Analysis and design of controllers for cooperative and automated driving

Document status and date:
Published: 01/01/2014

Document Version:
Publisher's PDF, also known as Version of Record (includes final page, issue and volume numbers)

Please check the document version of this publication:

Analysis and design of controllers for cooperative and automated driving

TNO innovation for life

Analysis and design of controllers for cooperative and automated driving

PROEFSCHRIFT

ter verkrijging van de graad van doctor aan de
Technische Universiteit Eindhoven op gezag van de
rector magnificus prof.dr.ir. C.J. van Duijn, voor een
commissie, aangewezen door het College voor
Promoties, in het openbaar te verdedigen
op woensdag 9 april 2014 om 16.00 uur

door

Jeroen Ploeg

geboren te Velsen

Dit proefschrift is goedgekeurd door de promotoren en de samenstelling van de promotiecommissie is als volgt:

voorzitter:	prof.dr.ir. C.J. van Duijn
promotor:	prof.dr. H. Nijmeijer
copromotor:	dr.ir. N. van de Wouw
leden:	prof.dr.ir. B. van Arem (Technische Universiteit Delft)
	prof.dr.ir. P.P.J. van den Bosch
	dr. S. Shladover (University of California, Berkeley)
	prof.dr. H.J. Zwart (Universiteit Twente)

Summary

Analysis and design of controllers for cooperative and automated driving

The limited capacity of the road network has become an important factor in meeting the road transport demand. In addition, an increasing societal demand exists to reduce fuel consumption and emissions, and to improve traffic safety. Road capacity can be increased by improving the traffic efficiency, as an overall measure for throughput and time of travel, which is determined by the interaction between vehicles rather than by the characteristics of the individual vehicle and its driver. Although fuel efficiency and traffic safety can still be enhanced by optimizing the individual vehicle, acknowledgement of the fact that this vehicle is part of a traffic system creates new possibilities for further improvement of these aspects. To address this traffic-system approach, the field of Intelligent Transportation Systems (ITS) emerged in the past decade.

A promising ITS application is provided by Cooperative Adaptive Cruise Control (CACC), which allows for automatic short-distance vehicle following using intervehicle wireless communication in addition to onboard sensors. The CACC system is subject to performance, safety, and comfort requirements. To meet these requirements, a CACC-equipped vehicle platoon needs to exhibit string-stable behavior, such that the effect of disturbances is attenuated along the vehicle string, thereby avoiding congestion due to so-called ghost traffic jams. The notion of string stability is, however, not unambiguous in the literature, since both stability-based and performance-based interpretations for string stability exist. Therefore, in this thesis, a novel string stability definition of nonlinear cascaded systems is proposed, based on the notion of input–output stability. This definition is shown to characterize well-known string stability conditions for linear cascaded systems as a special case. Employing these conditions, the string stability properties of a CACC system using information of the directly preceding vehicle are analyzed.

Motivated by the proposed conditions for string stability of linear systems, a controller synthesis approach is developed that allows for explicit inclusion of the string stability requirement in the design specifications, thus preventing *a*

posteriori controller tuning to obtain string-stable CACC behavior. The potential of this approach is illustrated by its application to the design of controllers for CACC for a one-vehicle and a two-vehicle look-ahead communication topology. As a result, string-stable platooning strategies are obtained in both cases, also revealing that the two-vehicle look-ahead topology is particularly effective at a larger communication delay.

To validate the theoretical analysis, a prototype CACC system has been developed and installed in a platoon of six passenger vehicles. Experiments performed with this setup clearly show that the practical results match the theoretical analysis, thereby illustrating the practical feasibility for automatic short-distance vehicle following. At the same time, however, the experiments clearly indicate the need for graceful degradation mechanisms, due to the fact that wireless communication is subject to impairments such as packet loss. To address this need, a control strategy for graceful degradation is proposed to partially maintain the string stability properties of CACC in case of a failure of the wireless link.

The development of driver assistance systems, among which CACC, is supported by hardware-in-the-loop experiments. In such experiments, a test vehicle is placed on a roller bench, whereas wheeled mobile robots (WMRs) represent other traffic participants. These WMRs are overactuated, due to the fact that they have independently driven and steered wheels. Consequently, the WMRs can be regarded as automated vehicles, albeit with features far beyond those of nowadays road vehicles. To achieve a high degree of experiment reproducibility, in this thesis, focus is put on the design of an accurate position control system for the overactuated WMRs, taking the tire slip into account. A position controller based on input–output linearization by static state feedback is presented, using the so-called multicycle approach, which regards the robot as a set of identical unicycles. The controller thus aims for motion coordination of the four driven and steered wheels, such that a shared objective, i.e, trajectory tracking of the WMR body, is satisfied. In this sense, the control problem is conceptually similar to the aforementioned platoon control problem, in which also coordinated behavior of multiple systems is pursued. Practical experiments with the designed controller indicate that the WMR is capable of accurately following a desired spatial trajectory, thus allowing reproducible testing of intelligent vehicles in a controlled environment.

Summarizing, this thesis focusses on the analysis and the design of controllers for cooperative and automated driving, both theoretically and experimentally. As an important result, it can be concluded that short-distance vehicle following by means of CACC is technically feasible, due to, firstly, the availability of low-latency wireless communication technologies, and, secondly, fundamental insight into the mechanism of disturbance propagation in an interconnected vehicle string. A prerequisite, however, is that graceful degradation strategies are implemented to cope with wireless communication impairments such as packet loss. Consequently, safety-critical cooperative driving applications require a thorough development process, to which end advanced hardware-in-the-loop test facilities are currently available.

Contents

Nomenclature

Acronyms and abbreviations

ADAS	Advanced Driver Assistance System
(C)ACC	(Cooperative) Adaptive Cruise Control
CAN	Controller Area Network
CC	Cruise Control
dCACC	degraded Cooperative Adaptive Cruise Control
EGNOS	European Geostationary Navigation Overlay Service
ETSI	European Telecommunications Standards Institute
GCDC	Grand Cooperative Driving Challenge
GPS	Global Positioning System
HMI	Human–Machine Interface
I2V	Infrastructure-to-Vehicle communication
ITS	Intelligent Transport System
ITS-G5	Set of protocols and parameters specified in the ETSI Standard ES 202 663
LFT	linear fractional transformation
LMI	Linear Matrix Inequality
LQR	Linear-Quadratic Regulator
MIMO	Multiple-input multiple-output
MB	Moving Base
MPC	Model Predictive Control
P(I)D	Proportional–(Integral–)Derivative
SISO	Single-input single-output
SSCS	String Stability Complementary Sensitivity
TCP/IP	Transmission Control Protocol/Internet Protocol
UDP	User Datagram Protocol
UTM	Universal Transverse Mercator
V2X	Vehicle-to-Vehicle (V2V) or Vehicle-to-Infrastructure (V2I) communication
VeHIL	Vehicle Hardware-In-the-Loop
WGS84	World Geodetic System 1984
WMR	Wheeled Mobile Robot

Roman symbols

A	system matrix
a	acceleration
B	input matrix
C	output matrix; covariance; cornering slip stiffness
D	delay transfer function
d	distance
e	error
F	discrete-time system matrix; force
G	vehicle transfer function
g	gravitational constant
H	spacing policy transfer function
h	time gap
I	identity matrix; moment of inertia
j	imaginary number
K	controller gain vector; controller transfer function; slip stiffness
k	controller gain; discrete time
L	vehicle length; observer gain matrix
l	length
ℓ	number of outputs
M	frequency-domain magnitude
m	platoon length; vehicle mass
N	number of time samples; lower linear fractional transformation
n	number of states; discrete frequency
P	probability
$P(s), \mathcal{P}$	plant model
Q	state weighting matrix
q	position; number of inputs; state vector
R	input weighting matrix; radius
r	standstill distance; control signal; input vector
S	sensitivity transfer function
s	Laplace variable; generalized position
T	time period; torque; observer transfer function
t	time
u	vehicle input; lateral velocity
V	Lyapunov candidate function
v	controller input; (longitudinal) velocity; noise
W	weighting factor; vehicle width
w	exogenous input; disturbance; noise
x	state vector; position coordinate
y	output; position coordinate
z	exogenous output

Greek symbols

α class $\mathcal{K}$ function; reciprocal maneuver time constant; lateral slip
β class $\mathcal{K}$ function; road slope angle
Γ string stability complementary sensitivity
γ string stability complementary sensitivity impulse response; threshold value
Δ interval
δ steering angle
Θ transfer function relevant to semi-strict string stability
θ communication delay
κ longitudinal slip
ν new system input
ξ new vehicle input
σ singular value; standard deviation; tire relaxation length
τ time constant
ϕ vehicle delay
ψ orientation angle
ω frequency; rotational velocity

Subscripts

cp	control point	max	maximum
d	derivative action; drive line	min	minimum
dd	double derivative action	nom	nominal
fb; ff	feedback; feedforward	p	proportional action; process
h	host vehicle	r	reference; desired
$i; j; k$	indices	rl	road load
lat	lateral	s	sampling; steering system
long	longitudinal	t	target vehicle
m	measurement	z	vertical direction

Miscellaneous

$\mathbb{C}$	set of complex numbers	sup	supremum
$\mathscr{F}(\cdot)$	Fourier transform	x^{T}	transpose of x
$f(\cdot)$	real-valued function	$\dot{x}\ (\ddot{x})$	(second) time derivative of x
$h(\cdot)$	real-valued function	$\bar{x}$	equilibrium; maximum of x
$k(\cdot)$	real-valued function	$\hat{x}$	estimated value of x
$\mathscr{L}(\cdot)$	Laplace transform	$\langle \cdot, \cdot \rangle$	inner product
max	maximum	$|\cdot|$	absolute value
$\mathbb{N}$	set of positive integer numbers	$\|\cdot\|$	vector norm
$\mathbb{R}^{n \times m}$	set of real $n \times m$ matrices	$\|\cdot\|_{\mathcal{H}_\infty}$	$\mathcal{H}_\infty$ system norm
$\mathrm{Re}(\cdot)$	real part	$\|\cdot\|_{\mathcal{L}_p}$	$\mathcal{L}_p$ signal norm, $p \in \{1, 2, \infty\}$
S_m	set of all vehicles in a platoon of length m		

Chapter 1

Introduction

Cooperative driving is a promising field of research in view of overall improvement of traffic efficiency and safety. The technology necessary to implement cooperative driving involves partial or full vehicle automation, supported by information retrieved through wireless communications between vehicles and/or between vehicles and roadside units. Before focussing on the control-relevant aspects of a closed-loop cooperative driving system in the coming chapters of this thesis, Section 1.1 of this chapter first briefly introduces some important aspects of cooperative driving in general. Section 1.2 then identifies the main challenges in the field of controller design for cooperative vehicle following, being a promising real-time closed-loop cooperative driving application. Section 1.3 further addresses these challenges by formulating the objectives of this thesis and by summarizing the specific contributions, after which Section 1.4 presents an outline of the thesis.

1.1 Cooperative driving

This section introduces the typical features of cooperative driving, identifies important technical aspects of real-time closed-loop applications in this field, and briefly describes the development process of cooperative driving control systems, the latter focussing on the use of hardware-in-the-loop simulations in this process.

1.1.1 The nature of cooperative driving

Vehicle automation by means of Advanced Driver Assistance Systems (ADASs) is believed to reduce the risk of accidents, improve safety, increase road capacity, reduce fuel consumption, and enhance overall comfort for drivers (Vahidi and Eskandarian, 2003). Based on all these potential benefits of automation, research on automating some or all aspects of the driving task has been pursued for several decades now. Initially aiming for increased driver comfort, this research resulted in Cruise Control and Adaptive Cruise Control (Piao and McDonald, 2008), both

of which are widespread in nowadays commercially available vehicles. The new generation of ADASs is primarily directed towards increasing safety of both passengers and vulnerable road users such as pedestrians and bicyclists. While this type of systems is still under development, the first safety-oriented ADASs already entered the market some time ago, focussing on collision mitigation and collision avoidance (Lu et al., 2005).

In parallel to the aforementioned developments, it is recognized that the current generation of advanced driver assistance systems still aims for optimizing the individual vehicle, which is an inherent consequence of the fact that onboard sensors such as radar, scanning laser (lidar), and vision systems, only provide information about other road users in the line-of-sight of the sensor. To optimize the road traffic system as a whole, either by centralized, decentralized, or distributed control systems, real-time information on other road users beyond the immediate line-of-sight is generally required. In addition, real-time information may be required that cannot be obtained through onboard sensors, or requires state observers, thereby introducing inaccuracy and/or phase lag. With wireless communications, local information from cooperating vehicles significantly extends the driver's perception and the detection range of onboard sensors, thus creating a wider information horizon. Vehicle automation systems utilizing wireless communications are generally referred to as cooperative driving systems (Shladover, 2012), although the mere fact of employing wireless communications does not necessarily imply true cooperation.

Cooperative driving may be described as *influencing the individual vehicle behavior, either through advisory or automated actions, so as to optimize the collective behavior with respect to road throughput, fuel efficiency and/or safety*, although a formal definition of cooperative driving does not exist to the best of the author's knowledge. Within the field of cooperative driving systems, numerous applications are under investigation, ranging from warning systems, supporting the driver in potentially dangerous situations, to partial or even full vehicle automation (Piao and McDonald, 2008). These applications are not limited to intervehicle wireless communications, but also include infrastructure-to-vehicle communications (and vice-versa) to even further extend the information horizon.

Besides the technical aspects of cooperative driving systems, which will be further addressed in the next subsection, the market introduction is of special importance since this involves a variety of stakeholders. In the European project DRIVE C2X[1], which currently runs under the 7th Framework Programme, three groups of stakeholders are identified, being the user, public bodies, and private companies, as schematically depicted in Figure 1.1. Furthermore, two types of cooperative driving systems are distinguished: *cooperative vehicular functions and services*, which involve the user and private companies, and *traffic services*, involving the user and public bodies. The figure further indicates the main prerequisites for a successful market introduction of both types of systems, relating to technical maturity, impact assessment, user awareness and acceptance, standardization, business models, and legislation. These topics are currently under investigation on a world-wide scale.

---

[1]http://www.drive-c2x.eu/project
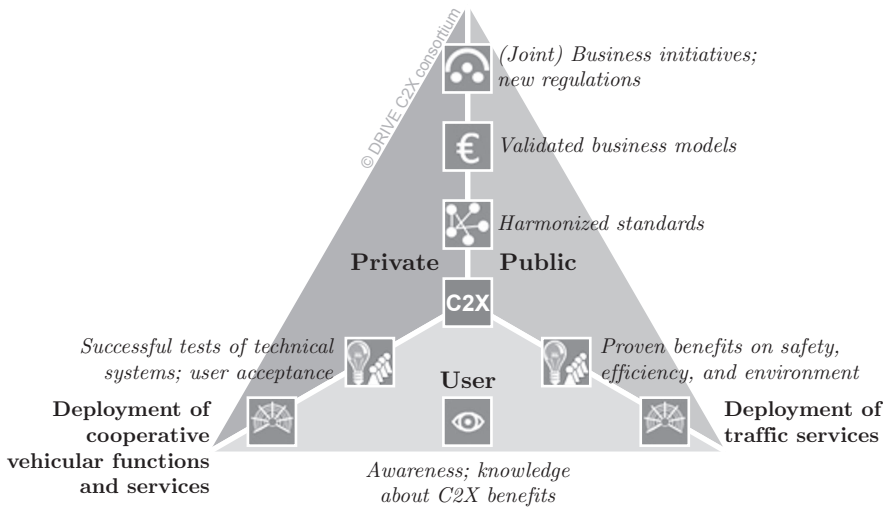
Figure 1.1: Requirements for successful market introduction of cooperative driving systems (source: http://www.drive-c2x.eu/road-to-market).

1.1.2 Technical aspects[2]

Of special interest, from a control perspective, are cooperative driving systems that employ wireless communications in a closed-loop configuration, thus constituting a *networked control system* (Heemels and Wouw, 2010), being subject to time delay and sampled data effects. An example of such a system, employing longitudinal vehicle automation, is Cooperative Adaptive Cruise Control (CACC). CACC is a vehicle-following system that allows for short-distance following while maintaining a high level of safety, thus potentially improving road throughput and fuel efficiency due to reduced aerodynamic drag (Shladover et al., 2012; Ramakers et al., 2009). CACC can in principle be extended so as to incorporate lateral automation as well. Real-time closed-loop cooperative driving applications are characterized by a number of key technical aspects, as explained below.

Robust fail-safe real-time control

CACC can be regarded as the main real-time closed-loop cooperative driving application that has been under investigation in academia and industry. A frequently adopted approach is based on well-defined vehicle platoons, i.e., a platoon leader is present and all platoon members are known. As opposed to this structured environment, the application of automated vehicle following in everyday traffic will most likely be characterized by an unstructured environment consisting of vehicles of various types and instrumentation. Moreover, in practice, a natural platoon leader need not be present and the platoon may not be well-defined, in the sense that all members of the platoon may not have been explicitly identified as such.

---

[2]This section is based on Ploeg et al. (2012).

This situation can be handled by either implementing a negotiation mechanism to determine the platoon leader and the platoon members, thereby increasing the communication load, or an *ad hoc* vehicle-following approach, which is characterized by a cluster of cooperative vehicle followers that are not necessarily aware of all members and do not rely on a leader. Note that these considerations not only apply to longitudinally automated vehicle systems, but just as well to systems consisting of fully automated vehicles, i.e., including lateral automation. Research into these implementation-relevant aspects has emerged only recently (compared to the system-theoretical aspects), see, e.g., Shaw and Hedrick (2007b) and Naus et al. (2010).

Furthermore, application in everyday traffic of automated vehicle-following systems, either incorporating longitudinal automation or lateral automation or both, requires a high level of reliability and safety. Especially when wireless communications are employed, careful network planning and message handling is required to achieve the necessary reliability. A high level of redundancy may not be the *a priori* solution since this also increases system costs. Consequently, the actual challenge which has yet to be solved, is to design a system that achieves a sufficient level of reliability and includes mechanisms for graceful degradation, capable of coping with flawed or missing data from other vehicles, to ensure safety, while keeping system costs to a minimum.

Finally, the impact of automation on the driver necessitates a very fundamental understanding of human factors in relation to (semi-)automated driving control or assistance systems. Hence, user acceptance and driver behavior are important aspects to be addressed before a safety-critical cooperative driving application, such as CACC, can be employed (Shladover et al., 2009).

Distributed real-time information structures

Cooperative driving technologies rely to a large extent on information exchange between traffic participants and/or between traffic participants and roadside units. To cooperate successfully, communicating nodes must have a common understanding of the exchanged information, which involves standardization of message formats, and communication and interaction protocols (Russo et al., 2008).

Road users and roadside units fuse data from their own sensors and from communicated information to construct their local view of the world or "world model." A world model includes a representation of the local traffic situation and the status of neighboring vehicles and roadside units and provides the input for control (Brignolo et al., 2008). On a traffic level, however, road users and roadside units have to maintain some level of consistency in the distributed world view to support cooperative (and safe) behavior. Consequently, a complex large-scale information flow arises, exchanging motion data and events on a real-time basis. This requires a well-defined information architecture, achieving a high level of reliability and scalability.

Wireless communication in real-time environments

It is well known that wireless and mobile communications are subject to failure by their very nature. Examples of phenomena, impeding flawless communications, are varying signal strengths due to varying propagation conditions, multi-path fading including intersymbol interference, Doppler shifts due to station mobility, and many types of interference signals, such as man-made noise and intermodulation (Tse and Viswanath, 2005). In ad hoc networks, including vehicle-to-vehicle networks, where stations communicate without the use of fixed infrastructure, additional problems arise. For instance, transmitting stations may cause mutual interference at a receiver, known as the hidden terminal problem (Hekmat, 2006). The latter problem actually becomes more dominant in the typical real-time setting, in which vehicles exchange motion data at relatively high update rates (10 Hz or higher) and require low latencies (significantly less than 100 ms).

Despite a plethora of mitigation strategies found in modern wireless communication systems, none of these are fail-safe. The control system should therefore be robust against wireless communication impairments such as latency, fading, frame and packet loss, and limited range and bandwidth. A careful balance is needed between the use of and dependency on information obtained through wireless communications and the use of onboard sensors to obtain the required situation awareness and to ensure safety at all times. Finding this balance is an important objective in wireless communications research in view of large-scale deployment, which is more important than the communication technologies by themselves.

Research activities into the technical aspects of cooperative driving are still ongoing. These activities also include experimental evaluation of cooperative driving applications, a unique example of which is provided by the Grand Cooperative Driving Challenge (GCDC), see Figure 1.2, which exclusively focussed on CACC. The GCDC took place in May 2011 in The Netherlands and involved nine international teams, each one having its own specific implementation of control algorithms, while employing a common message set for the wireless intervehicle communication (Nunen et al., 2012). The GCDC contributed in identifying directions for further research, one of the most important being the implementation of mechanisms for fault tolerance and graceful degradation. Although not addressed in the GCDC, it may be expected that cybersecurity will also be an important topic in this context.

Figure 1.2: The GCDC participants with the organization's lead vehicle.
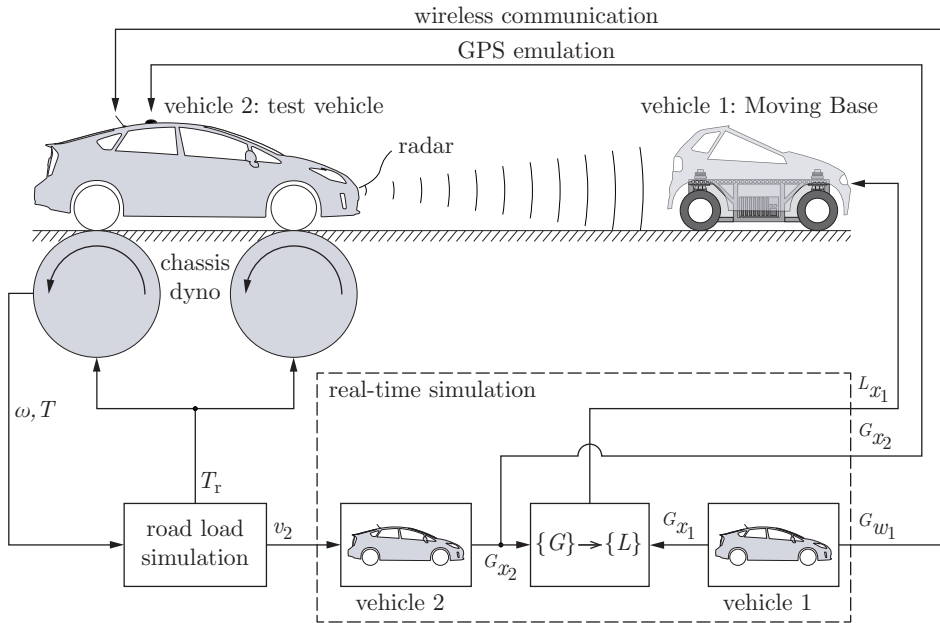
Figure 1.3: Schematic representation of the VeHIL test bed.

1.1.3 Development process

The development process of cooperative driving systems as performed by the automotive industry follows the so-called V-cycle, which identifies the steps in the design flow at different hierarchical levels, with every specification or design step having a corresponding validation or verification step (Naus, 2010). This process is supported by hardware-in-the-loop testing of components. Especially for safety-critical systems, it is desired to first test the entire vehicle in a hardware-in-the-loop setting before commencing road tests. To this end, a test bed called VeHIL (Vehicle Hardware-In-the-Loop) has been developed, which allows to test ADAS-equipped vehicles in a controlled (indoor) environment, while emulating other traffic by wheeled mobile robots (Gietelink et al., 2006). VeHIL is especially useful to test closed-loop vehicle control systems, among which cooperative driving systems, that aim to support the driver based on the detection of other traffic participants.

The working principle of VeHIL is schematically depicted in Figure 1.3 by means of an example involving a platoon consisting of a lead vehicle (vehicle 1) and a follower vehicle (vehicle 2) equipped with CACC. The core of VeHIL is a real-time simulation model, describing the dynamic behavior of relevant traffic participants. Starting from an equilibrium situation, in this case defined by a constant velocity of both vehicles whereas vehicle 2 follows at a desired distance, the simulated lead vehicle performs a maneuver, such as accelerating or braking, which is captured by its "state" vector $^{G}x_1$. This state vector contains the position

and orientation of vehicle 1, and possibly the first and second time derivatives, expressed with respect to the origin of a global fixed coordinate system $\{G\}^3$. The current measured state $^G x_2$ of the test vehicle, which is placed on a chassis dynamometer, is then used to perform a coordinate transformation of $^G x_1$ to a coordinate frame $\{L\}$ which is attached to the test vehicle, yielding $^L x_1$. This relative motion vector is subsequently sent as a control command to a wheeled mobile robot, the so-called Moving Base, which represents vehicle 1. The Moving Base motion is detected by the test vehicle's environmental sensor, e.g., a radar, upon which the test vehicle velocity response is measured through the chassis dynamometer rotational velocity ω and subsequently forwarded as the vehicle velocity v_2 to the simulation model. Finally, the test vehicle state vector $^G x_2$ is determined based on v_2 through numerical integration and differentiation. The chassis dynamometer is torque controlled, where the desired torque T_r stems from the vehicle inertia and the estimated friction forces caused by aerodynamic drag and the tires. In addition, the test vehicle GPS signal and the wireless message $^G w_1$ from the lead vehicle can be emulated as well, e.g. to perform tests with vehicles equipped with CACC.

In summary, VeHIL simulates the motion of traffic participants with respect to the test vehicle, which is safe and space efficient, thus allowing for indoor testing under controlled and reproducible circumstances. The application of VeHIL in the development process of ADASs is extensively described in Gietelink (2007), which also contains a case study regarding CACC system validation.

Of particular interest, from a control perspective, is the Moving Base. This wheeled mobile robot (WMR) is equipped with four independently driven and steered wheels to be able to independently control the orientation and the direction of motion, the reason for which is shown in Figure 1.4. Figure 1.4(a) shows an example manoeuver, consisting of a test vehicle (vehicle 2) with velocity vector $^G v_2$ and a preceding vehicle (vehicle 1) that performs a cut-in, thus having a velocity vector $^G v_1$ and a yaw rate $^G \dot{\psi}_1$. As a result of the relative motion principle of VeHIL, the Moving Base, representing vehicle 1, has a velocity vector $^L v_1$, whereas its yaw rate $^L \dot{\psi}_1$ is equal to $^G \dot{\psi}_1$, as shown in Figure 1.4(b). Consequently, the orientation of the Moving Base no longer corresponds to the direction of motion, hence requiring an all-wheel steered vehicle.

The Moving Base platform thus constitutes an overactuated system, consisting of eight actuators (four steering and four driving motors), whereas the motion control objective only incorporates the three degrees of freedom in the horizontal plane. As a result, the motion of the four wheels needs to be coordinated, in order to impose the required moment and forces on the center of gravity of the robot platform, such that the desired trajectory in the horizontal plane is tracked. Consequently, the control problem can be characterized as actuator-level motion coordination. In this respect, a conceptual link exists with the vehicle-following problem, which, in fact, also requires motion coordination of dynamic systems, in this case vehicles in a platoon. For this reason, and because of the relevance of hardware-in-the-loop validation of cooperative driving systems, the motion control

---

[3]Since VeHIL involves various coordinate systems, the particular coordinate system in which a certain variable is expressed, is explicitly indicated by a left superscript.
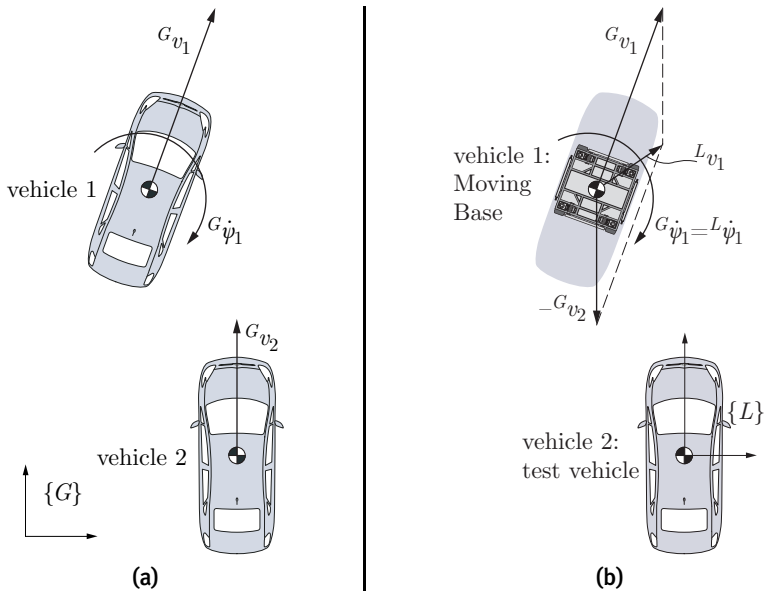
Figure 1.4: Vehicle motion with respect to (a) a global fixed coordinate frame $\{G\}$ and (b) a local coordinate frame $\{L\}$, attached to the test vehicle.

of the Moving Base, or, in general, an overactuated WMR, is incorporated in the challenges that are identified in the field of cooperative vehicle-following systems, as presented in the next section.

1.2 Challenges in dynamics and control of cooperative vehicle-following systems

Ad hoc cooperative vehicle following by means of longitudinal vehicle automation (i.e., CACC) is a closed-loop real-time cooperative driving application which has the potential to increase road throughput (Shladover et al., 2012) and reduce fuel consumption (Ramakers et al., 2009). Nevertheless, a number of challenges in the field of controller design for CACC still exist, as will be explained hereafter.

The concept of automated vehicle following with road vehicles has been well known for decades. One of the first control-oriented publications on the subject dates back to 1966 (Levine and Athans, 1966). Since then, a large amount of relevant research has been published, see, e.g., Sheikholeslam and Desoer (1993), Swaroop and Hedrick (1996), and Vahidi and Eskandarian (2003). This research invariably takes *string stability* into account, which can be roughly described as the attenuation along the string of vehicles of the effects of disturbances, such as initial condition perturbations or unexpected velocity variations of vehicles in the string (Seiler et al., 2004). String stability is generally considered a prerequisite for safety, driver comfort, and scalability with respect to platoon length.

Especially in case of ad hoc vehicle following (see Section 1.1.2), the scalability property is of the essence since the platoon length is unknown. Nevertheless, from the literature review on string stability as presented in Chapter 2 of this thesis, it appears that this notion is not unambiguous, since both stability and performance interpretations exist. Consequently, to allow for rigorous analysis of string stability properties of a vehicle platoon, a unifying (or at least general) definition of string stability is required first.

Despite the existing ambiguity of the notion of string stability, various types of controllers that realize a specific form of string-stable behavior have been proposed, see, e.g., Rajamani and Zhu (2002) for a PD-like controller, employing a one-vehicle look-ahead communication topology, and Swaroop et al. (2001), describing a sliding-mode controller that uses communicated lead vehicle information in addition. These controller synthesis methods, however, do not take the string stability requirement explicitly into account. Consequently, string-stable behavior has to be realized through *a posteriori* controller tuning. Moreover, in the scope of ad hoc vehicle following, communication of lead vehicle information is not possible since no vehicle is explicitly classified as such. Due to its capability of including constraints in the controller design, Model Predictive Control can enforce the attenuation of the $\mathcal{L}_\infty$ signal norm of the disturbance responses; this is investigated in Dunbar and Caveney (2012), but only for a one-vehicle look-ahead communication topology. Furthermore, a mixed $\mathcal{H}_2/\mathcal{H}_\infty$ problem formulation is applied in Maschuw et al. (2008), resulting in string-stable behavior of the vehicle platoon, albeit with a centralized controller that requires the states of all platoon vehicles to be available. From the aforementioned literature references and other relevant publications as thoroughly reviewed in Chapter 3 of this thesis, it appears that systematic controller design methods in which the string stability requirement is *a priori* included as a design specification, are investigated to a very limited extent. This conclusion especially holds when considering ad hoc vehicle following for the general multiple-vehicle look-ahead communication topology.

As already mentioned in Section 1.1.2, fail-safety of CACC is of the essence due to wireless communication impairments such as (varying) latency and packet loss. Current research in the field of networked control systems, focussing on the effects of varying latency (Öncü, 2014), contributes to rigorous knowledge regarding the maximum allowable latency and, consequently, to fail-safe controller design. However, also when the wireless link completely fails, it is necessary to guarantee safety, driver comfort, and platoon scalability. Consequently, it is required to design a controller which is robust to the loss of wireless communication, in the sense that performance degradation with respect to string stability is predictable and limited. This requirement constitutes yet another challenge for controller design, which is currently not addressed in the literature.

The aforementioned challenges all relate to various aspects of string stability of controlled vehicle platoons. To establish the practical feasibility of developed theoretical solutions, practical experiments are necessary. Although vehicle-following control systems have been evaluated in practice (see, for instance, Gehring and Fritz (1997) and Shladover et al. (2009)), such practical experiments in general do not focus on string stability. Vice versa, theoretical work on string stability,

as described in the literature, is rarely validated in practice. Consequently, the execution of real-life tests of CACC technology, to validate theoretical results regarding string stability properties, can be considered a challenge in itself.

Finally, the development of real-time safety-critical cooperative driving applications, such as CACC, can be strongly supported by hardware-in-the-loop tests that allow for safe and reproducible evaluation of these systems. As described in Section 1.1.3, VeHIL establishes such a testing environment. However, VeHIL heavily relies on accurate motion control of the wheeled mobile robots (WMRs), which simulate other traffic participants. Due to the relative-motion principle of VeHIL, these WMRs are equipped with four independently driven and steered wheels to independently control the orientation of the body and the direction of motion. Consequently, the WMR itself can be regarded as an automated vehicle, albeit with features far beyond those of nowadays road vehicles. When neglecting tire slip, this type of robot falls within the classification system as developed for wheeled mobile robots in Campion et al. (1996) and control solutions are readily available, see, e.g., Canudas de Wit et al. (1996), Bendtsen et al. (2002), and Ploeg et al. (2006). However, the added value of VeHIL is to be able to simulate safety-critical maneuvers, which inherently implies high decelerations and accelerations of the WMRs. Hence, tire slip plays an important role in the dynamic behavior of the WMR and needs to be taken into account in the control design, thus requiring a new controller design approach, incorporating the motion coordination on the actuator level, i.e., the four wheels.

1.3   Research objectives and contributions

Following the aforementioned challenges, this thesis aims to contribute to the analysis and control of the dynamics of a cooperative vehicle-following control system, in particular CACC, which requires a form of motion coordination of the consecutive vehicles in a platoon. In addition, the controller design for a wheeled mobile robot is pursued; This robot not only serves as a component in a hardware-in-the-loop test facility for cooperative road vehicles, but can also be regarded as an autonomous vehicle in itself, the trajectory control of which requires motion coordination of the four actuated wheels. Consequently, the following objectives are defined:

- Rigourously formulate the notion of string stability and subsequently investigate the possibilities for controller synthesis such that the string stability requirement is explicitly incorporated in the design specifications, while also taking into account fail-safety with respect to wireless communication impairments;

- Experimentally validate the theoretical results regarding (controller design for) string stability, using a CACC-equipped vehicle platoon;

- Develop and experimentally validate a trajectory controller for an over-actuated wheeled mobile robot, thereby illustrating actuator-level motion coordination.

These objectives are addressed by means of the following contributions, corresponding to the challenges as described in Section 1.2.

1. **String stability definition and analysis**
   String stability basically involves stability in the time domain and in the spatial domain, the latter referring to stability "over the cascaded vehicles". Based on a review of the various string stability definitions and criteria as published in the literature, a novel generic definition regarding $\mathcal{L}_p$ string stability for nonlinear cascaded systems is proposed in Chapter 2 of this thesis. This definition is applied to derive string stability criteria for linear systems, while introducing semi-strict and strict $\mathcal{L}_p$ string stability as special (stronger) forms of $\mathcal{L}_p$ string stability. These theoretical contributions are used to analyze the string stability properties of vehicle platoons, both with and without the application of wireless communication to retrieve information about the preceding vehicle(s).

2. **Controller synthesis for string stability**
   Next to string stability analysis, this thesis also contributes to controller synthesis aiming for string stability. A literature review regarding controller synthesis methods for vehicle platooning and other applications that require string-stable behavior reveals that the vast majority of applied controllers realizes string-stable behavior by ad hoc tuning of the controller parameters. Therefore, in Chapter 3 a structured method is proposed, employing $\mathcal{H}_\infty$ optimal control, which allows for explicit inclusion of the $\mathcal{L}_2$ string stability requirement in the controller synthesis specifications. The potential of this approach is illustrated by its application to the design of controllers for CACC for a one- and a two-vehicle look-ahead communication topology.

3. **Fail-safe controller design for CACC**
   Fail-safety by means of graceful degradation is an important prerequisite for a successful market introduction of CACC. Therefore, Chapter 4 presents a method for graceful degradation in case the wireless link fails due to, e.g., packet loss over an extended period of time. This method is based on estimation of the preceding vehicle's acceleration using onboard sensors and has a clear advantage in terms of $\mathcal{L}_2$ string stability compared to the alternative fallback scenario consisting of conventional Adaptive Cruise Control (ACC).

4. **Experimental evaluation using a platoon of passenger vehicles**
   A platoon of CACC-equipped passenger vehicles has been developed to experimentally validate all theoretical results. This may be considered an important contribution to the maturity level of CACC technology since practical implementation not only involves the platooning controller itself, but also requires mechanisms for graceful degradation, algorithms for object tracking, and human–machine interfacing. To structure this variety of algorithms, a layered control system architecture is developed in Chapter 5, consisting of a perception layer, containing observers for both the host vehicle motion pattern and that of target vehicles, a control layer, which includes

the control algorithms for CACC, and a supervisory layer that coordinates controller settings received from the driver or from roadside equipment, and ensures safe operation of the vehicle.

5. **Controller design for an overactuated wheeled mobile robot**
Finally, this thesis contributes to the design of position controllers for all-wheel steered mobile robots employing the so-called multicycle approach as described in Chapter 6. Such robots are used to emulate traffic participants in the VeHIL hardware-in-the-loop setup to test entire vehicles equipped with ADASs, among which CACC. A distributed position controller based on input–output linearization by state feedback appears to allow for highly dynamic maneuvers of the wheeled mobile robots, thus realizing an agile fully automated vehicle.

1.4 Outline

This thesis is organized as follows. Chapter 2 introduces a new generic $\mathcal{L}_p$ string stability definition, based on which string stability conditions for linear systems are derived. Subsequently, the string stability properties of a vehicle platoon equipped with CACC are analyzed, both in theory and in practice. Note that this chapter is based on Ploeg et al. (2014b), extended with experimental results taken from Ploeg et al. (2011).

Next, Chapter 3, which is directly based on Ploeg et al. (2014a), presents a controller design method that allows for explicit inclusion of the $\mathcal{L}_2$ string stability requirement in the controller synthesis specifications. The potential of this approach is illustrated by its application to the design of controllers for CACC for a one- and a two-vehicle look-ahead communication topology.

Chapter 4 fully focusses on the fact that CACC relies on communicated information, thus inherently causing a certain vulnerability to communication impairments such as packet loss. To cope with this property, a graceful degradation mechanism is presented that involves estimation of the preceding vehicle's acceleration. The resulting string stability properties are analyzed and experimentally validated. This chapter is based on Ploeg et al. (2013), with additional experimental results. It is noted that, due to the fact that this chapter and the previous two chapters are based on literature publications, the introductory parts of these chapters are redundant, to a limited extent.

As a part of the validation process, the previous three chapters all contain experimental results obtained with a CACC-equipped platoon of passenger vehicles. This test setup is described in more detail in Chapter 5, both with respect to vehicle instrumentation and to software, i.e., the algorithms that appear to be necessary to implement CACC in practice, next to the control algorithm itself.

Having explored the theoretical and practical aspects of the control of cascaded systems in general and vehicle platoons in particular, Chapter 6 is concerned with the position control of the wheeled mobile robots used in the VeHIL test site for cooperative systems such as CACC. This chapter is, in fact, a revised version of Ploeg et al. (2009).

Finally, Chapter 7 summarizes the main conclusions of this thesis regarding string stability, vehicle platooning, and vehicle automation, and presents recommendations for future research into these and related topics.

Chapter **2**

String stability of cascaded systems: Application to vehicle platooning[1]

Abstract   Nowadays, throughput has become a limiting factor in road transport. An effective means to increase the road throughput is to decrease the intervehicle time gap. A small time gap, however, may lead to string instability, being the amplification of velocity disturbances in upstream direction. String-stable behavior is thus considered an essential requirement for the design of automatic distance control systems, which are needed to allow for safe driving at time gaps well below 1 s. However, the formal notion of string stability is not unambiguous in literature, since both stability interpretations and performance interpretations exist. Therefore, a novel definition for string stability of nonlinear cascaded systems is proposed, using input–output properties. This definition is shown to result in well-known string stability conditions for linear cascaded systems. Employing these conditions, string stability is obtained by a controller that uses wireless intervehicle communication to provide information of the preceding vehicle. The theoretical results are validated by implementation of the controller, known as Cooperative Adaptive Cruise Control, on a platoon of six passenger vehicles. Experiments clearly show that the practical results match the theoretical analysis, thereby indicating the practical feasibility for short-distance vehicle following.

2.1   Introduction

Limited highway capacity regularly causes traffic jams, which tend to increase over the years with respect to both the number of traffic jams and their length. An effective means to increase road capacity is to decrease the intervehicle distance while maintaining the same velocity. This would, however, seriously compromise traffic safety. Moreover, human drivers are known to overreact to velocity variations, thereby amplifying these variations in upstream direction (Sugiyama

---

[1]This chapter is based on Ploeg et al. (2014b), extended with experimental results taken from Ploeg et al. (2011).

et al., 2008). Consequently, vehicle automation in longitudinal direction is required. To this end, the application of Adaptive Cruise Control (ACC) can be beneficial. ACC automatically adapts the velocity of a vehicle so as to realize a desired distance to the preceding vehicle, or, in the absence of one, a desired velocity (Venhovens et al., 2000; Corona and Schutter, 2008). The intervehicle distance and the relative velocity are measured by means of a radar or a scanning laser (lidar). However, ACC is primarily intended as a comfort system. Therefore, relatively large intervehicle distances are adopted (Vahidi and Eskandarian, 2003), with a standardized minimum of 1 s time gap (International Organization for Standardization, 2010), the latter referring to the geometric distance divided by the vehicle velocity[2].

Decreasing the ACC time gap to a value significantly smaller than 1 s is expected to yield an increase in traffic throughput (Santhanakrishnan and Rajamani, 2003; Arem et al., 2006). Moreover, a significant reduction in the aerodynamic drag force is possible in case of heavy-duty vehicles, thereby decreasing fuel consumption and emissions (Bose and Ioannou, 2003a; Shladover, 2005; Alam et al., 2010). It has however been shown that the application of ACC amplifies disturbances in upstream direction at small time gaps, see, e.g., Yanakiev and Kanellakopoulos (1998) and Naus et al. (2010), similar to the disturbance amplification in case of human drivers. These disturbances may be induced by velocity variations of the first vehicle in a string of vehicles, for instance. As a result, fuel consumption and emissions increase, and so-called ghost traffic jams may occur, negatively influencing throughput, whereas safety might be compromised as well. Note that this type of disturbance amplification becomes even worse when applying a constant-distance spacing policy instead of the common constant time gap policy, as assumed above (Swaroop and Hedrick, 1999).

Disturbance attenuation along the vehicle string is therefore an essential requirement, to be achieved by appropriately designed vehicle-following controllers. The disturbance evolution along a string of vehicles, or, in general, along a number of interconnected systems, is covered by the notion of string stability, where string-stable behavior can be loosely defined as the attenuation of the effect of disturbances in upstream direction. Automatic vehicle following based on data exchange by means of wireless communication, in addition to the data obtained by radar or lidar, is commonly referred to as Cooperative ACC (CACC), and is known to achieve string stability at time gaps significantly smaller than 1 s.

A vast amount of literature on string stability is available, where the first application to vehicle following systems probably dates from 1966 (Levine and Athans, 1966). In Swaroop and Hedrick (1996), Wang et al. (2006), and Curtain et al. (2009), for instance, several types of string stability definitions are given, focussing on a specific type of perturbations, or on specific interconnection topologies or other characteristics such as infinite string length. Consequently, a variety of string stability definitions exists. In addition, publications that focus on controller design for linear interconnected systems, in particular vehicle

---

[2]In literature, this measure is regularly referred to as the "time headway." In this thesis, however, the term "time gap" is adopted, in accordance with the ISO standard 15622 (International Organization for Standardization, 2010).

strings, tend to interpret string stability as a performance criterion, rather than a stability property (Sheikholeslam and Desoer, 1993; Rajamani and Zhu, 2002; Naus et al., 2010), the advantage being that control design is directly supported. As a result, however, the notion of string stability has become rather ambiguous over the years.

This chapter, therefore, first aims to formally define string stability, providing a rigorous basis for often-used string stability criteria for linear systems, thus including and generalizing existing results. To this end, the well-known notion of input–output stability is utilized. Second, it is shown that, employing these criteria, controller design for string stability is not only theoretically, but also practically feasible, using an experimental setup consisting of six passenger vehicles equipped with CACC, that has been specifically developed for the purpose of evaluating string stability properties.

The outline of this chapter is as follows. Section 2.2 first provides an overview of existing string stability concepts. Section 2.3 derives a model of a string of vehicles that are interconnected through their vehicle-follower control laws (hereafter shortly referred to as "platoon"). Adopting this model as a general model for an interconnected system, it forms the basis for the definition of string stability in Section 2.4 and the analysis thereof for vehicle platoons in Section 2.5. Next, Section 2.6 introduces the test vehicles and their instrumentation, after which Section 2.7 presents experimental results, obtained with the test vehicles. Finally, Section 2.8 summarizes the main conclusions.

2.2   String stability review

As opposed to conventional stability notions for dynamical systems, which are essentially concerned with the evolution of system states over time, string stability focusses on the propagation of system responses along a cascade of systems. Several approaches exist in the literature regarding the notion of string stability, as reviewed below.

Probably the most formal approach can be characterized as a Lyapunov-stability approach, of which Sheikholeslam and Desoer (1992a) provide an early description, which has been comprehensively formalized later in Swaroop and Hedrick (1996) and applied for controller design and analysis in Swaroop and Hedrick (1999). In this approach, the notion of Lyapunov stability is employed, which focusses on initial condition perturbations. Since, however, initial condition perturbations can be randomly distributed across the interconnected systems, a disturbance propagation in a clear direction cannot be distinguished anymore, thereby abandoning the original idea behind string stability to a certain extent. Instead, string stability is interpreted as asymptotic stability of an arbitrary number of interconnected systems, of which Yadlapalli et al. (2006) provide an elegant analysis. Recently, new results appeared in Klinge and Middleton (2009a), regarding a one-vehicle look-ahead control architecture in a homogeneous vehicle platoon. Herein, the response to an initial condition perturbation of a single vehicle in the platoon is considered, thereby conserving the disturbance-propagation idea

behind string stability. The drawback of this approach, however, is that only this special case is regarded, ignoring the effects of initial condition perturbations of other vehicles in the platoon, as well as the effects of (possibly persistent) external disturbances to the interconnected system. Consequently, the practical relevance of this approach is limited, since external disturbances, such as velocity variations of the first vehicle in a platoon, are of utmost importance in practice. Summarizing, although the string stability definitions in the Lyapunov-stability approach are rigorous, they only capture the notion of disturbance propagation along a set of interconnected systems to a limited extent. An attempt to overcome this apparent limitation has been made in Wang et al. (2006), which extends the focus on initial condition perturbations of the states by including external system inputs, ultimately leading to input-to-state string stability. The presented analysis, however, assumes that the interconnected system can be described by a singular perturbation model, and is therefore limited to weakly coupled interconnected systems.

The perspective of infinite-length strings of interconnected systems also gave rise to a clear mathematical formulation of string stability, described in Melzer and Kuo (1971) in the context of a centralized control scheme and then in Chu (1974) for a decentralized controller. Various applications regarding optimal controller design for interconnected systems such as seismic cables and vehicle platoons are reported in El-Sayed and Krishnaprasad (1981), Barbieri (1993), and Liang and Peng (1999), whereas Bamieh et al. (2002) and Curtain et al. (2009) provide extensive analyzes of the properties of infinite-length interconnected systems. In this approach, the model of such a system is formulated in an infinite-dimensional state space form and subsequently transformed using the bilateral Z-transform. The Z-transform is executed over the vehicle index instead of over (discrete) time, resulting in a model formulated in the "discrete spatial frequency" domain (Bamieh et al., 2002), related to the subsystem index, as well as in the continuous-time domain. String stability can then be assessed by inspecting the eigenvalues of the resulting system matrix as a function of the spatial frequency. In practice, however, vehicle platoons will be finite. Unfortunately, the stability properties of finite-length strings might not converge to those of infinite-length strings as length increases. This can be understood intuitively by recognizing that in a finite-length platoon, there will always be a first and a last vehicle, whose dynamics may significantly differ from those of the other vehicles in the platoon, depending on the controller topology. Consequently, the infinite-length platoon model does not always serve as a useful paradigm for a finite-length platoon as it becomes increasingly long (Curtain et al., 2009).

Finally, a performance-oriented approach for string stability is frequently applied, since this appears to directly offer tools for synthesis and analysis of *linear* vehicle-following control systems. An early application to vehicle platooning is presented in Peppard (1974), focussing on the analysis of a PID-controlled system. In Sheikholeslam and Desoer (1993) and in Lu and Hedrick (2004), the performance-oriented approach is employed to investigate the control of a vehicle platoon with and without lead vehicle information, whereas Naus et al. (2010) and Rajamani and Zhu (2002) apply intervehicle communication to obtain in-

formation of the directly preceding vehicle only. In Stanković et al. (2000), a decentralized optimal controller is designed by decoupling the interconnected systems to a certain extent using the so-called inclusion principle, and in Khatir and Davison (2004) optimal decentralized control is pursued as well, resulting in nonidentical controllers. Furthermore, Middleton and Braslavsky (2010) extensively investigate the limitations on performance, whereas Chien and Ioannou (1992) compare the performance of a vehicle-following controller with three types of human driver models. In González-Villaseñor et al. (2007), a controller design methodology is presented, adopting the performance-oriented approach. This approach is basically also used in Chakravarthy et al. (2009) to investigate a warning system for preventing head-tail collisions, taking mixed traffic (i.e., controlled and uncontrolled vehicles) into account. In the performance-oriented approach, string stability is characterized by the amplification in upstream direction of either distance error, velocity, or acceleration, the specific choice depending on the design requirements at hand. Let the signal of interest be denoted by y_i for vehicle i, and let $\Gamma_i(j\omega)$ denote the frequency response function, with the frequency $\omega \in \mathbb{R}$, describing the relation between the scalar output y_{i-1} of a preceding vehicle $i-1$ and the scalar output y_i of the follower vehicle i. Then the interconnected system is considered string stable if

$$\sup_\omega |\Gamma_i(j\omega)| \leq 1, \quad 2 \leq i \leq m, \tag{2.1}$$

where m is the string length; the supremum of $|\Gamma_i(j\omega)|$ is equal to the scalar version of the $\mathcal{H}_\infty$ norm. Since the $\mathcal{H}_\infty$ norm is induced by the $\mathcal{L}_2$ norms of the respective signals (Zhou et al., 1996), this approach in fact requires the $\mathcal{L}_2$ norm $\|y_i(t)\|_{\mathcal{L}_2}$ to be nonincreasing for increasing index i (i.e., in upstream direction) for string stability. Because of its convenient mathematical properties, the $\mathcal{L}_2$ gain is mostly adopted, according to (2.1); nevertheless, approaches that employ the induced $\mathcal{L}_\infty$ norm are also reported (Gehring and Fritz, 1997; Eyre et al., 1998; Klinge and Middleton, 2009b). Regardless of the specific norm that is employed, the major limitation of the performance-oriented approach is that only linear systems are considered, usually without considering the effect of nonzero initial conditions. Moreover, (2.1) should be considered as a *criterion* for string stability of linear systems, rather than a *definition* of this notion.

Summarizing, string stability appears to be defined in various ways, focusing on specific system properties. Building on these earlier results, a novel generic definition of string stability is proposed, based on the notion of input–output stability, which is applicable to both linear and nonlinear systems, while taking both the effects of initial conditions and external disturbances into account. Furthermore, for the special case of linear systems, a rigorous basis is obtained for the frequency-domain string stability conditions discussed above and it is proven that (2.1) indeed serves as a condition for string stability for a certain class of linear interconnected systems. To this end, the next section will first introduce a model of a homogeneous vehicle platoon, which motivates the formal definition of string stability as proposed in Section 2.4.
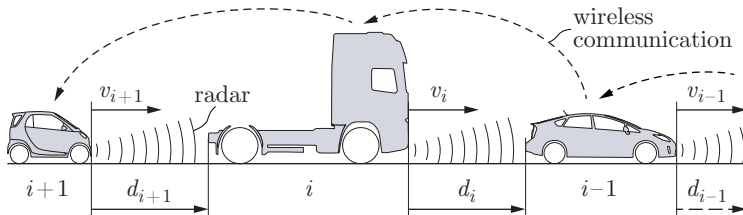
Figure 2.1: CACC-equipped vehicle platoon.

2.3 Platoon dynamics

In order to arrive at a model that describes the dynamics of a vehicle platoon, the control problem is formulated first. Next a controller is designed, which then allows for the formulation of a homogeneous (closed-loop) platoon model.

2.3.1 Control problem formulation

Consider a platoon of m vehicles, schematically depicted in Figure 2.1, with d_i being the distance between vehicle i and its preceding vehicle $i - 1$, and v_i the velocity of vehicle i. The main objective of each vehicle is to follow its preceding vehicle at a desired distance $d_{r,i}$. The first vehicle in the platoon (with index $i = 1$), not having a preceding vehicle, can be velocity controlled, for instance. Another option, adopted here, is to make the lead vehicle follow a so-called *virtual reference vehicle* (with index $i = 0$), which has the advantage that the lead vehicle will employ the same controller as the other vehicles in the platoon. The model for the virtual reference vehicle will be further explained in Section 2.3.3.

The desired distance $d_{r,i}$ is defined according to a constant time gap spacing policy, formulated as

$$d_{r,i}(t) = r_i + h v_i(t), \quad i \in S_m, \tag{2.2}$$

where h is the time gap, and r_i is the standstill distance. Herein, $S_m = \{i \in \mathbb{N} \mid 1 \leq i \leq m\}$ is the set of all vehicles in a platoon of length $m \in \mathbb{N}$. The spacing policy (2.2) is not only known to improve string stability (Rajamani and Zhu, 2002; Naus et al., 2010), but also contributes to safety (Ioannou and Chien, 1993). This is essentially due to the fact that (2.2) represents a differential feedback of the vehicle position, contributing to a well-damped behavior of the vehicle, as will be further explained in Section 2.4. Furthermore, a homogeneous platoon is assumed, which is why the time gap h is the same for all i. The spacing error $e_i(t)$ can now be defined as

$$\begin{aligned} e_i(t) &= d_i(t) - d_{r,i}(t) \\ &= \big(q_{i-1}(t) - q_i(t) - L_i\big) - \big(r_i + h v_i(t)\big), \quad i \in S_m, \end{aligned} \tag{2.3}$$

with q_i being the rear-bumper position of vehicle i and L_i its length. The platoon control problem now encompasses two requirements: one being the vehicle-

following control objective, to be formulated as $\lim_{t \to \infty} e_i(t) = 0 \; \forall \, i \in S_m$, and the other being the string stability requirement. The next subsection will focus on the first requirement, whereas the second requirement will be addressed in Section 2.4.

2.3.2 CACC design

As a basis for controller design, the following vehicle model is adopted, omitting the time argument t for readability:

$$\begin{pmatrix} \dot{d}_i \\ \dot{v}_i \\ \dot{a}_i \end{pmatrix} = \begin{pmatrix} v_{i-1} - v_i \\ a_i \\ -\frac{1}{\tau} a_i + \frac{1}{\tau} u_i \end{pmatrix}, \quad i \in S_m, \tag{2.4}$$

where a_i is the acceleration of vehicle i, u_i the external input, to be interpreted as desired acceleration, and τ a time constant representing driveline dynamics. This model is in fact obtained by formulating a more detailed model and then applying a precompensator, designed by means of input–output linearization by state feedback (Sheikholeslam and Desoer, 1993; Stanković et al., 2000). Also note that the time constant τ is assumed to be identical for all vehicles, corresponding to the above mentioned homogeneity assumption. With different types of vehicles in the platoon, as suggested by Figure 2.1, homogeneity may be obtained by low-level acceleration controllers so as to arrive at identical vehicle behavior according to (2.4).

A suitable method to arrive at a controller for CACC is based on formulation of the error dynamics. Define to this end the error states

$$\begin{pmatrix} e_{1,i} \\ e_{2,i} \\ e_{3,i} \end{pmatrix} = \begin{pmatrix} e_i \\ \dot{e}_i \\ \ddot{e}_i \end{pmatrix}, \quad i \in S_m \tag{2.5}$$

with e_i defined by (2.3). Then, obviously, $\dot{e}_{1,i} = e_{2,i}$ and $\dot{e}_{2,i} = e_{3,i}$. The third error state equation is obtained by differentiating $e_{3,i} = \ddot{e}_i$, while using (2.3) and (2.4), eventually resulting in:

$$\dot{e}_{3,i} = -\frac{1}{\tau} e_{3,i} - \frac{1}{\tau} \xi_i + \frac{1}{\tau} u_{i-1}, \quad i \in S_m \tag{2.6}$$

with

$$\xi_i := h \dot{u}_i + u_i, \tag{2.7}$$

which can be regarded as the new input to vehicle i. From (2.6), it is immediately clear that the input ξ_i should be used so as to stabilize the error dynamics while compensating for the (original) input u_{i-1} of the preceding vehicle in order to obey the vehicle-following control objective. Hence, the control law for ξ_i is chosen as follows:

$$\xi_i = K \begin{pmatrix} e_{1,i} \\ e_{2,i} \\ e_{3,i} \end{pmatrix} + u_{i-1}, \quad i \in S_m \tag{2.8}$$

with $K := \begin{pmatrix} k_p & k_d & k_{dd} \end{pmatrix}$. Note that the feedforward term u_{i-1} is obtained through wireless communication with the preceding vehicle and, therefore, is the reason for the employment of a wireless communication link in the scope of CACC.

Due to the additional controller dynamics (2.7), the error dynamics must be extended, to which end the input definition (2.7) can be employed, while substituting the control law (2.8):

$$\dot{u}_i = -\frac{1}{h}u_i + \frac{1}{h}(k_p e_{1,i} + k_d e_{2,i} + k_{dd} e_{3,i}) + \frac{1}{h}u_{i-1}, \quad i \in S_m. \qquad (2.9)$$

As a result, the 4$^{\text{th}}$-order closed-loop model reads

$$\begin{pmatrix} \dot{e}_{1,i} \\ \dot{e}_{2,i} \\ \dot{e}_{3,i} \\ \dot{u}_i \end{pmatrix} = \left(\begin{array}{ccc|c} 0 & 1 & 0 & 0 \\ 0 & 0 & 1 & 0 \\ -\frac{k_p}{\tau} & -\frac{k_d}{\tau} & -\frac{1+k_{dd}}{\tau} & 0 \\ \hline \frac{k_p}{h} & \frac{k_d}{h} & \frac{k_{dd}}{h} & -\frac{1}{h} \end{array} \right) \begin{pmatrix} e_{1,i} \\ e_{2,i} \\ e_{3,i} \\ u_i \end{pmatrix}$$

$$+ \left(\begin{array}{c} 0 \\ 0 \\ 0 \\ \hline \frac{1}{h} \end{array} \right) u_{i-1}, \quad i \in S_m. \quad (2.10)$$

This error model has an equilibrium in the origin for $u_{i-1} = 0$. Applying the Routh-Hurwitz stability criterion while using the fact that the system matrix in (2.10) is lower block-triangular, it follows that this equilibrium is asymptotically stable for any time gap $h > 0$, and with any choice for $k_p, k_d > 0$, $k_{dd} + 1 > 0$, such that $(1 + k_{dd})k_d - k_p \tau > 0$, thereby fulfilling the vehicle-following control objective. The second objective, being string stability, is not necessarily fulfilled yet. Note that the stability of the dynamics (2.10) is sometimes referred to as *individual vehicle stability* (Swaroop and Hedrick, 1999; Rajamani, 2006).

2.3.3   Homogeneous platoon model

Since string stability is commonly evaluated by analyzing the amplification in upstream direction of either distance error, velocity, and/or acceleration, a platoon model is formulated in terms of these state variables. Using the spacing error (2.3), the vehicle model (2.4), and the control law (2.9), the following homogeneous platoon model is obtained:

$$\begin{pmatrix} \dot{e}_i \\ \dot{v}_i \\ \dot{a}_i \\ \dot{u}_i \end{pmatrix} = \begin{pmatrix} 0 & -1 & -h & 0 \\ 0 & 0 & 1 & 0 \\ 0 & 0 & -\frac{1}{\tau} & \frac{1}{\tau} \\ \frac{k_p}{h} & -\frac{k_d}{h} & -k_d - \frac{k_{dd}(\tau-h)}{h\tau} & -\frac{k_{dd}h+\tau}{h\tau} \end{pmatrix} \begin{pmatrix} e_i \\ v_i \\ a_i \\ u_i \end{pmatrix}$$

$$+ \begin{pmatrix} 0 & 1 & 0 & 0 \\ 0 & 0 & 0 & 0 \\ 0 & 0 & 0 & 0 \\ 0 & \frac{k_d}{h} & \frac{k_{dd}}{h} & \frac{1}{h} \end{pmatrix} \begin{pmatrix} e_{i-1} \\ v_{i-1} \\ a_{i-1} \\ u_{i-1} \end{pmatrix}, \quad i \in S_m \quad (2.11)$$

or, in short,

$$\dot{x}_i = A_0 x_i + A_1 x_{i-1}, \quad i \in S_m \tag{2.12}$$

with state vector $x_i^{\mathrm{T}} = \begin{pmatrix} e_i & v_i & a_i & u_i \end{pmatrix}$, and the matrices A_0 and A_1 defined accordingly. Note that (2.11) is not similar to (2.10), since the former encompasses two controlled vehicles i and $i-1$, with external input u_{i-1} as a result, whereas the latter describes a controlled vehicle i, using the state of the vehicle $i-1$ as external "input".

Based on the vehicle model (2.4) and the input dynamics (2.7), the virtual reference vehicle $i = 0$ may be formulated as

$$\begin{pmatrix} \dot{e}_0 \\ \dot{v}_0 \\ \dot{a}_0 \\ \dot{u}_0 \end{pmatrix} = \begin{pmatrix} 0 & 0 & 0 & 0 \\ 0 & 0 & 1 & 0 \\ 0 & 0 & -\frac{1}{\tau} & \frac{1}{\tau} \\ 0 & 0 & 0 & -\frac{1}{h} \end{pmatrix} \begin{pmatrix} e_0 \\ v_0 \\ a_0 \\ u_0 \end{pmatrix} + \begin{pmatrix} 0 \\ 0 \\ 0 \\ \frac{1}{h} \end{pmatrix} q_0 \tag{2.13}$$

or, in short,

$$\dot{x}_0 = A_{\mathrm{r}} x_0 + B_{\mathrm{r}} u_{\mathrm{r}} \tag{2.14}$$

with state vector $x_0^{\mathrm{T}} = \begin{pmatrix} e_0 & v_0 & a_0 & u_0 \end{pmatrix}$, input $u_{\mathrm{r}} = q_0$, being the external input to the platoon, and the matrices A_{r} and B_{r} defined accordingly. Here, the state variables are chosen in accordance with the real vehicles in the platoon. Consequently, (2.13) represents a nonminimal realization, in which e_0 (where $e_0(t) = e_0(0)$) is a dummy state variable, having no further influence since the first column of both A_{r} and A_1 are equal to the zero column. In the remainder of this chapter, $e_0(0) = 0$ is chosen. The equilibrium state of (2.13) is then equal to $\bar{x}_0^{\mathrm{T}} = \begin{pmatrix} 0 & \bar{v}_0 & 0 & 0 \end{pmatrix}$ for $u_{\mathrm{r}} = 0$, where $\bar{v}_0$ is a constant velocity. Note that this equilibrium is only marginally stable since the virtual reference vehicle is in fact an uncontrolled vehicle model. In Kim et al. (2012), the same virtual reference vehicle concept is applied, but using a velocity-controlled vehicle model as virtual reference vehicle instead. This is considered unnecessary in the scope of the current application, since the virtual reference vehicle does not involve uncertainties or unknown disturbances.

Returning to the homogeneous platoon model (2.11), it can be easily established that $x_i = \bar{x}_0$, with $i = 1, 2, \ldots, m$, is an equilibrium of the vehicle platoon for $x_0 = \bar{x}_0$ and $u_{\mathrm{r}} = 0$; in other words, the platoon equilibrium is characterized by a constant velocity $\bar{v}_0$ of all vehicles. This equilibrium is asymptotically stable under the same conditions as mentioned for the error dynamics (2.10), which can be easily understood by replacing the first state e_i in (2.11) by a newly defined state $z_i := -e_i - hv_i$. As a result, the system matrix A_0 transforms into the system matrix of the error dynamics (2.10).

2.4 String stability

Having derived a homogeneous platoon model, this section will first generalize this model to a nonlinear cascaded state-space system, after which a new string stability definition is proposed. It is then shown that this definition serves as

a rigorous basis for $\mathcal{L}_2$ and $\mathcal{L}_\infty$ string stability conditions commonly used in the performance-oriented approach for string stability (see Section 2.2), and the relation to the other string stability notions is briefly discussed.

2.4.1 $\mathcal{L}_p$ string stability

The homogeneous platoon model (2.12), (2.14) is a special, linear case of the following cascaded state-space system:

$$\dot{x}_0 = f_{\mathrm{r}}(x_0, u_{\mathrm{r}}) \tag{2.15a}$$

$$\dot{x}_i = f_i(x_i, x_{i-1}), \quad i \in S_m \tag{2.15b}$$

$$y_i = h(x_i), \qquad i \in S_m, \tag{2.15c}$$

representing a general, possibly nonlinear, heterogeneous interconnected system with the same interconnection structure as (2.12), (2.14). Here, $u_{\mathrm{r}} \in \mathbb{R}^q$ is the external input, $x_i \in \mathbb{R}^n$, $i \in S_m \cup \{0\}$, is the state vector, and $y_i \in \mathbb{R}^\ell$, $i \in S_m$, is the output. Moreover, $f_{\mathrm{r}} : \mathbb{R}^n \times \mathbb{R}^q \mapsto \mathbb{R}^n$, $f_i : \mathbb{R}^n \times \mathbb{R}^n \mapsto \mathbb{R}^n$, $i \in S_m$, and $h : \mathbb{R}^n \mapsto \mathbb{R}^\ell$. In the scope of vehicle platooning, the state is typically defined as $x_i^{\mathrm{T}} = \begin{pmatrix} e_i & v_i & a_i & \ldots \end{pmatrix}$, $i \in S_m \cup \{0\}$, indicating a possible extension with additional states, due to, e.g., controller dynamics or spacing policy dynamics, see Section 2.3. Note that the heterogeneity property usually refers to the uncontrolled interconnected systems having different dynamical properties. In very rare cases, the (decentralized) controllers are nonidentical (Khatir and Davison, 2004). Furthermore, although the majority of platooning applications is based on linear models, nonlinear models will arise due to, e.g., nonlinear spacing policies (Yanakiev and Kanellakopoulos, 1998). Using the model (2.15), the following string stability definition is now proposed.

Definition 2.1 ($\mathcal{L}_p$ string stability). *Consider the interconnected system* (2.15). *Let* $x^{\mathrm{T}} = \begin{pmatrix} x_0^{\mathrm{T}} & x_1^{\mathrm{T}} & \ldots & x_m^{\mathrm{T}} \end{pmatrix}$ *be the lumped state vector and let* $\bar{x}^{\mathrm{T}} = \begin{pmatrix} \bar{x}_0^{\mathrm{T}} & \ldots & \bar{x}_0^{\mathrm{T}} \end{pmatrix}$ *denote a constant equilibrium solution of* (2.15) *for* $u_{\mathrm{r}} \equiv 0$. *The system* (2.15) *is* $\mathcal{L}_p$ *string stable if there exist class* $\mathcal{K}$ *functions*[3] α *and* β, *such that, for any initial state* $x(0) \in \mathbb{R}^{(m+1)n}$ *and any* $u_{\mathrm{r}} \in \mathcal{L}_p^q$,

$$\|y_i(t) - h(\bar{x}_0)\|_{\mathcal{L}_p} \leq \alpha(\|u_{\mathrm{r}}(t)\|_{\mathcal{L}_p}) + \beta(\|x(0) - \bar{x}\|), \quad \forall i \in S_m \text{ and } \forall m \in \mathbb{N}.$$

If, in addition, with $x(0) = \bar{x}$ *it also holds that*

$$\|y_i(t) - h(\bar{x}_0)\|_{\mathcal{L}_p} \leq \|y_{i-1}(t) - h(\bar{x}_0)\|_{\mathcal{L}_p}, \quad \forall i \in S_m \backslash\{1\} \text{ and } \forall m \in \mathbb{N} \backslash\{1\},$$

the system (2.15) *is* strictly $\mathcal{L}_p$ *string stable with respect to its input* $u_{\mathrm{r}}(t)$.

Here, $\| \cdot \|$ denotes any vector norm, $\| \cdot \|_{\mathcal{L}_p}$ denotes the signal p-norm (Desoer and Vidyasagar, 2009), and $\mathcal{L}_p^q$ is the q-dimensional space of vector signals that are bounded in the $\mathcal{L}_p$ sense.

---

[3]A continuous function $\alpha : \mathbb{R}_{\geq 0} \mapsto \mathbb{R}_{\geq 0}$ is said to belong to class $\mathcal{K}$ if it is strictly increasing and $\alpha(0) = 0$.

Remark 2.1. The interconnected system formulation (2.15) could be further generalized with respect to the interconnection structure (or "topology"), so as to include multiple-vehicle look-ahead, or even bidirectional interconnections. This has no principal consequences for Definition 2.1 since output responses are considered due to external inputs or initial condition perturbations. ◆

Clearly, Definition 2.1 takes the external disturbance $u_{\rm r}$ into account, imposed by the virtual reference vehicle, through the class $\mathcal{K}$ function $\alpha(\|u_{\rm r}(t)\|_{\mathcal{L}_p})$, as well as initial condition perturbations through the class $\mathcal{K}$ function $\beta(\|x(0) - \bar{x}\|)$. It should be mentioned, that, as a consequence of the latter, only initial condition perturbations are considered for which the norm $\|x(0) - \bar{x}\|$ exists, which limits the allowable class of perturbations in view of the fact that x will be infinite-dimensional for $m \to \infty$. Studies of string stability specifically focussing on initial condition perturbations can be found in, e.g., Yadlapalli et al. (2006) and Klinge and Middleton (2009a). Furthermore, Definition 2.1 obviously applies to both linear and nonlinear systems, and includes homogeneous as well as heterogeneous strings, providing a rigorous basis for the string stability analysis of heterogeneous strings pursued in Liang and Peng (2000) and Shaw and Hedrick (2007b).

It is important to note that Definition 2.1 closely resembles the common input–output or $\mathcal{L}_p$ stability definition (Khalil, 2000) as far as (nonstrict) $\mathcal{L}_p$ string stability is concerned, except for the fact that the norm requirements must hold *for all string lengths* $m \in \mathbb{N}$. Consequently, if an interconnected system is $\mathcal{L}_p$ string stable, it is also $\mathcal{L}_p$ stable. The reverse statement, however, does not hold since $\mathcal{L}_p$ stability of a string with a given finite length m does not imply $\mathcal{L}_p$ stability for all $m \in \mathbb{N}$, i.e., $\mathcal{L}_p$ string stability. The latter is essential to string stability, indicating that a string-stable system is *scalable* in terms of the number of subsystems (Yadlapalli et al., 2006).

The notion of *strict* $\mathcal{L}_p$ string stability, for which not only the first inequality but also the second inequality in Definition 2.1 must hold, dictates that the $\mathcal{L}_p$ norm of the outputs of the interconnected systems must be nonincreasing along the string, in the direction of increasing system index. As such, it is a stronger requirement than $\mathcal{L}_p$ string stability *per se*, which only requires the outputs to be bounded in response to a bounded input and a bounded initial condition perturbation. This notion has been introduced to accommodate the requirement of upstream disturbance attenuation as mentioned before. The definition of strict string stability differs from the one introduced in Bose and Ioannou (2003a), in that the latter explicitly excludes the possibility that $\|y_i(t) - h(\bar{x}_0)\|_{\mathcal{L}_p} = \|y_{i-1}(t) - h(\bar{x}_0)\|_{\mathcal{L}_p}$. Section 2.5, however, shows that in case of platooning, the equality is the best possible result. This is due to the vehicle following objective, which implies that with a constant velocity v_0 of the virtual reference vehicle, all velocities should asymptotically converge to v_0. Note that the system (2.15a), which may be referred to as the virtual reference system, does not have an output associated with it, since a "virtual output" is considered practically irrelevant. Therefore, $i = 1$ has been excluded in the norm requirement for strict string stability.

The proposed string stability definition provides a rigorous basis for the often-used frequency-domain string stability conditions for linear interconnected systems, as shown hereafter.

2.4.2   String stability conditions for linear systems

In order to derive string stability conditions for linear systems, (2.15) is assumed to describe a linear homogeneous system, i.e., f_i is a linear function of the states and considered to be independent of the vehicle index i. Consequently, (2.15) can be reformulated into a linear state-space model, which, in lumped form, is denoted by

$$\begin{pmatrix} \dot{x}_0 \\ \dot{x}_1 \\ \vdots \\ \dot{x}_m \end{pmatrix} = \begin{pmatrix} A_{\mathrm{r}} & & & \mathrm{O} \\ A_1 & A_0 & & \\ & \ddots & \ddots & \\ \mathrm{O} & & A_1 & A_0 \end{pmatrix} \begin{pmatrix} x_0 \\ x_1 \\ \vdots \\ x_m \end{pmatrix} + \begin{pmatrix} B_{\mathrm{r}} \\ 0 \\ \vdots \\ 0 \end{pmatrix} u_{\mathrm{r}} \qquad (2.16)$$

or, in short,

$$\dot{x} = Ax + Bu_{\mathrm{r}} \qquad (2.17)$$

with $x^{\mathrm{T}} = \begin{pmatrix} x_0^{\mathrm{T}} & x_1^{\mathrm{T}} & \dots & x_m^{\mathrm{T}} \end{pmatrix}$, and the matrices A and B defined accordingly. The matrices A_0, A_1, A_{r}, and B_{r} can, e.g., be chosen identical to those used in (2.12) and (2.14). In addition, consider linear output functions according to

$$y_i = Cx_i = C_i x, \quad i \in S_m \qquad (2.18)$$

with output matrix C and $C_i = \begin{pmatrix} 0_{\ell \times n(i-1)} & C & 0_{\ell \times n(m-i)} \end{pmatrix}$. Also, the equilibrium state $\bar{x}^{\mathrm{T}} = \begin{pmatrix} \bar{x}_0^{\mathrm{T}} & \dots & \bar{x}_0^{\mathrm{T}} \end{pmatrix} = 0$ is chosen, hence $h(\bar{x}_0) = C_i \bar{x} = 0 \ \forall i \in S_m$. This choice is without loss of generality because there is always a coordinate transformation possible such that $\bar{x} = 0$. The model (2.17), (2.18) can then be formulated in the Laplace domain as follows:

$$y_i(s) = P_i(s)u_{\mathrm{r}}(s) + O_i(s)x(0), \quad i \in S_m \qquad (2.19)$$

with outputs $y_i(t) \in \mathbb{R}^{\ell}$ and exogenous input $u_{\mathrm{r}}(t) \in \mathbb{R}^{\ell}$, whose Laplace transforms are denoted by $y_i(s)$ and $u_{\mathrm{r}}(s)$, with $s \in \mathbb{C}$, respectively. Note that, with a slight abuse of mathematical notation, $\cdot(s)$ denotes the Laplace transform of the corresponding time-domain variable $\cdot(t)$ throughout this chapter; if the argument is omitted, then the domain is either irrelevant or can be easily determined from the context. $x(0) \in \mathbb{R}^{(m+1)n}$ denotes the initial (time-domain) condition. $P_i(s)$ and $O_i(s)$, $i \in S_m$, are the complementary sensitivity transfer function and the initial condition transfer function, respectively, according to

$$\begin{aligned} P_i(s) &= C_i(sI - A)^{-1}B \\ O_i(s) &= C_i(sI - A)^{-1}. \end{aligned} \qquad (2.20)$$

$P_i(s)$ is thus assumed to be square, i.e., $\dim(u_{\mathrm{r}}) = \dim(y_i) = \ell$; this property is adopted in view of the upcoming analysis.

Since (2.16) describes a controlled system, the matrix A_0 is typically Hurwitz. However, this may not be the case for the matrix A_{r}, related to the virtual reference vehicle in case of vehicle following. As indicated by (2.13), for instance, A_{r} has a marginally stable mode associated with v_0 (besides the mode associated with the dummy state e_0). Hence, the system matrix A in (2.17) is not

Hurwitz in case of the vehicle following control problem. In the remainder of this section, however, it is assumed that the pair (C_i, A) is such that unstable (including marginally stable) modes are unobservable by a specific choice of C_i. Consequently, it suffices to only analyze the output response to the external input in view of string stability (or, equivalently, to choose $x(0) = \bar{x} = 0$), in accordance with the following remark.

Remark 2.2. If (2.15a), (2.15b) represents a linear system, the existence of α implies that β exists, provided that unstable and marginally stable modes are unobservable. This can be shown as follows. Consider the system (2.15a), (2.15b) for a fixed but otherwise arbitrary index $i = k$. Then this system is $\mathcal{L}_p$ *stable* if

$$\|y_k(t) - h(\bar{x}_0)\|_{\mathcal{L}_p} \leq \alpha_k(\|u_{\mathrm{r}}(t)\|_{\mathcal{L}_p}) + \beta_k(\|x(0) - \bar{x}\|)$$

with class $\mathcal{K}$ functions α_k and β_k (Khalil, 2000). If (2.15a), (2.15b) represents a linear system, with possible unstable or marginally stable modes being unobservable, the existence of α_k implies that β_k exists (Hespanha, 2009). Because this statement holds for any $k \in S_m$, it also applies to α and β in Definition 2.1. ◆

In order to arrive at conditions for $\mathcal{L}_2$ string stability, the $\mathcal{H}_\infty$ norm is introduced first, being defined as

$$\|P_i(s)\|_{\mathcal{H}_\infty} := \sup_{\mathrm{Re}(s)>0} \bar{\sigma}(P_i(s)). \tag{2.21}$$

Here, $\bar{\sigma}(\cdot)$ denotes the maximum singular value, which, according to the maximum modulus theorem (Zhou et al., 1996), can also be computed by evaluation of $\bar{\sigma}(P_i(s))$ along the imaginary axis, i.e., $\sup_{\mathrm{Re}(s)>0} \bar{\sigma}(P_i(s)) = \sup_{\omega \in \mathbb{R}} \bar{\sigma}(P_i(j\omega))$, provided that $P_i(s)$ represents a causal and stable system. It can then be shown (Zhou et al., 1996, p. 101) that $\|P_i(s)\|_{\mathcal{H}_\infty}$ is equal to the $\mathcal{L}_2$ induced system norm related to the input $u_{\mathrm{r}}(t)$ and the output $y_i(t)$:

$$\|P_i(s)\|_{\mathcal{H}_\infty} = \sup_{u_{\mathrm{r}} \neq 0} \frac{\|y_i(t)\|_{\mathcal{L}_2}}{\|u_{\mathrm{r}}(t)\|_{\mathcal{L}_2}}, \tag{2.22}$$

where the $\mathcal{L}_2$ norm is defined on the interval $t \in [0, \infty)$. Consequently, from (2.19) it follows that, with $x(0) = 0$,

$$\begin{aligned} \|y_i(t)\|_{\mathcal{L}_2} &\leq \|P_i(s)\|_{\mathcal{H}_\infty} \|u_{\mathrm{r}}(t)\|_{\mathcal{L}_2} \\ &\leq \max_{i \in S_m} \|P_i(s)\|_{\mathcal{H}_\infty} \|u_{\mathrm{r}}(t)\|_{\mathcal{L}_2}, \quad \forall i \in S_m. \end{aligned} \tag{2.23}$$

It is important to note that, due to (2.22), (2.23) is not conservative, in the sense that there is always a subsystem $i \in S_m$ and a specific signal $u_{\mathrm{r}}(t)$ for which the right-hand sides in (2.23) are equal and become arbitrarily close to $\|y_i(t)\|_{\mathcal{L}_2}$. Therefore, according to Definition 2.1 and under the assumptions as mentioned in Remark 2.2, the existence of $\max_{i \in S_m} \|P_i(s)\|_{\mathcal{H}_\infty}$, for all $m \in \mathbb{N}$, is a necessary and sufficient condition for $\mathcal{L}_2$ string stability of the interconnected system (2.17), (2.18). For further analysis, a specific type of interconnection topology will be adopted, as mentioned in the following remark.

Remark 2.3. In the case of a look-ahead topology, such as described by (2.16), the interconnection is unidirectional, from which it directly follows that the dynamics of the first $n < m$ systems in a string of length m do not depend on the systems $n+1, n+2, \ldots, m$. Consequently, if an infinite-length unidirectionally-interconnected string of cascaded systems has a bounded output response to a bounded input, then all finite-length strings as a subset thereof have a bounded output response as well. Therefore, in order to assess string stability, not all values for the string length $m \in \mathbb{N}$ need to be evaluated, but only the case where $m \to \infty$. This implies that the sets S_m, $m \in \mathbb{N}$, can be reduced to a single set $\mathbb{N}$.   ♦

As a result, the interconnected system (2.17), (2.18) is $\mathcal{L}_2$ string stable if and only if $\sup_{i \in \mathbb{N}} \|P_i(s)\|_{\mathcal{H}_\infty}$ exists (under the assumptions as mentioned in Remark 2.2). The class $\mathcal{K}$ function α in Definition 2.1 can then be chosen as

$$\alpha(\|u_{\mathrm{r}}(t)\|_{\mathcal{L}_2}) = \sup_{i \in \mathbb{N}} \|P_i(s)\|_{\mathcal{H}_\infty} \|u_{\mathrm{r}}(t)\|_{\mathcal{L}_2}. \tag{2.24}$$

Because of the linear form of α in (2.24), this type of string stability may be referred to as finite-gain $\mathcal{L}_2$ string stability, similar to the notion of finite-gain $\mathcal{L}_2$ stability (Khalil, 2000).

The existence of the supremum of the $\mathcal{L}_2$ gain can be further analyzed by factorization, leading to the theorem below. As a preliminary to this theorem, the *string stability complementary sensitivity* is introduced first. From (2.19), it directly follows that, with $x(0) = 0$,

$$y_i(s) = \Gamma_i(s) y_{i-1}(s) \tag{2.25}$$

with the string stability complementary sensitivity

$$\Gamma_i(s) := P_i(s) P_{i-1}^{-1}(s), \tag{2.26}$$

assuming that $P_i(s)$ is nonsingular[4] for all i, thus guaranteeing the existence of $P_{i-1}^{-1}(s)$ in (2.26). The following theorem, formulating conditions for (strict) $\mathcal{L}_2$ string stability, can now be stated.

Theorem 2.1. *Let* (2.17), (2.18) *represent a linear unidirectionally-interconnected system of which the input–output behavior is described by* (2.19), (2.20). *Assume that the pair* (C_i, A) *is such that unstable and marginally modes are unobservable and that* $P_i(s)$ *is square and nonsingular for all* $i \in \mathbb{N}$. *Then the system* (2.17), (2.18) *is* $\mathcal{L}_2$ *string stable if*

1. $\|P_1(s)\|_{\mathcal{H}_\infty} < \infty$ *and*

2. $\|\Gamma_i(s)\|_{\mathcal{H}_\infty} \leq 1$, $\quad \forall i \in \mathbb{N} \backslash \{1\}$

with $\Gamma_i(s)$ *as in* (2.26). *Moreover, the system is strictly* $\mathcal{L}_2$ *string stable if and only if conditions* 1 *and* 2 *hold.*

---

[4]A transfer function matrix $P(s)$ is nonsingular if it is invertible for almost all s.

Proof. Using (2.19), (2.25), and (2.26), the input–output relation for a specific subsystem $i \geq 2$ can be formulated as

$$y_i(s) = P_i(s)u_{\mathrm{r}}(s)$$
$$= \left(\prod_{k=2}^{i} \Gamma_k(s) \right) P_1(s)u_{\mathrm{r}}(s), \quad i \in \mathbb{N}\backslash\{1\}.$$

Having factorized $P_i(s)$ in this way, the submultiplicative property dictates that $\|P_i(s)\|_{\mathcal{H}_\infty}$ is subject to the following inequality:

$$\|P_i(s)\|_{\mathcal{H}_\infty} \leq \left(\prod_{k=2}^{i} \|\Gamma_k(s)\|_{\mathcal{H}_\infty} \right) \|P_1(s)\|_{\mathcal{H}_\infty}, \quad i \in \mathbb{N}\backslash\{1\}.$$

Consequently, under the conditions 1 and 2 in Theorem 2.1, $\sup_{i\in\mathbb{N}} \|P_i(s)\|_{\mathcal{H}_\infty}$ exists. Because it is also assumed that the pair (C_i, A) is such that unstable and marginally stable modes are unobservable for all $i \in \mathbb{N}$, it thus follows that the linear system is $\mathcal{L}_2$ string stable, according to Definition 2.1 and Remark 2.2, while using (2.24). Moreover, from (2.25) and condition 2, it follows that

$$\|y_i(t)\|_{\mathcal{L}_2} \leq \|\Gamma_i(s)\|_{\mathcal{H}_\infty} \|y_{i-1}(t)\|_{\mathcal{L}_2}$$
$$\leq \|y_{i-1}(t)\|_{\mathcal{L}_2}, \quad \forall\, i \in \mathbb{N}\backslash\{1\},$$

which yields the interconnected system strictly $\mathcal{L}_2$ string stable. Note that $i = 1$ must be excluded here because y_0, which would be the output of the virtual reference system, has not been defined.

Let us now show the necessity of condition 1 and 2 for strict $\mathcal{L}_2$ string stability. Clearly, condition 1 is necessary for both $\mathcal{L}_2$ string stability and strict $\mathcal{L}_2$ string stability. Moreover, if condition 2 is not satisfied, then there exists an $i \in \mathbb{N}\backslash\{1\}$ such that $\|\Gamma_i(s)\|_{\mathcal{H}_\infty} > 1$ yielding $\|y_i(t)\|_{\mathcal{L}_2} > \|y_{i-1}(t)\|_{\mathcal{L}_2}$, which contradicts the strict string stability requirement in Definition 2.1. Therefore, condition 2 is also a necessary condition for strict $\mathcal{L}_2$ string stability. ∎

It is important to note that condition 2 in fact very closely resembles the well-known string stability criterion (2.1). As such, Definition 2.1 together with Theorem 2.1 provide a rigorous basis for this criterion. The fact that Theorem 2.1 only yields sufficient conditions for $\mathcal{L}_2$ string stability is basically due to the submultiplicative property. In specific cases, however, the submultiplicative property becomes an equality, upon which the $\mathcal{L}_2$ string stability conditions become not only sufficient but also necessary. The following corollary deals with such a specific case, which nevertheless appears to be practically relevant, as described in Section 2.5 and 2.7.

Corollary 2.2. *Let* (2.17), (2.18) *represent a linear unidirectionally-interconnected system, with* $u_{\mathrm{r}} \in \mathbb{R}$ *and* $y_i \in \mathbb{R}$ $\forall\, i \in \mathbb{N}$, *for which the input–output behavior is described by* (2.19), (2.20). *Assume that the pair* (C_i, A) *is such that unstable and marginally stable modes are unobservable and that* $P_i(s)$ *is nonsingular for all* $i \in \mathbb{N}$. *Furthermore, let the string stability complementary sensitivity*

$\Gamma(s) = P_i(s)P_{i-1}^{-1}(s)$, $i \in \mathbb{N}\setminus\{1\}$, be independent of the vehicle index i. Then the system (2.17), (2.18) is $\mathcal{L}_2$ string stable if and only if

1. $\|P_1(s)\|_{\mathcal{H}_\infty} < \infty$ and

2. $\|\Gamma(s)\|_{\mathcal{H}_\infty} \leq 1$.

Moreover, $\mathcal{L}_2$ string stability and strict $\mathcal{L}_2$ string stability are equivalent notions in this case.

Proof. Referring to the factorization of $P_i(s)$ used in the proof of Theorem 2.1, the following equalities hold for systems with scalar input and output:

$$\begin{aligned} \|P_i(s)\|_{\mathcal{H}_\infty} &= \sup_\omega |P_i(j\omega)| \\ &= \sup_\omega \left|\Gamma(j\omega)^{i-1} P_1(j\omega)\right| \\ &= \sup_\omega \left\{ |\Gamma(j\omega)|^{i-1} |P_1(j\omega)| \right\}, \quad i \in \mathbb{N}, \end{aligned}$$

using the fact that the $\mathcal{H}_\infty$ norm can be computed by evaluation along the imaginary axis $s = j\omega$, as mentioned earlier. Hence, $\|P_i(s)\|_{\mathcal{H}_\infty}$ exists for all $i \in \mathbb{N}$, and especially for $i \to \infty$, if and only if $|P_1(j\omega)| < \infty$ and $|\Gamma(j\omega)| \leq 1$ for all $\omega \in \mathbb{R}$, rendering the interconnected system $\mathcal{L}_2$ string stable. Since $|\Gamma(j\omega)| \leq 1$, the system is also strictly $\mathcal{L}_2$ string stable.   ∎

From Corollary 2.2, it follows that for linear unidirectionally-interconnected systems with scalar input and output, $\mathcal{L}_2$ string stability and strict $\mathcal{L}_2$ string stability are equivalent in case of homogeneous strings, rendering the notion of (nonstrict) $\mathcal{L}_2$ string stability only relevant for heterogeneous strings of this type.

Until now, only $\mathcal{L}_2$ string stability has been considered. Physically, this can be motivated by the requirement of energy dissipation along the string. Alternatively, it is also possible to use the induced $\mathcal{L}_\infty$ norm instead, which then leads to $\mathcal{L}_\infty$ string stability. In the scope of vehicle following, the motivation for using this norm would be traffic safety, since the $\mathcal{L}_\infty$ norm is directly related to maximum overshoot. As will be shown below, the analysis of $\mathcal{L}_\infty$ string stability is similar to that of $\mathcal{L}_2$ string stability.

Let $p_i(t)$ denote the impulse response matrix, corresponding to the transfer function $P_i(s)$. Then, the $\mathcal{L}_1$ signal norm $\|p_i(t)\|_{\mathcal{L}_1}$ is induced by the $\mathcal{L}_\infty$ signal norms of input and output (Desoer and Vidyasagar, 2009), i.e.,

$$\|p_i(t)\|_{\mathcal{L}_1} = \sup_{u_\mathrm{r} \neq 0} \frac{\|y_i(t)\|_{\mathcal{L}_\infty}}{\|u_\mathrm{r}(t)\|_{\mathcal{L}_\infty}}. \tag{2.27}$$

Consequently, the unidirectionally interconnected system is $\mathcal{L}_\infty$ string stable if and only if $\sup_{i \in \mathbb{N}} \|p_i(t)\|_{\mathcal{L}_1}$ exists. The class $\mathcal{K}$ function α in Definition 2.1 can then be chosen as

$$\alpha(\|u_\mathrm{r}(t)\|_{\mathcal{L}_\infty}) = \left(\sup_{i \in \mathbb{N}} \|p_i(t)\|_{\mathcal{L}_1} \right) \|u_\mathrm{r}(t)\|_{\mathcal{L}_\infty}. \tag{2.28}$$

This leads to the following theorem, formulating conditions for (strict) $\mathcal{L}_\infty$ string stability.

Theorem 2.3. *Let* (2.17), (2.18) *represent a linear unidirectionally-interconnected system for which the input–output behavior is described by* (2.19), (2.20). *Assume that the pair* (C_i, A) *is such that unstable and marginally stable modes are unobservable and that* $P_i(s)$ *is square and nonsingular for all* $i \in \mathbb{N}$. *Then the system* (2.17), (2.18) *is* $\mathcal{L}_\infty$ *string stable if*

1. $\|p_1(t)\|_{\mathcal{L}_1} < \infty$ *and*

2. $\|\gamma_i(t)\|_{\mathcal{L}_1} \leq 1, \quad \forall \, i \in \mathbb{N} \backslash \{1\}$,

where $p_1(t)$ *and* $\gamma_i(t)$ *are the impulse response functions corresponding to* $P_1(s)$ *and* $\Gamma_i(s)$, *respectively, with* $\Gamma_i(s)$ *as in* (2.26). *Moreover, the system is strictly* $\mathcal{L}_\infty$ *string stable if and only if conditions* 1 *and* 2 *hold.*

Proof. Expressing the factorization of $P_i(s)$, $i \geq 2$, used in the proof of Theorem 2.1, in the time domain results in

$$
\begin{aligned}
y_i(t) &= (p_i * u_{\mathrm{r}})(t) \\
&= (\gamma_i * \gamma_{i-1} * \ldots * \gamma_2 * p_1 * u_{\mathrm{r}})(t), \quad i \in \mathbb{N} \backslash \{1\},
\end{aligned}
$$

where $*$ denotes the convolution operator. Applying Young's inequality for convolutions, the following inequality is obtained:

$$
\|p_i(t)\|_{\mathcal{L}_1} \leq \left(\prod_{k=2}^{i} \|\gamma_k(t)\|_{\mathcal{L}_1} \right) \|p_1(t)\|_{\mathcal{L}_1}, \quad i \in \mathbb{N} \backslash \{1\},
$$

from which it follows that $\sup_{i \in \mathbb{N}} \|p_i(t)\|_{\mathcal{L}_1}$ exists, under the conditions 1 and 2 in Theorem 2.3. Since it is also assumed that the pair (C_i, A) is such that unstable and marginally stable modes are unobservable for all $i \in \mathbb{N}$, it thus follows that the linear system is $\mathcal{L}_\infty$ string stable, according to Definition 2.1 and Remark 2.2, while using (2.28). Moreover, using the $\mathcal{L}_\infty$ gain definition of the system with impulse response $\gamma_i(t)$ and condition 2 yields

$$
\begin{aligned}
\|y_i(t)\|_{\mathcal{L}_\infty} &\leq \|\gamma_i(t)\|_{\mathcal{L}_1} \|y_{i-1}(t)\|_{\mathcal{L}_\infty} \\
&\leq \|y_{i-1}(t)\|_{\mathcal{L}_\infty}, \quad \forall \, i \in \mathbb{N} \backslash \{1\},
\end{aligned}
$$

implying that the interconnected system is strictly $\mathcal{L}_\infty$ string stable.

The necessity of the conditions 1 and 2 for strict $\mathcal{L}_\infty$ string stability can be proven with the same type of reasoning as used in the proof of Theorem 2.1. ∎

Again, Theorem 2.3 only provides sufficient conditions for $\mathcal{L}_\infty$ string stability. In this case, however, the additional assumption that u_{r} and y_i are scalar, similar to the assumption used in Corollary 2.2, does not lead to necessary and sufficient conditions for $\mathcal{L}_\infty$ string stability. Since the induced $\mathcal{L}_2$ norm is used far more often, in practice, than the induced $\mathcal{L}_\infty$ norm, no further attention will be paid to this issue in the scope of this chapter.

Note that a general treatment of the relation between $\|\gamma(t)\|_{\mathcal{L}_1}$ and $\|\Gamma(s)\|_{\mathcal{H}_\infty}$ is given in Desoer and Vidyasagar (2009). Using a Lyapunov-stability approach

for linear systems, Swaroop (2002) discusses the relation between $\mathcal{L}_\infty$ and $\mathcal{L}_2$ string stability, the main results of which can be extended to the new framework by defining the output y_i to contain all states x_i (subject to the remark in the next subsection), while focussing on initial condition perturbations $x(0) \neq 0$.

2.4.3   Discussion

From the previous section, it is clear that the performance-oriented approach to string stability (see, e.g., Sheikholeslam and Desoer (1993), Rajamani and Zhu (2002), and Naus et al. (2010)) is captured by Definition 2.1 as a special case for linear unidirectionally interconnected systems. In addition, the Lyapunov-stability approach (see, e.g., Swaroop and Hedrick (1996) and Wang et al. (2006)) is captured as well by the inclusion of initial condition perturbations in Definition 2.1. An apparent difference, however, is that the Lyapunov-stability approach focusses on the system states, whereas Definition 2.1 regards the system outputs. Nevertheless, there is no essential limitation in choosing the output so as to include all states, albeit that the string stability complementary sensitivity can no longer be computed using (2.26). As a result, it follows that Definition 2.1 encompasses and extends the aforementioned approaches to string stability.

   In the framework of spatially invariant linear systems, which focusses on infinite-length interconnected systems (see, e.g., Curtain et al. (2009) and Barbieri (1993)), string stability requires the norm of the states to (exponentially or, at least, asymptotically) decay both over time and system index as a result of initial condition perturbations. As such, it can be argued that such behavior corresponds to strict string stability as in Definition 2.1, although further research is required to establish the exact relation.

2.5   String stability of vehicle platoons

The string stability conditions derived in the previous section will now be applied to the platoon model presented in Section 2.3.3. Focussing on $\mathcal{L}_2$ string stability first, the outputs y_i for the platoon model (2.11), (2.13) need to be chosen such that Theorem 2.1 (or Corollary 2.2) can be applied. To this end, it is helpful to first formulate the closed-loop model of a platoon vehicle in the frequency domain. Therefore, the vehicle transfer function $G(s) = q_i(s)/u_i(s)$ is introduced, according to:

$$G(s) = \frac{1}{s^2(\tau s + 1)} \tag{2.29}$$

which follows from $\ddot{q}_i = a_i$ and $\dot{a}_i = -\frac{1}{\tau}a_i + \frac{1}{\tau}u_i$, see (2.4). Furthermore, let us introduce the *spacing policy transfer function* $H(s) = \xi_i(s)/u_i(s)$, derived from (2.7):

$$H(s) = hs + 1 \tag{2.30}$$

and the feedback law $K(s)$ with input $e_i(s)$, defined in (2.8):

$$K(s) = k_{\mathrm{p}} + k_{\mathrm{d}}s + k_{\mathrm{dd}}s^2. \tag{2.31}$$
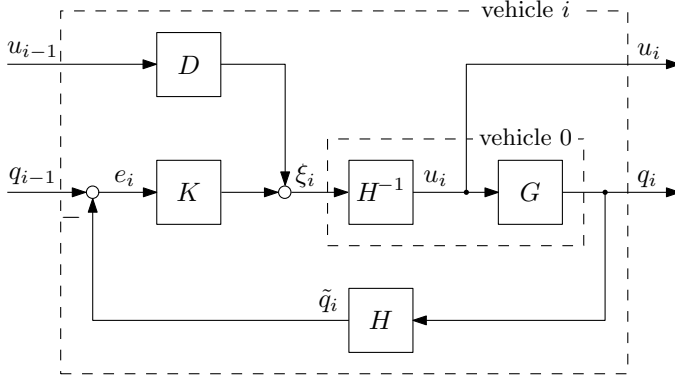
Figure 2.2: Block scheme of a controlled platoon vehicle $i \geq 1$ and of the virtual reference vehicle, indicated by the index 0.

The controlled vehicle, with index i, can then be represented by the block scheme as shown in Figure 2.2. Here, the occurrence of the spacing policy transfer function $H(s)$ in the feedback loop can be readily explained. Transforming the distance error $e_i(t)$ as formulated in (2.3), while using (2.30), yields

$$
\begin{aligned}
e_i(s) &= q_{i-1}(s) - q_i(s) - hsq_i(s) \\
&= q_{i-1}(s) - H(s)q_i(s), \quad i \in \mathbb{N},
\end{aligned}
\tag{2.32}
$$

in which $r_i = L_i = 0 \; \forall \; i$ is chosen without loss of generality, since these parameters can always be removed by a coordinate transformation. Consequently, $\tilde{q}_i(s) = H(s)q_i(s)$, as depicted in the block scheme, can be interpreted as the "virtual control point" of vehicle i, that must be as close as possible to the actual position $q_{i-1}(s)$ of the preceding vehicle $i-1$. Furthermore, since the frequency-domain approach allows for the inclusion of the latency θ induced by the wireless communication network due to queueing, contention, transmission, and propagation, the block scheme also includes a time delay $D(s) = e^{-\theta s}$.

The virtual reference vehicle model in the frequency domain is equal to that of the other vehicles, but without the feedback and the input feedforward, leaving the open-loop series connection of $H^{-1}(s)$ and $G(s)$, indicated in Figure 2.2 by the box named "vehicle 0", with $u_r(t) = \xi_0(t)$ as external input. Consequently, the vehicle platoon system has a scalar input u_r, upon which a scalar output needs to be selected according to Theorem 2.1. To this end, the vehicle acceleration is selected as output, i.e., $y_i = a_i$, since the acceleration is physically relevant on the one hand, and guarantees the existence of $\|P_1(s)\|_{\mathcal{H}_\infty}$ on the other, as will be shown later in this section. Moreover, it can be shown that with this output, the marginally stable mode associated with the reference vehicle is not observable, such that the corresponding requirement in Corollary 2.2 is met.

Given the chosen output, the string stability complementary sensitivity is thus equal to $\Gamma_i(s) = a_i(s)/a_{i-1}(s)$. Using the block scheme in Figure 2.2, $\Gamma_i(s) = \Gamma(s)$

(independent of i) can be shown to satisfy

$$\Gamma(s) = \frac{1}{H(s)} \frac{G(s)K(s) + D(s)}{1 + G(s)K(s)}. \tag{2.33}$$

Note that, since $\Gamma(s) = \frac{a_i(s)}{a_{i-1}(s)} = \frac{sv_i(s)}{sv_{i-1}(s)} = \frac{v_i(s}{v_{i-1}(s)}$, (2.33) also holds if the vehicle velocity v_i would have been chosen as output. Also when taking the distance error e_i as output, $\Gamma(s)$ still satisfies (2.33). This is a direct consequence of the homogeneity of the vehicle platoon.

Due to the specific choice for the virtual reference vehicle model, $\Gamma(s)$ is also equal to the transfer function from $a_0(s)$ to $a_1(s)$. It therefore follows that, using (2.13),

$$a_1(s) = \Gamma(s)a_0(s)$$
$$= \frac{\Gamma(s)}{H(s)} \frac{1}{\tau s + 1} u_r(s). \tag{2.34}$$

Hence,

$$P_1(s) = \frac{\Gamma(s)}{H(s)} \frac{1}{\tau s + 1} \tag{2.35}$$

from which it directly follows that $\|P_1(s)\|_{\mathcal{H}_\infty}$ exists if $\|\Gamma(s)\|_{\mathcal{H}_\infty}$ exists, due to the submultiplicative property of the $\mathcal{H}_\infty$ norm and the fact that $(H(s)(\tau s + 1))^{-1}$ is a stable transfer function (provided that $h \geq 0$). Furthermore, it follows from (2.33) that without delay ($D(s) = 1$), $\|\Gamma(s)\|_{\mathcal{H}_\infty}$ exists, since in that case $\|\Gamma(s)\|_{\mathcal{H}_\infty} = \sup_\omega |H^{-1}(j\omega)| = 1$. According to Theorem 2.1, the system without delay is thus strictly $\mathcal{L}_2$ string stable for any choice of controller gains and time gap.

Choosing e_i as output of interest would also have implied the existence of $\|P_1(s)\|_{\mathcal{H}_\infty}$ under the condition that $\|\Gamma(s)\|_{\mathcal{H}_\infty}$ exists, as can be shown when formulating $P_1(s)$ in this case. Choosing v_i as output, however, would introduce an open-loop integrator in $P_1(s)$, as a consequence of which $\|P_1(s)\|_{\mathcal{H}_\infty}$ would not exist. In addition, it can also be shown that, using the state-space realization (2.17), (2.18), the marginally stable mode associated with the virtual reference vehicle (2.13) is unobservable, except for the case where the velocity v_i is chosen as output. Although it may be surprising that the velocity cannot be chosen as output, this is merely a technical matter, originating in the definition of the virtual reference vehicle. Moreover, as mentioned after (2.33), $\Gamma(s)$ is independent of the output choice.

Note that, according to the vehicle-following objective, the states of all vehicles in the platoon will asymptotically converge to the equilibrium state $\bar{x}_0^T = \begin{pmatrix} 0 & \bar{v}_0 & 0 & 0 \end{pmatrix}$ if $u_r = 0$ and the virtual reference vehicle has a constant velocity $\bar{v}_0$; see Section 2.3.3. In other words, $\lim_{\omega \to 0} (v_i(j\omega) - v_{i-1}(j\omega)) = 0$. Hence,

$$\lim_{\omega \to 0} |\Gamma(j\omega)| = 1 \Rightarrow \|\Gamma(j\omega)\|_{\mathcal{H}_\infty} \geq 1, \tag{2.36}$$

which is why the strict $\mathcal{L}_p$ string stability definition allows for the fact that the $\mathcal{L}_p$ norm of the outputs neither increases, nor decreases in upstream direction. As
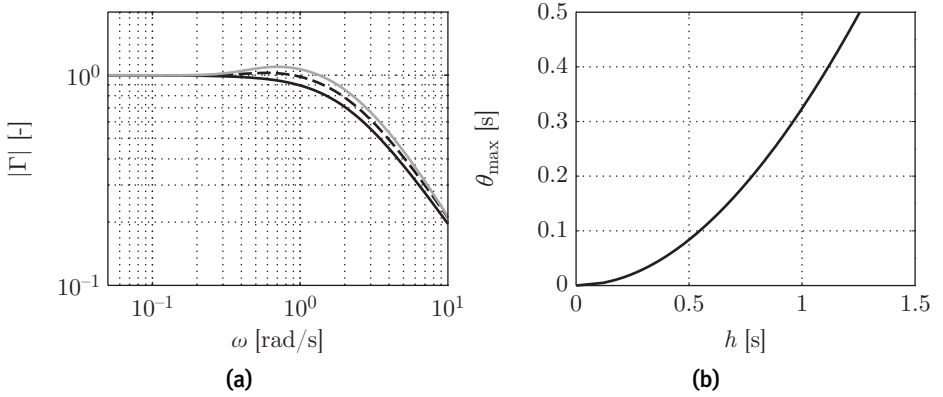
Figure 2.3: $\mathcal{L}_2$ string stability properties: (a) string stability complementary sensitivity magnitude $|\Gamma(j\omega)|$ for communication delay $\theta = 0\,s$ (solid black), $\theta = 0.15\,s$ (dashed black), $\theta = 0.3\,s$ (gray), and (b) maximum communication delay $\theta_{\max}$, as a function of the time gap h.

a consequence, however, string stability robustness with respect to, e.g., model uncertainties, may be poor in case these uncertainties cause $|\Gamma(j\omega)|$ to increase in the lower frequency region.

As already mentioned, wireless communications exhibit latency, which in general increases with increasing communication load. This time delay compromises string stability to a certain extent (Liu et al., 2001; Naus et al., 2010; Ploeg et al., 2011; Öncü et al., 2011, 2012), as illustrated in Figure 2.3(a), showing the gain $|\Gamma(j\omega)|$ for various values of the time delay θ. Here, $\tau = 0.1\,s$, $k_p = 0.2$, $k_d = 0.7$, $k_{dd} = 0$, and $h = 0.5\,s$ is used, yielding asymptotic stability of the platoon, thus fulfilling the vehicle following control objective, and at the same time resulting in comfortable driving behavior; see also Section 2.7.

According to Figure 2.3(a), an increasing time delay thus yields an increased value of $\|\Gamma(s)\|_{\mathcal{H}_\infty}$. From (2.33), it also follows that increasing the time gap h, decreases $\|\Gamma(s)\|_{\mathcal{H}_\infty}$, in the case of a nonzero communication delay θ or without communication ($D(s) = 0$). The latter can be understood as follows. Introducing the complementary sensitivity $\Gamma'(s)$:

$$\Gamma'(s) = \frac{G(s)K(s)}{1 + G(s)K(s)} \tag{2.37}$$

it follows that, due to Bode's complementary sensitivity integral (Middleton and Braslavsky, 2010), $\|\Gamma'(s)\|_{\mathcal{H}_\infty} > 1$. Because $|\Gamma'(j0)| = 1$, the peak value must occur at some $\omega > 0$. Since also $|H^{-1}(j\omega)| < 1$ for all $\omega > 0$ and $|H^{-1}(j\omega)|$ will decrease with increasing value for h according to (2.30), it follows that $\|\Gamma(s)\|_{\mathcal{H}_\infty} = \|H^{-1}(s)\Gamma'(s)\|_{\mathcal{H}_\infty}$ will decrease for increasing h. The same type of reasoning applies in the case of a nonzero communication delay θ.

The influence of the time gap h on string stability in the presence of a communication delay is illustrated in Figure 2.3(b), showing the maximum commu-

nication delay $\theta_{\max}$ that yields $\|\Gamma(s)\|_{\mathcal{H}_\infty} \leq 1$, as a function of the time gap h. The curve shown here is calculated iteratively by taking a fixed value for θ and then searching for the smallest value of h for which $\|\Gamma(s)\|_{\mathcal{H}_\infty} = 1$. For the given system, Corollary 2.2 can be applied as well, since, first, $y_i = a_i \in \mathbb{R}$, $\forall\, i \in \mathbb{N}$, and $u_\mathrm{r} \in \mathbb{R}$, second, $\Gamma(s)$ does not depend on the vehicle index i, and, third, it follows from (2.33) and (2.35) that $P_1(s)$ does not have poles on the imaginary axis that might be canceled by zeros in the product $\Gamma(s)P_1(s)$. Consequently, $\|P_1(s)\|_{\mathcal{H}_\infty} < \infty$ and $\|\Gamma(s)\|_{\mathcal{H}_\infty} \leq 1$ together form necessary and sufficient conditions for $\mathcal{L}_2$ string stability, being equivalent to strict $\mathcal{L}_2$ string stability in this case. Hence, Figure 2.3(b) shows the maximum communication delay for which the system is (strictly) $\mathcal{L}_2$ string stable. It can thus be inferred that a vehicle string with $h = 0.5\,\mathrm{s}$ would require θ to be smaller than about $0.083\,\mathrm{s}$ in view of (strict) $\mathcal{L}_2$ string stability.

In practice, the control system and the wireless communication are implemented in discrete time, which may affect string stability as well (Liu et al., 2001; Öncü et al., 2011, 2012). Assuming a sufficiently high sampling frequency, these sampled data effects are ignored here. Furthermore, the wireless communication delay is likely to vary and the communication itself is subject to packet loss, both depending on the communication load, which obviously also may influence the system performance (Teo et al., 2010).

Finally, it is worth mentioning that the string stability complementary sensitivity without the application of intervehicle communication (which may thus be referred to as ACC), can be easily obtained from (2.33) by choosing $D(s) = 0$. As a result, the system appears to be (strictly) $\mathcal{L}_2$ string stable for $h \geq 3.16\,\mathrm{s}$ (which approximately amounts to about $70\,\mathrm{m}$ at $80\,\mathrm{km/h}$ with $r_i = 0$), given the aforementioned model and controller parameters. This would be an extremely large time gap that is certainly undesirable in view of traffic flow efficiency and user acceptance, thereby motivating the application of CACC.

As far as $\mathcal{L}_\infty$ string stability is concerned, it can be shown that $\|p_1(t)\|_{\mathcal{L}_1}$ exists when $\|\gamma(t)\|_{\mathcal{L}_1}$ exists, similar to the result obtained for the existence of $\|P_1(s)\|_{\mathcal{H}_\infty}$. To this end, apply the inverse Laplace transform to (2.35) to obtain the impulse response, and subsequently use Young's inequality for convolutions. Concentrating on the second requirement in Theorem 2.3, $\Gamma(s) = H^{-1}(s)$ in case there is no communication delay. Consequently, the impulse response is equal to $\gamma(t) = h^{-1}e^{-t/h}$ from which it follows that $\|\gamma(t)\|_{\mathcal{L}_1} = 1$, rendering the system strictly $\mathcal{L}_\infty$ string stable for all time gaps and controller parameters, according to Theorem 2.3.

Again, including a communication delay compromises $\mathcal{L}_\infty$ string stability, as illustrated in Figure 2.4. Using the same parameter values as before, Figure 2.4(a) shows the impulse response function $\gamma(t)$ for various values of the delay θ. As could be expected, it appears that $\|\gamma(t)\|_{\mathcal{L}_1}$ is an increasing function of θ, the effect of which is illustrated in Figure 2.4(b). This figure shows the maximum communication delay $\theta_{\max}$ that yields $\|\gamma(t)\|_{\mathcal{L}_1} \leq 1$, as a function of the time gap h. The curve is obtained by determining $\Gamma(j\omega)$ from (2.33), applying the inverse Fourier transform, and subsequently calculating the $\mathcal{L}_1$ norm by numerical integration. For comparison, also the maximum time delay for $\mathcal{L}_2$ string stability
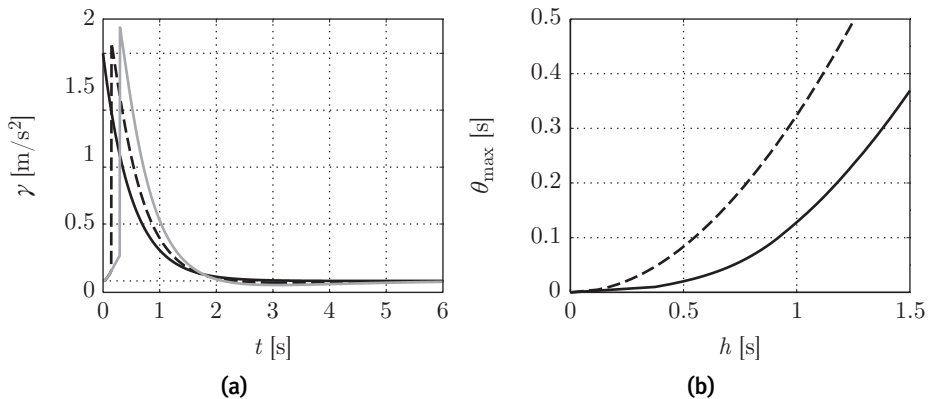
Figure 2.4: $\mathcal{L}_\infty$ string stability properties: (a) impulse response $\gamma(t)$ for communication delay $\theta = 0\,s$ (solid black), $\theta = 0.15\,s$ (dashed black), $\theta = 0.3\,s$ (gray), and (b) maximum communication delay $\theta_{\max}$, as a function of the time gap h, for strict $\mathcal{L}_\infty$ string stability (solid) and for strict $\mathcal{L}_2$ string stability (dashed).

(according to Figure 2.3) is shown here, from which it can be very clearly seen that $\|\gamma(t)\|_{\mathcal{L}_1} \leq 1$ is a more stringent string stability criterion than $\|\Gamma(s)\|_{\mathcal{H}_\infty} \leq 1$, in the sense that a significantly larger time gap is required to guarantee $\mathcal{L}_\infty$ string stability. This could be expected since, from linear system theory,

$$\|\Gamma(s)\|_{\mathcal{H}_\infty} \leq \|\gamma(t)\|_{\mathcal{L}_1}. \tag{2.38}$$

From Figure 2.4(b), it follows that a vehicle platoon with $h = 0.5\,s$ would require θ to be smaller than about 0.017 s in view of strict $\mathcal{L}_\infty$ string stability, compared to 0.083 s for strict $\mathcal{L}_2$ string stability.

Note that, due to Theorem 2.3, $\|\gamma(t)\|_{\mathcal{L}_1} \leq 1$ is sufficient for (nonstrict) $\mathcal{L}_\infty$ string stability, but not necessary. Consequently, it cannot be concluded that for time delays greater than $\theta_{\max}$, the system is $\mathcal{L}_\infty$ string unstable. However, it can be concluded that the system is not strictly $\mathcal{L}_\infty$ string stable for $\theta > \theta_{\max}$, according to the same theorem.

Similar to the $\mathcal{L}_2$ string stability case, choosing $D(s) = 0$ in order to obtain an ACC-like controller, and subsequently determining the time gap for which $\|\gamma(t)\|_{\mathcal{L}_1} \leq 1$, results in the rather large value $h \geq 3.87$ s, compared to $h \geq 3.16$ s for strict $\mathcal{L}_2$ string stability as mentioned above.

2.6   Experiment setup

To validate the theoretical results and to demonstrate its technical feasibility, CACC has been implemented in six similarly adapted vehicles as shown in Figure 2.5. The Toyota Prius III Executive was selected because of its modular setup and ex-factory ACC. Figure 2.6 shows a schematic representation of the components related to the experimental setup. From this figure, it appears that

Figure 2.5: Test fleet, consisting of CACC-equipped passenger vehicles.

the CACC-related components can be categorized into original vehicle components, CACC-specific components, and the vehicle gateway. These three groups are briefly explained below; further details regarding the test vehicle software and instrumentation are presented in Chapter 5.

By making use of many original vehicle systems, only a limited number of components had to be added. The long-range radar determines the relative position and speed of multiple objects with an update rate of 20 Hz. The onboard sensors measure acceleration in two directions, as well as yaw rate. The Power Management Control (PMC) determines the setpoints for the electric motor, the hydraulic brakes, and the engine. Finally, the Human–Machine Interface (HMI) consists of levers and a display in order to be able to set the maximum vehicle velocity (the so-called cruise speed) and the time gap, and to obtain information about the status of the wireless connection and other system components.

Some CACC-specific components have been installed in order to be able to implement the CACC control system. The main component is a real-time computer platform that executes the CACC control software. The wireless communication device, operating according to the IEEE 802.11p-based ETSI ITS G5 standard (Ström, 2011), allows for communication of the desired vehicle acceleration between the CACC vehicles with an update rate of 10 Hz. An EGNOS GPS receiver, with an update rate of 1 Hz, has been installed to serve as a basis for position estimation of the vehicle. This estimated position is also included in the wireless message in order to allow other vehicles to determine which vehicle is the directly preceding one, and to match its wireless message with radar measurements.

Finally, the in-house developed MOVE gateway is the interface between the original vehicle systems and the real-time CACC Platform. It runs at 100 Hz, converting the acceleration setpoints u_i from the CACC Platform, into vehicle actuator setpoints, such that the requested acceleration is accurately realized. The gateway also processes the vehicle sensor data and presents these to the CACC
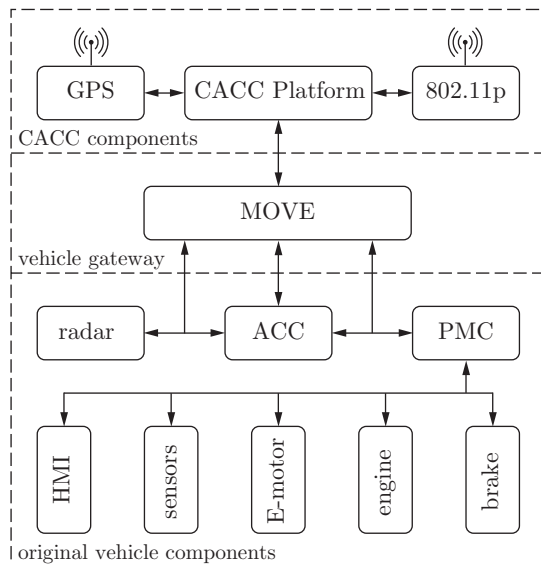
Figure 2.6: Schematic representation of the test vehicle instrumentation.

Platform. Furthermore, the gateway is connected to the native vehicle HMI. As a result, the CACC can be operated like the ex-factory ACC system, using the build-in levers to set cruise speed and time gap, and the vehicle dashboard to obtain information about the current status. To guarantee safe and reliable operation, the gateway also contains several safety features. The gateway employs multiple types of interfacing protocols for the communication with the vehicle systems, whereas a single CAN bus is used for communication with the real-time CACC Platform. Because of the integrated low-level controllers, safety-related functions, and sensor preprocessing, the MOVE gateway allows for evaluation of high-level vehicle controllers, such as CACC, in a safe, reliable and efficient way.

2.7 Experimental validation

To validate the designed controller, especially with respect to its string stability properties, experiments have been performed using the test fleet depicted in Figure 2.5. To this end, the vehicle model is identified first, based on which the controller parameters are chosen. Next, ACC as well as CACC are evaluated to compare the performance of both control systems. Note that the current tests are, therefore, fully focussed on string stability. A similar experiment setup is described in Rajamani et al. (2000a,b), which does not focus on string stability, but on other interesting aspects of practical platooning, among which lateral automation and intra-platoon maneuvers such as exiting the platoon.
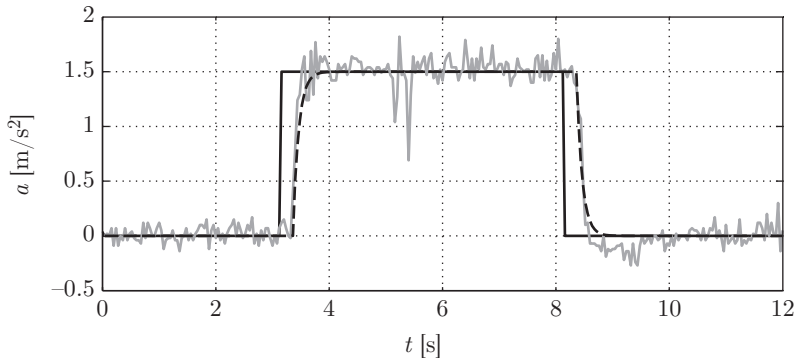
Figure 2.7: Step response of the test vehicle with low-level control only: desired acceleration (solid black), simulated acceleration (dashed black), and measured acceleration (gray).

2.7.1   Vehicle model validation

The vehicle model, including a low-level precompensator implemented in the MOVE gateway, is identified based on measurement of the response of the acceleration $a(t)$ to test signals such as step functions and (swept) sines applied to the vehicle input $u(t)$, to be physically interpreted as the desired acceleration. Subsequently, the model parameters are estimated using a least-squares method. From this, it appears that the vehicle model (2.4) needs to be adapted so as to include a time delay ϕ, having the following frequency-domain model as a result:

$$G(s) = \frac{1}{s^2(\tau s + 1)} e^{-\phi s} \qquad (2.39)$$

with $\tau = 0.1\,s$ and $\phi = 0.2\,s$. The time delay originates in the hybrid driveline of the test vehicle, which in itself is a complex control system.

Figure 2.7 illustrates a validation measurement, showing the test input signal $u(t)$, and the measured as well as the simulated acceleration $a(t)$ using the identified parameters. It can be concluded that the simple vehicle model adequately describes the longitudinal vehicle dynamics; it is fair to mention that the well-designed drive train of the test vehicles highly contributes to this result. Obviously, this longitudinal model does not hold for limit situations, characterized by nonlinear behavior due to tire slip or power limitations, for instance.

Considering the speed of response and passenger comfort, suitable controller parameters were found to be $k_{\mathrm{p}} = 0.2$ and $k_{\mathrm{d}} = 0.7$, whereas k_{dd} is set to zero to prevent feedback of the vehicle's jerk, which is in practice unfeasible. With these controller parameters, asymptotic stability of the error dynamics (2.10) is obtained, thus fulfilling the vehicle following objective.
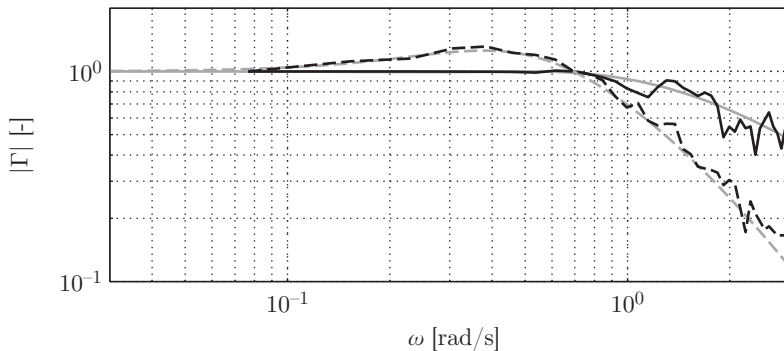
Figure 2.8: String stability complementary sensitivity magnitude $|\Gamma(j\omega)|$: CACC measured (solid black), CACC theoretical (solid gray), ACC measured (dashed black), and ACC theoretical (dashed gray).

2.7.2 String stability experiments

The wireless communication delay in the current test setup is equal to $\theta \approx 0.15\,\mathrm{s}$. From the analysis presented in Section 2.5, it follows that for this delay, and with the aforementioned vehicle and controller parameters, the minimum necessary time gap to guarantee (strict) $\mathcal{L}_2$ string stability is equal to $h_{\min} = 0.67\,\mathrm{s}$. Therefore, tests have been performed with $h = 0.7\,\mathrm{s}$, thus primarily focussing on $\mathcal{L}_2$ string stability.

In view of a high level of reproducibility, the lead vehicle tracks a prescribed trajectory of the virtual reference vehicle. The prescribed test trajectory is defined by a given acceleration $a_0(t)$ of the virtual reference vehicle, consisting of three superimposed swept sine signals in the frequency ranges $[0.06, 1.13]\,\mathrm{rad/s}$, $[1.13, 2.26]\,\mathrm{rad/s}$, and $[2.26, 3.14]\,\mathrm{rad/s}$, respectively. The reference vehicle input $u_{\mathrm{r}}(t)$ is then computed through differentiation, essentially employing the dynamic inverse of the model (2.13).

The test trajectory provides sufficient frequency content to allow for identification of the frequency response function of the string stability complementary sensitivity $\Gamma(j\omega)$. Employing Welch's averaged periodogram method (Stoica and Moses, 1997), the gain $|\Gamma(j\omega)|$ has been estimated, the result of which is shown in Figure 2.8. This figure shows the estimated gain for both ACC and CACC, as well as the theoretical gain $|\Gamma(j\omega)|$, calculated using (2.33), whereas the ACC controller is simply obtained by disabling the input feedforward, i.e., choosing $u_{i-1} = 0$ in (2.8). This experiment confirms the fact that ACC leads to $\mathcal{L}_2$ string unstable behavior, whereas CACC realizes strict $\mathcal{L}_2$ string stable behavior, thereby validating the theoretical analysis presented in Section 2.4. Another important observation is that string stability may not always be easy to assess in practice, since $|\Gamma(j\omega)|$ will be close to 1 for low frequencies, see (2.36), as a result of which estimation inaccuracy may compromise the second string stability criterion in Theorem 2.1 or Corollary 2.2.

Next, Figure 2.9 illustrates time-domain test results for an ACC setup and for
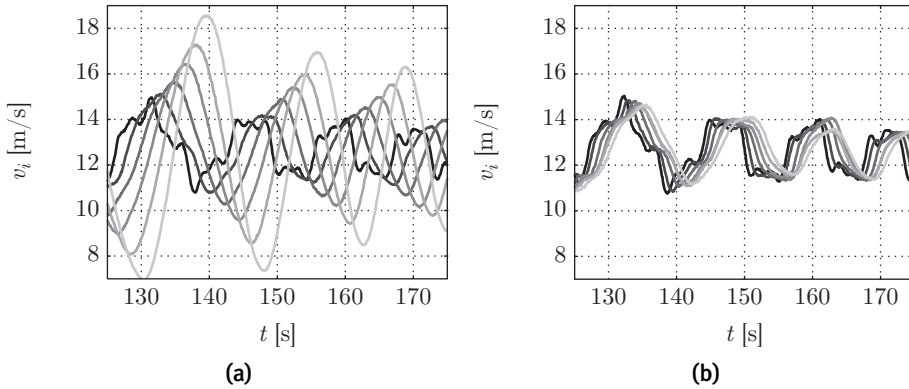
Figure 2.9: Measured velocity response of vehicle 1–6 (black–light gray) with (a) ACC and (b) CACC.

CACC, respectively. Both figures show the velocity responses of all six vehicles for part of the aforementioned test trajectory, where the velocity response of the lead vehicle is exactly the same in both cases since the same virtual reference vehicle input has been used. The responses provide a clear indication that the CACC system is strictly $\mathcal{L}_2$ string stable, whereas the ACC system is not. Noteworthy is the fast increase in overshoot for increasing vehicle index in case of ACC: the maximum velocity (in the time interval shown) of the last vehicle is equal to $18.6\,\mathrm{m/s}$ ($67\,\mathrm{km/h}$), whereas for CACC, this is $14.6\,\mathrm{m/s}$ ($53\,\mathrm{km/h}$).

Finally, Figure 2.10 shows the velocity response to a constant acceleration of the lead vehicle for both ACC and CACC, respectively. These responses too clearly point in the direction of string stability for CACC and the lack thereof for ACC. Note that with ACC, the last vehicle starts to accelerate after $15.5\,\mathrm{s}$, whereas with CACC, this is already after $8.5\,\mathrm{s}$, indicating that CACC may also be effective at traffic lights.

From Figure 2.4(b), it follows that the time gap must be greater than $1\,\mathrm{s}$ for the system to be strictly $\mathcal{L}_\infty$ string stable, given a communication delay $\theta = 0.15\,\mathrm{s}$. Nevertheless, both Figure 2.9(b) and Figure 2.10(b) suggest strict $\mathcal{L}_\infty$ string stability. The fact that there is no overshoot for these specific input signals, however, does not imply strict $\mathcal{L}_\infty$ string stability, since this would require the absence of overshoot for *all* possible types of input signals. Due to estimation inaccuracy, the identified frequency response, as shown in Figure 2.8, leads to an inaccurate impulse response function using the inverse Fourier transformation, which is why $\mathcal{L}_\infty$ string stability is not further investigated here.

Summarizing, the experiments clearly show that the practical results regarding string stability are consistent with the theoretical analysis, also indicating that short-distance vehicle following is technically feasible.
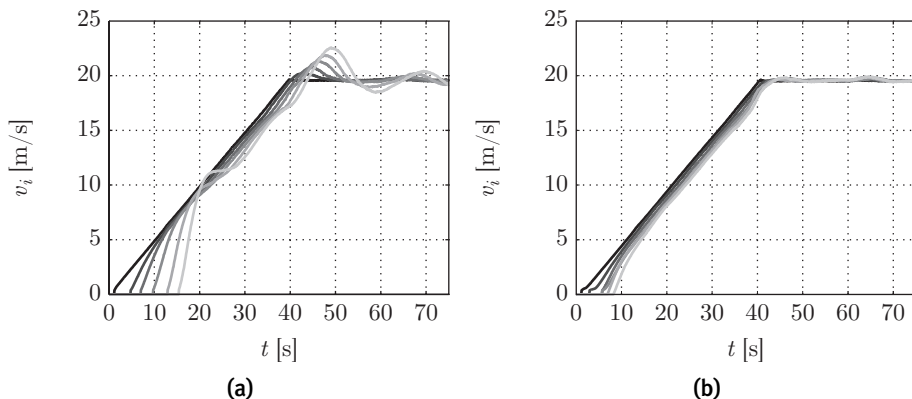
Figure 2.10: Measured velocity response of vehicle 1–6 (black–light gray) with (a) ACC and (b) CACC.

2.8   Conclusion

It is widely recognized that string stability is an essential requirement for the design of vehicle-following control systems that aim for short-distance following. Nevertheless, string stability is not unambiguously defined in literature, describing various stability-like definitions, but also containing performance interpretations. Therefore, a novel string stability definition was proposed, based on the concept of $\mathcal{L}_p$ stability, which applies to both linear and nonlinear systems, while accommodating initial condition perturbations as well as external disturbances, independent of the interconnection topology. The definition appeared to provide a rigorous basis for well-known string stability conditions, employing $\mathcal{L}_2$ and/or $\mathcal{L}_\infty$ gains, for linear unidirectionally interconnected systems.

Employing the derived string stability conditions, it was shown that CACC for vehicle platoons, which is based on common ACC sensors and a wireless intervehicle communication link, allows for time gaps significantly smaller than 1 s while retaining $\mathcal{L}_2$ and $\mathcal{L}_\infty$ string stability.

To demonstrate the technical feasibility of CACC, and to assess the string stability properties in practice, a test fleet of six identical passenger vehicles was developed. From practical experiments with this fleet, a time gap of 0.7 s appeared to yield strict $\mathcal{L}_2$ string-stable behavior, in accordance with the theoretical analysis, which also indicates that time gaps down to 0.3 s are feasible when optimizing the wireless link with respect to latency. As a result, a significant increase in road throughput and, in case of heavy-duty vehicles, decrease of fuel consumption and emissions due to reduced aerodynamic drag can be expected.

The string stability analysis as presented in this chapter, was based on a platoon model with a given controller, which was not specifically designed for string stability. Having rigorously formulated (conditions for) string stability, the immediate question is, whether it would be possible to explicitly include the string stability requirement in the controller design specifications, or, in other

words, to guarantee string-stable behavior by design. This particular controller synthesis problem will be addressed in the next chapter.

Chapter 3

Controller synthesis for string stability of vehicle platoons[1]

Abstract   Cooperative Adaptive Cruise Control (CACC) allows for short-distance automatic vehicle following using intervehicle wireless communication in addition to onboard sensors, thereby potentially improving road throughput. In order to fulfill performance, safety, and comfort requirements, a CACC-equipped vehicle platoon should be string stable, attenuating the effect of disturbances along the vehicle string. Therefore, a controller design method is developed that allows for explicit inclusion of the string stability requirement in the controller synthesis specifications. To this end, the notion of string stability is introduced first, and conditions for $\mathcal{L}_2$ string stability of linear systems are presented that motivate the development of an $\mathcal{H}_\infty$ controller synthesis approach for string stability. The potential of this approach is illustrated by its application to the design of controllers for CACC for one- and two-vehicle look-ahead communication topologies. As a result, $\mathcal{L}_2$ string stable platooning strategies are obtained in both cases, also revealing that the two-vehicle look-ahead topology is particularly effective at a larger communication delay. Finally, the results are experimentally validated using a platoon of three passenger vehicles, illustrating the practical feasibility of this approach.

3.1   Introduction

Cooperative Adaptive Cruise Control (CACC) can be regarded as an extension of the well-known Adaptive Cruise Control (ACC) functionality. ACC is a vehicle-following control system that automatically accelerates and decelerates a vehicle to keep a desired distance or time gap (depending on the spacing policy) to the preceding vehicle and, in the absence of one, aims for a constant cruise speed (Piao and McDonald, 2008). The intervehicle distance and its rate of change are commonly measured by a long-range radar. A CACC system arises when ACC is extended with wireless intervehicle communications (Rajamani and Shladover, 2001). This enables vehicles to obtain information beyond the line-of-sight of

---

[1]This chapter is based on Ploeg et al. (2014a).

onboard sensors and to obtain information regarding other vehicles' states that cannot be retrieved otherwise, or would require a state observer, thereby introducing phase lag. As a result, short intervehicle distances can be realized, thus increasing traffic throughput, without compromising safety (Bose and Ioannou, 2003b; Shladover et al., 2012). In addition, significant fuel savings are possible, particularly for trucks (Ramakers et al., 2009).

The vehicle-following objective, which is essential to CACC, is subject to requirements related to safety, passenger comfort, and scalability with respect to platoon length. In order to fulfil these requirements, the vehicle platoon is desired to exhibit string-stable behavior (Seiler et al., 2004), which can be loosely characterized as the attenuation of the effects of disturbances along the platoon. Typical disturbances are, e.g., velocity variations of the lead vehicle and initial condition perturbations of the platoon vehicles.

Various types of controllers that realize string-stable behavior have been proposed in the literature; see, e.g., Rajamani and Zhu (2002) for a PD-like controller and Swaroop et al. (2001), describing a sliding-mode controller. These controller synthesis methods, however, do not allow taking the string stability requirement explicitly into account. Consequently, string-stable behavior has to be realized through *a posteriori* controller tuning. Due to its capability of including constraints in the controller design, the application of Model Predictive Control (MPC) for vehicle platooning also received quite some attention. As a relevant example, Dunbar and Caveney (2012) proposes a predictive controller employing a one-vehicle look-ahead communication topology, with one of the constraints being the attenuation of the $\mathcal{L}_\infty$ norm of the disturbance responses. In Seiler and Sengupta (2005), an $\mathcal{H}_\infty$ optimal platoon controller is synthesized, also using a one-vehicle look-ahead topology, which focusses on the effect of packet loss on performance in terms of disturbance attenuation, thus being very closely related to string stability. A mixed $\mathcal{H}_2/\mathcal{H}_\infty$ problem formulation is applied in Maschuw et al. (2008), with string stability as one of the optimization criteria for controller synthesis, resulting in a centralized controller that requires the states of all platoon vehicles to be available.

Due to its relevance for application in everyday traffic, this chapter focusses on *ad hoc* vehicle platooning, i.e., a decentralized solution without designated platoon leader, aiming to develop a systematic controller design method in which the string stability requirement is *a priori* included as a design specification. To this end, $\mathcal{H}_\infty$ optimal controller synthesis is applied, since this approach appears to naturally fit the $\mathcal{L}_2$ string stability conditions for linear cascaded systems, among which vehicle platoon models. In addition, $\mathcal{H}_\infty$ control allows to explicitly make tradeoffs between vehicle-following performance and string stability, as these may be conflicting requirements (Maschuw et al., 2008). It is illustrated through controller synthesis for one- and two-vehicle look-ahead schemes that the controller design method supports the generic n-vehicle look-ahead communication topology. Finally, the practical feasibility of the controllers is shown through experimental evaluation in a platoon of three passenger vehicles.

The outline of this chapter is as follows: Section 3.2 first provides a literature overview of controllers for vehicle platooning, motivating the aforementioned

problem statement. Next, Section 3.3 formulates the control problem and derives a platoon model that forms the basis for the controller synthesis approach. Section 3.4 introduces the notion of $\mathcal{L}_2$ string stability and presents string stability conditions for linear systems, upon which Section 3.5 casts the control problem into the $\mathcal{H}_\infty$ framework. The actual controller synthesis is performed in Section 3.6, and experimental results obtained with the designed controllers are described in Section 3.7. Section 3.8 finally summarizes the main conclusions.

3.2   CACC synthesis review

Various controllers for CACC functionality have been proposed over the past decades, a concise review of which will follow below, focusing on the controllers' capability of attaining string stability. In this review, CACC controllers are categorized along two dimensions, being the controller synthesis method and the employed communication topology.

   As in many applications, PD-like controllers, employing feedback of measurable error states with additional feedforward of the preceding vehicles' motion information, have been applied extensively. The most common communication topologies utilized with this type of controller involve communication with the directly preceding vehicle (Ioannou and Chien, 1993; Sheikholeslam and Desoer, 1993; Kato et al., 2002; Rajamani and Zhu, 2002; Naus et al., 2010; Lidström et al., 2012; Nieuwenhuijze et al., 2012), sometimes extended with communication of lead vehicle information (Sheikholeslam and Desoer, 1992b; Swaroop et al., 1994; Shaw and Hedrick, 2007a). In very rare cases, a bidirectional control structure is studied, assuming communication with the directly preceding vehicle and the follower vehicle (Peppard, 1974; Barooah and Hespanha, 2005). Despite the apparent popularity of PD-like controllers, string-stable behavior is only obtained *a posteriori* by tuning the controller parameters.

   The application of sliding mode control for CACC also received quite some attention, probably because of its robustness properties. Here, the same communication topologies are employed as mentioned before: communication with the directly preceding vehicle only (Hedrick et al., 1991; Lu et al., 2004), possibly extended with lead vehicle communication (Gehring and Fritz, 1997; Rajamani et al., 2000b; Swaroop et al., 2001). String stability is obtained by a specific choice of sliding surface parameters, to which end the work in Swaroop et al. (2001) provides guidelines based on a specific platoon model. The string stability requirement, however, cannot be taken into account explicitly during the controller synthesis.

   An automated approach to controller synthesis for CACC is obtained by model predictive control (MPC) or receding horizon control. MPC is applied in Bu et al. (2010), but without taking string stability requirements into account. In Dunbar and Caveney (2012) and in Kianfar et al. (2012), the predictive controller is designed with one of the constraints being $\mathcal{L}_\infty$ string stability, i.e., attenuation of the $\mathcal{L}_\infty$ norm of the disturbances. The aforementioned papers on predictive control all focus on a one-vehicle look-ahead communication topology. Assuming

full state information of all platoon vehicles, Wang et al. (2012) presents an MPC controller that allows for "competitive" as well as cooperative vehicle behavior, but without taking string stability into account.

As a next category, optimal control is considered. Using the Linear-Quadratic Regulator (LQR) problem formulation, a quadratic cost criterion is minimized in Stanković et al. (2000), Huppé et al. (2003), and in Mårtensson et al. (2012), employing a one-vehicle look-ahead topology. String stability is not explicitly included in the controller design, but can be obtained by tuning the state and input weighting matrices in the cost criterion. Notably, Stanković et al. (2000) derives a set of constraints on the controller gains to obtain string stability, which can be satisfied by tuning the appropriate elements of the weighting matrices. The communication topology is extended with lead vehicle communication in Guo and Yue (2012), focusing on $\mathcal{H}_2$ optimal control. Here, string stability is obtained by an iterative procedure for choosing the state and input weighting matrices. The topology is extended to n-vehicle look-ahead in Geiger et al. (2012), where a set of optimal controllers is synthesized, one for each preceding vehicle, after which the controller with the smallest output (desired acceleration) is selected. Although string stability is indeed realized, there is no direct way to guarantee disturbance attenuation. Next, in Seiler and Sengupta (2005), an $\mathcal{H}_\infty$ optimal platoon controller is synthesized, using a one-vehicle look-ahead topology. The focus here is on the effect of packet loss on the $\mathcal{H}_\infty$ norm of the transfer function from certain disturbances to distance error and control effort. Although this approach potentially allows for the inclusion of a string stability requirement, the design is not put in this context since only a two-vehicle system is considered. A mixed $\mathcal{H}_2/\mathcal{H}_\infty$ problem formulation is applied in Maschuw et al. (2008), synthesizing a controller that *a priori* guarantees string stability, possibly at the cost of vehicle-following performance. This paper illustrates that, with this type of controller synthesis, it is possible to explicitly weigh vehicle-following performance against string stability, which may be conflicting requirements. However, the resulting solution is centralized, essentially requiring the states of all vehicles to be available.

A field of research in its own right is the theory of spatially invariant linear systems, concerned with the analysis and control of infinitely long interconnected systems. Application of the Z-transform over the vehicle index leads to a concise string model, after which an optimal state-feedback controller can be synthesized in the Z-domain, using the LQR problem formulation, that guarantees string stability for any (allowable) choice of weighting matrices. One of the early papers on this topic, see Melzer and Kuo (1971), assumes that all vehicles have full state information of all other vehicles, followed later by LQR controller synthesis with limited state information, i.e., the n nearest-neighbors case (Chu, 1974; El-Sayed and Krishnaprasad, 1981; Liang and Peng, 1999). In Bamieh et al. (2002) and in Jovanović and Bamieh (2005), this approach is reformulated based on a continuous spatial variable, upon which the Fourier transform is used to obtain a finite-dimensional model as a basis for both LQR, $\mathcal{H}_2$ and $\mathcal{H}_\infty$ controller synthesis, using an arbitrary, but *a priori* chosen information topology. Recently, interesting results are reported regarding a co-design of both the LQR controller and the information topology (Firooznia, 2012; Zwart et al., 2013). Because of the infinite
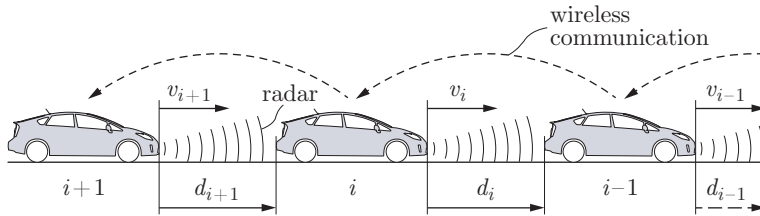
Figure 3.1: CACC-equipped homogeneous vehicle platoon.

length paradigm, the practical meaning of the spatially invariant linear systems approach is still limited. Nevertheless, Firooznia (2012) also proposes a design method for finite-length strings.

In summary, it can be concluded that various controllers have been proposed in the literature that may be suitable for ad hoc platooning. However, most of the synthesis methods do not explicitly formulate string stability as an *a priori* design requirement, hence requiring *a posteriori* tuning to realize this requirement, which may be complex, depending on the communication topology. The main exception is MPC design for $\mathcal{L}_\infty$ string stability; in this case, however, the control algorithm may be computationally demanding, especially when considering application in an embedded computer. Therefore, a method is proposed for systematic controller design for ad hoc platooning that allows for explicit inclusion of the $\mathcal{L}_2$ string stability requirement. To this end, the next section first formulates the vehicle-following control problem employed in this chapter.

3.3 Control problem formulation

Consider a homogeneous platoon of m vehicles, as depicted in Figure 3.1, where d_i is the distance between vehicle i and its preceding vehicle $i-1$, and v_i is the velocity of vehicle i. The main objective of each vehicle in the platoon (except the lead vehicle) is to follow its preceding vehicle at a desired distance $d_{\mathrm{r},i}$. Adopting the constant time gap spacing policy, which is known to improve string stability (Rajamani and Zhu, 2002; Naus et al., 2010), the desired distance reads

$$d_{\mathrm{r},i}(t) = r_i + hv_i(t), \quad i \in S_m\backslash\{1\}, \tag{3.1}$$

where h is the time gap, and r_i the standstill distance. The set of all vehicles in a platoon of length $m \in \mathbb{N}$ is denoted by $S_m = \{i \in \mathbb{N} \mid 1 \leq i \leq m\}$. This chapter focusses on homogeneous platoons, which is why h does not depend on the vehicle index. The spacing error $e_i(t)$ is then equal to

$$\begin{aligned} e_i(t) &= d_i(t) - d_{\mathrm{r},i}(t) \\ &= \big(q_{i-1}(t) - q_i(t) - L_i\big) - \big(r_i + hv_i(t)\big), \end{aligned} \tag{3.2}$$

where q_i is the rear-bumper position of vehicle i, and L_i is its length. The platoon control problem is now twofold. First, the platoon is subject to the vehicle-
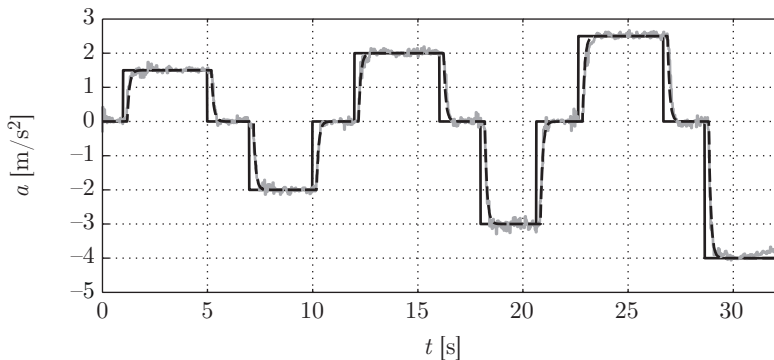
Figure 3.2: Step response of an acceleration-controlled test vehicle: desired acceleration (solid black), measured acceleration (gray), and simulated acceleration (dashed black).

following objective, which is formulated here as

$$a_1(t) = 0 \ \forall t \geq 0 \ \Rightarrow \ \lim_{t \to \infty} e_i(t) = 0 \ \forall i \in S_m \backslash \{1\}, \tag{3.3}$$

where a_1 is the acceleration of the first vehicle; in other words, with the first vehicle driving at a constant velocity, the spacing errors e_i should converge to zero. Second, the string stability requirement is imposed, as described in Section 3.4.

Adopting the platoon model as employed in Ploeg et al. (2011) and Ploeg et al. (2014b), the vehicle dynamics are described in the Laplace domain by the transfer function $G(s)$, with $s \in \mathbb{C}$, according to

$$G(s) = \frac{q_i(s)}{u_i(s)} = \frac{1}{s^2(\tau s + 1)} e^{-\phi s}, \tag{3.4}$$

where τ is a time constant and ϕ a time delay. u_i is the vehicle input, which can be interpreted as the desired acceleration, whereas the position q_i is the output. Note that, slightly abusing formal mathematical notation, $\cdot(s)$ denotes the Laplace transform of the corresponding time-domain variable $\cdot(t)$; if the argument is omitted, then the domain is either irrelevant or can be easily devised from the context. Due to the homogeneity assumption, $G(s)$ is identical for all vehicles. Despite its simplicity, $G(s)$ adequately describes the dynamics of the native force-controlled hybrid drive line of the test vehicles (see Section 3.7), including a precompensator to convert the desired acceleration to the desired force, taking into account the actual vehicle mass and the estimated drag forces. This is confirmed by the validation measurement in Figure 3.2, which shows the desired acceleration, the measured acceleration response, and the simulated response of the model $G_a(s) = 1/(\tau s + 1)e^{-\phi s}$, with $\tau = 0.1$ s and $\phi = 0.2$ s. Obviously, this model does not hold for limit situations, such as emergency braking, which are characterized by nonlinear behavior due to tire slip and complex braking system dynamics. Such limit situations, however, should be handled by control systems specifically developed for that purpose, e.g., a collision avoidance system, and are considered to be outside the operational range of CACC.

Formulating the spacing error $e_i(t)$ in (3.2) in the Laplace domain yields

$$e_i(s) = q_{i-1}(s) - H(s)q_i(s) \tag{3.5}$$

with the spacing policy transfer function $H(s)$ defined as

$$H(s) = hs + 1. \tag{3.6}$$

Without loss of generality, $r_i = L_i = 0$ is assumed in the remainder of this chapter. Inspired by Ploeg et al. (2014b), the structure of the controller of each vehicle is chosen according to

$$
\begin{aligned}
u_i(s) &= H^{-1}(s) \left(K_{\text{fb}}(s)e_i(s) + \sum_{j=1}^{k} K_{\text{ff},j}(s)u_{i-j}^*(s) \right) \\
&= H^{-1}(s)K(s) \begin{pmatrix} e_i(s) \\ u_{i-1}^*(s) \\ \vdots \\ u_{i-k}^*(s) \end{pmatrix} \\
&:= H^{-1}(s)\xi_i(s),
\end{aligned} \tag{3.7}
$$

where $K_{\text{fb}}(s)$ represents the feedback control law, $K_{\text{ff},j}(s)$, $j = 1, 2, \ldots, k$, the feedforward controllers, and $K(s) = \begin{pmatrix} K_{\text{fb}}(s) & K_{\text{ff},1}(s) & \ldots & K_{\text{ff},k}(s) \end{pmatrix}$. $\xi_i(s)$ is the output of the controller $K(s)$. Note that the precompensator $H^{-1}(s)$ in (3.7) cancels the spacing policy transfer function $H(s)$, which is located in the feedback loop according to (3.5), such that the driver can select any time gap h without compromising individual vehicle stability. Due to the ad hoc platooning concept, $K(s)$ is desired to be independent of the vehicle index i. u_{i-j}^*, $j = 1, 2, \ldots, k$, are the measured inputs of k preceding vehicles, which are obtained through wireless intervehicle communication. Obviously, (3.7) only holds for vehicles $i > k$; in case $i \leq k$, $K(s)$ is adapted to only take the $i-1$ preceding vehicles into account. The wireless communication has a latency θ, i.e., $u_{i-j}^*(t) = u_{i-j}(t - \theta)$, which, in the Laplace domain, is modeled by a transfer function

$$D(s) = e^{-\theta s}. \tag{3.8}$$

This latency is (approximately) the same for all preceding vehicles because all vehicles broadcast their information. It should be mentioned that the usage of wireless communication introduces time-varying sampling intervals, which may be relevant to the string stability characteristics (Öncü et al., 2012). Assuming a sufficiently high sampling frequency of the discrete-time controller implementation, these sampled-data effects are ignored here.

The controller (3.7) is thus required to realize asymptotic tracking of the preceding vehicle according to (3.3), under the additional requirement of string stability, with the latter being formally introduced in the next section.

3.4   String stability

A comprehensive overview of the various interpretations of string stability that exist in the literature is given in Chapter 2, based on which a novel definition for $\mathcal{L}_p$ string stability was introduced. Here, this definition is extended to better support multiple-vehicle look-ahead CACC design. In doing so, we focus on $\mathcal{L}_2$ string stability since the controller synthesis to be developed in Section 3.6 will specifically support this type of string stability. Consider to this end the cascaded state-space system

$$
\begin{aligned}
\dot{x}_1 &= f_1(x_1, u_1) \\
\dot{x}_2 &= f_2(x_2, x_1, u_1) \\
&\ \vdots \\
\dot{x}_m &= f_m(x_m, x_{m-1}, \ldots, x_1, u_1) \\
y_i &= h(x_i), \quad i \in S_m,
\end{aligned}
\tag{3.9}
$$

representing a homogeneous system with a unidirectional interconnection topology. $u_1 \in \mathbb{R}^\ell$ is the external input, and $x_i \in \mathbb{R}^n$ and $y_i \in \mathbb{R}^\ell$, $i \in S_m$, are the state and the output, respectively. Note that, in view of the upcoming conditions for string stability of linear systems, the system is assumed to be square, having ℓ inputs and outputs. The functions f_i $(i = 1, 2, \ldots, m)$ and h may be nonlinear. In case (3.9) represents a controlled vehicle platoon, the state may be defined as $x_i^\mathrm{T} = \begin{pmatrix} e_i & v_i & a_i & \ldots \end{pmatrix}$, where e_i is the distance error, v_i is the vehicle velocity, and a_i is the vehicle acceleration, whereas additional states may be present due to controller dynamics. With $u_1 \equiv 0$, the system (3.9) may then have constant equilibrium states $\bar{x}_i^\mathrm{T} = \bar{x}_1^\mathrm{T} = \begin{pmatrix} 0 & \bar{v}_1 & 0 & \ldots \end{pmatrix} \ \forall\, i \in S_m$, where $\bar{v}_1$ is a constant lead vehicle velocity. This can be readily understood, since the string would be in equilibrium when all vehicles drive at the same constant speed with zero spacing error. String stability can now be defined as follows.

Definition 3.1 ($\mathcal{L}_2$ string stability). *Consider the interconnected system* (3.9). *Let* $x^\mathrm{T} = \begin{pmatrix} x_1^\mathrm{T} & x_2^\mathrm{T} & \ldots & x_m^\mathrm{T} \end{pmatrix}$ *be the lumped state vector and let* $\bar{x}^\mathrm{T} = \begin{pmatrix} \bar{x}_1^\mathrm{T} & \ldots & \bar{x}_1^\mathrm{T} \end{pmatrix}$ *denote a constant equilibrium solution of* (3.9) *for* $u_1 \equiv 0$. *The system* (3.9) *is* $\mathcal{L}_2$ *string stable if there exist class* $\mathcal{K}$ *functions*[2] α *and* β, *such that, for any initial state* $x(0) \in \mathbb{R}^{mn}$ *and any* $u_1 \in \mathcal{L}_2^\ell$,

$$
\|y_i(t) - h(\bar{x}_1)\|_{\mathcal{L}_2} \leq \alpha(\|u_1(t)\|_{\mathcal{L}_2}) + \beta(\|x(0) - \bar{x}\|),
$$
$$
\forall\, i \in S_m \ and \ \forall\, m \in \mathbb{N}. \quad (3.10)
$$

If, in addition to (3.10), *with* $x(0) = \bar{x}$ *it also holds that*

$$
\|y_i(t) - h(\bar{x}_1)\|_{\mathcal{L}_2} \leq \|y_1(t) - h(\bar{x}_1)\|_{\mathcal{L}_2},
$$
$$
\forall\, i \in S_m \backslash \{1\} \ and \ \forall\, m \in \mathbb{N} \backslash \{1\}, \quad (3.11)
$$

---

[2]A continuous function $\alpha : \mathbb{R}_{\geq 0} \mapsto \mathbb{R}_{\geq 0}$ is said to belong to class $\mathcal{K}$ if it is strictly increasing and $\alpha(0) = 0$.

the system (3.9) *is* semi-strictly $\mathcal{L}_2$ string stable *with respect to its input $u_1(t)$.*
If, in addition to (3.10), *with $x(0) = \bar{x}$ it also holds that*

$$\|y_i(t) - h(\bar{x}_1)\|_{\mathcal{L}_2} \leq \|y_{i-1}(t) - h(\bar{x}_1)\|_{\mathcal{L}_2},$$
$$\forall\, i \in S_m \backslash \{1\} \text{ and } \forall\, m \in \mathbb{N} \backslash \{1\}, \quad (3.12)$$

the system (3.9) *is referred to as* strictly $\mathcal{L}_2$ string stable *with respect to its input*
$u_1(t)$.

Here, $\|\cdot\|$ denotes any vector norm, $\|\cdot\|_{\mathcal{L}_2}$ denotes the signal 2-norm (Zhou
et al., 1996), and $\mathcal{L}_2^{\ell}$ is the ℓ-dimensional space of vector signals that are bounded
in the $\mathcal{L}_2$ sense. It is noted that Definition 3.1 closely resembles the common
$\mathcal{L}_2$ stability definition (Khalil, 2000) as far as (nonstrict) $\mathcal{L}_2$ string stability is
concerned, except for the fact that the inequality (3.10) must hold *for all* string
lengths $m \in \mathbb{N}$.

The notion of (semi-)strict $\mathcal{L}_p$ string stability, for which not only (3.10) must
hold but also (3.11) or (3.12), has been introduced to accommodate the require-
ment of upstream disturbance attenuation, as already mentioned in Section 3.1.
Compared to Chapter 2 (see also Ploeg et al. (2014b)), the novel notion of semi-
strict string stability has been introduced here to support the controller design in
the two-vehicle look-ahead scheme, as will become clear in Section 3.6.

The interconnected system formulation could be generalized so as to also in-
clude other interconnection topologies, e.g., a bidirectional one, without principal
consequences for Definition 3.1. However, in the scope of the look-ahead schemes
considered here, this is not relevant. It is noted that the first system ($i = 1$) may
be either uncontrolled or, in case of vehicle platoons, velocity controlled. Alterna-
tively, as described in Chapter 2 (and in Ploeg et al. (2014b)), it is also possible
to apply a vehicle-following controller with a so-called virtual reference vehicle.
Choosing the input u_1 of vehicle $i = 1$ as the external platoon input encompasses
all such options, thus yielding the most generic approach.

Although formulated for general nonlinear systems, Definition 3.1 provides
a basis for deriving easy-to-check string stability conditions for linear systems.
Consider to this end the linear equivalent of the state equations in (3.9):

$$\dot{x}_i = \sum_{j=1}^{i} A_{i-j} x_j + B_{i-1} u_1, \quad i \in S_m, \quad (3.13)$$

where A_k and B_k ($k = 0, 1, \ldots, m-1$) are the system and input matrices, respec-
tively. Introducing the lumped state vector $x^{\mathrm{T}} = \begin{pmatrix} x_1^{\mathrm{T}} & x_2^{\mathrm{T}} & \ldots & x_m^{\mathrm{T}} \end{pmatrix}$, (3.13) can be
reformulated as

$$\dot{x} = Ax + Bu_1 \quad (3.14)$$

with input matrix $B^{\mathrm{T}} = \begin{pmatrix} B_0^{\mathrm{T}} & B_1^{\mathrm{T}} & \ldots & B_{m-1}^{\mathrm{T}} \end{pmatrix}$ and system matrix A, the latter
being lower block-triangular, with the matrices A_0 on the main diagonal, the
matrices A_1 on the subdiagonal, etc. In addition, consider linear output functions
according to

$$y_i = Cx_i = C_i x, \quad i \in S_m \quad (3.15)$$

with output matrix C and $C_i = \begin{pmatrix} 0_{\ell \times n(i-1)} & C & 0_{\ell \times n(m-i)} \end{pmatrix}$. Furthermore, the equilibrium state $\bar{x}^{\mathrm{T}} = \begin{pmatrix} \bar{x}_1^{\mathrm{T}} & \dots & \bar{x}_1^{\mathrm{T}} \end{pmatrix} = 0$ is chosen, hence $h(\bar{x}_1) = C_i \bar{x} = 0$ $\forall\, i \in S_m$. This choice is without loss of generality since there always exists a coordinate transformation such that $\bar{x} = 0$. The model (3.14), (3.15) can now be formulated in the Laplace domain as follows:

$$y_i(s) = P_i(s) u_1(s) + O_i(s) x(0), \quad i \in S_m \tag{3.16}$$

with outputs y_i and exogenous input u_1. $x(0)$ denotes the initial (time-domain) condition, whereas $P_i(s) = C_i(sI - A)^{-1}B$ and $O_i(s) = C_i(sI - A)^{-1}$.

Because the system with index $i = 1$ is assumed to be uncontrolled, (3.14) may contain unstable and/or marginally stable modes. Consequently, $P_1(s)$ may be unstable, leading to the following assumption.

Assumption 3.1. *The output y_i, $i \in S_m$, is chosen such that unstable and marginally stable modes of the system* (3.14), (3.15) *are unobservable.*

As a consequence of Assumption 3.1, it holds that, for linear time-invariant systems, if the function α in (3.10) exists, then also the function β exists. In view of string stability, it therefore suffices to only analyze the input–output behavior, characterized by $P_i(s)$, which is equivalent to assuming $x(0) = \bar{x} = 0$ in (3.16).

In order to further analyze the ($\mathcal{L}_2$) string stability properties, the $\mathcal{H}_\infty$ norm $\|P_i(s)\|_{\mathcal{H}_\infty}$ of $P_i(s)$ is employed, which is defined as

$$\|P_i(s)\|_{\mathcal{H}_\infty} := \sup_{\mathrm{Re}(s) > 0} \bar{\sigma}(P_i(s)), \tag{3.17}$$

where $\bar{\sigma}(\cdot)$ denotes the maximum singular value[3]. It can then be shown (Zhou et al., 1996, p. 101) that $\|P_i(s)\|_{\mathcal{H}_\infty}$ is equal to the $\mathcal{L}_2$ induced norm related to the input $u_1(t)$ and the output $y_i(t)$:

$$\|P_i(s)\|_{\mathcal{H}_\infty} = \sup_{u_1 \neq 0} \frac{\|y_i(t)\|_{\mathcal{L}_2}}{\|u_1(t)\|_{\mathcal{L}_2}}, \tag{3.18}$$

where the $\mathcal{L}_2$ norm is defined on the interval $t \in [0, \infty)$. Hence

$$\begin{aligned} \|y_i(t)\|_{\mathcal{L}_2} &\leq \|P_i(s)\|_{\mathcal{H}_\infty} \|u_1(t)\|_{\mathcal{L}_2} \\ &\leq \max_{i \in S_m} \|P_i(s)\|_{\mathcal{H}_\infty} \|u_1(t)\|_{\mathcal{L}_2}, \quad \forall\, i \in S_m. \end{aligned} \tag{3.19}$$

Note that (3.19) is not conservative, in the sense that there is always a subsystem $i \in S_m$ and a specific signal $u_1(t)$ for which the right-hand sides in (3.19) are equal and become arbitrarily close to $\|y_i(t)\|_{\mathcal{L}_2}$. Therefore, according to Definition 3.1 and under the conditions as mentioned in Assumption 3.1, the existence of $\max_{i \in S_m} \|P_i(s)\|_{\mathcal{H}_\infty}$, for all $m \in \mathbb{N}$, is a necessary and sufficient condition for $\mathcal{L}_2$ string stability of the interconnected system (3.14), (3.15).

---

[3]According to the maximum modulus theorem (Zhou et al., 1996), the $\mathcal{H}_\infty$ norm can be computed by evaluation of $\bar{\sigma}(P_i(s))$ along the imaginary axis, i.e., $\sup_{\mathrm{Re}(s)>0} \bar{\sigma}(P_i(s)) = \sup_{\omega \in \mathbb{R}} \bar{\sigma}(P_i(j\omega))$, provided that $P_i(s)$ represents a causal and stable system. Therefore, s and $j\omega$ are sometimes used interchangeably in this chapter.

If an infinite-length string consisting of linear *unidirectionally-coupled* systems has a bounded output response to a bounded input, then also finite-length strings have a bounded output response. It therefore suffices to consider only the infinite-length string $m \to \infty$ instead of all possible string lengths $m \in \mathbb{N}$. The sets S_m, $m \in \mathbb{N}$, over which the inequality (3.10) must hold, can then be simplified to a single set $\mathbb{N}$. As a result, the following string stability condition can be formulated.

Condition 3.1 ($\mathcal{L}_2$ string stability)**.** *The interconnected system* (3.14)*,* (3.15)*, with input–output representation* (3.16)*, is $\mathcal{L}_2$ string stable, under the condition as mentioned in Assumption 3.1, if and only if*

$$\sup_{i \in \mathbb{N}} \|P_i(s)\|_{\mathcal{H}_\infty} < \infty. \tag{3.20}$$

Assuming functional controllability (Patel and Munro, 1982) of the system (3.16) for $i = 1$, i.e., $P_1^{-1}(s)$ exists (which is why the system is assumed to be square), the transfer function $\Theta_i(s)$ from "input" $y_1(s)$ to output $y_i(s)$ can be defined according to

$$\Theta_i(s) := P_i(s)P_1^{-1}(s) \tag{3.21}$$

such that $P_i(s) = \Theta_i(s)P_1(s)$. The following condition for semi-strict $\mathcal{L}_2$ string stability can now be formulated.

Condition 3.2 (Semi-strict $\mathcal{L}_2$ string stability)**.** *Subject to Assumption 3.1, the interconnected system* (3.16) *is semi-strictly $\mathcal{L}_2$ string stable with respect to its input u_1 if and only if*

$$\|P_1(s)\|_{\mathcal{H}_\infty} < \infty \tag{3.22a}$$
$$\|\Theta_i(s)\|_{\mathcal{H}_\infty} \leq 1, \quad \forall\, i \in \mathbb{N}\backslash\{1\}. \tag{3.22b}$$

The sufficiency of the conditions (3.22a) and (3.22b) for $\mathcal{L}_2$ string stability follows from the fact that $\|P_i(s)\|_{\mathcal{H}_\infty} \leq \|\Theta_i(s)\|_{\mathcal{H}_\infty} \|P_1(s)\|_{\mathcal{H}_\infty}$ and Condition 3.1. Furthermore, since $y_i(s) = \Theta_i(s)y_1(s)$, it follows that the system is also semi-strictly $\mathcal{L}_2$ string stable if (3.22b) holds. The necessity of condition (3.22a) is immediate. Moreover, if (3.22b) is not satisfied for some i, it follows that $\|y_i(t)\|_{\mathcal{L}_2} > \|y_1(t)\|_{\mathcal{L}_2}$ for some $y_1(t)$, indicating the necessity of condition (3.22b).

Along the same line of thought, the transfer function $\Gamma_i(s)$ from $y_{i-1}(s)$ to $y_i(s)$ is introduced, assuming functional controllability of $P_{i-1}(s)$, according to

$$\Gamma_i(s) := P_i(s)P_{i-1}^{-1}(s), \tag{3.23}$$

which is referred to as the string stability complementary sensitivity. This leads to the following strict $\mathcal{L}_2$ string stability condition, a formal proof of which is given in Ploeg et al. (2014b).

Condition 3.3 (Strict $\mathcal{L}_2$ string stability)**.** *Subject to Assumption 3.1, the system* (3.16) *is strictly $\mathcal{L}_2$ string stable with respect to its input u_1 if and only if*

$$\|P_1(s)\|_{\mathcal{H}_\infty} < \infty \tag{3.24a}$$
$$\|\Gamma_i(s)\|_{\mathcal{H}_\infty} \leq 1, \quad \forall\, i \in \mathbb{N}\backslash\{1\}. \tag{3.24b}$$
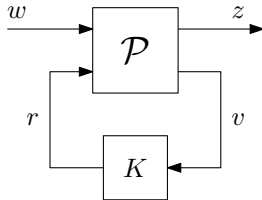
Figure 3.3: $\mathcal{H}_\infty$ optimal control configuration.

The Conditions 3.2 and 3.3 now provide a basis for controller design by means of $\mathcal{H}_\infty$ optimization for the vehicle-following control problem, as introduced in the next section.

3.5   The $\mathcal{H}_\infty$ control problem

Before casting the platoon control problem into the $\mathcal{H}_\infty$ synthesis framework (Zhou et al., 1996), the general $\mathcal{H}_\infty$ control configuration, as shown in Figure 3.3, is described first. Here, the plant $\mathcal{P}$ is the system to be controlled, whereas w denotes the exogenous inputs, r denotes the control signals, z denotes the exogenous outputs, and v denotes the controller inputs, i.e.,

$$\begin{pmatrix} z(s) \\ v(s) \end{pmatrix} = \mathcal{P}(s) \begin{pmatrix} w(s) \\ r(s) \end{pmatrix}. \tag{3.25}$$

In the scope of the platooning problem, the control signal is scalar and equal to $r = \xi_i$, and the controller inputs are equal to $v^{\mathrm{T}} = \begin{pmatrix} e_i & u^*_{i-1} & \dots & u^*_{i-k} \end{pmatrix}$, corresponding to (3.7).

The feedback loop is closed by the controller K according to

$$r(s) = K(s)v(s) \tag{3.26}$$

upon which the controlled system is described by

$$z(s) = N(s)w(s) \tag{3.27}$$

with

$$N = \mathcal{P}_{11} + \mathcal{P}_{12}K\left(I - \mathcal{P}_{22}K\right)^{-1}\mathcal{P}_{21}, \tag{3.28}$$

omitting the argument s for readability. Here, $\mathcal{P}(s)$ is partitioned in block matrices $\mathcal{P}_{ij}(s)$, $i,j \in \{1,2\}$, of dimensions corresponding to the inputs and outputs in (3.25). $N(s)$ is known as the lower Linear Fractional Transformation (LFT) (Zhou et al., 1996). $\mathcal{H}_\infty$ optimal control now involves finding a stabilizing controller $K_{\mathrm{opt}}(s)$ subject to

$$K_{\mathrm{opt}}(s) = \arg\min_K \|N(K)\|_{\mathcal{H}_\infty} \tag{3.29}$$

yielding an *internally* stable system, i.e., without cancelation of unstable or marginally stable plant poles by the controller. To this end, either a Riccati-based approach or an LMI-based approach can be applied (Doyle et al., 1989; Chiang and Safonov, 1998).

The specific form of the $\mathcal{H}_\infty$ synthesis objective in (3.29) motivates the choice for this type of controller design strategy for the platoon problem, since the conditions (3.22b) and (3.24b) for (semi-)strict $\mathcal{L}_2$ string stability are also concerned with minimizing the $\mathcal{H}_\infty$ norm of a transfer function. Hence, if the exogenous input w and the exogenous output z are chosen such that $N(s)$ contains either $\Theta_i(s)$ or $\Gamma_i(s)$, then (semi-)strict $\mathcal{L}_2$ string stability is actively pursued by the controller synthesis procedure, and condition (3.22b) or (3.24b) is satisfied if $N(s)$ in (3.28) satisfies $\|N(s)\|_{\mathcal{H}_\infty} \leq 1$. In addition, the error e_i must be included in z, in view of the vehicle-following objective (3.3). The specific choices for w and z, however, depend on the particular communication topology under study, as will be further described in the next section.

3.6 Controller synthesis for string-stable platooning

Having formulated the control problem, a platooning controller for a one-vehicle look-ahead topology and subsequently for a two-vehicle look-ahead topology will be designed. The motivation for the latter is to investigate the benefits of a more complex communication topology, illustrating at the same time that the controller synthesis procedure is able to go beyond the basic one-vehicle look-ahead topology.

3.6.1 One-vehicle look-ahead topology

In case of the one-vehicle look-ahead CACC scheme, the input u_{i-1} of the preceding vehicle is employed to obtain string stability. Since u_{i-1} and q_{i-1} are related through the vehicle model $G(s)$ (bearing in mind the homogeneity of the vehicle dynamics), the block scheme as shown in Figure 3.4 arises. From this scheme, it can be concluded that $K(s)$ includes both output feedback and input feedforward; hence, $K(s)$ can be characterized as a two degree-of-freedom controller (Skogestad and Postlethwaite, 2005).

From Figure 3.4, it immediately follows that the exogenous input w corresponds to u_{i-1} in this specific application. Next, the (weighted) distance error e_i is chosen as the first element of the exogenous output z, since it directly relates to the vehicle-following objective. The weighting is implemented in the Laplace domain by a function $W_e(s)$, providing a means to further specify the control objectives as commonly employed in $\mathcal{H}_\infty$ controller synthesis. Consequently, $e_i'(s) = W_e(s)e_i(s)$ becomes the first exogenous output. Finally, since u_{i-1} is the exogenous input, u_i is chosen as the second exogenous output, as a result of which the lower LFT $N(s)$ will contain the following SISO relation:

$$u_i(s) = \Gamma_i(s)u_{i-1}(s). \tag{3.30}$$

$\Gamma_i(s)$ can be interpreted as the string stability complementary sensitivity, defined in (3.23) with the output of $P_i(s)$ chosen as $y_i(s) = u_i(s)$, i.e., $u_i(s) = P_i(s)u_1(s)$.
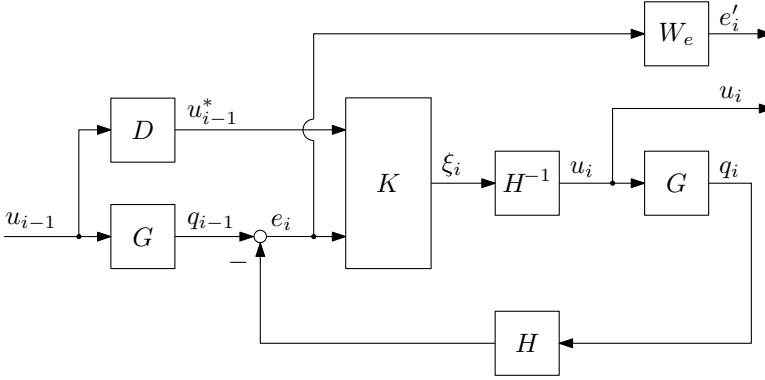
Figure 3.4: One-vehicle look-ahead CACC configuration.

The controller design thus aims for strict $\mathcal{L}_2$ string stability, subject to Condition 3.3, which is preferable above semi-strict $\mathcal{L}_2$ string stability in view of disturbance attenuation. In addition, choosing u_i as the second exogenous output has the advantage that the control effort is minimized at the same time. Note that $P_1(s) = 1$ due to the choice of u_i as the relevant output for string stability; therefore, condition (3.24a) is satisfied by definition. As can be directly seen from Figure 3.4, the control signal r corresponds to ξ_i, being the output of the controller $K(s)$, whereas the controller input vector v has e_i and u_{i-1}^* as its elements.

The (mixed-sensitivity) $\mathcal{H}_\infty$ control problem is now to compute a stabilizing controller $K(s) = \begin{pmatrix} K_{\mathrm{fb}}(s) & K_{\mathrm{ff}}(s) \end{pmatrix}$, with

$$\xi_i(s) = \begin{pmatrix} K_{\mathrm{fb}}(s) & K_{\mathrm{ff}}(s) \end{pmatrix} \begin{pmatrix} e_i(s) \\ u_{i-1}^*(s) \end{pmatrix}, \tag{3.31}$$

such that $\|N(s)\|_{\mathcal{H}_\infty}$ is minimized, where

$$\begin{pmatrix} e_i'(s) \\ u_i(s) \end{pmatrix} = \begin{pmatrix} W_e(s)S(s) \\ \Gamma(s) \end{pmatrix} u_{i-1}(s)$$
$$:= N(s)u_{i-1}(s). \tag{3.32}$$

Here,

$$S(s) = \tilde{S}(s)G(s)\big(1 - K_{\mathrm{ff}}(s)D(s)\big) \tag{3.33}$$

is the sensitivity and

$$\Gamma(s) = \tilde{S}(s)H^{-1}(s)\big(K_{\mathrm{fb}}(s)G(s) + K_{\mathrm{ff}}(s)D(s)\big) \tag{3.34}$$

is the string stability complementary sensitivity, with

$$\tilde{S}(s) = \big(1 + K_{\mathrm{fb}}(s)G(s)\big)^{-1}. \tag{3.35}$$

It is noted that $\Gamma(s)$ does not depend on the index i, which can be readily understood when realizing that the block scheme in Figure 3.4 holds for all vehicles $i > 1$. As desired, the synthesized controller is also independent of i.

From $N(s)$ in (3.32), it follows that

$$\|N(s)\|_{\mathcal{H}_\infty} = \gamma \;\Rightarrow\; \|\Gamma(s)\|_{\mathcal{H}_\infty} \leq \gamma. \tag{3.36}$$

According to condition (3.24b), string stability is thus obtained for any value $\gamma \leq 1$. On the other hand, if the vehicle-following objective is realized, it must hold that $\lim_{\omega \to 0}\big(v_i(j\omega) - v_{i-1}(j\omega)\big) = 0$, where $\omega \in \mathbb{R}$ is the frequency. Also taking into account the homogeneity of the vehicle dynamics, due to which $u_i(j\omega)/u_{i-1}(j\omega) = v_i(j\omega)/v_{i-1}(j\omega)$, this implies

$$\lim_{\omega \to 0} |\Gamma(j\omega)| = 1 \;\Rightarrow\; \|\Gamma(s)\|_{\mathcal{H}_\infty} \geq 1. \tag{3.37}$$

From (3.36) and (3.37), it thus follows that

$$\|N(s)\|_{\mathcal{H}_\infty} = 1 \tag{3.38}$$

is the $\mathcal{H}_\infty$ synthesis objective for the design of a strictly $\mathcal{L}_2$ string-stabilizing controller. Note that, considering (3.37) and $N(s)$ in (3.32), (3.38) is a sufficient condition for strict $\mathcal{L}_2$ string stability and asymptotic tracking.

The weighting function $W_e(s)$ in (3.32) is employed to specify the vehicle-following performance in terms of comfort and speed of response, possibly at the cost of string stability. $W_e(s)$ thus allows to balance vehicle-following performance against string stability. However, since the focus here is on string stability, $W_e = 1$ is chosen, thus equally penalizing amplification of disturbances in u_{i-1} over the entire frequency range.

To synthesize the controller, the vehicle parameters are set to $\tau = 0.1\,\mathrm{s}$ and $\phi = 0.2\,\mathrm{s}$, with $\theta = 0.02\,\mathrm{s}$ representing the communication delay[4]. In addition, both the vehicle and the communication delay are described by a 3rd-order Padé approximation, yielding a sufficiently accurate phase in the frequency interval of interest[5]. Finally, a design time gap $h = 1\,\mathrm{s}$ is chosen, being the standardized minimum time gap for ACC (International Organization for Standardization, 2010). The $\mathcal{H}_\infty$ optimization procedure then yields a 10th-order state-space model of the controller. This controller is reduced by removing those states that are associated with small Hankel singular values (which are a measure of the energy transfer from input to state or state to output) upon which the controller is written as a transfer function $K(s)$. After a further reduction by manually removing those poles and zeros of $K(s)$ that are outside the frequency region of interest and, at the same time, do not significantly influence the string stability properties of the controlled system, the final controller design reads

$$
\begin{aligned}
K_{\mathrm{fb}}(s) &= \frac{2.6880(s+23.22)(s+10)(s+1)(s+0.3646)}{(s+24.65)(s+5.926)(s+5.049)(s+0.9947)} \\
K_{\mathrm{ff}}(s) &= \frac{1.0391(s+24.1)(s+7.233)(s+4.051)(s+1)}{(s+24.65)(s+5.926)(s+5.049)(s+0.9947)}.
\end{aligned}
\tag{3.39}
$$

---

[4]This value is significantly smaller than the delay $\theta = 0.15\,\mathrm{s}$ as used in Chapter 2 (Section 2.7) due to a different hard- and software implementation of the wireless communication system; see also Section 3.7.

[5]Alternatively, the method proposed in Meinsma and Zwart (2000) can be applied, involving a Smith predictor parameterization of the controller. This potentially reduces the order of the resulting controller, compared to the "classical" Padé approximation approach.
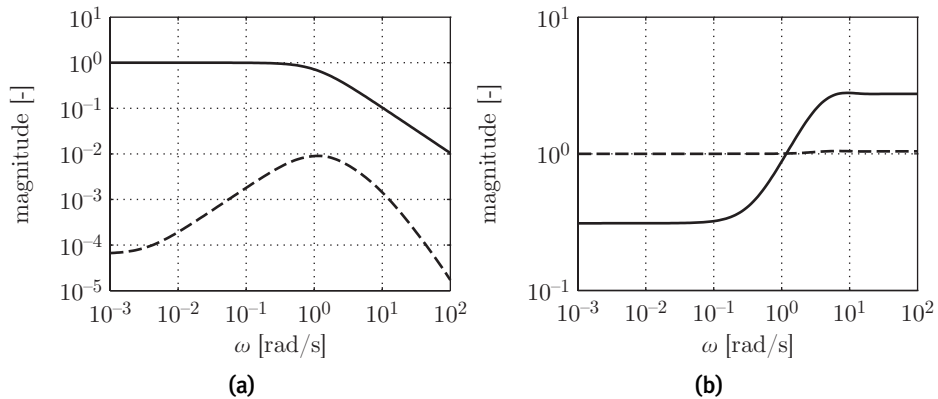
Figure 3.5: Frequency response magnitude of (a) $N(j\omega)$: $|\Gamma(j\omega)|$ (solid) and $|S(j\omega)|$ (dashed), and (b) $K(j\omega)$: $|K_{\text{fb}}(j\omega)|$ (solid) and $|K_{\text{ff}}(j\omega)|$ (dashed).

This controller realizes a stable platooning system, which can, e.g., readily be checked by computing the poles of $\Gamma(s)$. Because the controller does not cancel the marginally stable poles of $G(s)$, the system is also internally stable[6].

Indeed, with this controller, $\|N(s)\|_{\mathcal{H}_\infty} = 1$ is obtained, indicating strict $\mathcal{L}_2$ string stability, while also satisfying the requirement on the sensitivity $S(s)$. This is confirmed by Figure 3.5(a), showing the frequency response magnitudes $|S(j\omega)|$ and $|\Gamma(j\omega)|$, from which it can be concluded that $|S(j\omega)| \leq 1$ and $|\Gamma(j\omega)| \leq 1$. In addition, Figure 3.5(b) shows the controller magnitudes $|K_{\text{fb}}(j\omega)|$ and $|K_{\text{ff}}(j\omega)|$, which illustrates that the feedforward gain is very close to 1 over the entire frequency range. This, in fact, corresponds to the controller designed in Ploeg et al. (2011), where the feedforward gain was chosen identical to 1. Note that the magnitude response $|K_{\text{fb}}(j\omega)|$ exhibits a slope of approximately $+1$ around $\omega = 1\,\text{rad/s}$, indicating that the feedback controller contains a differential action.

Figure 3.6 shows the time responses of 5 vehicles for $h = 1\,\text{s}$, with vehicle 1, which is velocity controlled (see Section 3.7), performing a smooth velocity step upward and downward, based on a trapezoidal acceleration profile. The acceleration responses (which are very similar to the control actions, given the relatively small values for τ and ϕ) clearly show a decreasing amplitude along the string, indicating *strict* $\mathcal{L}_2$ string-stable behavior. This is confirmed by the absence of overshoot in the velocity responses. Furthermore, the distance responses reflect the velocity-dependent spacing policy, whereas from the distance error response, it can be concluded that the vehicle-following objective is reached. The error response also indicates strict $\mathcal{L}_2$ string stability, bearing in mind that, due to the homogeneity assumption, $\Gamma(s) = e_i(s)/e_{i-1}(s)$.

---

[6]In some cases, the poles in zero of $G(s)$ shift slightly into the left half-plane during the controller synthesis procedure due to numerical inaccuracy, upon which they may actually be cancelled by the controller. This can be prevented by either formulating the $\mathcal{H}_\infty$ problem as a "four-block" problem, which involves an additional exogenous disturbance at the input of $G(s)$, or by applying a bilinear pole-shifting transformation (Safonov, 1987; Chiang and Safonov, 1992).
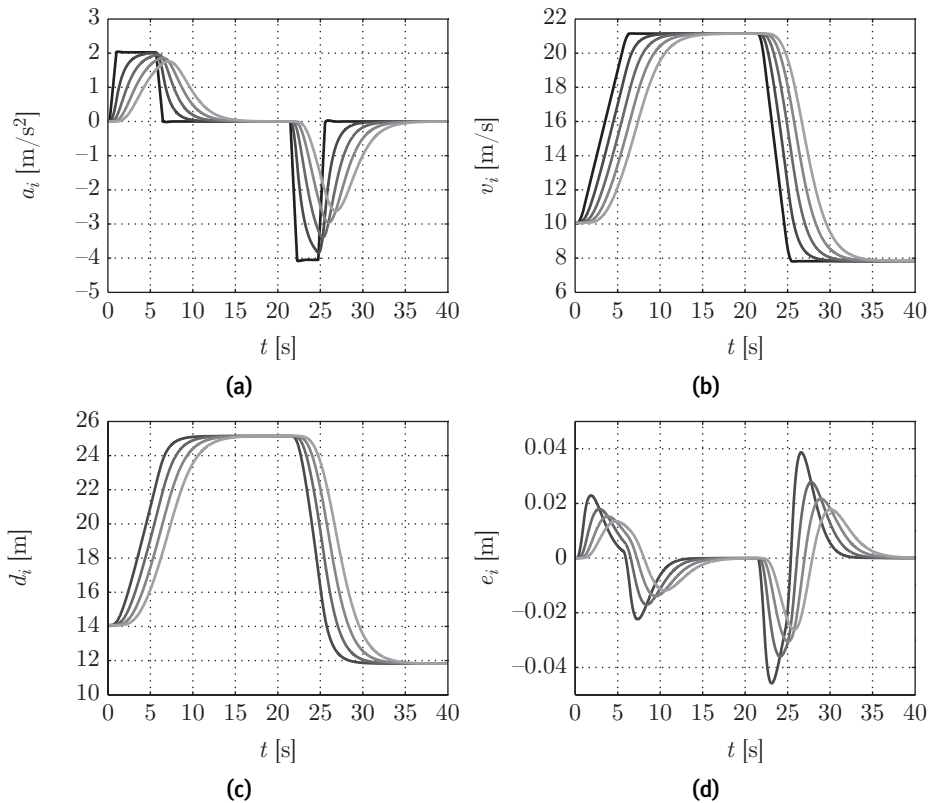
Figure 3.6: Time responses of (a) the acceleration $a_i(t)$ and (b) the velocity $v_i(t)$ (black–light gray: $i = 1, 2, \ldots, 5$); (c) the distance $d_i(t)$ and (d) the distance error $e_i(t)$ (dark–light gray: $i = 2, 3, 4, 5$).

Although (semi-)strict $\mathcal{L}_2$ string stability characterizes the propagation of the effects of input disturbances, satisfying this property also implies that the system outputs are bounded with respect to bounded initial condition perturbations, according to Definition 3.1. In other words, no (string-unstable) amplification of initial condition perturbations can occur. Moreover, since the controlled system is linear and time-invariant, the initial condition response is characterized by the transfer function that also describes the input–output behavior, i.e., $\Gamma(s)$. For these reasons, initial condition perturbations are not explicitly considered here.

3.6.2 Two-vehicle look-ahead topology

To illustrate the design procedure in case of a more complex information topology and to investigate the possible benefits of this topology with respect to string stability, this section is concerned with a two-vehicle look-ahead topology, taking an additional controller input u_{i-2}^* into account. In this case, however, u_{i-1}^* and u_{i-2}^* are not independent inputs, since they both depend on u_{i-3}^*, whereas u_{i-2}^*
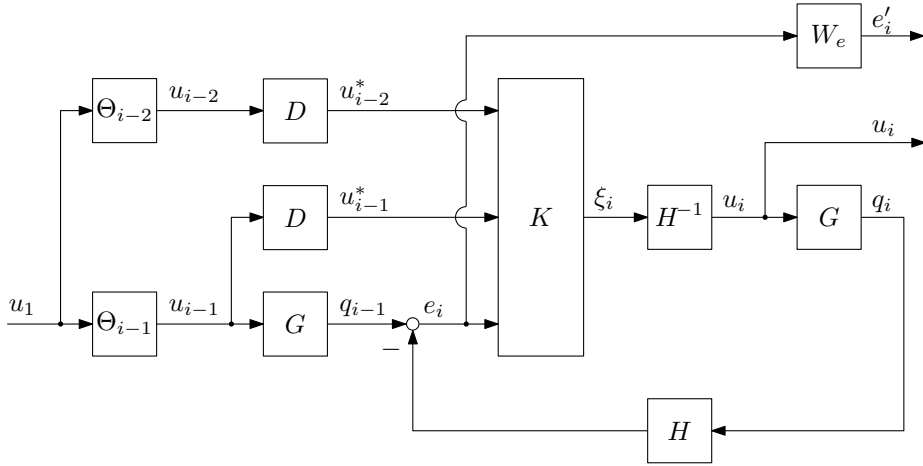
Figure 3.7: Two-vehicle look-ahead CACC configuration.

and u_{i-3}^* both depend on u_{i-4}^*, etc. In other words, a single-vehicle subsystem with an independent input cannot be isolated, as was the case with the one-vehicle look-ahead topology. Consequently, the lead vehicle input u_1 is chosen to be the independent input, yielding the block scheme as shown in Figure 3.7. In this figure, the following input–output relation is introduced:

$$u_i(s) = \Theta_i(s)u_1(s). \tag{3.40}$$

$\Theta_i(s)$ can be interpreted as the transfer function, defined in (3.21), relevant for semi-strict string stability. This implies that u_1 should be chosen as the exogenous input and u_i as exogenous output in order to cast the string stability problem into the $\mathcal{H}_\infty$ synthesis framework. Again choosing the weighted distance error e_i' as additional exogenous output, the mixed-sensitivity $\mathcal{H}_\infty$ control problem now involves computing a stabilizing controller $K(s) = \begin{pmatrix} K_{\text{fb}}(s) & K_{\text{ff},1}(s) & K_{\text{ff},2}(s) \end{pmatrix}$ according to

$$\xi_i(s) = \begin{pmatrix} K_{\text{fb}}(s) & K_{\text{ff},1}(s) & K_{\text{ff},2}(s) \end{pmatrix} \begin{pmatrix} e_i(s) \\ u_{i-1}^*(s) \\ u_{i-2}^*(s) \end{pmatrix}, \tag{3.41}$$

such that $\|N_i(s)\|_{\mathcal{H}_\infty}$ is minimized, with

$$\begin{pmatrix} e_i'(s) \\ u_i(s) \end{pmatrix} = \begin{pmatrix} W_e(s)S_i(s) \\ \Theta_i(s) \end{pmatrix} u_1(s)$$
$$:= N_i(s)u_1(s). \tag{3.42}$$

Here, the sensitivity $S_i(s)$ is equal to (omitting the argument s for readability)

$$S_i = \tilde{S}G\big((1 - K_{\text{ff},1}D)\,\Theta_{i-1} - K_{\text{ff},2}D\Theta_{i-2}\big) \tag{3.43}$$

with $\tilde{S}$ as in (3.35), whereas $\Theta_i(s)$, $i \geq 3$, is equal to

$$\Theta_i = \tilde{S}H^{-1}\big((K_{\text{fb}}G + K_{\text{ff},1}D)\,\Theta_{i-1} + K_{\text{ff},2}D\Theta_{i-2}\big) \tag{3.44}$$

with $\Theta_1(s) = 1$ and $\Theta_2(s) = \Gamma_2(s)$ by definition. Assuming that the second vehicle, having only one preceding vehicle, is controlled using the one-vehicle look-ahead controller (3.39), it follows that $\Gamma_2(s) = \Gamma(s)$ according to (3.34).

The controller design thus naturally aims for semi-strict $\mathcal{L}_2$ string stability, subject to Condition 3.2, where the inequality (3.22a) is met by definition since $P_1(s) = 1$. As opposed to the one-vehicle look-ahead case, however, $N_i(s)$ now appears to depend on the vehicle index i, and so will the synthesized controller. In other words, the $\mathcal{H}_\infty$ optimal controller for a specific vehicle depends on the position in the platoon of that vehicle, which is undesired in view of the ad hoc platooning approach and, in addition, leads to a time-consuming controller synthesis procedure. This property is a direct consequence of the fact that a single-vehicle subsystem with an independent input cannot be isolated, as mentioned before. To overcome this limitation, a controller is synthesized for the third vehicle only, being the first vehicle in the string with two preceding vehicles, aiming for $\|N_3(s)\|_{\mathcal{H}_\infty} = 1$. This controller is then applied to all upstream vehicles $i \geq 4$ as well, after which the resulting string stability properties will be analyzed through the assessment of condition (3.22b).

Using the same motivation as before, $W_e(s) = W_e = 1$ is chosen. Then, the controller is synthesized with the model parameters from the previous subsection and a design time gap of $h = 1\,\mathrm{s}$, while employing a 3rd-order Padé approximation for the vehicle and the communication delay. In addition, $\Gamma(s)$ is approximated by $H^{-1}(s)$ (by substituting $K_{\mathrm{ff}}(s) = 1$ with communication delay $\theta = 0$) to decrease the order of the controller. As a result, the following reduced-order controller is obtained:

$$
\begin{aligned}
K_{\mathrm{fb}}(s) &= \frac{1.8517(s+23.22)(s+10)(s+1.39)(s+1)(s+0.3893)}{(s+23.97)(s+8.201)(s+2.783)(s+1.272)(s+1.185)} \\
K_{\mathrm{ff},1}(s) &= \frac{0.4299(s+23.22)(s+10.03)(s+1)(s^2+2.904s+3.617)}{(s+23.97)(s+8.201)(s+2.783)(s+1.272)(s+1.185)} \\
K_{\mathrm{ff},2}(s) &= \frac{0.2664(s+23.14)(s+10.49)(s+1)(s^2+2.411s+7.145)}{(s+23.97)(s+8.201)(s+2.783)(s+1.272)(s+1.185)}.
\end{aligned}
\tag{3.45}
$$

This controller realizes an internally stable system since the poles of $\Theta_3(s)$ are in the left half-plane, whereas the controller does not cancel the marginally stable poles of $G(s)$. Furthermore, $\|N_3(s)\|_{\mathcal{H}_\infty} = 1$ is obtained, which is confirmed in Figure 3.8(a), showing that $|S_3(j\omega)| \leq 1$ and $|\Theta_3(j\omega)| \leq 1$. In addition, Figure 3.8(b) shows the controller magnitudes $|K_{\mathrm{fb}}(j\omega)|$, $|K_{\mathrm{ff},1}(j\omega)|$, and $|K_{\mathrm{ff},2}(j\omega)|$, from which it can be concluded that a weighted feedforward of u_1 and u_2 is obtained. Note that $|K_{\mathrm{ff},1}(j\omega) + K_{\mathrm{ff},2}(j\omega)| \to 1$ for $\omega \to 0$.

For semi-strict $\mathcal{L}_2$ string stability, condition (3.22b) must hold, which requires to investigate $\|\Theta_i(s)\|_{\mathcal{H}_\infty}$ with $i \in \mathbb{N}$. This can be done by formulating (3.44) as a state-space model that is a discrete function of the vehicle index i. Introducing the state vector

$$
X_i(j\omega) = \begin{pmatrix} \Theta_{i-1}(j\omega) \\ \Theta_i(j\omega) \end{pmatrix}
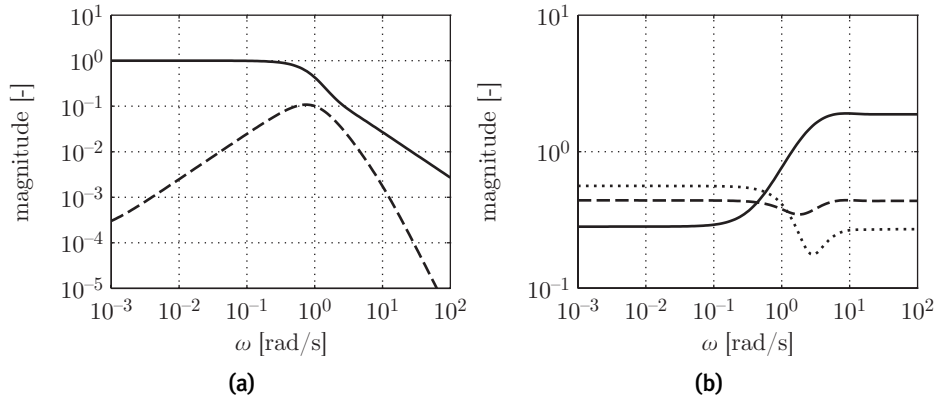\tag{3.46}
$$

Figure 3.8: Frequency response magnitude of (a) the LFT $N(j\omega)$: $|\Theta_3(j\omega)|$ (solid) and $|S_3(j\omega)|$ (dashed), and (b) the controller $K(j\omega)$: $|K_{\text{fb}}(j\omega)|$ (solid), $|K_{\text{ff},1}(j\omega)|$ (dashed), and $|K_{\text{ff},2}(j\omega)|$ (dotted).
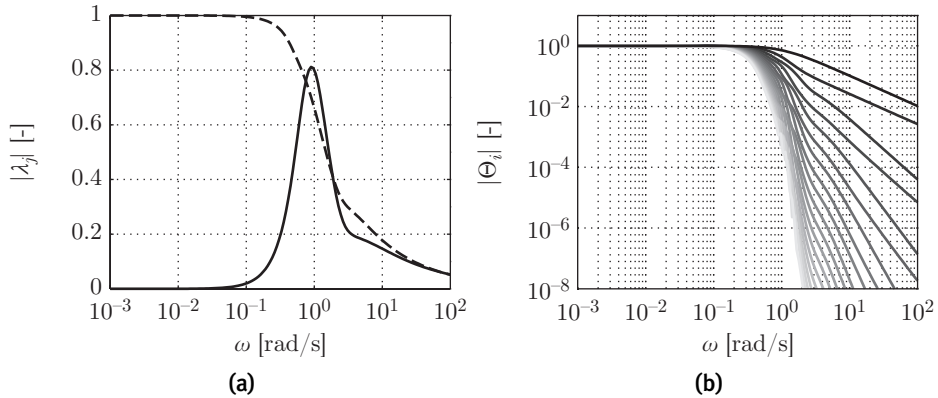

Figure 3.9: Frequency response magnitude of (a) the eigenvalues $\lambda_j(j\omega)$, $j = 1, 2$, of A and (b) $\Theta_i(j\omega)$ (black–light gray: $i = 2, 3, \ldots, 20$).

then yields the state-space model

$$X_{i+1}(j\omega) = A(j\omega)X_i(j\omega), \quad i \geq 2 \tag{3.47}$$

with system matrix

$$A(j\omega) = \begin{pmatrix} 0 & 1 \\ \tilde{S}H^{-1}K_{\text{ff},2}D & \tilde{S}H^{-1}\left(K_{\text{fb}}G + K_{\text{ff},1}D\right) \end{pmatrix} \tag{3.48}$$

and initial condition $X_2^{\mathsf{T}}(j\omega) = \begin{pmatrix} 1 & \Gamma(j\omega) \end{pmatrix}$. Both the state vector X_i and the system matrix A are complex functions of the frequency ω. Hence, the eigenvalues $\lambda_j(j\omega)$, $j = 1, 2$, of $A(j\omega)$ indicate the exponential stability properties of (3.47) pointwise in frequency, i.e., for each fixed value of ω. Figure 3.9(a) shows these
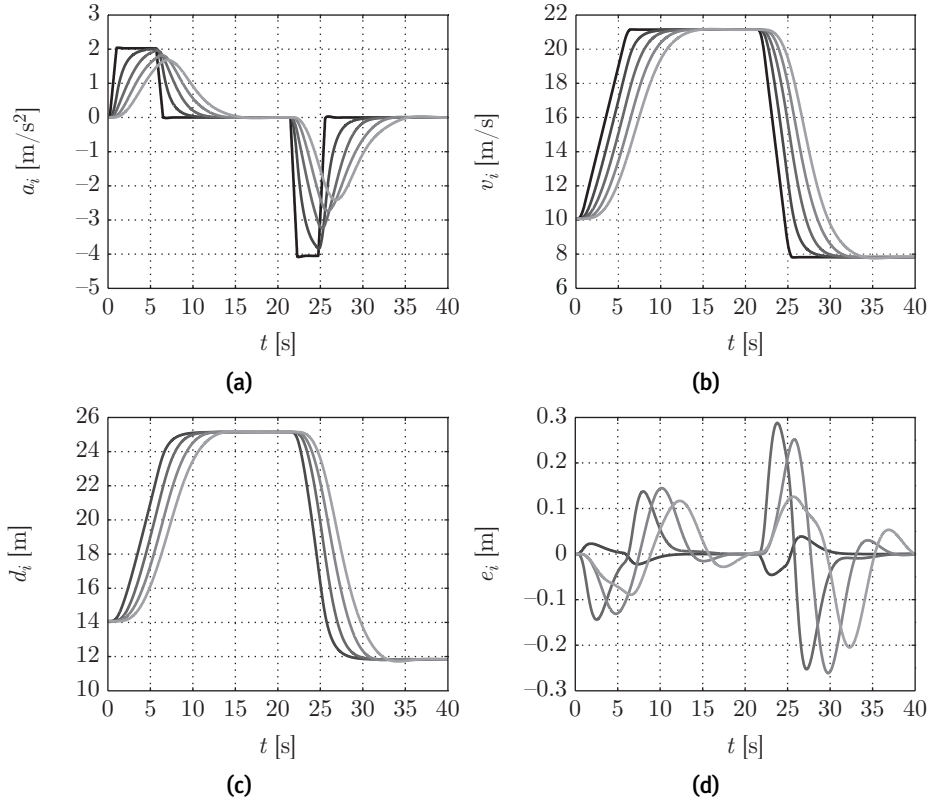
Figure 3.10: Time responses of (a) the acceleration $a_i(t)$ and (b) the velocity $v_i(t)$ (black–light gray: $i = 1, 2, \ldots, 5$); (c) the distance $d_i(t)$ and (d) the distance error $e_i(t)$ (dark–light gray: $i = 2, 3, 4, 5$).

eigenvalues, from which it can be concluded that they are inside the unit circle for all $\omega > 0$. For $\omega = 0$, it appears that $|\lambda_1(j0)| = 0$ and $|\lambda_2(j0)| = 1$, implying that both states remain at their initial value $\Gamma(j0) = 1$. Hence, for all $\omega > 0$, $\Theta_i(j\omega) \to 0$ for $i \to \infty$, which suggests semi-strict $\mathcal{L}_2$ string stability. The latter is confirmed by numerical evaluation of $|\Theta_i(j\omega)|$ for various values of i using (3.47) (or, similarly, (3.44)) with initial conditions $\Theta_1(j\omega) = 1$ and $\Theta_2(j\omega) = \Gamma(j\omega)$, the result of which is shown in Figure 3.9(b) for $i = 2, 3, \ldots, 20$.

Figure 3.10 shows the time response of 5 vehicles to a smooth velocity step of vehicle 1, which is the same as the one used in Figure 3.6, obtained with $h = 1$ s. It appears that the response of the acceleration, the velocity, and the distance are very similar to those of the one-vehicle look-ahead controlled system, as shown in Figure 3.6. The distance error response, however, shows significantly larger error amplitudes, although asymptotic tracking behavior is certainly obtained. Note that, using (3.30) and (3.40), the string stability complementary sensitivity

is equal to

$$\Gamma_i(s) = \Theta_i(s)\Theta_{i-1}^{-1}(s) \tag{3.49}$$

based on which it can be established that the controlled system is not strictly $\mathcal{L}_2$ string stable (not shown here). Nevertheless, $|\Gamma_i(j\omega)|$ slightly exceeds 1 only for $i \geq 10$ and only at frequencies beyond the bandwidth of $\Theta_i(j\omega)$, which is why this effect only becomes visible in the distance error responses.

In summary, $\mathcal{H}_\infty$ optimal control allows for the explicit inclusion of the (semi-)strict $\mathcal{L}_2$ string stability requirement for linear systems. However, string stability cannot be *a priori* guaranteed since the controller synthesis procedure only minimizes the $\mathcal{H}_\infty$ norm of the relevant transfer function without guarantee that the minimum will be smaller than or equal to 1. Nevertheless, the chosen norm requirement appears to be fulfilled in both the one- and the two-vehicle look-ahead case, which is basically due to the fact that the norm requirement on the sensitivity $S(s)$ appears to be less restrictive than the norm requirement on $\Gamma(s)$ or $\Theta_i(s)$. In addition, there is no fundamental limitation preventing the $\mathcal{L}_2$ string stability requirement from being fulfilled. Such a limitation would, e.g., have occurred in case of a constant distance spacing policy (Naus et al., 2010). Finally, it is noted that the two-vehicle look-ahead solution is scalable, in the sense that the topology can be straightforwardly extended so as to include any number of preceding vehicles.

In addition to the controller synthesis aspects of both control strategies and the controller performance in frequency and time domain, the relation between the communication topology employed by both controllers and the resulting string stability properties is investigated in the next subsection.

3.6.3   Performance comparison

Based on the results so far, the two-vehicle look-ahead strategy does not seem to improve upon the string stability properties of the one-vehicle look-ahead strategy for this particular case study. To further compare both communication topologies, the influence of the time gap h on string stability in relation to the communication delay θ is investigated.

With respect to the one-vehicle look-ahead controller, it appears that the factor $H^{-1}(s) = 1/(hs + 1)$ in $\Gamma(s)$, see (3.34), decreases the peak value of the magnitude of the remaining transfer functions in $\Gamma(s)$, the effect of which is smaller for decreasing values of h. Hence, in the presence of a communication delay $\theta > 0$, a minimum time gap $h_{\min}$ must exist that realizes string stability[7]. Indeed, it appears that, with $\theta = 0.02$ s, the controlled system is string stable for $h \geq h_{\min} = 0.11$ s. From a practical perspective, this implies that the driver can choose any time gap $h \geq 0.11$ s without compromising individual vehicle stability or string stability, while using the same controller[8].

---

[7]Without communication delay, i.e., $D(s) = 1$, while substituting $K_{\text{ff}}(s) = 1$, $\Gamma(s) = H^{-1}(s)$ is obtained, such that $\|\Gamma(s)\|_{\mathcal{H}_\infty} = 1$, regardless of the value of the time gap h.

[8]In addition, because of that same factor $H^{-1}(s)$ in $\Gamma(s)$, the vehicle has a faster response to velocity changes of the preceding vehicle at smaller time gaps, which conforms to expected behavior from a driver point of view.
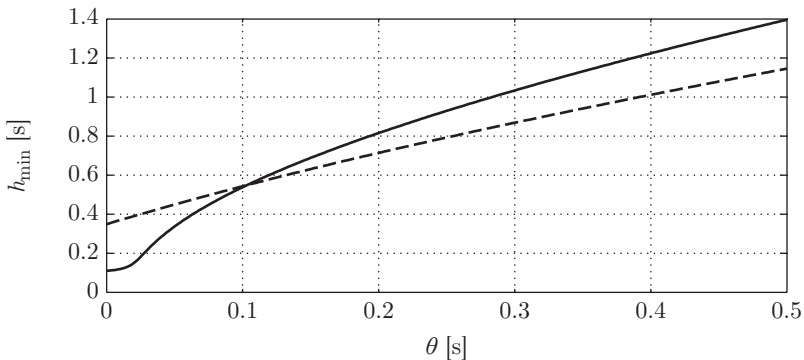
Figure 3.11: Minimum string-stable time gap $h_{\min}$ as a function of communication delay θ for one-vehicle and two-vehicle look-ahead control (solid and dashed, respectively).

For the two-vehicle look-ahead topology, however, a significantly larger value of $h_{\min} = 0.35\,\mathrm{s}$ is found. Intuitively, this result can be understood as follows: Without communication delay ($D(s) = 1$), while approximating the feedforward transfer function by $K_{\mathrm{ff}}(s) = 1$, the one-vehicle look-ahead sensitivity (3.33) is equal to $S = 0$, indicating perfect following behavior. Consequently, additional information, which is obtained from the second preceding vehicle, would not yield additional benefit. On the other hand, for increasing communication delay, one may expect to benefit from the information of the second preceding vehicle at some point, because it provides "preview" disturbance information, given the fact that the delay is (approximately) identical for all vehicles. This intuition is confirmed by determining the minimum string-stable time gap $h_{\min}$ as a function of the communication delay θ for both communication topologies, the result of which is shown in Figure 3.11. This figure has been obtained by taking a fixed value for θ and then searching for the smallest value of h, such that $\|\Gamma(s)\|_{\mathcal{H}_\infty} = 1$ for the one-vehicle look-ahead case, or $\|\Theta_3(s)\|_{\mathcal{H}_\infty} = 1$ for the two-vehicle look-ahead case. Indeed, it appears that above a certain break-even communication delay, here about 0.1 s, the two-vehicle look-ahead topology allows for smaller time gaps in view of string stability.

It can therefore be concluded that a multiple-vehicle look-ahead scheme provides a benefit with respect to minimum string-stable time gap when the communication delay exceeds a certain threshold. Hence, it may be worthwhile, in practice, to actively switch between communication topologies, depending on the actual latency of the wireless communication.

Another benefit of multiple-vehicle look-ahead is the fact that it provides a certain level of robustness against non-communicating vehicles. This can be illustrated by comparison of the one- and the two-vehicle look-ahead controller implemented in vehicle 3, in case vehicle 2 does not communicate, i.e., $u_2^* = 0$. The result is illustrated in Figure 3.12, showing the magnitude $|\Theta_3(j\omega)|$ and the distance error response $e_3(t)$ as a result of vehicle 1 performing the same smooth velocity step as before (with $h = 1\,\mathrm{s}$). It can be clearly seen that both the
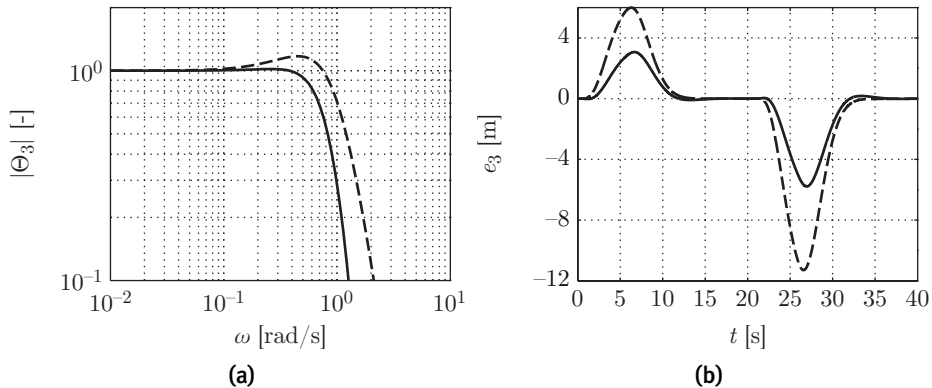
Figure 3.12: Response of vehicle 3 without vehicle 2 communication, employing the two-vehicle look-ahead topology (solid) and the one-vehicle look-ahead topology (dashed); (a) magnitude $|\Theta_3(j\omega)|$ and (b) distance error $e_3(t)$.

peak value of $|\Theta_3(j\omega)|$ and the amplitude of $e_3(t)$ are significantly smaller for the two-vehicle look-ahead controller. The two-vehicle look-ahead strategy thus outperforms the one-vehicle look-ahead strategy in terms of robust fault tolerance with respect to failures of the wireless link used for CACC implementation.

3.7 Experimental validation

To validate the theoretical results, both controllers have been implemented in a platoon of three passenger vehicles, as shown in Figure 3.13, equipped with a prototype CACC system. This system encompasses a forward-looking radar, wireless communications according to the ETSI ITS G5 standard (Ström, 2011), and a computer system that executes the CACC controller and allows for computer-controlled vehicle acceleration through interaction with the native vehicle control system; see Ploeg et al. (2011) and Chapter 5 of this thesis for more details. This section first presents experimentally obtained frequency responses to validate the string stability properties, after which measured time responses are shown to validate controller performance in general.

3.7.1 Frequency response experiments

Experiment design

The lead vehicle is required to follow a predefined velocity profile $v_r(t)$, which is designed to excite the follower vehicles in the frequency region of interest for the assessment of string stability. To this end, a "random-phase multisine signal" (Pintelon and Schoukens, 2012) is generated as follows. First the spectral properties of the velocity variations $v_\Delta(t)$ are defined by choosing the frequency-domain magnitudes M_n:

$$M_n = |v_\Delta(j\omega_n)|, \quad n = 0, 1, \ldots, \tfrac{N}{2} - 1, \tag{3.50}$$

Figure 3.13: Experimental vehicle platoon, consisting of three CACC-equipped passenger vehicles.

where the discrete frequency $\omega_n = n\Delta\omega$ is an integer multiple of a chosen frequency interval $\Delta\omega \approx 0.05\,\text{rad/s}$. N is the even number of frequency intervals such that $N\Delta\omega = \omega_\text{s}$, where $\omega_\text{s} = 314.16\,\text{rad/s}$ (50 Hz) is the sampling frequency. Hence, the maximum frequency in (3.50) is just below $\frac{N}{2}\Delta\omega = \frac{1}{2}\omega_\text{s}$, which corresponds to the Nyquist frequency. The sequence M_n is chosen such that the frequency interval $[\Delta\omega, 5]\,\text{rad/s}$ is covered, while emphasizing the region $[2\Delta\omega, 3]\,\text{rad/s}$ because it is expected that string stability may be violated in this interval. The resulting sequence is shown in Figure 3.14(a). Note that $M_0 = 0$, avoiding a static component.

Upon choosing a uniformly distributed random phase $\varphi_n \in [0, 2\pi)$ and concatenating the conjugate mirrored sequence to create a conjugate symmetric series, the inverse Fast Fourier Transform is applied, yielding the time-domain signal

$$v_\Delta(t_k) = \frac{2}{N}\sum_{n=0}^{\frac{N}{2}-1} M_n \cos(\omega_n t_k + \varphi_n), \quad k = 0, 1, \ldots, N-1 \tag{3.51}$$

at time $t_k = kt_\text{s}$, where $t_\text{s} = 2\pi/\omega_\text{s} = 0.02\,\text{s}$ is the sampling time interval. From (3.51), it directly follows that a time period $T = 2\pi/\omega_1 = 2\pi/\Delta\omega = 125.7\,\text{s}$ is required to capture at least one period of all frequencies, thus imposing the minimum test duration. The reference velocity profile $v_\text{r}(t_k)$ is now chosen according to

$$v_\text{r}(t_k) = Wv_\Delta(t_k) + \bar{v}, \tag{3.52}$$

where $\bar{v} = 15\,\text{m/s}$ is the nominal test velocity and $W = 160$ scales the velocity amplitude, such that the acceleration covers the interval $[-3, 3]\,\text{m/s}^2$. Figure 3.14(b) shows a part of $v_\text{r}(t_k)$. The test signal used in the experiments is finally constructed by repeating the excitation signal in (3.52) 4 times to improve the test
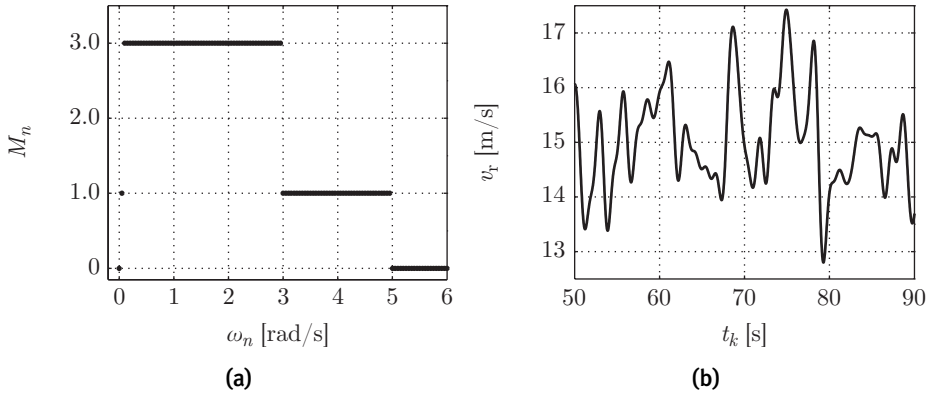
Figure 3.14: Test signal: (a) magnitude $M_n = |v_\Delta(j\omega_n)|$ and (b) excerpt of the corresponding time-domain signal $v_r(t_k)$.

results, after an initial platoon formation phase during which steady-state platoon behavior is obtained at the nominal velocity $\bar{v}$.

The excitation signal is applied as the desired velocity for a proportional velocity-feedback controller implemented in the lead vehicle, whereas the velocity-tracking performance is greatly enhanced by adding a feedforward signal u_{ff} on the vehicle's input, which is derived from (3.4), according to

$$u_{ff}(t_k) = \tau \ddot{v}_r(t_k + \theta) + \dot{v}_r(t_k + \theta), \tag{3.53}$$

thus taking care that the frequency content of the velocity profile (3.52) remains intact. The derivatives of v_r in (3.53) are obtained by numerical differentiation, which is sufficiently accurate considering the smoothness of v_r. Note that the same velocity controller was used in the time-domain simulations presented in Section 3.6.

String stability results

Based on earlier experiments, the round-trip time of a wireless message appeared to be on average equal to $40\,\mathrm{ms}$, which seems to be primarily determined by the update rate of $25\,\mathrm{Hz}$ of the wireless communication network. Consequently, $\theta \approx 0.02\,\mathrm{s}$, as used earlier in the controller design.

The first experiment is conducted with two vehicles, focusing on the one-vehicle look-ahead topology. Here, the lead vehicle is velocity controlled with the aforementioned desired velocity profile and the follower vehicle is equipped with the one-vehicle look-ahead controller (3.39). Upon measuring the communicated input $u_1^*(t_k)$ of the lead vehicle and the local input $u_2(t_k)$ of the follower vehicle, the magnitude of the frequency response function of the string stability complementary sensitivity $\Gamma(j\omega)$ is estimated, employing Welch's averaged periodogram method (Stoica and Moses, 1997), using 4 non-overlapping, rectangular windows of length N. Note that the delayed lead vehicle input $u_1^*(t_k)$ can be used instead of the real input $u_1(t_k)$ since only the magnitude of $\Gamma(j\omega)$ is of interest.
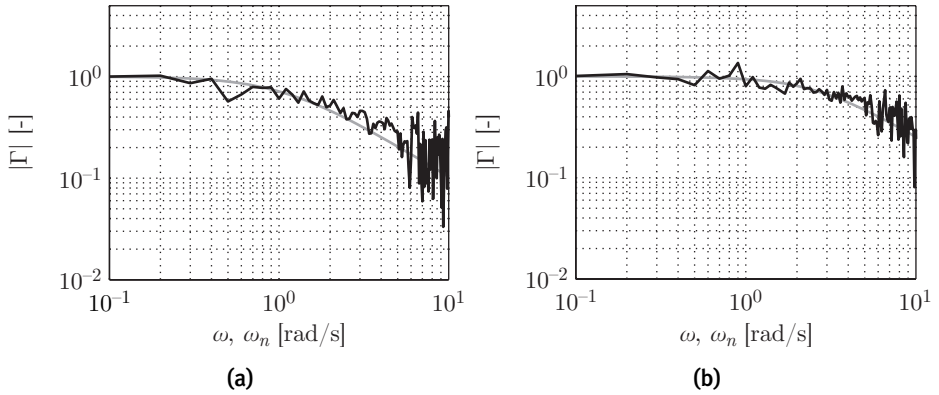
Figure 3.15: Frequency response magnitude with (a) $h = 1.0\,\mathrm{s}$ and (b) $h = 0.4\,\mathrm{s}$; estimated magnitude $|\hat{\Gamma}(j\omega_n)|$ (black) and theoretical magnitude $|\Gamma(j\omega)|$ (gray).

Figure 3.15(a) shows the estimated magnitude $|\hat{\Gamma}(j\omega_n)|$ as well as the theoretical magnitude $|\Gamma(j\omega)|$ according to (3.34) in case the design time gap $h = 1\,\mathrm{s}$ is applied. Despite the noise level due to estimation inaccuracy, this figure clearly shows the similarity between both frequency response magnitudes, thus validating the theoretical results. Note that the quality of the estimate $|\hat{\Gamma}(j\omega_n)|$ strongly degrades for $\omega_n > 5\,\mathrm{rad/s}$, which is of course due to the fact that the test signal does not contain any frequency content in this region.

A second, similar experiment is carried out with a time gap of $h = 0.4\,\mathrm{s}$. As mentioned in Section 3.6.1, strict $\mathcal{L}_2$ string stability is expected for this value, which appears to be consistent with the frequency response magnitude shown in Figure 3.15(b). It must, however, be mentioned that the experimental assessment of string stability may be sensitive to estimation errors, as can be seen in Figure 3.15(b), which is caused by the fact that the relevant transfer function magnitude, here $|\Gamma(j\omega)|$, approaches 1 for $\omega \to 0$, inherent to the vehicle-following objective.

The next experiment focusses on the two-vehicle look-ahead topology and is, therefore, carried out with 3 vehicles. The lead vehicle is again velocity controlled, with the same velocity reference profile as before, whereas the first follower vehicle is controlled by the one-vehicle look-ahead controller (3.39) and the second follower vehicle by the two-vehicle look-ahead controller (3.45). The resulting estimated frequency response magnitude $|\hat{\Theta}_3(j\omega_n)|$ as well as the theoretical results using (3.44) are shown in Figure 3.16(a) for $h = 1\,\mathrm{s}$ and in Figure 3.16(b) for $h = 0.4\,\mathrm{s}$. Again, the experimental results are consistent with the theoretical results, especially for $h = 0.4\,\mathrm{s}$, which just yields semi-strict $\mathcal{L}_2$ string stable behavior, as mentioned in Section 3.6.2. Hence, the experiments validate the theory as presented in this chapter for both the one- and the two-vehicle look-ahead topology.
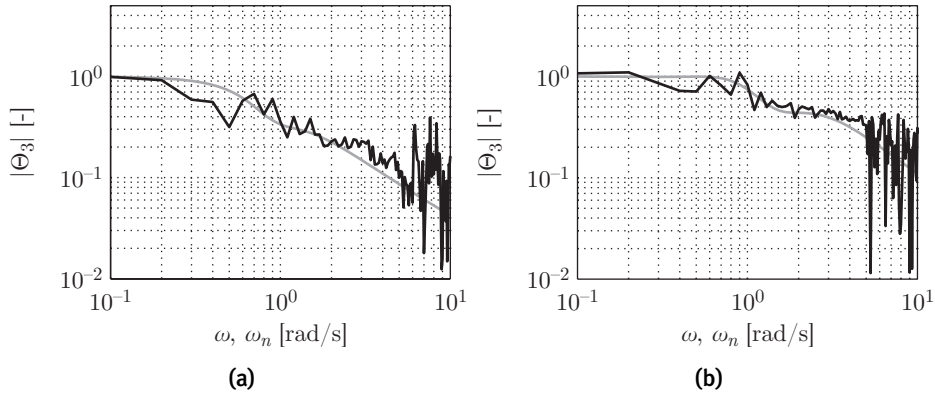
Figure 3.16: Frequency response magnitude with (a) $h = 1.0\,\text{s}$ and (b) $h = 0.4\,\text{s}$; estimated magnitude $|\hat{\Theta}_3(j\omega_n)|$ (black) and theoretical magnitude $|\Theta_3(j\omega)|$ (gray).

3.7.2   Time response experiments

The second type of experiment aims to validate the simulated time responses as shown in Section 3.6. First, the simulation shown in Figure 3.6 for the one-vehicle look-ahead controlled system with $h = 1\,\text{s}$ is repeated, in practice, with three vehicles, where the first vehicle is velocity controlled with the same controller as used in the simulation, subject to the same desired velocity profile. Figure 3.17 shows the measured acceleration, velocity, distance, and distance error, which can be directly compared with the simulation results in Figure 3.6.

The acceleration, velocity, and distance are clearly very similar to those shown in the simulation. In particular the acceleration directly indicates strict $\mathcal{L}_2$ string stability since the acceleration amplitude decreases in upstream direction. Furthermore, there is no overshoot during the acceleration section of the test scenario and (almost) no undershoot at the rather strong deceleration, thus ensuring safe behavior within the operational range of the CACC system.

The distance error, however, appears to be significantly larger than in the simulation. This is partly caused by measurement noise: even in the constant-velocity sections, the distance error is already in the order of magnitude of $0.3\,\text{m}$. Yet another cause can be found as follows. It is known that, due to the feedforward of the preceding vehicle's input, the system behavior is sensitive to inhomogeneity of the vehicle string, i.e., uncertainties in the vehicle model (3.4) that vary along the string. Even though all test vehicles are of the same type, these inhomogeneities occur, among others, because the batteries of the hybrid driveline do not have the same state of charge. Since particularly the second vehicle in the string shows a relatively large distance error, it is therefore believed that the first vehicle behaves slightly differently than the other vehicles, negatively influencing the input feedforward for the second vehicle. This also explains why the velocity as well as the distance of the second vehicle show a slight undershoot at the end of the braking action, whereas the third vehicle in the string does not exhibit this effect. Nevertheless, taking into account the relatively high level of acceleration

Figure 3.17: Measured one-vehicle look-ahead CACC time responses of (a) the accelera-
tion $a_i(t)$ and (b) the velocity $v_i(t)$ (black–light gray: $i = 1, 2, 3$); (c) the distance $d_i(t)$
and (d) the distance error $e_i(t)$ (black, light gray: $i = 2, 3$).

and deceleration, it can be concluded that the designed controller performs at a
satisfactory level.

The same experiment is performed with the two-vehicle look-ahead controller,
the results of which are shown in Figure 3.18, to be compared to Figure 3.10. The
aforementioned remarks also apply here, apart from the fact that the inhomo-
geneity now influences both follower vehicles due to the communication topology.
It is noted that the velocity and the distance are slightly less damped, compared
in the one-vehicle look-ahead case. This is also observed in Figure 3.10.

3.8 Conclusion

String stability is an important requirement for the design of controllers for ve-
hicle platoons, because it allows for short intervehicle following distances and
scalability of the platoon with respect to its length. The application of the $\mathcal{H}_\infty$
synthesis framework appeared to enable the explicit inclusion in the controller
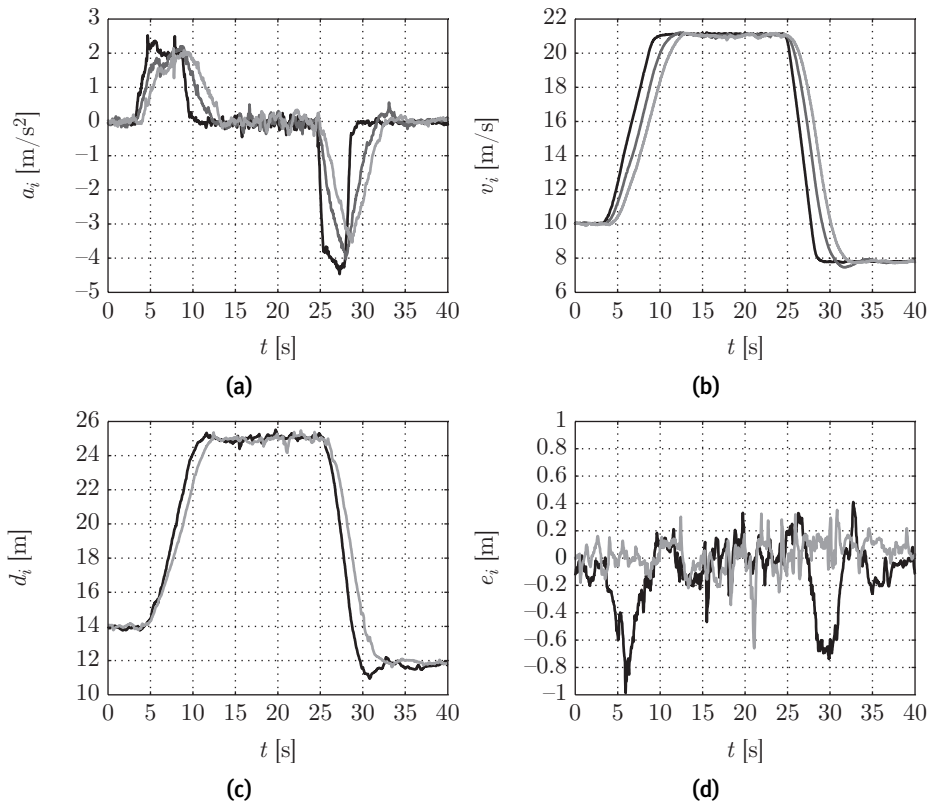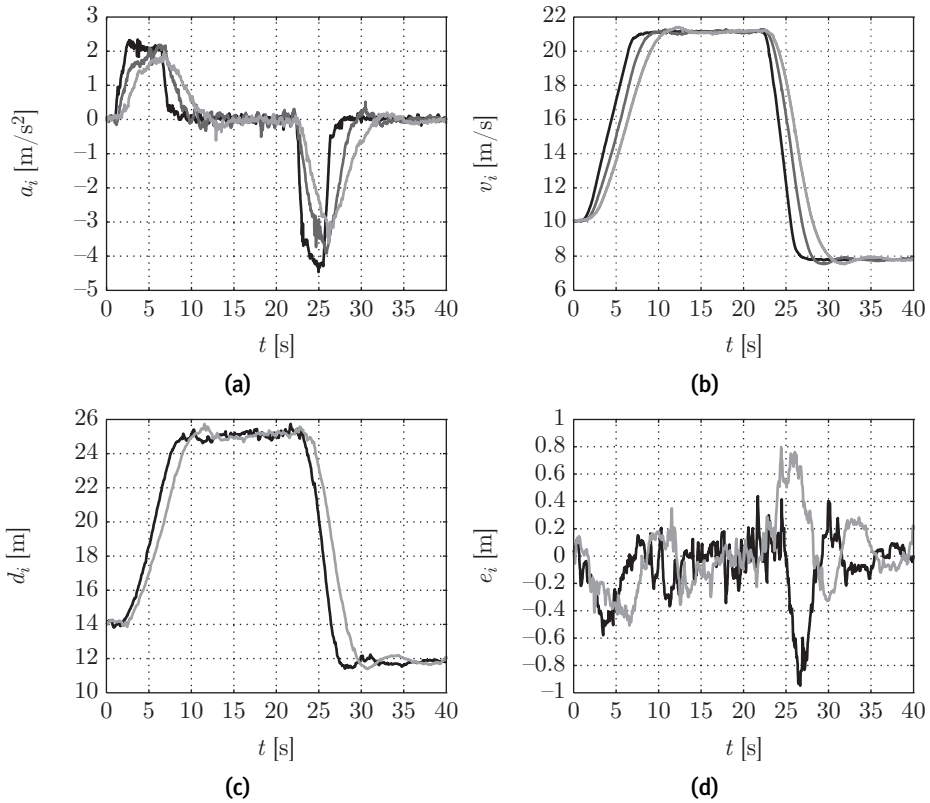
Figure 3.18: Measured two-vehicle look-ahead CACC time responses of (a) the accelera-
tion $a_i(t)$ and (b) the velocity $v_i(t)$ (black–light gray: $i = 1, 2, 3$); (c) the distance $d_i(t)$
and (d) the distance error $e_i(t)$ (black, light gray: $i = 2, 3$).

design specification of the $\mathcal{L}_2$ string stability requirement for linear cascaded sys-
tems, in general, and vehicle platoons in particular. As a result, strict (pre-
ceding vehicle to follower vehicle) $\mathcal{L}_2$ string-stable behavior was obtained for a
one-vehicle look-ahead communication topology, whereas semi-strict (lead vehi-
cle to follower vehicle) $\mathcal{L}_2$ string-stable behavior was realized for a two-vehicle
look-ahead topology. In addition, it was found that the two-vehicle look-ahead
topology only provides a benefit with respect to minimum string-stable time gap
when the communication delay exceeds a certain threshold. Moreover, the two-
vehicle look-ahead controller is more robust against the presence of vehicles not
equipped with wireless communication or for wireless link failures.

Both controllers were evaluated, in practice, using a platoon of three passenger
vehicles, which were specifically instrumented to test platooning controllers. A
frequency- and time-domain analysis of the test results validated the theoretical
results, while illustrating the practical feasibility of the presented approach at the
same time.

Besides the controller synthesis itself, this chapter briefly touched upon the loss of wireless communication over an extended period of time, albeit without specifically taking this issue into account in the controller design. Since wireless communication is inherently subject to impairments such as packet loss, it is of paramount importance that the vehicle-following controller is robust against the loss of communication, or, at least, allows for some form of graceful degradation. To this end, the next chapter proposes an alternative control strategy, which is based on estimation of the actual acceleration of the preceding vehicle in the case that its desired acceleration cannot be communicated. The resulting platoon behavior is then analyzed with respect to string stability, from which it appears that this strategy can be truly characterized as a form of "degraded" CACC.

Graceful degradation of Cooperative Adaptive Cruise Control subject to unreliable wireless communication[1]

Abstract   Cooperative Adaptive Cruise Control (CACC) employs wireless intervehicle communication, in addition to onboard sensors, to obtain string-stable vehicle-following behavior at small intervehicle distances. As a consequence, however, CACC is vulnerable to communication impairments such as latency and packet loss. In the latter case, it would effectively degrade to conventional Adaptive Cruise Control (ACC), thereby increasing the minimal intervehicle distance needed for string-stable behavior. To partially maintain the favorable string stability properties of CACC, a control strategy for graceful degradation of one-vehicle look-ahead CACC is proposed, based on estimating the preceding vehicle's acceleration using the onboard sensors. Whenever needed, the CACC can switch to this strategy, as an alternative to the desired acceleration transmitted through wireless communication for this type of CACC. It is shown through simulations and experiments that the proposed strategy results in a noticeable improvement of string stability characteristics, when compared to the situation in which ACC is used as a fallback scenario.

4.1   Introduction

Cooperative Adaptive Cruise Control (CACC) can be characterized as a vehicle-following control system that automatically accelerates and decelerates so as to keep a desired distance to the preceding vehicle (Rajamani and Zhu, 2002). To this end, onboard sensors are employed, such as radar, that measure the intervehicle distance and relative velocity. In addition, extra information of the preceding vehicle(s), e.g., the desired acceleration, is cast through a wireless communication link. As a consequence, the performance in terms of minimizing the intervehicle distance while guaranteeing string stability, i.e., shock wave attenuation

---

[1]This chapter is based on Ploeg et al. (2013).

in upstream direction, is significantly enhanced when compared to conventional Adaptive Cruise Control (ACC), which is operated without a wireless communication link (Naus et al., 2010). As a result, traffic throughput is increased, while maintaining a sufficient level of safety (Shladover et al., 2012), although string-stable behavior *per se* does not guarantee the avoidance of collisions. In addition, significant fuel savings are possible, especially for trucks (Ramakers et al., 2009).

Inherent to the CACC concept is its vulnerability to unreliable wireless communication due to high latency or packet loss, which will inevitably occur with an increasing amount of communicating vehicles employing the same network. In Eckhoff et al. (2013), for instance, it was found that the ratio of correctly received packets drops to values below 10% on a motorway junction with high traffic density, assuming all vehicles are equipped with wireless communication devices. The relation between latency or packet loss and CACC performance in terms of string stability already attracted interest, see, e.g., Seiler and Sengupta (2005), which focusses on $\mathcal{H}_\infty$ controller synthesis taking packet loss into account, the experimental study described in Lei et al. (2012), and the analysis framework incorporating uncertain sampling intervals and delays as developed in Öncü (2014). In contrast to the existing literature on this topic, the focus in this chapter is on how to cope with losing the wireless communication link for an extended period of time. In this case, while not taking any compensating actions, CACC inherently degrades to ACC, which requires a significantly larger time gap to guarantee string-stable behavior. As an example, Ploeg et al. (2011) shows that the minimum string-stable time gap increases from $0.7\,\mathrm{s}$ (depending on the latency of the wireless communication link) to more than $3\,\mathrm{s}$. It is, therefore, important to have an alternative control technique that exhibits string-stable behavior for a less dramatic increase in time gap, which comes into action when a failure in the wireless communication is detected (or when there is no network in the first place). To this end, this chapter presents a fallback strategy to gracefully degrade functionality of a one-vehicle look-ahead CACC, based on estimating the preceding vehicle's acceleration using the available data from an onboard sensor.

This chapter is organized as follows. Section 4.2 first provides an overview of the adopted CACC and the notion of string stability used in the present work. Next, Section 4.3 introduces the graceful degradation strategy, upon which Section 4.4 analyses the string stability properties of the controlled system, in comparison to those of ACC and CACC. Section 4.5 then presents experimental results obtained with three CACC-equipped passenger vehicles. Finally, Section 4.6 summarizes the main conclusions.

4.2   Control of vehicle platoons

Consider a homogeneous platoon of m vehicles, as shown in Figure 4.1, where the vehicles are enumerated with index $i = 1, \ldots, m$, with $i = 1$ indicating the lead vehicle. From the perspective of road usage efficiency, it is desired that a short intervehicle distance d_i is maintained within this platoon. However, this can only be done by regulating the intervehicle distances in an automatic way, i.e., by using
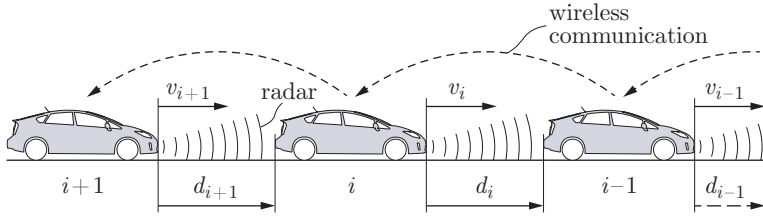
Figure 4.1: A homogeneous platoon of vehicles equipped with CACC.

a controller to guarantee that the longitudinal distance of the vehicles is regulated to a desired value. ACC addresses this need with the help of vehicle measurement devices, e.g., radar or lidar, which measure the relative velocity and the distance with respect to the preceding vehicle. However, the main weakness of ACC is its inability to attenuate traffic shock waves in an upstream direction, caused by, e.g., sudden braking or velocity decrease by a vehicle within the platoon, unless a relatively large intervehicle distance is chosen (Naus et al., 2010). This property of shockwave attenuation is referred to as string stability (Seiler et al., 2004), and is formally introduced in the following subsection.

4.2.1 String stability of a vehicle platoon

In the literature, three main directions towards defining the notion of string stability can be distinguished: 1) a formal Lyapunov-stability approach (Swaroop and Hedrick, 1996), 2) a stability approach for spatially-invariant linear systems (Curtain et al., 2009), and 3) a performance-oriented frequency-domain approach (Rajamani and Zhu, 2002; Lu and Hedrick, 2004). Due to its capability of offering controller synthesis tools, the last approach is more often used in the literature. In Ploeg et al. (2014b), an overview of the most relevant literature in this respect is given, based on which a general string stability definition is proposed and, based on this generic definition, string stability conditions for linear unidirectionally-coupled homogeneous systems are given that correspond to the conditions used in the performance-oriented approach. This subsection briefly summarizes these conditions.

Let the homogeneous vehicle platoon, in which all follower vehicles are controlled by a one-vehicle look-ahead CACC, be formulated by the following state-space model (omitting the time argument t for readability):

$$\begin{pmatrix} \dot{x}_1 \\ \dot{x}_2 \\ \vdots \\ \dot{x}_m \end{pmatrix} = \begin{pmatrix} A_0 & & & \text{O} \\ \tilde{A}_1 & \tilde{A}_0 & & \\ & \ddots & \ddots & \\ \text{O} & & \tilde{A}_1 & \tilde{A}_0 \end{pmatrix} \begin{pmatrix} x_1 \\ x_2 \\ \vdots \\ x_m \end{pmatrix} + \begin{pmatrix} B_0 \\ 0 \\ \vdots \\ 0 \end{pmatrix} u_1 \tag{4.1}$$

or, in short,

$$\dot{x} = Ax + Bu_1 \tag{4.2}$$

with $x^{\mathrm{T}} = \begin{pmatrix} x_1^{\mathrm{T}} & x_2^{\mathrm{T}} & \dots & x_m^{\mathrm{T}} \end{pmatrix}$, and the matrices A and B defined accordingly. x_i, $i \in S_m$, is the state vector of vehicle i (typically containing distance or distance error, velocity, acceleration, and possibly additional variables), with $S_m = \{i \in \mathbb{N} \mid 1 \leq i \leq m\}$ denoting the set of all vehicles in a platoon of length $m \in \mathbb{N}$. u_1 is the external input, which, in this case, is the input of the *uncontrolled* lead vehicle. A_0 and B_0 are the system matrix and input matrix, respectively, of this lead vehicle, whereas $\tilde{A}_0$ and $\tilde{A}_1$ are the system and "input" matrix, respectively, of the *controlled* follower vehicles. In addition, consider linear output functions according to

$$y_i = C_i x, \quad i \in S_m, \tag{4.3}$$

where y_i is the output of vehicle i, and C_i the corresponding output matrix. The model (4.2), (4.3), which will be further detailed in Section 4.2.2, is considered $\mathcal{L}_p$ *string stable* if all outputs y_i are bounded (in the $\mathcal{L}_p$ sense), for a bounded input u_1 and bounded initial condition perturbations $x(0)$, with $m \to \infty$, i.e., infinite string length. Hence, $y_i(t)$ must be bounded for all $i \in \mathbb{N}$ and for all $t \geq 0$. If, in addition,

$$\|y_i(t) - C_i \bar{x}\|_{\mathcal{L}_p} \leq \|y_{i-1}(t) - C_{i-1}\bar{x}\|_{\mathcal{L}_p}, \quad \forall i \in \mathbb{N}\backslash\{1\}, \tag{4.4}$$

where $\bar{x}$ denotes the equilibrium state of (4.2) with $u_1 \equiv 0$ and $\|\cdot\|_{\mathcal{L}_p}$ denotes the signal p-norm, the interconnected system is said to be *strictly $\mathcal{L}_p$ string stable*.

Remark 4.1. For linear homogeneous cascaded systems with a unidirectional coupling, and with a scalar input u_1 and scalar outputs y_i, the notions of $\mathcal{L}_p$ string stability and strict $\mathcal{L}_p$ string stability are equivalent (Ploeg et al., 2014b). ◆

Reformulating (4.2), (4.3) in the Laplace domain, while exclusively focussing on input–output behavior, yields

$$y_i(s) = P_i(s)u_1(s), \quad i \in S_m, \tag{4.5}$$

where $y_i(s)$ and $u_1(s)$, $s \in \mathbb{C}$, denote the Laplace transforms of $y_i(t)$ and $u_1(t)$, respectively, and $P_i(s) = C_i(sI - A)^{-1}B$. Assuming that the system (4.5) is square and functionally controllable (i.e., $P_i^{-1}(s)$ exists for all $i \in S_m$), the *string stability complementary sensitivity* (SSCS) is defined according to

$$\Gamma_i(s) := P_i(s)P_{i-1}^{-1}(s) \tag{4.6}$$

such that

$$y_i(s) = \Gamma_i(s)y_{i-1}(s). \tag{4.7}$$

Adopting the $\mathcal{L}_2$ signal norm (i.e., $p = 2$), the following condition for strict $\mathcal{L}_2$ string stability holds (Ploeg et al., 2014b).

Condition 4.1 (Strict $\mathcal{L}_2$ String Stability). *The system* (4.2), (4.3), *with Laplace-domain representation* (4.5), *is strictly $\mathcal{L}_2$ string stable if and only if*

$$\begin{aligned} &\|P_1(s)\|_{\mathcal{H}_\infty} < \infty \\ &\|\Gamma_i(s)\|_{\mathcal{H}_\infty} \leq 1, \quad \forall i \in \mathbb{N}\backslash\{1\}, \end{aligned} \tag{4.8}$$

where $\Gamma_i(s)$ is the SSCS according to (4.6) *and $\|\cdot\|_{\mathcal{H}_\infty}$ denotes the $\mathcal{H}_\infty$ norm.*

As mentioned before, ACC requires a large time gap to obtain string-stable behavior. As a result, in the early 90's, the concept of platooning with the help of wireless information has been introduced (Sheikholeslam and Desoer, 1990). Initially, the control strategies were based on the concept of a well-defined platoon, meaning that a platoon leader is present (and all platoon members are known), thereby allowing for the possibility to employ communicated lead vehicle information. In everyday traffic, however, it may be more feasible to adopt the concept of *ad hoc* platooning, i.e., without designated leader and members, similar to ACC. This approach led to control strategies which are commonly referred to as Cooperative Adaptive Cruise Control (CACC). The following subsection presents an overview of the CACC strategy employed in this paper.

4.2.2 Cooperative Adaptive Cruise Control

The objective of CACC is to guarantee that, within a string of vehicles, the intervehicle distances d_i, $i \in S_m \backslash \{1\}$, are regulated to a safe but small value. In addition, this string should be able to attenuate the shock waves that arise as a result of a sudden change in the state of a vehicle in the platoon due to, e.g., sudden braking. In the following, a control design strategy is briefly explained which guarantees that the above objectives are satisfied. Although the results obtained in the present paper are rather generic and independent of the selected CACC strategy, in order to be able to proceed with the details of the proposed method, a specific CACC structure is chosen here. The strategy which is used as our reference is a one-vehicle look-ahead CACC as developed and experimentally validated in Ploeg et al. (2011).

Consider the following model of an uncontrolled vehicle within a platoon of m vehicles, as shown in Figure 4.1:

$$
\begin{aligned}
\begin{pmatrix} \dot{v}_1 \\ \dot{a}_1 \end{pmatrix} &= \begin{pmatrix} a_1 \\ -\frac{1}{\tau} a_1 + \frac{1}{\tau} u_1 \end{pmatrix} \\
\begin{pmatrix} \dot{d}_i \\ \dot{v}_i \\ \dot{a}_i \end{pmatrix} &= \begin{pmatrix} v_{i-1} - v_i \\ a_i \\ -\frac{1}{\tau} a_i + \frac{1}{\tau} u_i \end{pmatrix}, \quad i \in S_m \backslash \{1\}
\end{aligned}
\tag{4.9}
$$

with $d_i = q_{i-1} - q_i - L_i$ being the distance between vehicle i and $i-1$, where q_i and q_{i-1} are the rear bumper position of vehicle i and $i-1$, respectively, and L_i is the length of vehicle i; v_i is the velocity and a_i is the acceleration of vehicle i. Moreover, u_i is the vehicle input, to be interpreted as desired acceleration, and τ is the time constant representing the driveline dynamics. Also, the following policy for the intervehicle spacing is adopted:

$$
d_{r,i}(t) = r_i + h v_i(t), \quad i \in S_m \backslash \{1\},
\tag{4.10}
$$

where $d_{r,i}$ is the desired distance between vehicle i and $i-1$, h is the time gap, and r_i is the standstill distance. The main objective is to regulate the distance error

$$
e_i(t) = d_i(t) - d_{r,i}(t), \quad i \in S_m \backslash \{1\}
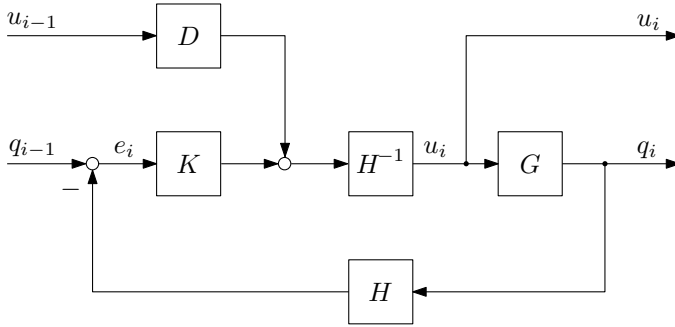\tag{4.11}
$$

Figure 4.2: Block scheme of the CACC system.

to zero, i.e.,

$$a_1(t) = 0 \ \forall \ t \geq 0 \ \Rightarrow \ \lim_{t \to \infty} e_i(t) = 0 \ \forall \ i \in S_m \backslash \{1\}, \tag{4.12}$$

taking into account that this objective is, in general, only satisfied if the lead vehicle drives with a constant velocity, i.e., $a_1 = 0$. In Ploeg et al. (2011), it is shown that the following dynamic controller achieves this vehicle-following objective:

$$\dot{u}_i = -\frac{1}{h} u_i + \frac{1}{h}(k_\mathrm{p} e_i + k_\mathrm{d} \dot{e}_i + k_\mathrm{dd} \ddot{e}_i) + \frac{1}{h} u_{i-1}, \quad i \in S_m \backslash \{1\}, \tag{4.13}$$

where k_p, k_d, and k_dd are the controller coefficients. Furthermore, it is shown that, for a bounded u_{i-1} and subject to the following constraints on the controller gains:

$$\begin{aligned} &k_\mathrm{p} > 0 \\ &k_\mathrm{d} > 0 \\ &k_\mathrm{dd} + 1 > 0 \\ &(1 + k_\mathrm{dd})k_\mathrm{d} - k_\mathrm{p}\tau > 0, \end{aligned} \tag{4.14}$$

the intervehicle distance d_i is regulated to $d_{\mathrm{r},i}$ as defined by the spacing policy (4.10), thus satisfying (4.12).

Based on the vehicle model (4.9)–(4.11) and the controller (4.13), the state-space model of the controlled vehicle platoon can be formulated as in (4.2), with states $x_i^\mathrm{T} = \begin{pmatrix} e_i & v_i & a_i & u_i \end{pmatrix}$, $i \in S_m$ (Ploeg et al., 2014b). However, since the string stability conditions (4.8) are formulated in the Laplace domain, the model of the controlled vehicle platoon is also formulated in the Laplace domain. This finally leads to the block diagram of the closed-loop system for vehicle i as shown in Figure 4.2, with

$$\begin{aligned} G(s) &= \frac{q_i(s)}{u_i(s)} = \frac{1}{s^2(\tau s + 1)} e^{-\phi s} \\ H(s) &= hs + 1 \\ K(s) &= k_\mathrm{p} + k_\mathrm{d} s + k_\mathrm{dd} s^2 \\ D(s) &= e^{-\theta s}. \end{aligned} \tag{4.15}$$

Here, $q_i(s)$ and $u_i(s)$ are the Laplace transforms of the vehicle position $q_i(t)$ and the desired acceleration $u_i(t)$, respectively; the vehicle transfer function $G(s)$ follows from $\ddot{q}_i = a_i$ and $\dot{a}_i = -\frac{1}{\tau} a_i + \frac{1}{\tau} u_i$, see (4.9), with an additional delay ϕ as experimentally identified (Ploeg et al., 2011). The spacing policy transfer function $H(s)$ is related to (4.10) and the controller $K(s)$ represents the error feedback in (4.13). Also, θ is the time delay induced by the wireless communication network. Note that, without loss of generality, $r_i = L_i = 0 \ \forall\, i \in S_m \backslash \{1\}$ is assumed here, as will be in the remainder of this chapter.

Now let the vehicle acceleration be taken as a basis for string stability, i.e., $y_i = a_i$, $\forall\, i \in S_m$, since it is physically relevant on the one hand, and satisfies the norm requirement on $P_1(s)$ in Condition 4.1 on the other hand. The latter can be easily understood, because, with this choice of outputs, $P_1(s) = \frac{1}{\tau s + 1} e^{-\phi s}$, hence $\|P_1(j\omega)\|_{\mathcal{H}_\infty} = 1$. The corresponding SSCS is then given by

$$\Gamma_{\mathrm{CACC}}(s) = \frac{a_i(s)}{a_{i-1}(s)} = \frac{1}{H(s)} \frac{G(s)K(s) + D(s)}{1 + G(s)K(s)}, \qquad (4.16)$$

where $a_i(s)$ and $a_{i-1}(s)$ are the Laplace transforms of $a_i(t)$ and $a_{i-1}(t)$, respectively. It is noted that the SSCS (4.16) would be the same in case the velocity v_i is chosen as output, since $\frac{a_i(s)}{a_{i-1}(s)} = \frac{sv_i(s)}{sv_{i-1}(s)} = \frac{v_i(s)}{v_{i-1}(s)}$, but that the first requirement in Condition 4.1 would not be satisfied in that case. In addition, it is worth mentioning that the SSCS is independent of the vehicle index i, which is a direct consequence of the homogeneity assumption. Finally, for an ACC system, i.e., where no feedforward path exists, the SSCS $\Gamma_{\mathrm{ACC}}(s)$ can be obtained from (4.16) with $D(s) = 0$, resulting in

$$\Gamma_{\mathrm{ACC}}(s) = \frac{1}{H(s)} \frac{G(s)K(s)}{1 + G(s)K(s)}. \qquad (4.17)$$

4.3 Graceful degradation under communication loss

The main difference of the CACC proposed in the previous section with its ACC counterpart is in the feedforward path, see Figure 4.2, which includes the effect of the preceding vehicle's desired acceleration u_{i-1} into the control loop. This difference enables the succeeding vehicle to follow the desired spacing policy more accurately due to the fact that string stability is obtained with smaller time gaps, compared to ACC. However, this feedforward path depends on the quality of the wireless intervehicle communication, in terms of latency and packet loss. Consequently, if the wireless communication fails (or when the preceding vehicle is not equipped with CACC), CACC would automatically degrade to ACC, leading to a significant increase in minimal time gap to maintain string-stable behavior. It is, therefore, desirable to implement an alternative fallback scenario, i.e., a graceful degradation technique, with less dramatic consequences. To this end, it is proposed to estimate the actual acceleration of the preceding vehicle, which can then be used as a replacement of the desired acceleration in case no communication updates are received. To arrive at an accurate acceleration estimation, Section 4.3.1

first describes a dynamic model for the target vehicle as a basis for state estimation, after which Section 4.3.2 incorporates the acceleration estimation algorithm into the CACC framework.

4.3.1 Object tracking

Since there might be several object vehicles close to the follower vehicle, a multi-object tracking algorithm needs to be applied, which is able to distinguish and track the desirable object in a multi-object environment. This involves, firstly, associating the correct measurement data with the various tracked objects; see, e.g., Mori et al. (2002) and the references contained therein. Secondly, the objects' states need to be estimated, using methods as comprehensively reviewed in Li and Jilkov (2002, 2003). In the scope of this paper, the focus is on the estimation technique. Moreover, regardless of the specific estimation technique, a dynamical object model has to be adopted for the estimation algorithm, representing the target's pattern of motion as accurately as possible. In the following, a concise description is given of the dynamic object model as well as the estimation technique applied here.

Dynamic object model

To describe an object's longitudinal motion, the Singer acceleration model (Singer, 1970) is adopted, since this model appears to provide a good approximation of the longitudinal vehicle dynamics (Lijster, 2012). This model takes into account the correlation in time of the acceleration, namely if a target is accelerating at time instant t, it is likely to be accelerating at time instant $t + \tau$ for a sufficiently small τ. This time correlation results in the following equation of a linear time-invariant system describing the vehicle acceleration:

$$\dot{a}(t) = -\alpha a(t) + u(t) \tag{4.18}$$

with a being the acceleration of the object vehicle and u the model input. α represents the inverse of the so-called maneuver time constant τ_m, the choice of which will be briefly exemplified at the end of Section 4.4. Since u is unknown, the *equivalent-noise approach* (Li and Jilkov, 2002) is chosen, by assuming that this input is a zero-mean uncorrelated random process (white noise). To arrive at the statistical characteristics of this white noise, the object vehicle is assumed to exhibit maximum acceleration $a_{\max}$ or deceleration $-a_{\max}$ with a probability $P_{\max}$ and to have a probability P_0 of zero acceleration, whereas other acceleration values are uniformly distributed. This results in the probability density function $p(a)$ for the object acceleration a as shown in Figure 4.3, which appears to provide a satisfactory representation of the object's instantaneous maneuver characteristics (Singer, 1970). Consequently, the variance σ_a^2 of the object acceleration is equal to

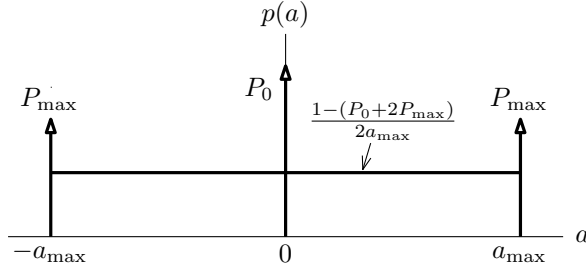$$\sigma_a^2 = \frac{a_{\max}^2}{3}(1 + 4P_{\max} - P_0). \tag{4.19}$$

Figure 4.3: Probability density function $p(a)$ of the object acceleration a.

It can then be shown (Singer, 1970) that, in order to satisfy $p(a)$, the covariance $C_{uu}(\tau)$ of the white-noise input u in (4.18) must be equal to

$$C_{uu}(\tau) = 2\alpha\sigma_a^2\delta(\tau), \tag{4.20}$$

where δ is the unit impulse function. As a result, the random variable a, satisfying a probability density function $p(a)$ with variance σ_a^2 as in (4.19), while being correlated in time through the maneuver time constant τ_m, is described as a random process $a(t)$ being the output of a 1$^\text{st}$-order system (4.18) with a white-noise input $u(t)$ satisfying (4.20).

Using the acceleration model (4.18), the corresponding equation of motion can be described in the state space as

$$\dot{x}(t) = A_\text{a}x(t) + B_\text{a}u(t) \tag{4.21a}$$
$$y(t) = C_\text{a}x(t), \tag{4.21b}$$

where $x^\text{T} = \begin{pmatrix} q & v & a \end{pmatrix}$, with q and v being the object vehicle's position and velocity, respectively. The vector $y^\text{T} = \begin{pmatrix} q & v \end{pmatrix}$ is the output of the model and the matrices A_a, B_a, and C_a are defined as follows:

$$A_\text{a} = \begin{pmatrix} 0 & 1 & 0 \\ 0 & 0 & 1 \\ 0 & 0 & -\alpha \end{pmatrix}, \; B_\text{a} = \begin{pmatrix} 0 \\ 0 \\ 1 \end{pmatrix}, \; C_\text{a} = \begin{pmatrix} 1 & 0 & 0 \\ 0 & 1 & 0 \end{pmatrix}. \tag{4.22}$$

Note that the state equation (4.21a) closely resembles the vehicle dynamics model (4.9) when replacing α by τ^{-1}. Finally, the exact discretization of (4.21) is given by

$$x(k+1) = F_\text{a}x(k) + w(k)$$
$$y(k) = C_\text{a}x(k) \tag{4.23}$$

with

$$F_\text{a} = e^{A_\text{a}t_\text{s}} = \begin{pmatrix} 1 & t_\text{s} & \frac{1}{\alpha^2}(-1 + \alpha t_\text{s} + e^{-\alpha t_\text{s}}) \\ 0 & 1 & \frac{1}{\alpha}(1 - e^{-\alpha t_\text{s}}) \\ 0 & 0 & e^{-\alpha t_\text{s}} \end{pmatrix} \tag{4.24a}$$

$$w(k) = \int_{kt_\text{s}}^{(k+1)t_\text{s}} e^{A_\text{a}((k+1)t_\text{s}-\tau)} B_\text{a}u(\tau)\, \text{d}\tau, \tag{4.24b}$$

where $\cdot(k)$ denotes the discrete-time variable associated with the continuous time instant kt_{s}, with t_{s} being the sampling interval. It is shown in Singer (1970) that $w(k)$ is a discrete-time white-noise sequence. Consequently, $w(k)$ can be regarded as the process noise in the estimator design, as described in the next subsection.

Object state estimation

The approach that is adopted for estimation of the object vehicle acceleration, is the stand-alone Kalman filter, where estimations of the internal state of a linear dynamical system are based on the observations of the sensors only (Maybeck, 1979). Obviously, for real-time implementation in the vehicle control computer, a discrete-time Kalman filter is required. However, to simplify the upcoming string stability analysis, a continuous-time approach is adopted here. Hence, the continuous-time equivalent of the Kalman filter will be employed, based on the state-space model

$$
\begin{aligned}
\dot{x}(t) &= A_{\mathrm{a}}x(t) + w(t) \\
y(t) &= C_{\mathrm{a}}x(t) + v(t).
\end{aligned}
\tag{4.25}
$$

This model corresponds to (4.21), (4.22) with an additional measurement noise vector $v(t)$ and the process noise equal to $w(t) := B_{\mathrm{a}}u(t)$, according to the equivalent-noise approach. $v(t)$ is a Gaussian white-noise signal, where the covariance matrix R is based on the noise parameters of the onboard sensor used in the implementation of the observer, which, in this case, is a radar (see Section 4.5). Hence,

$$
R = E\{v(t)v^{\mathrm{T}}(t)\} = \begin{pmatrix} \sigma_d^2 & 0 \\ 0 & \sigma_{\Delta v}^2 \end{pmatrix},
\tag{4.26}
$$

where σ_d^2 is the variance of the measured intervehicle distance and $\sigma_{\Delta v}^2$ the variance of the measured relative velocity. Note that here, the relative variables are taken as a basis for R, i.e., the distance d and relative velocity Δv, instead of the absolute variables q and v, the reason for which will be explained in Section 4.3.2. Furthermore, using (4.20), the continuous-time process noise covariance matrix Q equals

$$
Q = E\{w(t)w^{\mathrm{T}}(t)\} = B_{\mathrm{a}}E\{u(t)u^{\mathrm{T}}(t)\}B_{\mathrm{a}}^{\mathrm{T}} = \begin{pmatrix} 0 & 0 & 0 \\ 0 & 0 & 0 \\ 0 & 0 & 2\alpha\sigma_a^2 \end{pmatrix}.
\tag{4.27}
$$

With the given Q and R matrices, the following continuous-time observer is obtained:

$$
\dot{\hat{x}}(t) = A_{\mathrm{a}}\hat{x}(t) + L_{\mathrm{a}}\big(y(t) - C_{\mathrm{a}}\hat{x}(t)\big)
\tag{4.28}
$$

with A_{a} and C_{a} according to (4.22). $\hat{x}$ is the estimate of the object vehicle state $x^{\mathrm{T}} = \begin{pmatrix} q & v & a \end{pmatrix}$ and L_{a} is the continuous-time Kalman filter gain matrix. The measurement vector y consists of the position q and the velocity v of the object vehicle. Because neither of these can be measured by the onboard sensor of the follower vehicle, the observer needs to be adapted, as will be further explained in the next section.

4.3.2 CACC fallback scenario

In this section, a so-called "degraded" CACC (dCACC) strategy is proposed. This strategy aims to use the estimated actual acceleration rather than the desired acceleration of the preceding vehicle, as employed in CACC[2]. However, the measurement y in the acceleration estimator (4.28), containing the absolute object position and velocity, is not available. Instead, the onboard sensor provides distance and relative velocity. The estimation algorithm thus needs to be adapted, as explained below.

As a first step, the continuous-time estimator (4.28) is described in the Laplace domain by a transfer function $T(s)$, which takes the actual position q_{i-1} and velocity v_{i-1} of the preceding vehicle, contained in the measurement vector $y(t)$ in (4.28), as input. The output of $T(s)$ is the estimate $\hat{a}_{i-1}$ of the preceding vehicle's acceleration, being the third element of the estimated state. This yields the estimator

$$\hat{a}_{i-1}(s) = T(s) \begin{pmatrix} q_{i-1}(s) \\ v_{i-1}(s) \end{pmatrix}, \tag{4.29}$$

where $\hat{a}_{i-1}(s)$ denotes the Laplace transform of $\hat{a}_{i-1}(t)$, and $q_{i-1}(s)$ and $v_{i-1}(s)$ are the Laplace transforms of $q_{i-1}(t)$ and $v_{i-1}(t)$, respectively. Moreover, the 1×2 observer transfer function $T(s)$ is equal to

$$\begin{aligned} T(s) &= \hat{C}(sI - \hat{A})^{-1}\hat{B} \\ &=: \begin{pmatrix} T_{aq}(s) & T_{av}(s) \end{pmatrix} \end{aligned} \tag{4.30}$$

with

$$\hat{A} = A_{\mathrm{a}} - L_{\mathrm{a}}C_{\mathrm{a}}, \ \hat{B} = L_{\mathrm{a}}, \ \hat{C} = \begin{pmatrix} 0 & 0 & 1 \end{pmatrix}. \tag{4.31}$$

Note that $T(s)$ does not depend on the vehicle index i due to the homogeneity assumption.

The second step involves a transformation to relative coordinates, using the fact that (with $L_i = 0$)

$$\begin{aligned} q_{i-1}(s) &= d_i(s) + q_i(s) \\ v_{i-1}(s) &= \Delta v_i(s) + v_i(s), \end{aligned} \tag{4.32}$$

where $\Delta v_i(s)$ denotes the Laplace transform of the relative velocity $\Delta v_i(t) = \dot{d}_i(t)$. Substituting (4.32) into (4.29) yields

$$\hat{a}_{i-1}(s) = T(s) \begin{pmatrix} d_i(s) \\ \Delta v_i(s) \end{pmatrix} + T(s) \begin{pmatrix} q_i(s) \\ v_i(s) \end{pmatrix}. \tag{4.33}$$

As a result, the acceleration estimator is split into a relative-coordinate estimator

$$\widehat{\Delta a}_i(s) := T(s) \begin{pmatrix} d_i(s) \\ \Delta v_i(s) \end{pmatrix}, \tag{4.34}$$

---

[2]Technically, dCACC is not cooperative, since information exchange through wireless communication is no longer employed. However, to clearly indicate its purpose, the proposed degradation mechanism is put forward as degraded CACC rather than enhanced ACC.

where $\widehat{\Delta a}_i(s)$ can be regarded as the Laplace transform of the estimated relative acceleration $\widehat{\Delta a}_i(t)$, and an absolute-coordinate estimator

$$\hat{a}_i(s) = T(s) \begin{pmatrix} q_i(s) \\ v_i(s) \end{pmatrix}, \tag{4.35}$$

where $\hat{a}_i(s)$ is the Laplace transform of the estimated local acceleration $\hat{a}_i(t)$.

Finally, $\hat{a}_i(s)$ in (4.35) can be easily computed with

$$\begin{aligned} \hat{a}_i(s) &= \begin{pmatrix} T_{aq}(s) & T_{av}(s) \end{pmatrix} \begin{pmatrix} q_i(s) \\ v_i(s) \end{pmatrix} \\ &= \left(\frac{T_{aq}(s)}{s^2} + \frac{T_{av}(s)}{s} \right) a_i(s) \\ &=: T_{aa}(s) a_i(s), \end{aligned} \tag{4.36}$$

exploiting the fact that the local position $q_i(t)$ and velocity $v_i(t)$ are the result of integration of the locally measured acceleration $a_i(t)$, thereby avoiding the use of a potentially inaccurate absolute position measurement by means of a global positioning system (GPS). The transfer function $T_{aa}(s)$ (among others involving the estimator dynamics) acts as a filter for the measured acceleration a_i, yielding the "estimated" acceleration $\hat{a}_i$, effectively synchronizing the local vehicle acceleration measurement with the estimated relative acceleration.

Summarizing, the control law of the fallback dCACC system is obtained by replacing the preceding vehicle's input u_{i-1} in the controller (4.13) with the estimated acceleration $\hat{a}_{i-1}$. The control law is then formulated in the Laplace domain as:

$$u_i(s) = H^{-1}(s) \left\{ K(s) e_i(s) + T(s) \begin{pmatrix} d_i(s) \\ \Delta v_i(s) \end{pmatrix} + T_{aa}(s) a_i(s) \right\}, \tag{4.37}$$

which can be implemented using the radar measurement of the distance d_i and the relative velocity Δv_i, and the locally measured acceleration a_i and velocity v_i, the latter being required to calculate the distance error e_i according to (4.10) and (4.11). The corresponding block diagram of the closed-loop dCACC system as a result of this approach is shown in Figure 4.4.

4.4 String stability of degraded CACC

To analyze the string stability properties of the dCACC strategy, the output of interest is chosen to be the acceleration, since this directly guarantees the existence of $\|P_1(s)\|_{\mathcal{H}_\infty}$ being the first requirement in Condition 4.1 for strict $\mathcal{L}_2$ string stability, as mentioned in Section 4.2.2. The SSCS $\Gamma_{\mathrm{dCACC}}(s)$, as defined in (4.6), can then be computed using (4.7), with $y_j(s) = a_j(s)$, $j = i, i-1$. As a result, with the closed-loop configuration given in Figure 4.4, the following SSCS is obtained:

$$\Gamma_{\mathrm{dCACC}}(s) = \frac{1}{H(s)} \frac{G(s) \left(K(s) + s^2 T_{aa}(s) \right)}{1 + G(s) K(s)}. \tag{4.38}$$
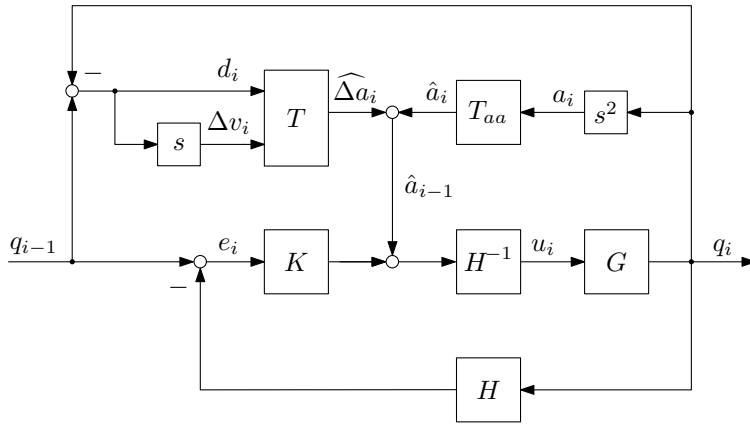
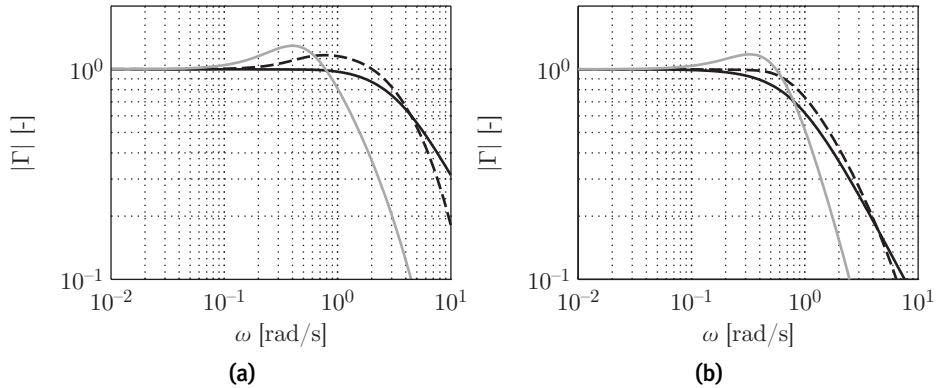**Figure 4.4:** Block scheme of the fallback dCACC system.

Figure 4.5: SSCS frequency response magnitude in case of CACC (solid black), dCACC (dashed black), and ACC (gray) with (a) $h = 0.3$ s and (b) $h = 1.3$ s.

Note that, according to Remark 4.1 in Section 4.2.2, strict $\mathcal{L}_2$ string stability is equivalent to $\mathcal{L}_2$ string stability for the current system. Moreover, since only (strict) $\mathcal{L}_2$ string stability is considered, this notion will be simply referred to as string stability in the remainder of this chapter.

The platoon of vehicles is string stable if also the second requirement as mentioned under Condition 4.1 holds, i.e., $\|\Gamma_{\mathrm{dCACC}}(s)\|_{\mathcal{H}_\infty} \leq 1$. Furthermore, if the system is string unstable, $\|\Gamma_{\mathrm{dCACC}}(s)\|_{\mathcal{H}_\infty}$ will exceed 1; still, in that case we would aim at making this norm as low as possible to minimize disturbance amplification. The frequency response magnitudes of $\Gamma_{\mathrm{CACC}}(j\omega)$ from (4.16), $\Gamma_{\mathrm{dCACC}}(j\omega)$ from (4.38), and $\Gamma_{\mathrm{ACC}}(j\omega)$ from (4.17) are shown in Figure 4.5(a) and 4.5(b) for $h = 0.3$ s and $h = 1.3$ s, respectively. Here, the model parameters, summarized in Table 4.1, are set according to the parameters of the test vehicles used for experiments, see Section 4.5. From the frequency response magnitudes, it

Table 4.1: Vehicle and controller parameters.

Symbol	Value	Description
θ	$0.02\,\text{s}$	Communication delay
τ	$0.1\,\text{s}$	Vehicle time constant
ϕ	$0.2\,\text{s}$	Vehicle internal time delay
k_{p}	0.2	Controller gain (proportional)
k_{d}	0.7	Controller gain (differential)
k_{dd}	0	Controller gain
$a_{\max}$	$3\,\text{m/s}^2$	Maximum acceleration
$P_{\max}$	0.01	Probability of maximum acceleration
P_0	0.1	Probability of zero acceleration
α	$1.25\,\text{s}^{-1}$	Reciprocal maneuver time constant $(1/\tau_m)$
σ_d^2	$0.029\,\text{m}^2$	Variance of measured distance
$\sigma_{\Delta v}^2$	$0.017\,\text{m}^2/\text{s}^2$	Variance of measured relative velocity

follows that for $h = 0.3\,\text{s}$, only CACC appears to result in string-stable behavior, whereas for $h = 1.3\,\text{s}$, both CACC and dCACC yield string stability. Clearly, ACC is not string stable in either case.

In addition to the frequency response functions, time domain responses, as shown in Figure 4.6, can be compared as well. In this figure, the (velocity controlled) lead vehicle in a platoon of 5 vehicles follows a smooth down-step velocity profile, whereas the remaining vehicles are controlled by either CACC, dCACC, or ACC, with $h = 0.6\,\text{s}$. As a result of this disturbance, the three systems respond very differently. From the velocity response (left column), it directly follows that the CACC system damps the shockwave completely, i.e., is string stable, whereas the dCACC and ACC systems start to propagate a shockwave. However, dCACC clearly outperforms ACC in terms of damping. The same effect can be seen in the responses of the distance error, defined as in (4.11), in the right column of Figure 4.6. Nevertheless, all systems show asymptotic tracking behavior, since the distance errors all converge to zero. For the given model and controller parameters, the string-stable time gap region for dCACC appears to be $h \geq 1.23\,\text{s}$, whereas for CACC and ACC this appears to be $h \geq 0.25\,\text{s}$ and $h \geq 3.16\,\text{s}$, respectively[3]. Consequently, dCACC represents a significant improvement over ACC when it comes to string stability characteristics.

The quality of the acceleration estimation as employed in dCACC can be illustrated as follows. For the same simulation as shown in Figure 4.6, Figure 4.7 shows the desired acceleration u_2 and the actual acceleration a_2 of vehicle $i = 2$, as well as the acceleration $\hat{a}_2$ that is estimated by the follower vehicle $i = 3$. As can be seen in the figure, $\hat{a}_2$, in itself providing a satisfactory estimation of a_2, shows a noticeable phase lag with respect to u_2, which is essentially the reason

---

[3]Hence, with $v_i = 80\,\text{km/h}$, for instance, these time gaps correspond to distances greater than $27.3\,\text{m}$, $5.6\,\text{m}$, and $70.2\,\text{m}$, respectively.
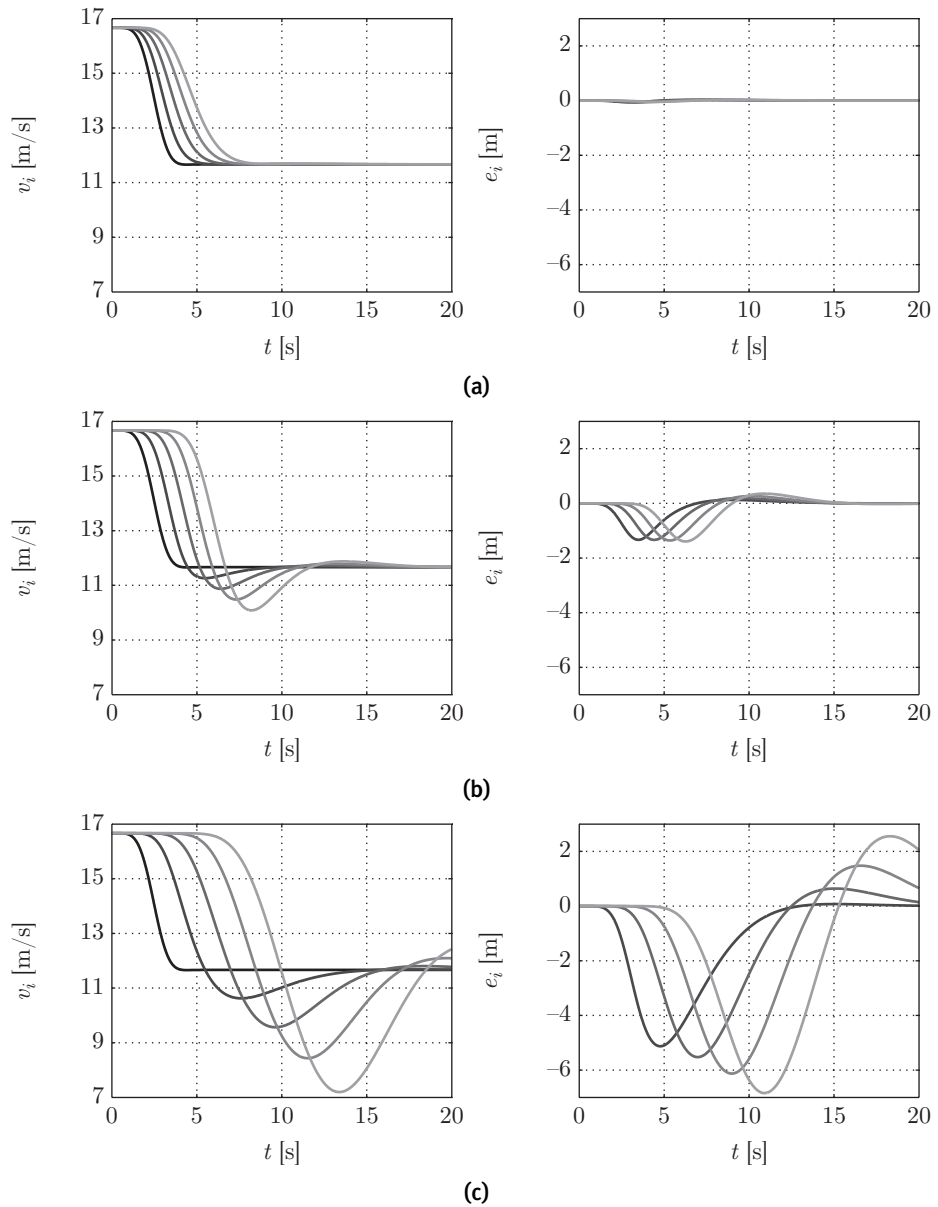
Figure 4.6: Response of the velocity $v_i(t)$ (left column; black–light gray: $i = 1, 2, \ldots, 5$) and the distance error $e_i(t)$ (right column; black–light gray: $i = 2, 3, 4, 5$) for (a) CACC, (b) dCACC, and (c) ACC.
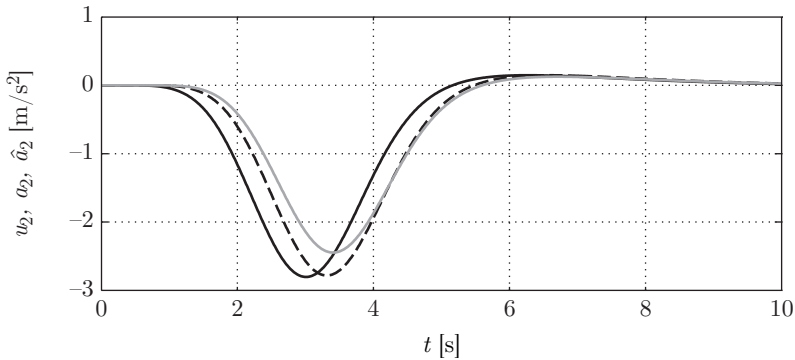
Figure 4.7: Vehicle 2 acceleration: desired acceleration u_2 (solid black), actual acceleration a_2 (dashed black) and estimated acceleration $\hat{a}_2$ (gray).

for the degraded string stability performance of dCACC.

To make the performance of the dCACC system even more efficient in terms of string stability, the reciprocal maneuver time constant $\alpha = 1.25$ of the Singer model can be increased so as to further reduce the frequency response peak of the SSCS function. However, it should be noted that there exists a trade-off between the value of α for the optimal string stability performance and the value needed for an acceptable level of ride comfort. As a rule of thumb, $0.5 \leq \alpha \leq 1.5$ appears to maintain both requirements at an acceptable level.

4.5 Experimental validation

The CACC system, with added graceful degradation feature, is implemented in three identical passenger cars (Toyota Prius III Executive), equipped with a wireless communication device that follows the ITS G5 standard (Ström, 2011), enabling the vehicles to communicate control-related information, e.g., the desired acceleration; see Chapter 5 for further details regarding the software and instrumentation of these test vehicles. The relative position of the preceding vehicle and its relative velocity are measured by a long-range radar, which is an original vehicle component in this case. Furthermore, a real-time platform executes the CACC with a sampling time $t_s = 0.01\,\text{s}$, yielding the desired vehicle acceleration which is then forwarded to a low-level acceleration controller of the vehicle. This section first presents experimentally obtained frequency responses to validate the string stability properties of dCACC, compared to those of CACC and ACC, after which measured time responses are shown to validate the performance of the controllers in general.

4.5.1 Frequency response experiments

The frequency response tests are conducted with two vehicles only. Here, the lead vehicle is velocity controlled, with a reference velocity profile $v_r(t)$. This test
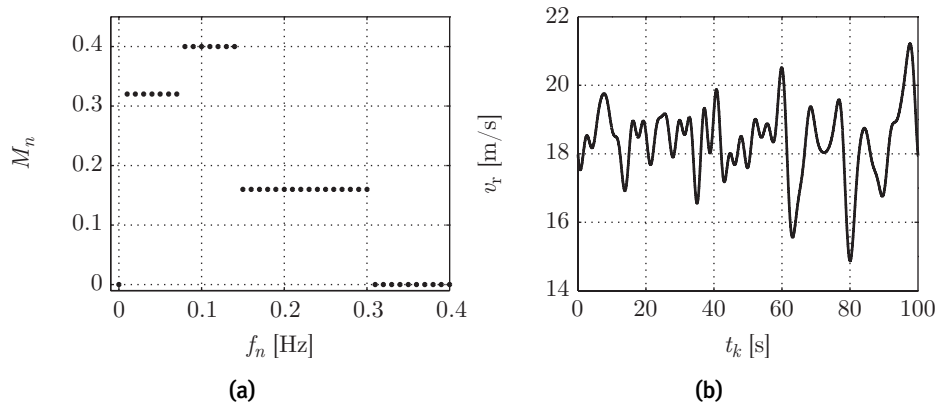
Figure 4.8: Velocity reference test signal used for identification of the controlled vehicle platoon: (a) frequency-domain magnitude M_n and (b) corresponding time-domain signal $v_r(k)$.

signal should provide sufficient frequency content for performing a nonparametric system identification, in particular to identify the SSCS function in the relevant frequency range. Towards this end, the selected signal is a random-phase multisine signal that covers the frequency range $f \in [0, 0.3]$ Hz ($[0, 1.9]$ rad/s). This range of excitation, as well as the frequency weighting factors M_n, with $n = 0, 1, \ldots, \frac{N}{2} - 1$ and N being the number of frequency intervals up to the sampling frequency $f_s = 1/t_s$, are chosen based on the frequency content needed for SSCS identification. The chosen frequency-domain magnitudes M_n of the test signal, as a function of the discrete frequency $f_n = n\Delta f$, with frequency interval $\Delta f = f_s/N$, are shown in Figure 4.8(a); the resulting discrete-time signal $v_r(k)$ at time $t_k = kt_s$ with $k = 0, 1, \ldots, N - 1$, is shown in Figure 4.8(b).

To run the dCACC system in the two test vehicles, the relative-acceleration estimator in (4.33) has been implemented in the follower vehicle ($i = 2$) using the discrete-time equivalent of the filter equation (4.28), with measurement input vector

$$y(k) = \begin{pmatrix} d_2(k) \\ \Delta v_2(k) \end{pmatrix}, \tag{4.39}$$

being the radar output, and with the state vector

$$\hat{x}(k) = \begin{pmatrix} \hat{d}_2(k) \\ \widehat{\Delta v}_2(k) \\ \widehat{\Delta a}_2(k) \end{pmatrix}. \tag{4.40}$$

This yields the estimated relative acceleration $\widehat{\Delta a}_2(k)$, based on which the absolute lead vehicle acceleration $a_1(k)$ is estimated by adding the filtered locally measured acceleration $\hat{a}_2(k)$, using the discrete-frequency equivalent of $T_{aa}(s)$ in (4.36), combined with an onboard acceleration sensor.

Using the measurement data obtained from the tests, a nonparametric system identification is performed to compute $|\Gamma_{\mathrm{CACC}}(j\omega_n)|$, $|\Gamma_{\mathrm{dCACC}}(j\omega_n)|$, and $|\Gamma_{\mathrm{ACC}}(j\omega_n)|$, with $\omega_n = n2\pi\Delta f$. Subsequently, these are compared with the theoretical values, i.e., through equations (4.16), (4.38), and (4.17), respectively, using $h = 0.6\,\mathrm{s}$ time gap. The result is shown in Figure 4.9. From this figure, it can be seen that the experimental results match with the theoretical ones in the frequency range of excitation as indicated by Figure 4.8(a), i.e., for frequencies up to $1.9\,\mathrm{rad/s} = 0.3\,\mathrm{Hz}$. It should be noted, however, that a larger excitation frequency interval may have been chosen, in order to obtain a more accurate estimate around the cut-off frequency in the case of dCACC. Nevertheless, it can be concluded that the experiments confirm the improvement with respect to string stability obtained with dCACC compared to the conventional ACC fallback scenario. Consequently, smaller time gaps are feasible under severe packet loss for the dCACC controller, compared to the ACC controller.

4.5.2 Time response experiments

The time response experiments are conducted with three vehicles and are identical to those shown in Figure 4.6, i.e., starting from a situation in which the platoon is in steady-state at $16.67\,\mathrm{m/s}$ ($60\,\mathrm{km/h}$) with $h = 0.6\,\mathrm{s}$, the velocity-controlled lead vehicle performs a smooth velocity step of $-5\,\mathrm{m/s}$. The measured velocity and distance error responses are shown in Figure 4.10. Comparing the velocity responses with the simulated responses in Figure 4.6 directly reveals that the practical experiments are very similar to the theoretical results: CACC is again clearly string stable, whereas dCACC and ACC are not. Nevertheless, the amount of overshoot is much smaller with dCACC than with ACC. Note that also the magnitude of the velocity responses is very close to that of the simulations. The distance error responses deviate slightly from the simulated responses as far as the amplitude is concerned, but still clearly show the same trend, despite the rather large noise level, which is inherent to the distance measurement by the radar. As will be seen in the last experiment, explained hereafter, this measurement noise leads to noise in the estimated acceleration, which is why the velocity response in case of dCACC is less smooth, compared to CACC and ACC. As already mentioned at the end of Section 4.4, a smoother behavior (hence, improved ride comfort) can be obtained by decreasing the value of the reciprocal maneuver time constant α, but at the cost of further increasing the string instability.

Finally, using the same experiment, Figure 4.11 shows the desired acceleration $u_2(t)$ and the actual measured acceleration $a_2(t)$ of the first follower vehicle, both received in the last follower vehicle via the communication link, as well as the estimated acceleration $\hat{a}_2(t)$, computed locally in the last follower vehicle. As can be seen in this figure, $\hat{a}_2(t)$ provides a satisfactory estimation of $a_2(t)$, but shows a significant phase lag with respect to $u_2(t)$, which corresponds to the simulation results as depicted in Figure 4.7. As mentioned earlier, this phase lag accounts for the degraded string stability performance of dCACC. Furthermore, $\hat{a}_2(t)$ shows a considerable noise level due to the quality of the radar measurements. This behavior could be improved by tuning the value of the reciprocal maneuver time
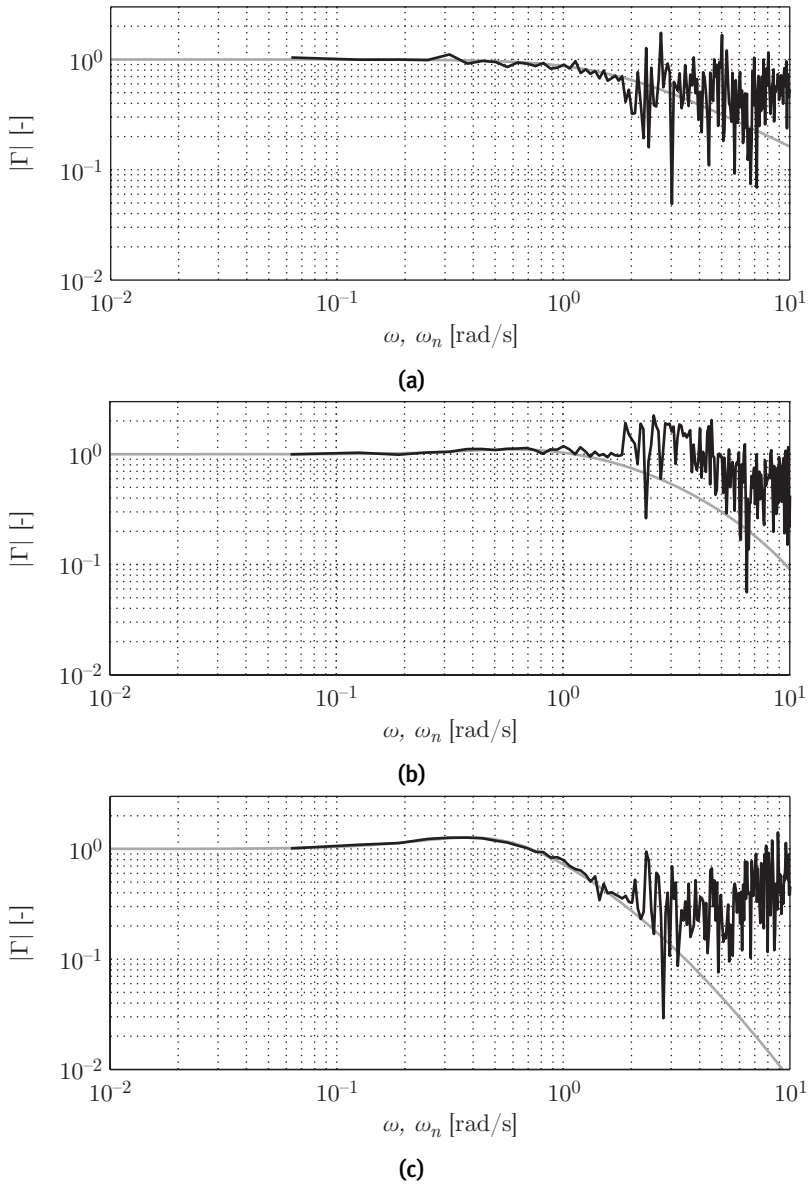
Figure 4.9: Experimental (black) and theoretical (gray) SSCS frequency response magnitude of the system subject to (a) CACC, (b) dCACC, and (c) ACC.
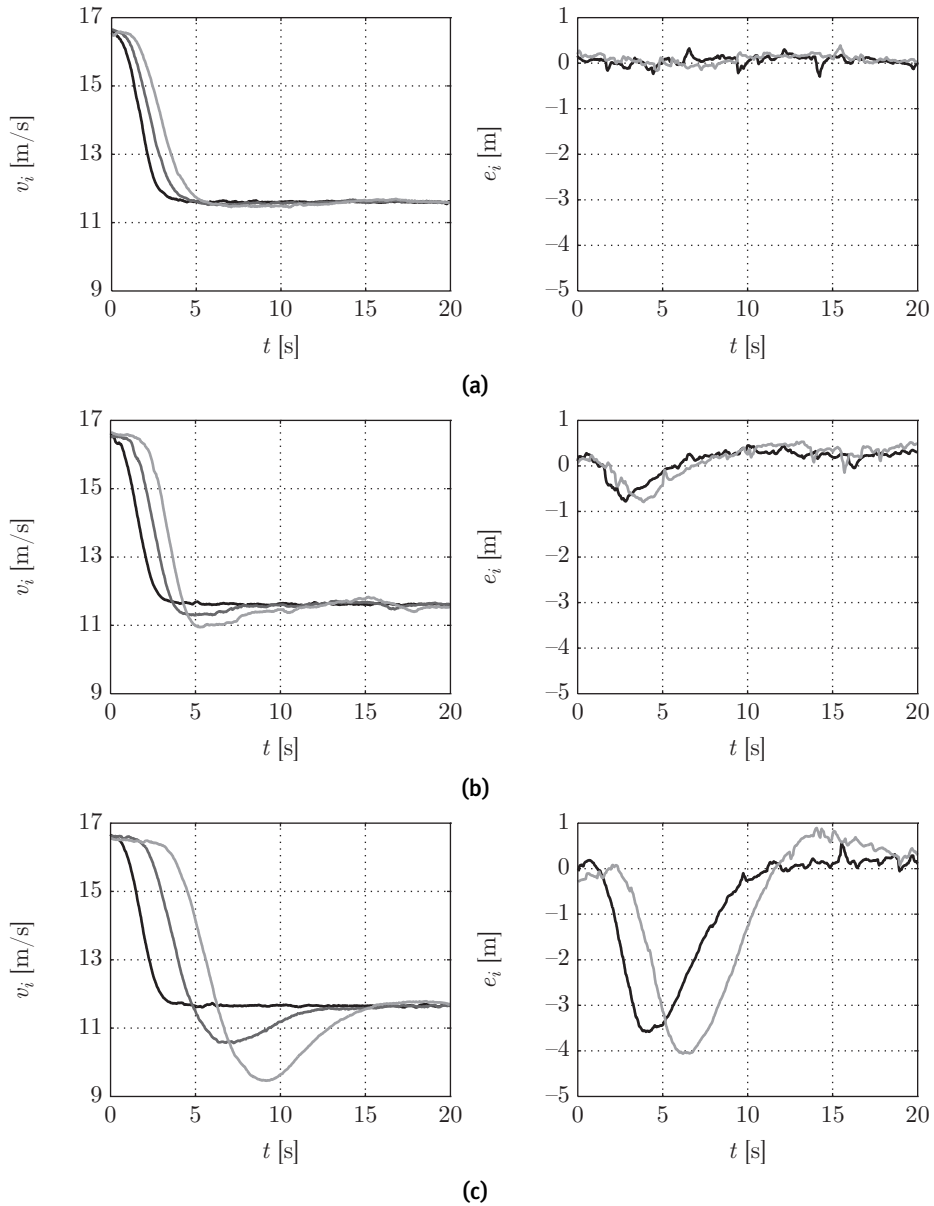
Figure 4.10: Measured response of the velocity $v_i(t)$ (left column; black–light gray: $i = 1, 2, 3$) and the distance error $e_i(t)$ (right column; black, light gray: $i = 2, 3$) for (a) CACC, (b) dCACC, and (c) ACC.
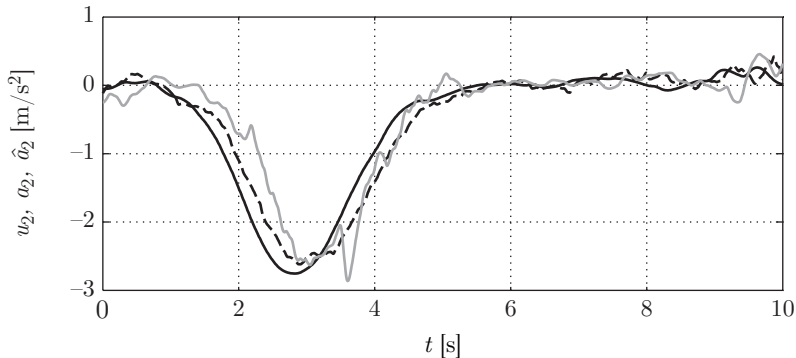
Figure 4.11: Measured vehicle 2 acceleration: desired acceleration u_2 (solid black), actual acceleration a_2 (dashed black), and estimated acceleration $\hat{a}_2$ (gray).

constant α. Fortunately, the measurement noise is hardly noticeable in vehicle 3, which uses $\hat{a}_2(t)$ as a feedforward signal, because the precompensator $H^{-1}(s)$ together with the vehicle dynamics act as a series connection of 1$^{\text{st}}$-order low-pass filters with time constant h and τ, respectively; see (4.15) and Figure 4.4.

4.6   Conclusion

A graceful degradation technique for CACC was presented, serving as an alternative fallback scenario to ACC. The idea behind the proposed approach is to obtain the minimum loss of functionality of CACC when the wireless communication link fails or when the preceding vehicle is not equipped with wireless communication means. The proposed strategy uses an estimation of the preceding vehicle's current acceleration as a replacement to the desired acceleration which would normally be communicated over a wireless link. It was shown that the performance, in terms of string stability of degraded CACC (dCACC), can be maintained at a much higher level compared to an ACC fallback scenario. Both theoretical as well as experimental results showed that the dCACC system outperforms the ACC fallback scenario with respect to string stability characteristics by reducing the minimum string-stable time gap to less than half of the required value in case of ACC.

This chapter, as well as Chapter 2 and 3, contained not only a theoretical analysis, but also illustrated the resulting platoon behavior by means of experiments with a platoon of CACC-equipped passenger vehicles. The control system software, as implemented in these vehicles, firstly comprised the particular vehicle-following controller of the respective chapters. For practical application, however, functions other than the controller itself need to be implemented as well. Examples of such functions are sensor fusion and object tracking, position estimation of the vehicle itself, and human-machine interfacing. These functional aspects of the control system implementation, as well as the required vehicle instrumentation, will be explained in more detail in the next chapter.

Chapter 5

Implementation of Cooperative Adaptive Cruise Control

Abstract Practical implementation of control algorithms for driver assistance systems generally also requires the implementation of functionality other than the controller itself. Especially for Cooperative Adaptive Cruise Control (CACC), mechanisms for graceful degradation, algorithms for object tracking, and human–machine interfacing are essential for reliable and safe operation in daily traffic. Therefore, a layered architecture for a real-time control system for CACC is developed, consisting of a perception layer, containing observers for both the host vehicle motion pattern and that of target vehicles, a control layer, which includes the control algorithms for CACC, and a supervisory layer that coordinates controller settings received from the driver or from roadside equipment, and ensures safe operation of the vehicle. In addition, the control system also needs to interface with the native vehicle systems, which requires a real-time gateway to the vehicle that also implements a lower-level acceleration controller. This architecture is implemented in prototype CACC test vehicles, from which it can be concluded that CACC implementation requires significant additional functionality on the one hand, but only limited additional vehicle instrumentation on the other hand.

5.1 Introduction

Practical implementation of a control algorithm on the vehicle to be controlled often requires additional adaptations. First of all, the algorithm needs to be implemented in the control computer in discrete-time, which thus requires discretization, using a sampling time which is small enough to not compromise the desired dynamical behavior of the controlled system on the one hand, but which is as large as possible in view of computational efficiency on the other (Åstrom and Wittenmark, 1997). Furthermore, the specific control computer may require to implement the algorithm using fixed-point arithmetic, which implies that the signal amplitude is discretized as well, known as quantization (Haimovic, 2006). Consequently, roundoff errors must be taken into account, as well as typical fixed-

point effects such as saturation and overflow.

Next to these technical aspects of real-time implementation of control algorithms, also functional aspects other than the controller itself may come into play. These aspects commonly include startup and shutdown procedures, sensor calibration procedures, and mechanisms for fault tolerance (Ding, 2008). Especially for driver assistance systems in road vehicles, such as Cooperative Adaptive Cruise Control (CACC) (Naus et al., 2008), the driver can interact with the control system, not only by (de-)activating it, but also by providing controller settings. In the case of CACC, these settings at least include the desired time gap and the so-called cruise speed, being the maximum allowable velocity of the follower vehicle. Furthermore, since CACC employs wireless intervehicle communication, the controller is prone to communication impairments such as latency and packet loss. Consequently, methods for graceful degradation, as described in Chapter 4, need to be implemented. In addition, the design and the analysis of controllers for platooning of road vehicles, as presented in Chapters 2 and 3, implicitly assumed that the preceding vehicle was known on beforehand. In real traffic, however, the radar as well as the wireless communication system may detect multiple vehicles, upon which it has to be determined which of those are relevant for CACC. This requires estimating the objects' states—especially position and velocity—using object tracking methods, a comprehensive overview of which is given in Li and Jilkov (2001, 2002, 2003).

This chapter aims to provide insight into the additional functionality that is required to implement a CACC system for operation under real-life circumstances, i.e., in the presence of multiple vehicles, either or not equipped with CACC, and intelligent roadside units that may also transmit certain data to the platoon vehicles, while also allowing for driver input regarding controller parameters. In addition, the instrumentation needed for implementation of CACC will be described, thus providing a complete overview of the aspects that are relevant for practical application of CACC. Both topics will be covered on the basis of the software and hardware that has been developed for the test vehicles as used in the previous chapters. Obviously, the control system implementation in a test setup may significantly differ from the final commercial implementation, both technically and functionally. Nevertheless, the test vehicle implementation still provides valuable insight into the implementation aspects of cooperative driving systems in general and CACC in particular.

This chapter is organized as follows. Section 5.2 describes the architecture of the real-time control system software necessary to implement the CACC functionality. Next, Section 5.3 presents the corresponding test vehicle instrumentation in terms of required hardware, among which sensors, wireless communication equipment, and processing units. Finally, Section 5.4 summarizes the main conclusions.

5.2   Real-time control system for CACC

The vehicle-following controller and related functionality is implemented on the so-called Real-Time CACC Platform, being a real-time processing unit. This

unit interacts with another (event-driven) processing unit that implements the Human–Machine Interface (HMI), referred to as the HMI Platform. This interaction is bidirectional, allowing the driver to set controller parameters and to obtain information about, e.g., the current controller settings, other transmitting vehicles and the specific vehicle that is currently being followed. The Real-Time CACC Platform is connected with the vehicle through the Vehicle Gateway, which is a real-time computer platform as well. The information exchange with the outside world takes place through wireless communication, in particular by means of wireless messages received from other vehicles, i.e., vehicle-to-vehicle communication (V2V), and from roadside units, i.e., infrastructure-to-vehicle communication (I2V). The vehicle also sends its own wireless message to both other vehicles (V2V) and roadside units (V2I); these are, in fact, the same message (hence, sometimes jointly referred to as V2X), which is periodically transmitted. The I2V message contains data of a more static nature and may be either event-triggered or periodically transmitted. An overview of the real-time control system software is given in Figure 5.1, showing its functional architecture.

In the remainder of this section, the software architecture of the Real-Time CACC Platform will be discussed in more detail, including a brief description of the wireless message content which is crucial to the CACC system. This section concludes with a description of the real-time software implemented on the Vehicle Gateway.

5.2.1 The Real-Time CACC Platform

The control system implemented on the Real-Time CACC Platform has a layered architecture, consisting of the following layers, as shown in Figure 5.1:

- Perception layer;
- Control layer;
- Supervisory layer.

Sensory inputs enter into the control system via the perception layer, which contains observers for both the (host) vehicle motion and the target vehicle motion. The control algorithms for CACC are implemented in the control layer, whereas the supervisory layer determines a number of controller parameters, taking into account driver inputs through the HMI and instructions from roadside units, if any. Moreover, the supervisory layer ensures safe operation of the vehicle by monitoring the quality of the target vehicle data and adapting the controller settings accordingly. The entire platform runs at a 100 Hz update rate in the test vehicles, although, given the bandwidth of the controlled system (see Chapter 3, for instance), an update rate of 25 Hz would suffice. The contents of each layer will be described in more detail below.

Perception layer

The perception layer generally performs postprocessing of sensor signals such as filtering, and estimation of those signals that cannot be directly measured, or
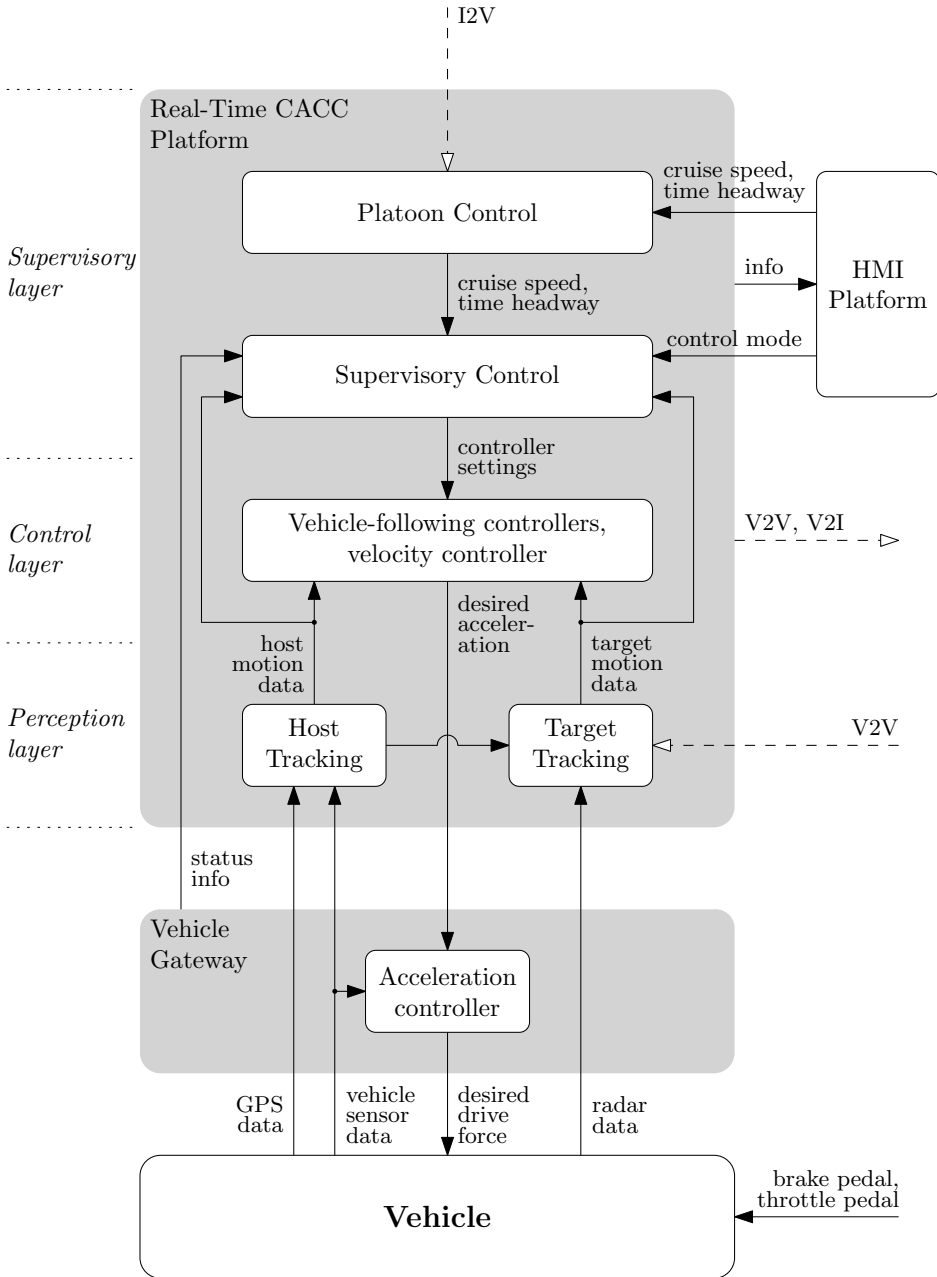
Figure 5.1: Functional architecture of the real-time control system software for CACC.
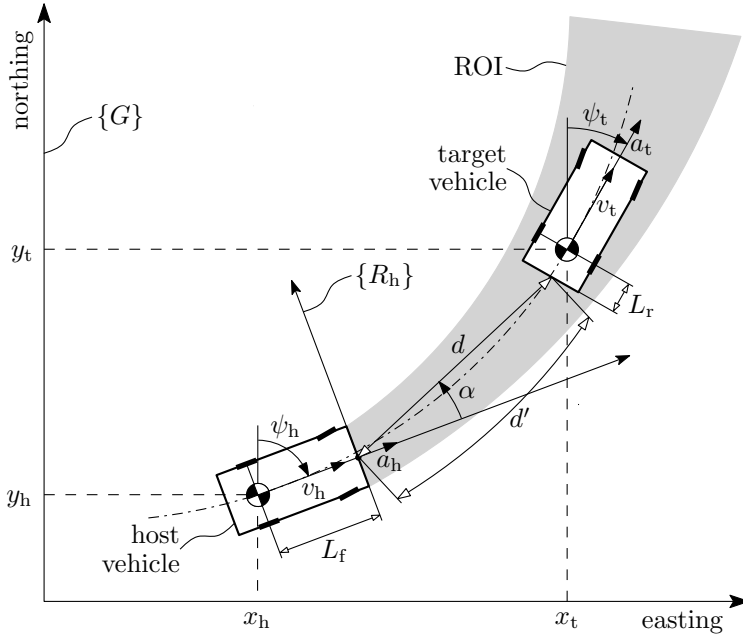
Figure 5.2: CACC-relevant coordinate systems.

only with insufficient accuracy. The perception layer in the test vehicles currently includes two components, being the Host Tracking and the Target Tracking. The Host Tracking aims to estimate the relevant kinematical host vehicle states[1], being the global position coordinates (x_h, y_h), the heading angle ψ_h, the longitudinal component v_h of the host vehicle velocity, and the longitudinal component a_h of the host vehicle acceleration. The longitudinal velocity and acceleration components are the components in the direction of the vehicle, whereas the vehicle position and orientation are expressed with respect to a fixed, global coordinate frame $\{G\}$; see Figure 5.2, showing the aforementioned kinematical states as well as the global coordinate system. In practice, the Universal Transverse Mercator (UTM) system (Hofmann-Wellenhof et al., 2001) is commonly chosen as the global coordinate system. The UTM system divides the earth surface in enumerated rectangular patches, each one with its own Cartesian coordinate system, with the x-axis pointing eastwards and the y-axis pointing in northern direction, which is why the x-coordinate is commonly referred to as "easting" and the y-coordinate as "northing". The kinematical states are determined by fusion of GPS readings and measurements from onboard vehicle sensors, i.e., the accelerometer, the wheel speed encoders, and the gyroscope. These vehicle sensors are present in all vehicles nowadays. The sensor fusion is implemented using an extended Kalman filter (Toledo-Moreo et al., 2011) which is based on a nonlinear kinematical model of

---

[1]In this chapter, the term "state" refers to all relevant kinematical variables of the vehicle, not necessarily to the states of a state-space model of that vehicle.

the vehicle. Note that all kinematical states relate to the rear axle center and are part of the message that is communicated to other vehicles.

The objective of the Target Tracking is to determine the relevant kinematical states of other ("target") vehicles, expressed in the host vehicle bound coordinate system $\{R_{\mathrm{h}}\}$, which has its origin in the front bumper center, with the x-axis pointing forward and the y-axis pointing to the left, see Figure 5.2. The origin of $\{R_{\mathrm{h}}\}$ is assumed to coincide with the forward-looking radar mounted in the grill of the vehicle. For CACC, the relevant kinematical variables are the object distance d, the magnitude of the relative velocity $\Delta v = \dot{d}$ and the desired longitudinal target vehicle acceleration u_{t}, being the input of the target vehicle (Ploeg et al., 2014b). The Target Tracking encompasses the following operations:

Coordinate transformation   Information regarding other vehicles is obtained by the onboard radar and through wireless communication. However, the radar provides the rear-bumper target vehicle position and velocity in the vehicle-fixed coordinate frame $\{R_{\mathrm{h}}\}$, whereas the wireless communicated message contains target vehicle states that relate to the target vehicle rear axle center, expressed in the global coordinate system $\{G\}$. Therefore, using the output of the Host Tracking and the distance L_{f} between the rear axle and the front bumper of the host vehicle, the target vehicle motion states (relating to the target vehicle's rear axle center) are transformed to coordinates in $\{R_{\mathrm{h}}\}$ of the rear axle center of the target vehicle. Next, from the target vehicle rear axle coordinates in $\{R_{\mathrm{h}}\}$, the target vehicle rear bumper coordinates in $\{R_{\mathrm{h}}\}$ are calculated using the target vehicle heading ψ_{t} and the distance L_{r} between the target vehicle rear axle and its rear bumper, both of which are also included in the wireless message. This finally results in the distance d, the relative velocity Δv, and the bearing angle α for each target vehicle that is detected by radar and/or wireless communication[2].

Region-of-interest filtering   In order to limit the computational effort, a first selection is made regarding objects that will be further processed, by dismissing all objects outside the region of interest (ROI). The ROI, as depicted in Figure 5.2, is determined using a kinematic prediction of the host vehicle motion. In a more advanced version, this region could be determined based on a digital map of the road network or by means of an onboard camera.

Data association   As a next step, the target vehicle distance d, bearing angle α, and relative velocity Δv, obtained through the radar measurements and wireless communication, need to be associated in case they originate from the same target vehicle. Moreover, these variables need to be associated with the correct Kalman filter used for data fusion in the next step, i.e., the Kalman filter that already "contains" that specific object, such that the correct measurements will be used. Many methods exist for data association, most of them employing a probabilistic approach, see, e.g., Li and Jilkov (2002) and Mori et al. (2002) and the references

---

[2]Here, the Euclidean distance d is used, whereas in fact the distance d' along the road curve should have been applied. However, the error as a result thereof is rather small: with a curve radius of 100 m and an intervehicle distance $d' = 35\,\mathrm{m}$ (which corresponds to about 1 s time gap at $100\,\mathrm{km/h}$), the Euclidean distance is equal to $d = 34.83\,\mathrm{m}$, i.e., an error of only $0.5\,\%$.

contained therein. In the current test setup, however, a deterministic method, known as Quality Threshold Clustering (Heyer et al., 1999), is used in view of minimal computational effort. With this method, those measurements are associated ("clustered") that are closest to each other in the Euclidean sense, within a certain distance threshold.

Data fusion   Having associated the radar measurements and the wireless information with a specific object, the information from both sources must be fused. To this end, a (linear) Kalman filter can be applied. However, it is also possible to just select the distance d and relative velocity Δv from the radar, since these are in practice sufficiently accurate to be used without any further processing. In either case, the desired target vehicle acceleration u_t can only be obtained through wireless communication. If the target vehicle is only detected by radar, the actual acceleration can be estimated using a linear Kalman filter and subsequently used as a feedforward signal for the controller, thereby providing a method for graceful degradation (see Chapter 4). If only wireless information is available, which is the case when the target vehicle is outside the field of view of the radar, then d and Δv as calculated from the wireless information (see the coordinate transformation item above) can be used. In this case, there is generally no need for any further signal processing to improve the signal-to-noise ratio since the communicated signals are already the result of an estimation algorithm, included in the Host Tracking module of each vehicle.

Object classification   The final step of the Target Tracking is to classify the objects as standing or moving and, in case of the latter, as oncoming traffic or traffic in the same direction. Based on these classifications, the CACC-relevant target vehicles are finally selected as follows. First, oncoming traffic will be ignored because CACC is not a collision avoidance system. Next, above a certain velocity of the host vehicle, standing objects are also ignored to prevent false detections, caused by road signs, viaducts, etc., at high velocities, whereas moving objects are always taken into account, provided they move in roughly the same direction as the host vehicle[3]. From the resulting subset of detected objects, the Most Important Object (MIO) is selected, being the directly preceding vehicle in case of one-vehicle look-ahead CACC. In the case of two-vehicle look-ahead CACC (see Chapter 3), the second preceding vehicle is also taken into account.

Control layer

The Target Tracking result, being the distance d, the relative velocity Δv and the desired target acceleration u_t (or the estimated target acceleration $\hat{a}_\mathrm{t}$) of the preceding vehicle and possibly the desired acceleration of the second preceding

---

[3]Ignoring standing objects at higher speed has important consequences, such as a complete lack of reaction when approaching the tail of a traffic jam. Nevertheless, this is still common behavior in commercially available Adaptive Cruise Control, thus putting more emphasis on the prevention of sudden braking due to false detections, especially on highways. One may however expect that, in the near future, this workaround is no longer necessary due to increasing reliability of radar sensors and advanced techniques to fuse radar and camera measurements.

vehicle, is used as input to the control layer. This layer contains the actual vehicle-following controller as extensively described in Chapters 2 and 3. In case no target vehicle is detected, the control system automatically reverts to a velocity-controlled mode, which simply aims to realize the cruise speed as set by the driver.

Supervisory layer

The purpose of the supervisory layer is twofold. First, it coordinates the controller settings from the driver and from roadside equipment, if any, by means of the Platoon Control unit. Second, the supervisory layer implements mechanisms to ensure safe operation of the controlled vehicle, referred to as the Supervisory Control unit.

Adopting the spacing policy

$$d_{\mathrm{r}} = r + h v_{\mathrm{h}}, \tag{5.1}$$

where d_{r} is the desired intervehicle distance, r the standstill distance, h the time gap, and v_{h} the (longitudinal component of the) host vehicle velocity, the Supervisory Control unit may increase h and/or r as set by the driver through the HMI, depending on the accuracy of the kinematical states of the detected target. To this end, the noise covariance and the active sensor set (radar and/or wireless communication) is forwarded to the Supervisory Control unit, upon which the latter calculates a safe intervehicle distance, thereby overruling the driver setting, while also taking into account the minimum time gap that is necessary for string-stable operation of the CACC system (Nunen et al., 2013; Ploeg et al., 2014b).

As an example, when the target vehicle is detected by radar only, the graceful degradation mechanism as described in Chapter 4 comes into operation, which *estimates* the actual target acceleration instead of using the communicated desired acceleration. As a result, both string stability and safety are compromised, albeit to a limited extent. The Supervisory Control unit then reacts by increasing the time gap h and/or the standstill distance r, such that safe and string-stable operation is again realized. When a target is not present in the first place or when it is not detected for some reason, the Supervisory Control unit instructs the control layer to switch to cruise control, being the common mechanism for vehicles with Adaptive Cruise Control (ACC). In case of CACC at small intervehicle distances, it could be argued that a slight deceleration and subsequent return of control to the driver is a safer alternative, taking into account a possible failure of both the radar and the wireless communication. Note that the driver can choose to only use cruise control, indicated by the "control mode" in Figure 5.1, in which case this setting is directly forwarded to the control layer.

Finally, the Platoon Control unit compares the time gap and cruise speed received from roadside equipment with the ones set by the driver, upon which the larger time gap and the smaller cruise speed is forwarded to the Supervisory Control unit. This functionality is implemented to allow for the future implementation of automated merging at up-ramps on highways. Here, it is envisioned that roadside equipment detects an upcoming vehicle on the up-ramp, and instructs a specific vehicle in the platoon to create a gap for the merging vehicle.

Table 5.1: V2X WIRELESS MESSAGE CONTENT (EXCERPT).

Signal	Description	Purpose
t	Time of transmission [s]	Determine message age; ignore message when exceeding a certain threshold.
$^W q_{\mathrm{long}}$	Position, longitude [°]	Data association; distance calculation in the absence of radar detection.
$^W q_{\mathrm{lat}}$	Position, latitude [°]	Data association; distance calculation in the absence of radar detection.
c_{p}	Position confidence interval (95 %)	Assess reliability of the wireless message content.
$^W \psi$	Heading [rad]	Object classification (oncoming traffic vs. traffic in the same direction); distance calculation in the absence of radar detection.
v	Velocity [m/s]	Object classification (standing vs. moving); relative velocity calculation in the absence of radar detection.
u	Vehicle input (desired acceleration) [m/s^2]	Vehicle-following control.
a	Longitudinal acceleration [m/s^2]	Vehicle-following control, if u is not available.
L_{r}	Distance from rear bumper to rear axle [m]	Calculation by receiving vehicle of the transmitting vehicle rear-bumper coordinates.

Wireless message content

As mentioned at the beginning of this section, the Real-Time CACC Platform interacts with the outside world through wireless communication. To this end, wireless messages are periodically transmitted to and received from other vehicles (V2X) at an update rate of 25 Hz in the current test setup. As may be concluded from the previous section, these messages contain more information than strictly needed for the vehicle-following controller: The controller only requires the desired target vehicle acceleration, assuming that the distance and relative velocity are measured by the onboard radar. However, in order to determine the CACC-relevant vehicles, and to be able to estimate distance and relative velocity if the radar does not detect the target vehicle (e.g., in sharp curves), the wireless message also includes the kinematical states of the transmitting vehicle.

Table 5.1 provides an overview of the most important information contained in the wireless message and mentions the main purpose of that information. Note that the subscripts "h" for host vehicle and "t" for target vehicle have been omitted since this message holds for all vehicles. The left superscript "W" indicates the so-called WGS84 coordinate system (Hofmann-Wellenhof et al., 2001), in which the position is expressed in degrees longitude and degrees latitude, the use of which in wireless communication is more common than the use of UTM coordinates.

Consequently, upon reception, these coordinates first have to be transformed to UTM coordinates to allow for distance calculation. Furthermore, the message also contains an indication of the reliability of the information, by means of the 95 % position confidence interval c_p; upon exceeding a predefined position confidence threshold, the wireless message will be ignored and only the radar will be used, using the control strategy for graceful degradation as described in Chapter 4.

From Table 5.1, it can be readily concluded that the message contains significantly more information than required for the vehicle-following controller *per se*. Note that Table 5.1 only contains a small part of the wireless message content: In the current test setup, 36 signals are included in the message, providing, e.g., information regarding the active controller in the target vehicle, and, if CACC is active, its time gap and cruise speed. In addition, the message also contains the accuracy of all vehicle states and, for future use, a merge-request signal indicating that the transmitting vehicle intends to join the platoon.

5.2.2   The Vehicle Gateway

The interaction between the Real-Time CACC Platform and the vehicle electronics takes place through the Vehicle Gateway, which is a real-time computer platform that forwards vehicle sensor readings to the perception layer and vehicle status information to the supervisory layer. The Vehicle Gateway processes information at a relatively high sampling rate (100 Hz) to minimize the time delay introduced by this system. In addition, the Vehicle Gateway also converts the desired acceleration u, being the main output of the Real-Time CACC Platform, into vehicle actuator setpoints, such that the requested acceleration is accurately realized. The Vehicle Gateway employs multiple types of interfacing protocols for the communication with the vehicle systems, as described in Section 5.3, whereas a single Controller Area Network (CAN) bus is used for communication with the Real-Time CACC Platform. The status of this CAN bus is continuously monitored to guarantee safe and reliable operation.

For the current type of test vehicle (Toyota Prius III), the actuator setpoint actually consists of a single signal, being the desired drive force $F_{d,r}$, which can be both positive and negative. The native hybrid drive line control system then controls the combustion engine, the electric drive and the disc brakes so as to realize the requested force, which is determined by the Vehicle Gateway through a feedforward controller. This feedforward controller converts the desired acceleration u to the desired drive force $F_{d,r}$, while compensating for the so-called road load force F_{rl} according to (omitting the subscript "h" for host or "t" for target)

$$F_{rl} = F_g + F_{drag}. \tag{5.2}$$

Here, F_g is the gravity force component due to the road slope according to

$$F_g = mg \sin \beta, \tag{5.3}$$

where m is the vehicle mass, g the gravity constant, and β the road slope angle. F_{drag} is a drag force caused by the rolling resistance and the aerodynamic drag,
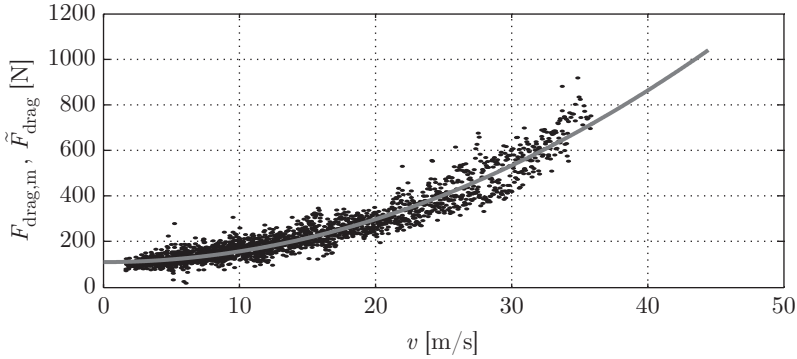
Figure 5.3: Coast-down test result: Measured drag force $F_{\mathrm{drag,m}}$ (dotted black) and 2nd-order polynomial approximation $\widetilde{F}_{\mathrm{drag}}$ (solid gray) as a function of the velocity v (with $m_{\mathrm{nom}} = 1627\,\mathrm{kg}$).

being approximately equal to

$$F_{\mathrm{drag}} = mgc_{\mathrm{r}}\cos\beta + c_1 v + c_2 v^2, \tag{5.4}$$

where v is the vehicle velocity; c_{r} is the rolling resistance coefficient, whereas the coefficients c_1 and c_2 are related to the aerodynamic drag.

The drag force coefficients c_{r}, c_1, and c_2 in (5.4) are determined *a priori* based on a so-called coast-down test. This test involves accelerating to a relatively high velocity on a flat road, and subsequently letting the vehicle come to a full stop with disengaged clutch while measuring the velocity v and the acceleration a. With a known vehicle mass m_{nom} at the time of measurement (through explicit weighing of the vehicle and its passengers), the "measured" drag force $F_{\mathrm{drag,m}}$ can then be determined by $F_{\mathrm{drag,m}} = m_{\mathrm{nom}}a$, upon which a curve-fitting procedure is applied, yielding a 2nd-order polynomial $\widetilde{F}_{\mathrm{drag}}$ as a function of the velocity v. The result is illustrated in Figure 5.3, which shows both the measured drag force $F_{\mathrm{drag,m}}$ and the 2nd-order polynomial $\widetilde{F}_{\mathrm{drag}}$. Subsequently, the drag force coefficients are calculated by setting the 2nd-order polynomial $\widetilde{F}_{\mathrm{drag}}$ equal to (5.4), with $m = m_{\mathrm{nom}}$ and $\beta = 0$.

Finally, in order to provide real-time estimates $\widehat{F}_{\mathrm{g}}$ of the gravity force component and $\widehat{F}_{\mathrm{drag}}$ of the drag force under CACC operation of the vehicle, the mass m and the road slope β are estimated simultaneously, using a recursive least squares method as proposed in Vahidi et al. (2005), based on the velocity v, the acceleration a, and the drive force F_d that are measured while driving. As a result, the road load can be approximated in real-time as

$$\begin{aligned}
\widehat{F}_{\mathrm{rl}} &= \widehat{F}_{\mathrm{g}} + \widehat{F}_{\mathrm{drag}} \\
&= \hat{m}g\sin\hat{\beta} + \hat{m}gc_{\mathrm{r}}\cos\hat{\beta} + c_1 v + c_2 v^2
\end{aligned} \tag{5.5}$$

with $\hat{m}$ and $\hat{\beta}$ being the estimated mass and the estimated road slope, respectively.
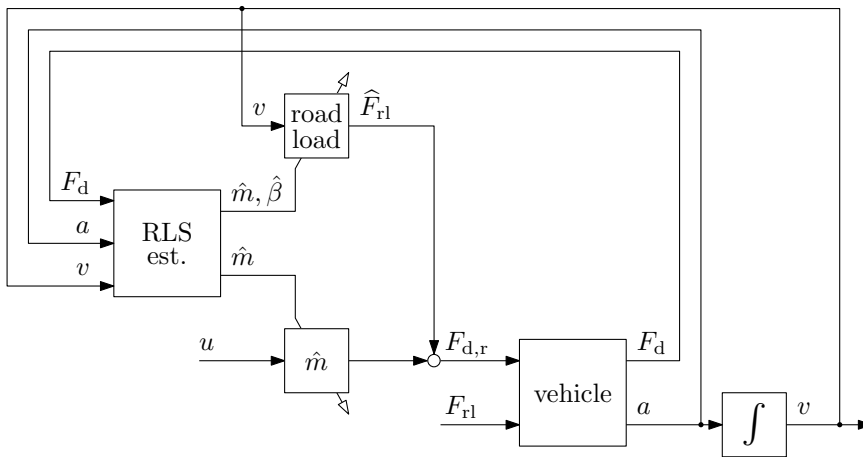
Figure 5.4: Acceleration controller as implemented in the Vehicle Gateway.

The Vehicle Gateway thus implements a feedforward acceleration controller with disturbance compensation, the block scheme of which is given in Figure 5.4. For the test vehicles, it appeared that the resulting dynamic behavior of the acceleration-controlled vehicle can be described by a 1st-order transfer function from the input $u(s)$ to the acceleration $a(s)$, which also appears to include a small time delay, as mentioned in the previous chapters.

5.3   Vehicle instrumentation

To implement the control software as described in the previous section, additional vehicle instrumentation is required, such as real-time computing platforms, sensors and a driver HMI. This section provides an overview of the hardware as implemented in the test vehicles, based on which an assessment is made which hardware would actually be needed for a commercial implementation of CACC.

Figure 5.5 shows the hardware layout of the test vehicles. Starting with the equipment that is installed in the trunk, the Real-Time CACC Platform is a small computer equipped with a real-time operating system. The Real-Time CACC Platform is connected to the Vehicle Gateway through a Controller Area Network (CAN) bus, whereas an ethernet connection, employing the User Datagram Protocol (UDP), is used for communication with the HMI Platform. The latter is a common PC, albeit with a small form factor.

The wireless messages are transmitted and received through a modem, the so-called ITS G5 Gateway, using an ethernet UDP connection as well. The ITS G5 wireless communication standard is based on the IEEE 802.11p standard (Ström, 2011), which determines, among others, the type of antenna that is mounted on the roof of the vehicle. The ethernet switch just serves as a hub, routing all ethernet messages in the vehicle.
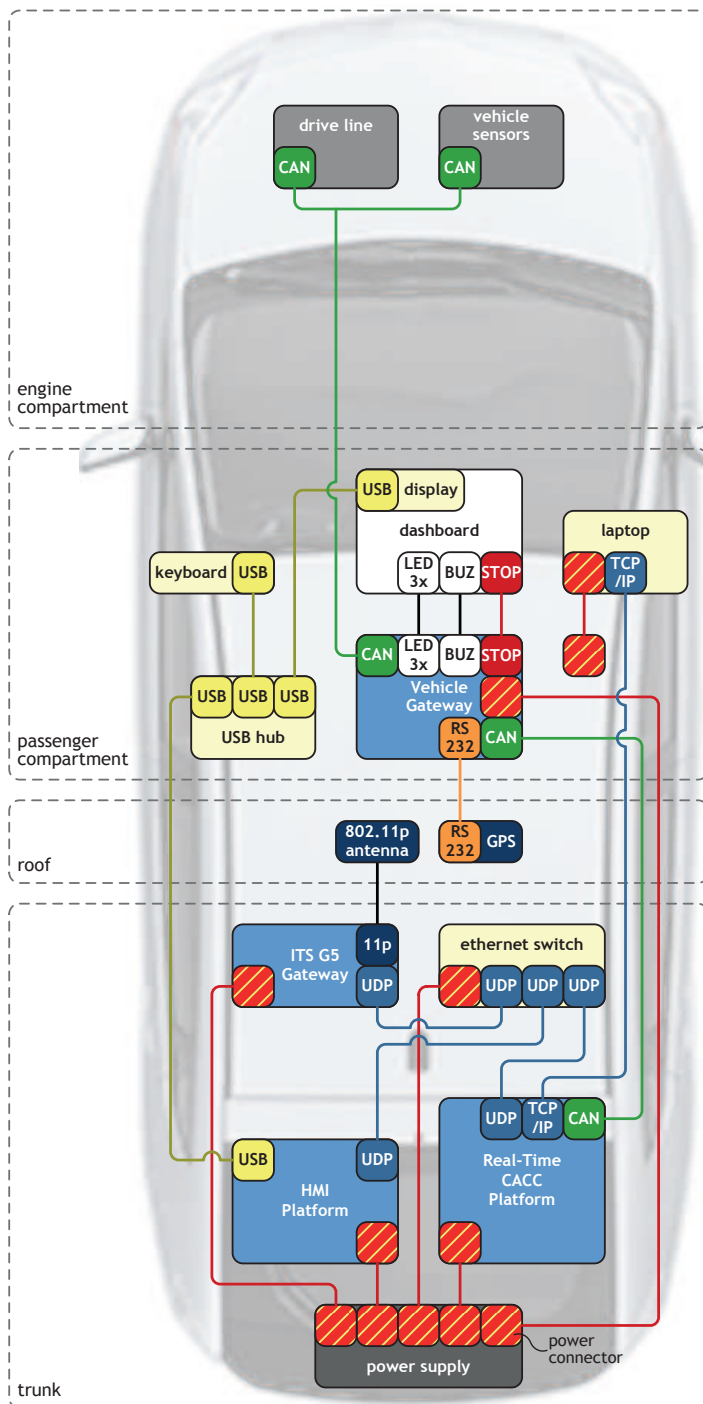
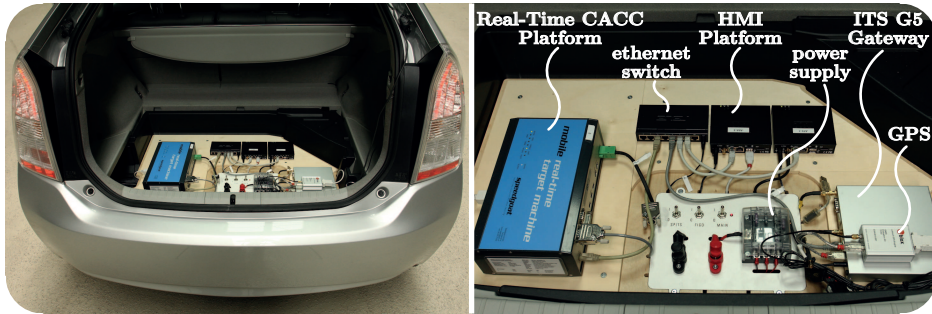**Figure 5.5:** Instrumentation of the test vehicles.

Figure 5.6: Overview (left) and close-up (right) of the CACC-related hardware in the vehicle trunk.

Figure 5.6 shows a photograph of the trunk of the test vehicle, including a close-up, from which the Real-Time CACC Platform, the HMI Platform, the ITS G5 Gateway and the ethernet switch can be identified.

The Vehicle Gateway, located in the passenger compartment, communicates with the native vehicle systems through a CAN bus. These native vehicle systems are the drive line, the accelerometer, the gyroscope, and the wheel speed encoders. In addition, the GPS receiver is connected to the Vehicle Gateway, using a serial bus (RS232) for reasons of convenience. In addition, the HMI Platform is connected by means of a Universal Serial Bus (USB) connection to a dedicated CACC display in the dashboard, which allows the driver to provide controller settings, as described in the previous section, and to obtain information about the current status. Figure 5.7 shows a photograph of the vehicle dashboard, including close-ups of the CACC display mounted in the dashboard and the native vehicle display. The CACC display shows with which sensors the target vehicle is currently detected, by means of a wireless communication icon on the target vehicle and a "radar beam" in front of the host vehicle. Note that the native vehicle display is normally used for the ACC, being an original feature of the vehicle. However, this display is now also updated with CACC information through the vehicle CAN bus that is connected to the Vehicle Gateway. For the purpose of control system development, the status of the Vehicle Gateway is also displayed on the dashboard using LEDs and, in addition, includes an auditory warning by means of a buzzer (indicated by "BUZ" in Figure 5.5) to indicate malfunctioning. Finally, an emergency button (indicated by "STOP" in Figure 5.5) is installed, which is capable of immediately de-activating the Vehicle Gateway, thereby disconnecting all CACC-related components and restoring the original vehicle settings.

Finally, peripheral equipment can be installed such as a laptop for programming the Real-Time CACC Platform over an ethernet TCP/IP connection using Matlab/Simulink®, and a USB keyboard for programming the HMI Platform.

From this brief description of the CACC-related vehicle instrumentation, it may appear as if a considerable amount of additional hardware is required to implement CACC. However, the final commercial implementation of CACC requires

Figure 5.7: Human–machine interfaces in the dashboard: overview (bottom left), close-up of the CACC display (bottom right), and close-up of the native vehicle display (top).

considerably less additional instrumentation, provided that the vehicle is already equipped with ACC, such that a processing computer as well as a radar are already available. In that case, the Real-Time CACC Platform and the Vehicle Gateway functionality can be implemented in the existing ACC processing unit, whereas the vehicle sensors (accelerometer, wheel speed encoders and gyroscope) are nowadays present in every vehicle. Also the HMI functionality can be easily integrated in the existing system. Consequently, only the wireless gateway and a GPS receiver need to be added, both of which are not very costly.

5.4 Conclusion

Next to the controller itself, practical implementation of CACC requires additional functionality related to position and velocity estimation of both the host vehicle and the target vehicle(s), the latter also including the association of radar signals with the corresponding wireless messages. In addition, the driver must be allowed to interact with the system and mechanisms for fault tolerance and graceful degradation need to be implemented. Therefore, a layered control system architecture was proposed, consisting of a perception layer, a control layer, and a supervisory layer, as implemented in the prototype CACC vehicles used for experiments. The hardware instrumentation of these vehicles was described, from which it was concluded that although the instrumentation is rather extensive for the purpose of CACC development, the actual commercial implementation would only require a GPS receiver and a wireless modem, provided that the vehicle is already equipped with ACC.

Chapter 6

Position control of a wheeled mobile robot[1]

Abstract   The design and implementation of driver assistance systems, among which Cooperative Adaptive Cruise Control, requires a thorough development procedure in view of safety and reliability.   An important part of such a development procedure consists of hardware-in-the-loop experiments in a controlled environment. To this end, a facility called Vehicle Hardware-In-the-Loop (VeHIL) is operated, aiming at testing the entire road vehicle in an artificial environment. In VeHIL, the test vehicle is placed on a roller bench, whereas other traffic participants are emulated using wheeled mobile robots (WMRs). To achieve a high degree of experiment reproducibility, focus is put on the design of an accurate position control system for the robots. Due to the required types of maneuvers, these robots have independently driven and steered wheels. Consequently, the robot is overactuated. Furthermore, since the robot is capable of highly dynamic maneuvers, slip effects caused by the tires can play an important role.   A position controller based on feedback linearization is presented, using the so-called multicycle approach, which regards the robot as a set of identical unicycles. As a result, the WMR is position controlled by means of four identical unicycle controllers, taking weight transfer as well as longitudinal and lateral tire slip into account.

6.1   Introduction

Advanced driver assistance systems, such as adaptive cruise control, collision warning, and collision mitigation systems, have become increasingly available on road vehicles (Vahidi and Eskandarian, 2003). Recently, research has also been directed toward a class of assistance systems, known as cooperative driving systems, that aim for a common goal, such as increased throughput, safety, and/or fuel efficiency (Kato et al., 2002; Arem et al., 2006), with Cooperative Adaptive Cruise Control as an important example. To support the development of this wide variety of assistance systems, a test facility called Vehicle Hardware-In-the-Loop (VeHIL)

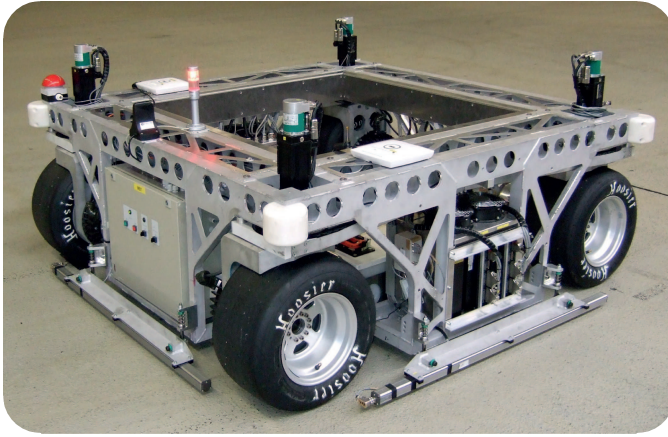[1]This chapter is based on Ploeg et al. (2009).

Figure 6.1: One of the wheeled mobile robots used in VeHIL (without vehicle body),
serving as a target vehicle for testing advanced driver assistance systems.

was put into operation several years ago (Gietelink et al., 2006) and, among oth-
ers, used to develop and evaluate a control algorithm for Cooperative Adaptive
Cruise Control (Gietelink, 2007). VeHIL enables the hardware-in-the-loop test-
ing of entire road vehicles equipped with advanced driver assistance functionality
based on environment sensors, such as radar, lidar, or vision. The principle of
VeHIL is to simulate the relative motion of other vehicles with respect to the
test vehicle, allowing for efficient, safe, and reproducible testing. The neighboring
vehicles are emulated by wheeled mobile robots (WMRs), one of which is shown
in Figure 6.1, with the vehicle body removed. This VeHIL WMR or *Moving Base*
(MB) differs from most wheeled robots used in the industry in that it is capable
of extreme maneuvers at velocities of up to 50 km/h in all directions (Ploeg et
al., 2002). Consequently, the control system has to be designed such that these
specifications are fully exploited, which is the focus of this chapter.

The main control objective of the MB is to let its center track a reference tra-
jectory consisting of the position and the orientation in the horizontal plane. This
is achieved by four independently driven and steered wheels. As a consequence,
the MB has eight actuators—four driving and four steering motors—whereas the
MB as a whole has 3 degrees of freedom only. The MB can therefore be charac-
terized as being *overactuated*. In Ploeg et al. (2006), a control method based on
feedback linearization is presented, which handles the overactuated nature of the
system by regarding the MB as four independent unicycles. Although the results
of this controller were promising, they can be improved by taking tire behavior
into account in the controller design since tires introduce slip effects that compro-
mise the position accuracy. A possible approach for counteracting this effect is to
incorporate a tire model, which is well known in the field of automotive engineer-
ing (Pacejka, 2002), in a feedback linearization-based controller, as is commonly
used in the field of robotics (Canudas de Wit et al., 1996; Bendtsen et al., 2002).

Following this proposed approach, Section 6.2 first introduces the main charac-

Table 6.1: MOVING BASE SPECIFICATIONS.

Characteristic	Specification
Vehicle mass with/without body	$756/694\,\mathrm{kg}$
Wheel base $\times$ track width	$1.4\,\mathrm{m} \times 1.4\,\mathrm{m}$
Center-of-gravity height	$0.40\,\mathrm{m}$
Maximum velocity (in all directions)	$50\,\mathrm{km/h}$
Maximum translational acceleration	$10\,\mathrm{m/s^2}$
Maximum centripetal acceleration	$12\,\mathrm{m/s^2}$
Installed power	$52\,\mathrm{kW}$
Steering angle range	$[-350°, 350°]$

teristics of the MB, upon which Section 6.3 states the control problem and presents the concept that will be employed to solve the control problem. Next, Section 6.4 introduces a dynamic unicycle model incorporating tire behavior, based on which the unicycle controller design is described. The resulting unicycle controller appears to require system states that have to be estimated, to which end Section 6.5 proposes two observers: One for the motion of the MB as a whole, and one specifically for the tire slip. Section 6.6 then briefly describes how the unicycle controllers are combined to create a so-called multicycle controller, suitable to control the MB. Finally, Section 6.7 presents experimental results obtained with the actual MB and Section 6.8 summarizes the main conclusions.

6.2 Moving Base characteristics

Table 6.1 summarizes the main MB characteristics relevant to the controller design. The high acceleration levels, together with the considerable mass, as mentioned in the table, lead to a significant weight transfer from one wheel to another, influencing the actual vertical load of the tires. The friction force that a tire can deliver is, in turn, approximately proportional to its actual vertical load (Pacejka, 2002). Consequently, the drive torque distribution across the four wheels should correspond to the actual vertical loads to obtain the maximum performance of the MB in terms of acceleration and maneuverability.

   The tire friction force also depends on the longitudinal slip κ and the lateral slip angle α, where κ is equal to the normalized velocity difference between the tire and the road, and α is the angle between the wheel plane and the velocity direction. This slip dependency is illustrated in Figure 6.2, which shows the longitudinal tire force F_{long}, which is normalized by the vertical load F_z, as a function of the slip κ according to the Magic Formula tire model (Pacejka, 2002). The lateral force characteristic is described by a similar function. This characteristic justifies the incorporation of tire slip into the control design. Note that Figure 6.2 also shows the linear approximation of the tire characteristic, which is valid for $\kappa \ll 1$. The same type of approximation applies to the lateral characteristic.
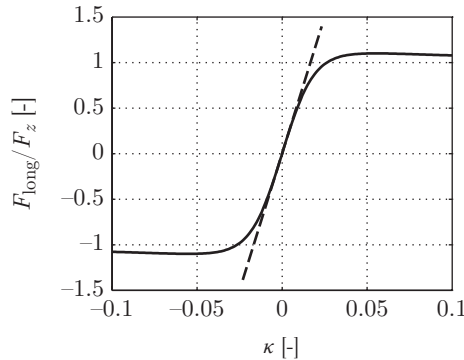
Figure 6.2: Normalized longitudinal tire characteristic of the MB (solid) and a linear approximation in the neighborhood of $\kappa = 0$ (dashed).

6.3   Control concept

The control objective of the MB is to let its center track a reference trajectory s_r in a global Cartesian coordinate system $\{G\}$ as shown in Figure 6.3, depicting the MB coordinate systems and the main kinematical variables. The reference trajectory s_r consists of the desired position $(x_\mathrm{r}, y_\mathrm{r})$ and the desired orientation ψ_r as a function of the time t, i.e.,

$$s_\mathrm{r}(t) = \begin{pmatrix} x_\mathrm{r}(t) \\ y_\mathrm{r}(t) \\ \psi_\mathrm{r}(t) \end{pmatrix}, \tag{6.1}$$

where the components of $s_\mathrm{r}(t)$ can be chosen independently (within certain operational limits), provided that $s_\mathrm{r}(t)$ is a continuously differentiable trajectory.

The controller is designed using a similar approach as that applied in Ploeg et al. (2006), being inspired by the idea presented in Borenstein (1995), which is to decentralize the tracking problem. To this end, the reference vector s_r is converted to reference positions $x_{\mathrm{r},i}$ and $y_{\mathrm{r},i}$, $i = 1, \ldots, 4$, for the separate wheels, enumerating them in a clockwise fashion, starting with $i = 1$ for the front left wheel; see Figure 6.3. The reference positions for the four wheels $i = 1, \ldots, 4$ thus read

$$\begin{aligned}
x_{\mathrm{r},1} &= x_\mathrm{r} + L_\mathrm{d} \cos\big(\psi_\mathrm{r} + \arctan(W/L)\big) \\
y_{\mathrm{r},1} &= y_\mathrm{r} + L_\mathrm{d} \sin\big(\psi_\mathrm{r} + \arctan(W/L)\big) \\
x_{\mathrm{r},2} &= x_\mathrm{r} + L_\mathrm{d} \cos\big(\psi_\mathrm{r} - \arctan(W/L)\big) \\
y_{\mathrm{r},2} &= y_\mathrm{r} - L_\mathrm{d} \sin\big(\psi_\mathrm{r} - \arctan(W/L)\big) \\
x_{\mathrm{r},3} &= x_\mathrm{r} - L_\mathrm{d} \cos\big(\psi_\mathrm{r} + \arctan(W/L)\big) \\
y_{\mathrm{r},3} &= y_\mathrm{r} - L_\mathrm{d} \sin\big(\psi_\mathrm{r} + \arctan(W/L)\big) \\
x_{\mathrm{r},4} &= x_\mathrm{r} - L_\mathrm{d} \cos\big(\psi_\mathrm{r} - \arctan(W/L)\big) \\
y_{\mathrm{r},4} &= y_\mathrm{r} + L_\mathrm{d} \sin\big(\psi_\mathrm{r} - \arctan(W/L)\big),
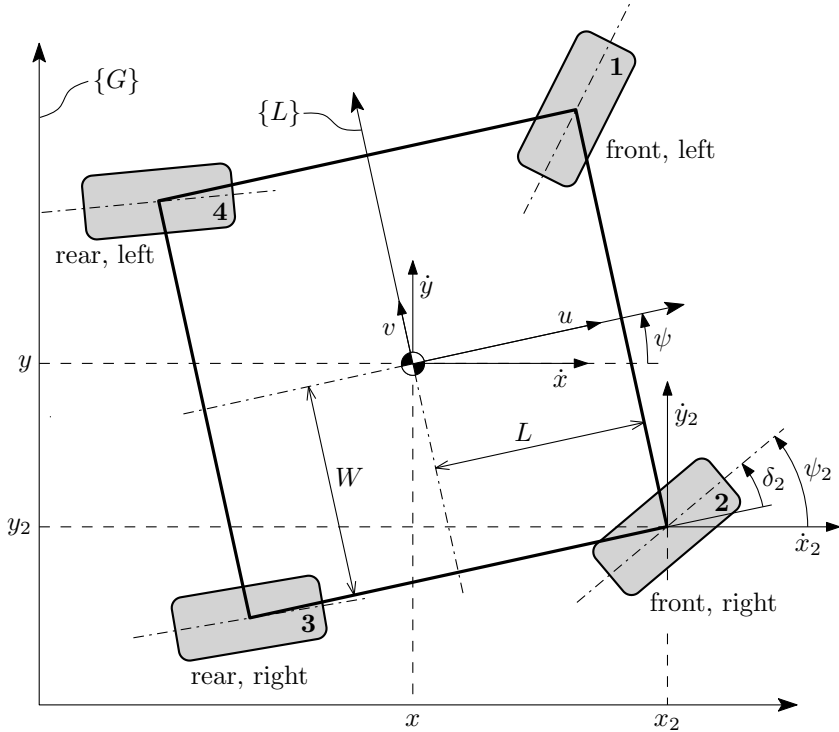\end{aligned} \tag{6.2}$$

Figure 6.3: Moving Base coordinate systems: The global Cartesian coordinate system $\{G\}$ and the local Cartesian coordinate system $\{L\}$.

where L and W are half the vehicle length and width respectively, and $L_{\mathrm{d}} = \sqrt{L^2 + W^2}$.

Although (6.2) uniquely defines the MB position and orientation, reference wheel orientation angles $\psi_{\mathrm{r},i}$ are also needed, because the MB should be able to move in all directions, i.e., the MB must be fully controllable. These angles are kinematically calculated according to

$$\psi_{\mathrm{r},i} = \arctan\left(\frac{\dot{y}_{\mathrm{r},i}}{\dot{x}_{\mathrm{r},i}}\right), \quad i = 1, \ldots, 4, \tag{6.3}$$

where the velocities $\dot{x}_{\mathrm{r},i}$ and $\dot{y}_{\mathrm{r},i}$ are determined by differentiation of the appropriate equations in (6.2). Note that in case $\dot{x}_{\mathrm{r},i} = 0$ and $\dot{y}_{\mathrm{r},i} \neq 0$, $\psi_{\mathrm{r},i} = \mathrm{sgn}(\dot{y}_{\mathrm{r},i})\pi$ is chosen. Yet another singularity occurs in (6.3) at $\dot{x}_{\mathrm{r},i} = \dot{y}_{\mathrm{r},i} = 0$, which can be directly understood because at standstill, the wheel orientations can have any value. This singularity can be handled in practice by requiring that the wheels resume their nominal steering angle (e.g., equal to zero) at very low values of both $\dot{x}_{\mathrm{r},i}$ and $\dot{y}_{\mathrm{r},i}$. This situation, however, is considered out of scope for the controller design described in this chapter; in other words, it is assumed that

$$\dot{x}_{\mathrm{r},i}^2 + \dot{y}_{\mathrm{r},i}^2 > 0. \tag{6.4}$$

The MB is thus regarded as a set of four identical subsystems, which are called *unicycles*, being single wheels that can be steered and driven. All four unicycles have their specific continuously differentiable reference trajectory

$$s_{\mathrm{r},i}(t) = \begin{pmatrix} x_{\mathrm{r},i}(t) \\ y_{\mathrm{r},i}(t) \\ \psi_{\mathrm{r},i}(t) \end{pmatrix}, \quad i = 1, \ldots, 4, \tag{6.5}$$

corresponding to the reference trajectory of the MB. Consequently, four identical tracking problems effectively remain.

As mentioned in Section 6.2, the mechanical coupling between the unicycles results in weight transfer from one wheel to another when accelerating, directly influencing the actual vertical load on each wheel. Recalling that the tire characteristic (see Figure 6.2) is approximately proportional to the actual vertical load, each tire will be operated with approximately the same amount of longitudinal slip if the drive torque distribution is equal to the vertical load distribution. This approach effectively yields optimal use of the tires, preventing the situation that some tires are operated far beyond the peak in their characteristic, whereas others are operated with a very low slip at the same time. The drive torque distribution requirement is met by introducing a fictitious equivalent unicycle mass $\tilde{m}_i$, $i = 1, \ldots, 4$, which is determined by the nominal mass and the weight transfer at each instant, assuming a force equilibrium regarding the tilt and pitch motion of the MB:

$$\begin{aligned}
\tilde{m}_1 &= \frac{m}{4} - \frac{hm}{4Lg}(\dot{u} - v\dot{\psi}) - \frac{hm}{4Wg}(\dot{v} + u\dot{\psi}) \\
\tilde{m}_2 &= \frac{m}{4} - \frac{hm}{4Lg}(\dot{u} - v\dot{\psi}) + \frac{hm}{4Wg}(\dot{v} + u\dot{\psi}) \\
\tilde{m}_3 &= \frac{m}{4} + \frac{hm}{4Lg}(\dot{u} - v\dot{\psi}) - \frac{hm}{4Wg}(\dot{v} + u\dot{\psi}) \\
\tilde{m}_4 &= \frac{m}{4} + \frac{hm}{4Lg}(\dot{u} - v\dot{\psi}) + \frac{hm}{4Wg}(\dot{v} + u\dot{\psi}),
\end{aligned} \tag{6.6}$$

where m is the total MB mass, h is the height of the center of gravity, g is the gravitational constant, and u and v are the velocity components of the MB expressed in the local MB coordinate frame $\{L\}$, as shown in Figure 6.3. In (6.6), $\dot{u} - v\dot{\psi}$ and $\dot{v} + u\dot{\psi}$ are the longitudinal and lateral MB accelerations, respectively. These accelerations affect the actual vertical wheel forces, which, when divided by g, result in the equivalent masses $\tilde{m}_i$ according to (6.6). These equivalent masses are now considered to be the "inertial masses" of the unicycles. Note that the hyperstaticity of the MB is dealt with by assuming a perfectly flat floor and a uniformly distributed MB mass, such that the nominal mass of each unicycle ia equal to the total MB mass divided by the number of wheels.

It should be mentioned that the mechanical coupling between the unicycles is likely to cause disturbances. It is however assumed that these disturbances are small and rather well damped due to the tire compliance. This assumption is justified by the practical experiments, as described in Section 6.7.

The next step is to design a position controller for each unicycle. If tire slip is neglected, the robotics theory based on motion constraints (Campion et al., 1996) could be applied to formulate a unicycle model and subsequently design a feedback linearizing controller (Canudas de Wit et al., 1996; Bendtsen et al., 2002). This method, as applied in Ploeg et al. (2006), appears to yield rather acceptable results. One might however expect that taking tire slip into account will improve the characteristics of the controlled unicycles and, consequently, of the MB as a whole, with respect to accuracy. Along this line of thinking, Andréa-Novel et al. (1995) and Motte and Campion (2000) provide a solution, based on the fact that tire dynamics are generally significantly faster than WMR dynamics, leading to a so-called *singular perturbation* model. Using this model, the feedback linearization procedure is essentially straightforward, even though it is mathematically complex. An explicit slip measurement appears not to be required, which is an advantage of the proposed controller. The resulting controller, however, has a rather complex structure, providing limited physical insight. Moreover, the singular perturbation model incorporates the linearized tire characteristics, whereas extension to the nonlinear characteristics (see Figure 6.2) is far from straightforward. The next section therefore explores a different approach, based on a unicycle model taken from the field of automotive engineering and feedback linearization in a master–slave structure.

6.4   Unicycle modeling and control

Before developing a controller for the MB, this section first focuses on the modeling and control design for a unicycle.

6.4.1   Modeling

Based on the physical description of a tire, as commonly used in the field of automotive engineering (Pacejka, 2002), this section will derive a unicycle model, including a linear tire model with 1st-order dynamics. Note that longitudinal and lateral slip, and the resulting forces are assumed to be independent, i.e., combined slip effects are ignored.

The equations of motion of the unicycle with index $i = 1, \ldots, 4$ in the horizontal plane are

$$\tilde{m}_i(\dot{u}_i - v_i\dot{\psi}_i) = F_{\text{long},i} \tag{6.7a}$$

$$\tilde{m}_i(\dot{v}_i + u_i\dot{\psi}_i) = F_{\text{lat},i} \tag{6.7b}$$

$$I_{\text{s}}\ddot{\psi}_i = T_{\text{s},i} \tag{6.7c}$$

with longitudinal velocity u_i, lateral velocity v_i, heading angle ψ_i, longitudinal force $F_{\text{long},i}$, and lateral force $F_{\text{lat},i}$. I_{s} is the inertia of the steering system, and $T_{\text{s},i}$ is the steer torque. A schematic of the unicycle model is shown in Figure 6.4. According to (6.7c), the steering system is modeled as a 2nd-order system without damping. This can be motivated by the fact that the wheels of the MB have
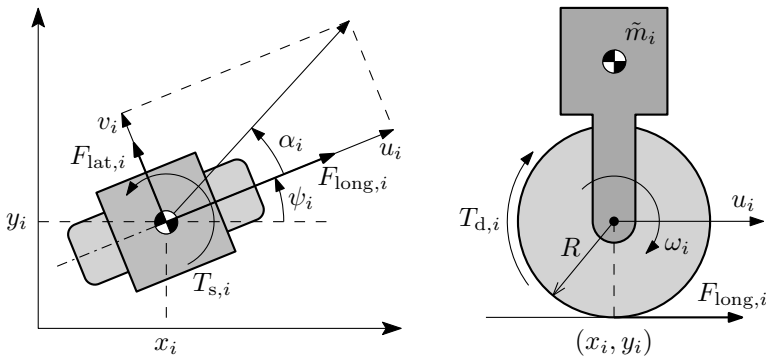
Figure 6.4: Top view (left) and side view (right) of the unicycle model.

center-point steering. Moreover, the self-aligning torque (Pacejka, 2002) is very small, compared with the maximum steering torque. Finally, the friction in the steering system is minimized through careful mechanical design. Note that the subscript i is omitted for those parameters that are identical for all unicycles.

After linearization with respect to the longitudinal tire slip κ_i, the longitudinal force $F_{\text{long},i}$ can be expressed as

$$F_{\text{long},i} = K(F_{z,i})\kappa_i \tag{6.8}$$

with longitudinal slip stiffness $K(F_{z,i})$, where $F_{z,i}$ is the actual vertical force acting on wheel i. $K(F_{z,i})$ is approximately proportional to the vertical load $F_{z,i} = \tilde{m}_i g$. Consequently, (6.8) can be rewritten as

$$F_{\text{long},i} = K_{\text{n}}\tilde{m}_i\kappa_i \tag{6.9}$$

with normalized longitudinal slip stiffness K_{n}. Tire relaxation effects are represented by the following 1st-order differential equation for the longitudinal tire slip:

$$\sigma_\kappa \dot{\kappa}_i + u_i\kappa_i = R\omega_i - u_i, \tag{6.10}$$

where σ_κ is the longitudinal relaxation length, R is the wheel radius, and ω_i the rotation velocity. Note that, for steady state, (6.10) yields $\kappa_i = (R\omega_i - u_i)/u_i$, i.e., the normalized velocity difference between the tire and the road. The longitudinal tire model is completed by the dynamics due to the inertia I_{d} of the tire/wheel/drive combination according to

$$I_{\text{d}}\dot{\omega}_i = T_{\text{d},i} - RF_{\text{long},i}, \tag{6.11}$$

where $T_{\text{d},i}$ is the drive torque.

Similarly, the lateral tire force is approximated by a linear function of the slip angle α_i:

$$F_{\text{lat},i} = -C_{\text{n}}\tilde{m}_i\alpha_i \tag{6.12}$$

with normalized cornering slip stiffness C_n. Introducing the lateral relaxation length σ_α, α_i is described by

$$\sigma_\alpha \dot{\alpha}_i + u_i \alpha_i = v_i, \tag{6.13}$$

where $\tan \alpha_i$ is approximated by α_i, assuming small slip angles (not to be confused with possible large *steering* angles). In steady state, (6.13) yields $\alpha_i = v_i/u_i$, which is, indeed, the tangent of the angle of the wheel velocity with respect to the wheel plane.

In summary, the complete unicycle model reads, for $i = 1, \ldots, 4$,

$$\dot{x}_i = u_i \cos \psi_i - v_i \sin \psi_i \tag{6.14a}$$

$$\dot{u}_i = K_\mathrm{n} \kappa_i + v_i \dot{\psi}_i \tag{6.14b}$$

$$\dot{\kappa}_i = \frac{R\omega_i - u_i - u_i \kappa_i}{\sigma_\kappa} \tag{6.14c}$$

$$\dot{\omega}_i = \frac{T_{\mathrm{d},i} - R K_\mathrm{n} \tilde{m}_i \kappa_i}{I_\mathrm{d}} \tag{6.14d}$$

$$\dot{y}_i = u_i \sin \psi_i + v_i \cos \psi_i \tag{6.14e}$$

$$\dot{v}_i = -C_\mathrm{n} \alpha_i - u_i \dot{\psi}_i \tag{6.14f}$$

$$\dot{\alpha}_i = \frac{v_i - u_i \alpha_i}{\sigma_\alpha} \tag{6.14g}$$

$$\ddot{\psi}_i = \frac{T_{\mathrm{s},i}}{I_\mathrm{s}}, \tag{6.14h}$$

where (x_i, y_i) is the position of the center of gravity (see Figure 6.4). The 9th-order unicycle model (6.14) has two external inputs, i.e., the drive torque $T_{\mathrm{d},i}$ and the steer torque $T_{\mathrm{s},i}$.

6.4.2 Controller design

The unicycle controller will be based on input–output linearization by time-invariant state feedback (Nijmeijer and Schaft, 1990), with the advantage of this approach being that it (partly) linearizes the system and, at the same time, decouples a multi-input multi-output system. A necessary condition for input–output linearization is that the system must be square. Consequently, two outputs have to be defined. A possible choice for the unicycle output function $z_{1,i}$, $i = 1, \ldots, 4$, is

$$z_{1,i} = \begin{pmatrix} z_{1,i,1} \\ z_{1,i,2} \end{pmatrix} = \begin{pmatrix} x_i + l_\mathrm{cp} \cos \psi_i \\ y_i + l_\mathrm{cp} \sin \psi_i \end{pmatrix} \tag{6.15}$$

with $l_\mathrm{cp} > 0$ being a constant parameter. This choice can be motivated from a physical point of view: Instead of controlling the position and the heading of the center of gravity of the unicycle, as indicated by (6.5), the position of a virtual control point $V_{\mathrm{cp},i}$ is controlled. This control point is located at a distance l_cp in front of the center of gravity as shown in Figure 6.5, which guarantees that not only the position (x_i, y_i), but also the heading ψ_i converge to their reference
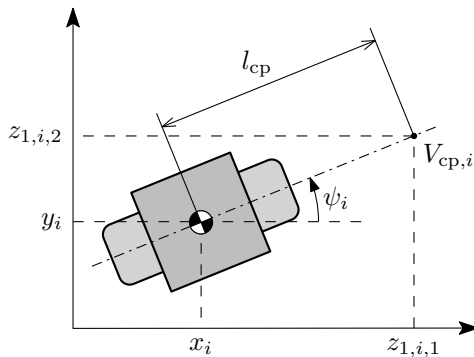
Figure 6.5: The virtual control point $V_{\text{cp},i}$, located on a distance l_{cp} from the unicycle center.

value as long as the forward velocity u_i is nonzero and the controlled system is stable. l_{cp} is, in fact, a tuning parameter, primarily influencing the damping of the controlled system. The latter can be readily understood: The effect of disturbances as a result of variations in the desired trajectory $z_{1,i}(t)$ perpendicular to the unicycle direction will be more attenuated as the length l_{cp} increases; with $l_{\text{cp}} \to \infty$, this type of disturbances no longer affects the unicycle motion at all.

Input–output linearization is basically performed by differentiating the outputs with respect to time until both inputs "appear" and then inverting the input–output relation. The number of differentiations of output $z_{1,i,k}$, $k = 1, 2$, that are necessary for at least one input to appear is called the *relative degree* d_k. Note that, because the unicycle models are identical, d_k is independent of i. For the unicycle model, d_1 and d_2 are both equal to 2. It appears, however, that only the second input $T_{\text{s},i}$ is then visible in both outputs, which renders the system not input–output linearizable by static state feedback[2]. The solution adopted here is to reduce the model by taking κ_i, instead of $T_{\text{d},i}$, as input, thereby removing (6.14c) and (6.14d) from the model (6.14). Consequently, the model order reduces to $n = 7$. The resulting model can be written as

$$\dot{q}_i = f(q_i) + G(q_i)r_i \tag{6.16}$$

with state vector q_i and input vector r_i according to

$$q_i = \begin{pmatrix} x_i & u_i & y_i & v_i & \alpha_i & \psi_i & \dot{\psi}_i \end{pmatrix}^{\text{T}} \tag{6.17a}$$

$$r_i = \begin{pmatrix} \kappa_i & T_{\text{s},i} \end{pmatrix}^{\text{T}}. \tag{6.17b}$$

The functions $f : \mathbb{R}^7 \mapsto \mathbb{R}^7$ and $G : \mathbb{R}^7 \mapsto \mathbb{R}^{7 \times 2}$, where $m = 2$ is the number of inputs, follow from (6.14). However, because the real input of the unicycle

---

[2]Only after four differentiations the input $T_{\text{d},i}$ appears in the outputs. Consequently, the second time derivative $\ddot{T}_{\text{s},i}$ then also appears in the outputs. Defining $\ddot{T}_{\text{s},i}$ as a new input would provide a solution, which is known as *dynamic extension*. This would however increase the system order, complicating the feedback controller design.

remains $T_{\mathrm{d},i}$, a slave controller that controls κ_i using $T_{\mathrm{d},i}$ is needed. In the remainder of this section, first, the position controller for the reduced unicycle model is designed, after which the κ controller will be described.

Since $d_1 = d_2 = 2$, the output vector $z_{1,i}$ has to be differentiated twice to construct the linearized model. To this end, the output function (6.15) is denoted by

$$z_{1,i} = \begin{pmatrix} x_i + l_{\mathrm{cp}} \cos \psi_i \\ y_i + l_{\mathrm{cp}} \sin \psi_i \end{pmatrix} = \begin{pmatrix} h_1(q_i) \\ h_2(q_i) \end{pmatrix} = h(q_i) \qquad (6.18)$$

with $h : \mathbb{R}^7 \mapsto \mathbb{R}^2$. Prior to the actual differentiation of (6.18), the Lie derivative $L_f\, h_k(q_i)$ (with, in this case, $k = 1, 2$) is introduced first, defined by(Khalil, 2000):

$$L_f\, h_k(q_i) := \langle \nabla h_k(q_i), f(q_i) \rangle, \qquad (6.19)$$

where $\nabla h_k(q_i)$ denotes the gradient of h_k with respect to q_i and $\langle \cdot, \cdot \rangle$ denotes the inner product. Since f is a vector field, the Lie derivative is, in fact, the directional derivative of h in the direction of f. Higher-order Lie derivatives can be defined recursively by

$$\begin{aligned} L_f^j\, h_k(q_i) &:= L_f\big(L_f^{j-1}\, h_k(q_i)\big) \\ &= \left\langle \nabla\big(L_f^{j-1}\, h_k(q_i)\big), f(q_i) \right\rangle, \quad j = 1, 2, \ldots, \end{aligned} \qquad (6.20)$$

where $L_f^0\, h_k(q_i) = h_k(q_i)$ by convention. Then, the first time derivative $\dot{z}_{1,i}$ yields

$$\begin{aligned} \dot{z}_{1,i} &= \begin{pmatrix} L_f\, h_1(q_i) \\ L_f\, h_2(q_i) \end{pmatrix} \\ &= \begin{pmatrix} u_i \cos \psi_i - (v_i + l_{\mathrm{cp}} \dot{\psi}_i) \sin \psi_i \\ u_i \sin \psi_i + (v_i + l_{\mathrm{cp}} \dot{\psi}_i) \cos \psi_i \end{pmatrix}. \end{aligned} \qquad (6.21)$$

Next, with the state vector $z_{2,i} = \dot{z}_{1,i}$, the second derivative is equal to

$$\dot{z}_{2,i} = b(q_i) + H(q_i) r_i \qquad (6.22)$$

with

$$\begin{aligned} b(q_i) &= \begin{pmatrix} L_f^2\, h_1(q_i) \\ L_f^2\, h_2(q_i) \end{pmatrix} \\ &= \begin{pmatrix} C_{\mathrm{n}} \alpha_i \sin \psi_i - l_{\mathrm{cp}} \dot{\psi}_i^2 \cos \psi_i \\ -C_{\mathrm{n}} \alpha_i \cos \psi_i - l_{\mathrm{cp}} \dot{\psi}_i^2 \sin \psi_i \end{pmatrix} \end{aligned} \qquad (6.23)$$

and

$$\begin{aligned} H(q_i) &= \begin{pmatrix} L_{g_1} L_f\, h_1(q_i) & L_{g_2} L_f\, h_1(q_i) \\ L_{g_1} L_f\, h_2(q_i) & L_{g_2} L_f\, h_2(q_i) \end{pmatrix} \\ &= \begin{pmatrix} K_{\mathrm{n}} \cos \psi_i & -\frac{l_{\mathrm{cp}}}{T_{\mathrm{s}}} \sin \psi_i \\ K_{\mathrm{n}} \sin \psi_i & \frac{l_{\mathrm{cp}}}{T_{\mathrm{s}}} \cos \psi_i \end{pmatrix}, \end{aligned} \qquad (6.24)$$

where g_1 and g_2 indicate the first and second columns of the matrix function G in (6.16), respectively. This clearly shows that the inputs appear in the differential equation after two differentiations. Note that the determinant $|H| = K_\mathrm{n} l_\mathrm{cp}/I_\mathrm{s}$ must be nonzero, because the inverse H^{-1} will be applied in the design. Consequently, l_cp must be nonzero, which can readily be understood because the wheel orientation would be undefined if $V_{\mathrm{cp},i}$ is located in the wheel center.

The differential equations (6.21) and (6.22), in fact, provide a new description of the linearizable part of the reduced unicycle model. The order of this subsystem is equal to $\sum_{k=1}^m d_k = 4$. Since the order of the reduced model is equal to 7, a subsystem of order 3 remains. Denoting the state of this subsystem by $z_{3,i}$, a possible choice for this state is $z_{3,i}^\mathrm{T} = \begin{pmatrix} v_i & \alpha_i & \dot\psi_i \end{pmatrix}$, which, after differentiation, results in an expression of the form

$$\dot z_{3,i} = k(z_{1,i}, z_{2,i}, z_{3,i}, r_i), \tag{6.25}$$

where $k : \mathbb{R}^2 \times \mathbb{R}^2 \times \mathbb{R}^3 \times \mathbb{R}^2 \mapsto \mathbb{R}^3$ appears to be a nonlinear function of the system input r_i and the states $z_{j,i}$, $j = 1, 2, 3$. This expression cannot be linearized using the input–output linearization procedure with the given choice of outputs (6.18), because the state $z_{3,i}$ is not "visible" in the output function (6.15).

With (6.21), (6.22), and (6.25), the reduced unicycle model is formulated in the so-called *normal form*. The actual feedback linearization is now obtained by choosing the input u_i according to the following feedback law:

$$r_i = H^{-1}(q_i)\left(\nu_i - b(q_i)\right), \tag{6.26}$$

which finally results in the unicycle model

$$\dot z_{1,i} = z_{2,i} \tag{6.27a}$$

$$\dot z_{2,i} = \nu_i \tag{6.27b}$$

$$\dot z_{3,i} = \tilde k(z_{1,i}, z_{2,i}, z_{3,i}, \nu_i) \tag{6.27c}$$

with new external input ν_i. The input r_i in the nonlinear state equation (6.27c) is also replaced by the new input ν_i, resulting in an adapted nonlinear function $\tilde k$. The model (6.27) shows that the dynamics of the reduced unicycle model have now been decomposed into a linear decoupled input–output part with states $z_{1,i}$ and $z_{2,i}$, and a nonlinear "unobservable" part with state $z_{3,i}$, which is generally referred to as the *internal dynamics*. Note that these dynamics may depend on the reference trajectory, according to (6.27c) and (6.28).

Tracking behavior of the linear input–output dynamics is obtained by a regular proportional–differential (PD) controller with feedforward:

$$\nu_i = \ddot z_{1,i,\mathrm{r}} + K_\mathrm{d}\left(\dot z_{1,i,\mathrm{r}} - \dot z_{1,i}\right) + K_\mathrm{p}\left(z_{1,i,\mathrm{r}} - z_{1,i}\right), \tag{6.28}$$

where K_p and K_d are diagonal 2×2 matrices containing the proportional and differential gains, respectively. To obtain equal dynamic behavior in the longitudinal and lateral directions, the elements of K_p and K_d that correspond to the longitudinal direction are chosen equal to those relating to the lateral direction. The

desired output $z_{1,i,\mathrm{r}}$ is calculated by substituting the reference trajectories (6.2) and (6.3) into (6.15). The resulting expression can subsequently be differentiated to obtain $\dot{z}_{1,i,\mathrm{r}}$ and $\ddot{z}_{1,i,\mathrm{r}}$.

The controller (6.28) stabilizes the input–output dynamics. To prevent undesirable phenomena, the internal dynamics, however, must also be stable or, in other words, the system should be minimum phase in the nonlinear sense. An example of such an undesirable phenomenon is the lateral oscillation of the unicycle wheel while the control point $V_{\mathrm{cp},i}$ "perfectly" tracks the reference trajectory. Due to the nonlinearity, the stability has to be checked for each reference trajectory. In case the unicycle is driving along a straight line with a constant forward velocity, the internal dynamics appear to be asymptotically stable for $u_i > 0$ and $l_{\mathrm{cp}} > \sigma_\alpha = 0.22\,\mathrm{m}$. Remarkably, the same stability requirement is also found regarding the effect of landing-gear shimmy for aircraft (Besselink, 2000). The requirement $u_i > 0$ can easily be understood from a physical point of view: When the unicycle is standing still, the heading angle ψ_i does not converge to the reference value. It should be noted that the stability proof is not pursued for a large number of trajectory types. In practice, however, the controlled MB appears to be stable, regardless of the specific trajectory, as illustrated in Section 6.7.

Finally, the slip controller is designed. The dynamics between the drive torque $T_{\mathrm{d},i}$ and the longitudinal slip κ_i are described by (6.14c) and (6.14d), where the forward velocity u_i is regarded as a relatively slowly varying parameter, which is indicated by the time argument t in the remainder of this section. Note that the longitudinal tire dynamics are thus assumed to be significantly faster than the MB dynamics (which, among others, are determined by the controller parameters K_{p} and K_{d} in (6.28)). This is the same fundamental idea as that used in Motte and Campion (2000). For this subsystem, it is possible to again apply input–output linearization using the same procedure as previously described. To this end, the model (6.14c) and (6.14d) is written as

$$\dot{q}_{\kappa,i} = f_\kappa(q_{\kappa,i}) + g_\kappa(q_{\kappa,i})r_{\kappa,i} \tag{6.29}$$

with vector functions $f_\kappa : \mathbb{R}^2 \mapsto \mathbb{R}^2$ and $g_\kappa : \mathbb{R}^2 \mapsto \mathbb{R}^2$. The states $q_{\kappa,i}$ and input $r_{\kappa,i}$ are defined as

$$\begin{aligned}
q_{\kappa,i} &= \begin{pmatrix} \kappa_i & \omega_i \end{pmatrix}^{\mathrm{T}} \\
r_{\kappa,i} &= T_{\mathrm{d},i}.
\end{aligned} \tag{6.30}$$

Choosing the controlled output $z_{\kappa,1,i}$ according to

$$z_{\kappa,1,i} = \kappa_i = h_\kappa(q_{\kappa,i}) \tag{6.31}$$

with $h_\kappa : \mathbb{R}^2 \mapsto \mathbb{R}$ being the output function, now leads to the 2$^{\mathrm{nd}}$-order linear system

$$\begin{aligned}
\dot{z}_{\kappa,1,i} &= z_{\kappa,2,i} \\
\dot{z}_{\kappa,2,i} &= \nu_{\kappa,i}
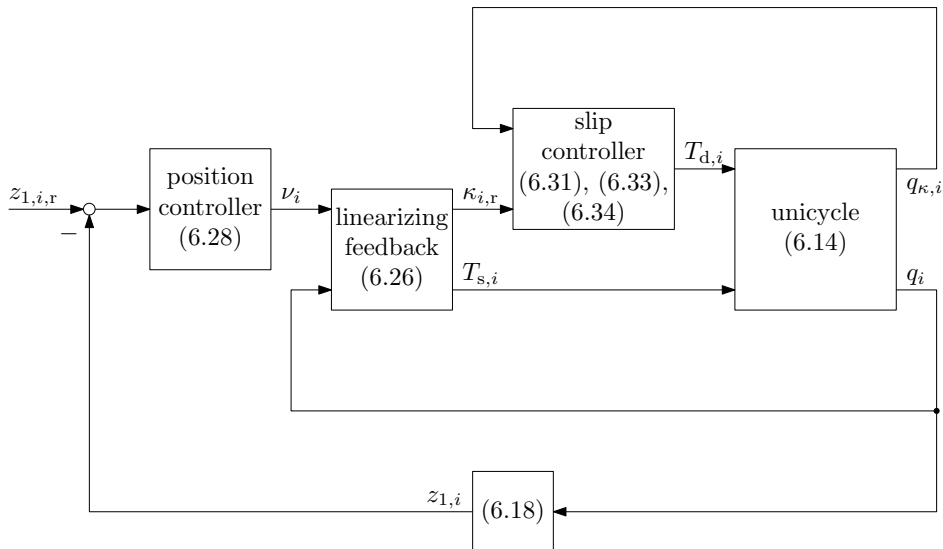\end{aligned} \tag{6.32}$$

Figure 6.6: Block scheme of the position-controlled unicycle.

with states $z_{\kappa,1,i}$ and $z_{\kappa,2,i}$, and new input $\nu_{\kappa,i}$ such that

$$
\begin{aligned}
r_{\kappa,i} &= L_{g_\kappa} L_{f_\kappa} h_\kappa(q_{\kappa,i})^{-1} \left(\nu_{\kappa i} - L_{f_\kappa}^2 h_\kappa(q_{\kappa,i}) \right) \\
&= \frac{\sigma_\kappa I_{\mathrm{d}}}{R} \left\{ \nu_{\kappa,i} + u_i(t) \frac{R\omega_i - u_i(t) - u_i(t)\kappa_i}{\sigma_\kappa^2} \right\} + R K_{\mathrm{n}} \tilde{m}_i \kappa_i, \qquad (6.33)
\end{aligned}
$$

which is obtained in a similar manner as in (6.26). Note that there are no internal dynamics because the relative degree is equal to the order of the system. Furthermore, it is noteworthy that the linearizing feedback law (6.33) explicitly contains the equivalent unicycle masses $\tilde{m}_i$. Hence, this feedback law effectively implements the drive torque distribution requirement, as stated in Section 6.3.

The system (6.32) can now be controlled using the following PD controller:

$$
\nu_{\kappa,i} = K_{\mathrm{d},\kappa}(\dot{z}_{\kappa,1,i,\mathrm{r}} - \dot{z}_{\kappa,1,i}) + K_{\mathrm{p},\kappa}(z_{\kappa,1,i,\mathrm{r}} - z_{\kappa,1,i}) \qquad (6.34)
$$

with differential gain $K_{\mathrm{d},\kappa}$ and proportional gain $K_{\mathrm{p},\kappa}$. $z_{\kappa,1,i,\mathrm{r}} = \kappa_{i,\mathrm{r}}$ is the longitudinal slip reference generated by the linearizing feedback law (6.26) of the "master" position controller. The first element of r_i in (6.17b) is thus regarded as the desired slip $\kappa_{i,\mathrm{r}}$ rather than the actual slip κ_i. Note that (6.34) does not include a feedforward term that is similar to $\ddot{z}_{1,i,\mathrm{r}}$ in (6.28), because double differentiation of the position controller output is expected to lead to a poor signal-to-noise ratio in practice.

In summary, the unicycle controller developed in this section consists of a slave slip controller and a master position controller, both of which are designed using input–output linearization involving time-invariant state feedback. Figure 6.6 shows the resulting block scheme, which provides an overview of the controller structure.

6.5   Observer design for the MB

The feedback-linearizing controller requires all states of the unicycle model (6.14) to be available, whereas not all states can be (accurately) measured. Moreover, some MB sensors, for instance an accelerometer and a gyroscope, are not repeatedly installed for each separate unicycle because of cost considerations; instead, a single sensor is mounted on the MB frame. Therefore, after a brief summary of the measured signals in Section 6.5.1, a linear observer is developed in Section 6.5.2, which estimates the position and the velocity of the geometric center of the MB as a basis for kinematical calculation of the position and velocity of the unicycles. In addition, two nonlinear observers are presented in Section 6.5.3 that estimate the lateral and the longitudinal slip for each unicycle.

6.5.1   Measurements

The following signals can be directly measured by sensors installed on the MB:

- The position (x, y) of the geometric center of the MB is measured using magnets mounted in the road surface in a regularly spaced grid. These magnets are detected by linear transducers (magnetostrictive waveguides) mounted on each side of the MB. Because the transducers only measure the position of a magnet along the transducer, some additional processing steps are required—among others involving a look-up procedure to determine the position of the magnet being detected—to calculate the MB center position. Although the measured position is relatively accurate (the position error is smaller than 2 cm), the position measurement becomes only available when at least one of the linear transducers moves over a magnet.

- For each unicycle, the wheel rotational velocity ω_i and the steering angle δ_i are measured by encoders. Here, the steering angle δ_i corresponds to the wheel orientation with respect to the MB body, as shown in Figure 6.3. Note that the wheel velocity encoder could be used to determine the longitudinal unicycle velocity u_i, but only when ignoring the longitudinal tire slip, whereas the lateral velocity v_i cannot be determined at all.

- The longitudinal acceleration a_{long} and the lateral acceleration a_{lat} of the geometrical MB center in the direction of the axes of the local MB coordinate system $\{L\}$ are measured by an accelerometer.

- The yaw rate $\dot{\psi}$ of the MB is measured by a very accurate fiber optic gyroscope.

- Both the drive torque $T_{\mathrm{d},i}$ and the steer torque $T_{\mathrm{s},i}$ can be directly measured at the electrical drives.

As a result, most of the available sensors cannot be used to directly and accurately measure the unicycle states, except for the wheel rotational velocity ω_i, which is measured by the wheel encoders. Nevertheless, the unicycle orientation ψ_i and the yaw rate $\dot{\psi}_i$ can be estimated without application of an observer. Consider

to this end the orientation ψ of the MB, which can be simply determined by integration of the measured yaw rate $\dot{\psi}$, using a calibration procedure to determine the initial orientation. Given the quality of the fiber optic gyroscope, this leads to a sufficiently accurate estimate, also taking into account that the MB only drives for short periods of time, which limits possible drift inherent to the open-loop integration. As a result, the unicycle orientation ψ_i can be easily calculated using the measured steering angle δ_i in addition, according to

$$\psi_i = \psi + \delta_i. \tag{6.35}$$

Furthermore, the unicycle yaw rate $\dot{\psi}_i = \dot{\psi} + \dot{\delta}_i$ can be determined by using the measured MB yaw rate $\dot{\psi}$ and the numerical derivative of the steering angle δ_i, which appears to be sufficiently accurate in practice due to the high-quality steering angle encoder.

In summary, the unicycle wheel velocity ω_i, orientation ψ_i, and yaw rate $\dot{\psi}_i$ can either be directly measured or calculated without using an observer. The remaining unicycle states x_i, y_i, u_i, v_i, κ_i, and α_i, however, require the use of observers, as will be described in the next two sections.

6.5.2 Motion observer

Since most sensors relate to the motion of the MB as a whole, it is decided to first develop an observer for the motion pattern of the geometrical center of the MB, specifically for the position (x, y) and the velocity $(\dot{x}, \dot{y})$. The resulting estimations then form a basis for the kinematical calculation of the unicycle position (x_i, y_i) and velocity (u_i, v_i).

The motion observer utilizes the following model:

$$\begin{aligned} \dot{q} &= Aq + Br + v_{\mathrm{p}} \\ z &= Cq + v_{\mathrm{m}} \end{aligned} \tag{6.36}$$

with state vector $q^{\mathrm{T}} = \begin{pmatrix} x & y & \dot{x} & \dot{y} \end{pmatrix}$ and input vector $r^{\mathrm{T}} = \begin{pmatrix} a_x & a_y \end{pmatrix}$, where a_x and a_y are the MB body accelerations with respect to the global coordinate system $\{G\}$, i.e., in x- and y-direction, respectively. Note that only the accelerations a_{long} and a_{lat} in the direction of the local MB coordinate system $\{L\}$ are measured. It is however relatively straightforward to convert $(a_{\mathrm{long}}, a_{\mathrm{lat}})$ to (a_x, a_y) using the MB orientation ψ. The measurement vector z contains the measured position and velocity (in two directions) of the MB center. From these definitions, the matrices A, B, and C directly follow as:

$$A = \begin{pmatrix} 0 & 0 & 1 & 0 \\ 0 & 0 & 0 & 1 \\ 0 & 0 & 0 & 0 \\ 0 & 0 & 0 & 0 \end{pmatrix}, \quad B = \begin{pmatrix} 0 & 0 \\ 0 & 0 \\ 1 & 0 \\ 0 & 1 \end{pmatrix}, \quad C = \begin{pmatrix} 1 & 0 & 0 & 0 \\ 0 & 1 & 0 & 0 \\ 0 & 0 & 1 & 0 \\ 0 & 0 & 0 & 1 \end{pmatrix}. \tag{6.37}$$

Finally, v_{p} is the process noise and v_{m} the measurement noise, both assumed to be Gaussian white noise with zero mean, essentially representing model and measurement uncertainties, respectively.

Based on the model (6.36), a Kalman filter is formulated, according to

$$\dot{\hat{q}} = A\hat{q} + Br + L\left(z - \hat{z}\right)$$
$$\hat{z} = C\hat{q},$$

(6.38)

where $\hat{q}$ and $\hat{z}$ are the estimated states and outputs, respectively, and z contains the measured outputs. The Kalman gain matrix L is calculated to minimize the covariance of the error $e = q - \hat{q}$, the result of which depends on (and can be tuned with) the noise covariance R_{v_p} of v_p and R_{v_m} of v_m. Note that L guarantees stable error dynamics

$$\dot{e} = \left(A - LC\right)e.$$

(6.39)

Some remarks apply to the measurement vector z in (6.38), which contains the measured position (x, y) and velocity $(\dot{x}, \dot{y})$ of the MB center. Here, the position is derived from the linear transducers. The velocity, however, is not directly measured. Instead, the MB velocity is kinematically calculated using the measured wheel velocities and steering angles, i.e., a so-called odometric approach. The fact that tire slip is ignored in this approach, is corrected in the Kalman filter by the position measurement and the use of the acceleration measurements as inputs. In fact, this is one of the reasons to apply this Kalman filter in the first place. The other reason is that the position measurement is only available if there is at least one magnet detected. If this is not the case, then the "measured" position (x, y) contained in z is set equal to the estimated value $(\hat{x}, \hat{y})$ contained in $\hat{z}$, effectively disabling the correction mechanism in the Kalman filter, thus resulting in open-loop integration of the estimated velocity $(\dot{\hat{x}}, \dot{\hat{y}})$.

From the estimated state $\hat{q}$ (and the orientation ψ_i and yaw rate $\dot{\psi}_i$), estimates of the position (x_i, y_i) and the velocity (u_i, v_i) of each unicycle are finally calculated straightforwardly using kinematical relations. As a result, these unicycle states are estimated using a linear observer without explicit knowledge regarding the tire slip. Nevertheless, explicit estimates of both the longitudinal tire slip κ_i and the lateral tire slip α_i are also required by the MB controller, which is the focus of the next section.

6.5.3 Slip observers

To estimate the longitudinal tire slip κ_i and the lateral tire slip α_i, two reduced-order observers are designed, using the same technique. To this end, the general approach used to design an observer with linear error dynamics (Sastry, 1999) is described first.

Consider a nonlinear system with input r, output z, and states q that is generally formulated as

$$\dot{q} = f(q, r)$$
$$z = h(q)$$

(6.40)

with $f : \mathbb{R}^n \times \mathbb{R}^m \mapsto \mathbb{R}^n$ and $h : \mathbb{R}^n \mapsto \mathbb{R}^\ell$ where n is the number of states, m the number of inputs, and ℓ the number of outputs. If (6.40) can be written in

the *observer form*

$$\dot{\tilde{q}} = A\tilde{q} + p(C\tilde{q}, r) \tag{6.41a}$$

$$z = C\tilde{q} \tag{6.41b}$$

with $\tilde{q}$ being the (possibly) redefined states, A and C being the system and output matrices, respectively, and $p : \mathbb{R}^\ell \times \mathbb{R}^m \mapsto \mathbb{R}^n$ being a nonlinear function of the inputs and the outputs, then the following observer can be formulated:

$$\dot{\hat{q}} = A\hat{q} + p(z, r) + L(z - \hat{z})$$
$$\hat{z} = C\hat{q}, \tag{6.42}$$

where $\hat{q}$ is the estimated state, $\hat{z}$ is the estimated output, and L is the $n \times \ell$ observer gain. Introducing the observer error $e = \tilde{q} - \hat{q}$, the resulting error dynamics appear to be linear due to cancelation of the nonlinear term $p(z, r)$, i.e.,

$$\dot{e} = (A - LC)e. \tag{6.43}$$

Note the similarity with the error dynamics (6.39) of the linear motion observer. Furthermore, if the pair (A, C) is observable, the error dynamics can be arbitrarily influenced by choosing L, within limits imposed by the measurement noise.

Based on the aforementioned approach, a longitudinal slip observer with linear error dynamics is designed. The objective of this observer is to estimate the longitudinal unicycle slip κ_i using the measurements mentioned in Section 6.5.1 and the estimated unicycle states from the motion observer, as described in Section 6.5.2. To this end, (6.14c) and (6.14d):

$$\dot{\kappa}_i = \frac{R\omega_i - u_i - u_i\kappa_i}{\sigma_\kappa} \tag{6.14c}$$

$$\dot{\omega}_i = \frac{T_{d,i} - RK_n\tilde{m}_i\kappa_i}{I_d}, \tag{6.14d}$$

describing part of the unicycle, will be applied. With input $r = T_{d,i}$, output $z = \omega_i$, and states $q^T = \tilde{q}^T = \begin{pmatrix} \kappa_i & \omega_i \end{pmatrix}$, (6.14c) and (6.14d) can be rewritten in the observer form (6.41) with

$$A_{\kappa,i} = \begin{pmatrix} -\frac{u_i(t)}{\sigma_\kappa} & \frac{R}{\sigma_\kappa} \\ -\frac{RK_n\tilde{m}_i}{I_d} & 0 \end{pmatrix} \tag{6.44a}$$

$$p_{\kappa,i}(z, r) = \begin{pmatrix} -\frac{u_i(t)}{\sigma_\kappa} \\ \frac{T_{d,i}}{I_d} \end{pmatrix} \tag{6.44b}$$

$$C_\kappa = \begin{pmatrix} 0 & 1 \end{pmatrix}. \tag{6.44c}$$

The system matrix A in (6.41a) is substituted by $A_{\kappa,i}$ and the nonlinear function p is substituted by $p_{\kappa,i}$. Similarly, the output matrix C in (6.41b) is substituted

by C_κ. The longitudinal velocity $u_i(t)$, appearing in (6.44a) and (6.44b), is estimated by the motion observer, whereas the wheel speed ω_i and the drive torque $T_{d,i}$ are directly measured. $u_i(t)$ is regarded as a time-varying parameter, which is indicated by the time argument t, although not necessarily a slowly varying parameter, as was the assumption for the design of the longitudinal slip controller in Section 6.4.2. As a consequence, however, both $A_{\kappa,i}$ and $p_{\kappa,i}$ are now time dependent, such that the observer gain L cannot be designed using techniques for linear time-invariant systems, such as, e.g., pole placement.

Denoting the observer gain vector as $L^{\mathrm{T}} = \begin{pmatrix} l_\kappa & l_\omega \end{pmatrix}$ and the estimation error for unicycle i as $e_i^{\mathrm{T}} = \begin{pmatrix} e_{\kappa,i} & e_{\omega,i} \end{pmatrix}$, with $e_{\kappa,i} = \kappa_i - \hat{\kappa}_i$ and $e_{\omega,i} = \omega_i - \hat{\omega}_i$, the observer error dynamics can be written in the form of (6.43) as follows:

$$\begin{pmatrix} \dot{e}_{\kappa,i} \\ \dot{e}_{\omega,i} \end{pmatrix} = \begin{pmatrix} -\frac{u_i(t)}{\sigma_\kappa} & \frac{R}{\sigma_\kappa} - l_\kappa \\ -\frac{RK_{\mathrm{n}}\tilde{m}_i}{I_{\mathrm{d}}} & -l_\omega \end{pmatrix} \begin{pmatrix} e_{\kappa,i} \\ e_{\omega,i} \end{pmatrix}. \tag{6.45}$$

The stability of these time-varying error dynamics can be investigated using Lyapunov's direct method with the following candidate Lyapunov function, where $e^{\mathrm{T}} = \begin{pmatrix} e_{\kappa,i} & e_{\omega,i} \end{pmatrix}$:

$$V(e) = \frac{1}{2}\frac{RK_{\mathrm{n}}\tilde{m}_i}{I_{\mathrm{d}}}e_{\kappa,i}^2 + \frac{1}{2}\left(\frac{R}{\sigma_\kappa} - l_\kappa\right)e_{\omega,i}^2 \tag{6.46}$$

which is a positive definite function for $l_\kappa < \frac{R}{\sigma_\kappa}$. The time derivative of V is given by

$$\dot{V}(e) = \frac{RK_{\mathrm{n}}\tilde{m}_i}{I_{\mathrm{d}}}e_{\kappa,i}\dot{e}_{\kappa,i} + \left(\frac{R}{\sigma_\kappa} - l_\kappa\right)e_{\omega,i}\dot{e}_{\omega,i}$$

$$= -\frac{RK_{\mathrm{n}}\tilde{m}_i u_i(t)}{I_{\mathrm{d}}\sigma_\kappa}e_{\kappa,i}^2 - l_\omega\left(\frac{R}{\sigma_\kappa} - l_\kappa\right)e_{\omega,i}^2, \tag{6.47}$$

which is negative definite if $u_i(t) > 0$ for all t and $l_\omega > 0$, provided that $l_\kappa < \frac{R}{\sigma_\kappa}$. Hence, the origin is a uniformly[3] globally asymptotically stable equilibrium point of the observer error dynamics (6.45) under the following conditions:

$$l_\kappa - \frac{R}{\sigma_\kappa} < 0$$
$$l_\omega > 0 \tag{6.48}$$
$$u_i(t) > \epsilon_\kappa \; \forall \, t,$$

where $\epsilon_\kappa > 0$ is an arbitrarily small number[4]. From (6.48), it inherently follows that the (time-varying) pair $(A_{\kappa,i}, C_\kappa)$ is observable. The condition on $u_i(t)$ implies, firstly, that the instantaneous center-of-rotation of the MB should not be

---

[3]V is decrescent, i.e., $V(e,t) \leq b(|e|)$ for some class $\mathcal{K}$ function b, since it does not explicitly depend on the time t.

[4]Due to the fact that $u_i(t)$ is a time-varying signal, the stability properties for $\epsilon_\kappa = 0$ require further analysis; this issue, however, has no practical consequences.

located exactly at the steering point of one of the unicycles (see Figure 6.3), imposing constraints on the desired trajectory s_r as formulated in (6.1); in practice, however, these constraints do not result in operational limitations. Secondly, the MB should not stand still, as was already explicitly formulated as a constraint by means of (6.4).

The observer for the lateral slip α_i is designed in a similar way, now based on (6.14f) and (6.14g):

$$\dot{v}_i = -C_n\alpha_i - u_i\dot{\psi}_i \tag{6.14f}$$

$$\dot{\alpha}_i = \frac{v_i - u_i\alpha_i}{\sigma_\alpha}. \tag{6.14g}$$

With input $r = \dot{\psi}_i$, output $z = v_i$, and states $q^T = \tilde{q}^T = \begin{pmatrix} v_i & \alpha_i \end{pmatrix}$, (6.14f) and (6.14g) can be rewritten in the observer form (6.41) with

$$
\begin{aligned}
A_{\alpha,i} &= \begin{pmatrix} 0 & -C_n \\ \frac{1}{\sigma_\alpha} & -\frac{u_i(t)}{\sigma_\alpha} \end{pmatrix} \\
p_{\alpha,i}(z,r) &= \begin{pmatrix} -u_i(t)\dot{\psi}_i \\ 0 \end{pmatrix} \\
C_\alpha &= \begin{pmatrix} 1 & 0 \end{pmatrix}
\end{aligned}
\tag{6.49}
$$

substituting A, p, and C in (6.41) by $A_{\alpha,i}$, $p_{\alpha,i}$, and C_α, respectively. The longitudinal velocity u_i and the lateral velocity v_i are estimated by the motion observer, whereas the unicycle yaw rate $\dot{\psi}_i$ is obtained from measurements as described in Section 6.5.1. u_i is again regarded as a time-varying parameter, as indicated by the time argument t, allowing for the specific observer form. Note that the lateral velocity v_i, estimated by the motion observer, is thus regarded as a "measurement" of the "true" lateral velocity included in the state q. Without using v_i as a state in the observer (i.e., omitting (6.14f) from the observer equations) only open-loop estimation of α_i using (6.14g) would be possible, which would require the initial condition to be exactly known.

The error dynamics of the lateral slip observer now read

$$
\begin{pmatrix} \dot{e}_{v,i} \\ \dot{e}_{\alpha,i} \end{pmatrix} = \begin{pmatrix} -l_v & -C_n \\ \frac{1}{\sigma_\alpha} - l_\alpha & -\frac{u_i(t)}{\sigma_\alpha} \end{pmatrix} \begin{pmatrix} e_{v,i} \\ e_{\alpha,i} \end{pmatrix}
\tag{6.50}
$$

with observer gains $\begin{pmatrix} l_v & l_\alpha \end{pmatrix} = L^T$. Using Lyapunov's direct method with candidate Lyapunov function

$$V(e) = \frac{1}{2}\left(\frac{1}{\sigma_\alpha} - l_\alpha\right)e_{v,i}^2 + \frac{1}{2}C_n e_{\alpha,i}^2, \tag{6.51}$$

with $e^T = \begin{pmatrix} e_{v,i} & e_{\alpha,i} \end{pmatrix}$, the origin $e^T = \begin{pmatrix} 0 & 0 \end{pmatrix}$ can be shown to be a uniformly

Table 6.2: Methods to obtain the unicycle states.

State	Method
x_i	Motion observer (6.38)
u_i	Motion observer (6.38)
κ_i	Longitudinal slip observer (6.42), (6.44)
ω_i	Direct measurement
y_i	Motion observer (6.38)
v_i	Motion observer (6.38)
α_i	Lateral slip observer (6.42), (6.49)
$\dot{\psi}_i$	Direct measurement
ψ_i	Open-loop integration of measured $\dot{\psi}_i$

globally asymptotically stable equilibrium if

$$
\begin{aligned}
l_\alpha - \frac{1}{\sigma_\alpha} &< 0 \\
l_v &> 0 \\
u_i(t) &> \epsilon_\alpha \ \forall \ t,
\end{aligned}
\tag{6.52}
$$

where $\epsilon_\alpha > 0$ is an arbitrarily small number. The first condition in (6.52) originates from the requirement dat V must be positive definite to serve as a Lyapunov function; the same remarks apply to the constraint on $u_i(t)$ as made in the context of the longitudinal slip observer.

Summarizing this section, all unicycle states can be estimated using a linear motion observer for the MB as a whole, combined with a nonlinear slip observer for the longitudinal tire slip and one for the lateral tire slip, for each unicycle separately. Table 6.2 presents an overview of the method with which each unicycle state is obtained. It is noted that the wheel rotational velocity ω_i is directly measured, but also estimated by the longitudinal slip observer (6.42), (6.44). Similarly, the lateral velocity v_i is estimated by the motion observer (6.38), but also by the lateral slip observer (6.42), (6.49). In both cases, however, it is decided not to use the values as estimated by the respective slip observers to prevent unnecessary phase delay.

6.6 Multicycle controller design

Having designed controllers and observers for the unicycles, the MB controller can now be established. As explained in Section 6.3, the MB controller consists of multiple identical unicycle controllers. It is therefore called the *multicycle* controller. One small adaptation, however, must be made, because the wheels have to be steered relative to the MB body only.

The unicycle steering torque $T_{\mathrm{s},i}$ is equal to $I_\mathrm{s}\ddot{\psi}_i$ for an ideal (frictionless) unicycle. Because the MB-body also rotates around its vertical axis with angular
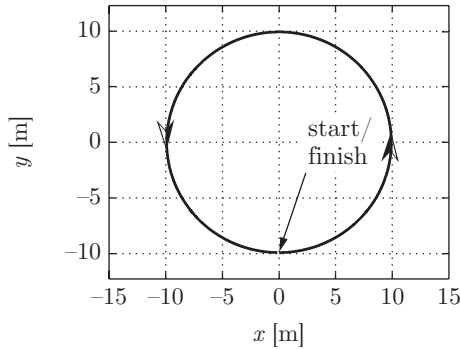
Figure 6.7: Desired position trajectory in the x–y plane for the observer experiment.

acceleration $\ddot{\psi}$, the net required steering torque $\tilde{T}_{s,i}$ for the multicycle is

$$\tilde{T}_{s,i} = I_s\ddot{\tilde{\delta}}_i = I_s(\ddot{\psi}_i - \ddot{\psi}) = T_{s,i} - I_s\ddot{\psi}. \tag{6.53}$$

As a consequence, a compensation term $-I_s\ddot{\psi}$ has to be added to $T_{s,i}$ to obtain the multicycle steering torque. The MB controller is now fully determined.

6.7   Experiments

After having tuned the designed controller and the observer gains on a simulation level, the final step in the design entails testing the controller in reality. To this end, first, the observer performance is assessed using the position-controlled MB. For this test, a position controller is applied, which differs from the one designed here in that it does not incorporate tire behavior and therefore does not need the slip to be estimated. The slip observers are implemented "in parallel", i.e., not in the closed control loop, which allows the slip observers to be evaluated independently of the position controller. The motion observer, however, is actively used in the position feedback control, because this is the only means of reliable position and velocity estimation.

A circular track is applied as desired trajectory, as shown in Figure 6.7. The desired velocity tangential to the track is increased from 0 to 30 km/h with a maximum acceleration of 7 m/s^2, then kept constant, and finally decreased to zero again with an acceleration of -7 m/s^2. The track radius is such that the centripetal acceleration[5] is equal to 7 m/s^2 at maximum velocity. The desired MB orientation is directed tangentially to the track. This test trajectory is applied to a simulation model of the controlled MB and to the real MB. The simulation model comprises a comprehensive physical model of the MB, which is implemented together with the controller in MATLAB/Simulink®.

---

[5]The term "centripetal" acceleration is used, instead of the more commonly used "lateral" acceleration to avoid ambiguity. Because the MB is an all-wheel steered robot, lateral acceleration could also be interpreted as a sideways translational acceleration.

Figure 6.8 shows the results of both the simulation and the experiment, displaying the longitudinal velocity of the MB center and the longitudinal slip, as well as the lateral slip of the front right tire ($i = 2$). The figure shows the following three types of signals:

1. *Simulated* signals: the simulated longitudinal velocity u, longitudinal slip κ_2, and the lateral slip α_2;

2. *Simulated estimated* signals: the velocity $\hat{u}$ and the slip $\hat{\kappa}_2$ and $\hat{\alpha}_2$, as estimated in the simulation by the motion observer and the slip observers, respectively;

3. *Measured estimated* signals: the observer results $\hat{u}_{\mathrm{m}}$, $\hat{\kappa}_{2,\mathrm{m}}$, and $\hat{\alpha}_{2,\mathrm{m}}$ from the practical experiment.

First, it can be concluded from Figure 6.8 that the longitudinal MB velocity u is rather accurately estimated in the simulation. Moreover, the estimated velocity $\hat{u}_{\mathrm{m}}$ during the practical experiment cannot be distinguished from the simulated signal $\hat{u}$. Furthermore, the simulated estimate $\hat{\kappa}_2$ of the longitudinal slip appears to be a little smaller (in absolute sense) than the simulated value κ_2. This is caused by the fact that the tire behavior is described by a linearized characteristic, yielding smaller slip values at the same tire force (see Figure 6.2). Nevertheless, the measured longitudinal slip estimate $\hat{\kappa}_{2,\mathrm{m}}$ shows a very high correlation with the simulated estimate $\hat{\kappa}_2$. The same observations hold for the lateral slip α_2, although there is a bigger difference between the simulated signal α_2 and the estimated signals $\hat{\alpha}_2$ and $\hat{\alpha}_{2,\mathrm{m}}$. This effect is again caused by the linearized tire characteristic. Furthermore, the lateral slip shows a significant higher noise level in the lower frequency region, compared to the longitudinal slip, as clearly shown by the simulated lateral slip. In addition, an increased noise level in the higher frequency region exists, particularly regarding the estimated lateral slip in the practical experiment. The low-frequency noise is actually caused by the motion observer, which updates the estimated position each time that a magnet is encountered. The high-frequency noise is caused by measurement noise of the gyroscope, to which the lateral slip observer is more sensitive than the longitudinal observer, because the former explicitly uses the measured yaw rate.

The aforementioned results for the front right tire also apply to the other tires, indicating that the estimates of the velocity and the slip are accurate, or at least show a high correlation with the real signals. It should however be noted that the experimental results do not provide certainty with respect to the observer performance, because the estimated signals cannot be compared with direct measurements since the latter are not available.

To test the overall system, i.e., the MB with unicycle observers and feedback-linearizing controllers, an "eight"-shaped test trajectory is designed, as shown in Figure 6.9. This figure shows both the reference trajectory and the resulting measured trajectory from the practical experiment. The centripetal acceleration during cornering is $9\,\mathrm{m/s}^2$, illustrating the MB behavior at a very high lateral acceleration level. The velocity tangential to the track is increased from 0 to $20\,\mathrm{km/h}$ with an acceleration of $5\,\mathrm{m/s}^2$, then kept constant, and finally decreased
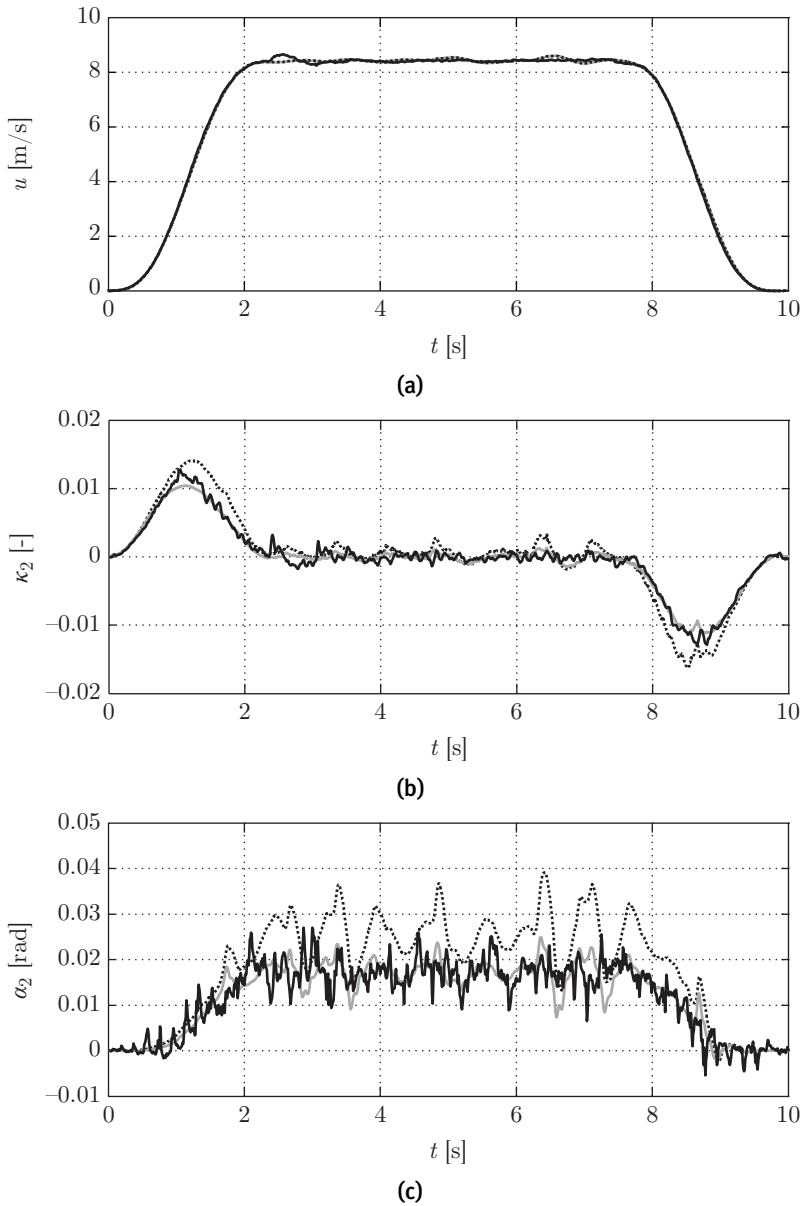
Figure 6.8: Observer results: Simulated signals (dotted black), simulated estimated signals (gray), and measured estimated signals (solid black) of (a) the longitudinal MB velocity u, (b) the longitudinal front right wheel slip κ_2, and (c) the lateral slip α_2.
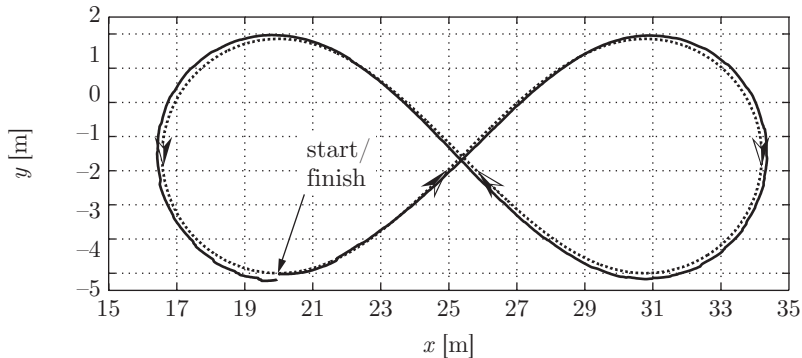
Figure 6.9: Desired position trajectory (dotted) and the experimentally measured trajectory (solid) in the x–y plane for the overall experiment.

to zero again with $5\,\mathrm{m/s^2}$ deceleration. The desired orientation is directed tangentially to the track. The test trajectory is again applied to the simulation model and the real MB.

From Figure 6.9, it can be observed that the position error is small, compared to the actual size of the trajectory. Furthermore, it appears that the measured trajectory is always outside the reference trajectory during cornering, indicating stable but not asymptotically stable internal dynamics. The simulated trajectory, which is not shown in Figure 6.9, leads to the same observations, albeit with a smaller position error.

Figure 6.10 displays the x-position error $e_x = x_\mathrm{r} - \hat{x}$, the y-position error $e_y = y_\mathrm{r} - \hat{y}$, and the orientation error $e_\psi = \psi_\mathrm{r} - \psi$ for the MB center as a function of time. Both the simulated and the measured error signals are shown, which were calculated using the positions estimated by the motion observer and the yaw angle as determined by open-loop integration of the measured yaw rate.

The noticeable differences between the simulated and the measured errors are due to model uncertainties and simplifications, particularly with respect to the tire characteristics and the floor flatness. Nevertheless, the simulation and the experiment show corresponding tendencies. Furthermore, it can be concluded from Figure 6.10 that the position error in the practical experiment is reasonable ($|e_x| < 0.3\,\mathrm{m}$, $|e_y| < 0.3\,\mathrm{m}$, and $|e_\psi| \le 0.1\,\mathrm{rad}$), given the high centripetal acceleration during the cornering part of the trajectory. The controller gains in (6.28) and (6.34) have, however, yet to be optimized with respect to these errors; further improvement might therefore be expected. Finally, the steady-state errors in the simulation and in reality should be noted. These are caused by the fact that the internal dynamics are stable but not asymptotically stable for $u_i = 0$, allowing for a final nonzero value of each wheel orientation ψ_i. Because, however, $z_{1,i}$ does converge to $z_{1,i,\mathrm{r}}$, i.e., the virtual control points converge to their desired values, the unicycle orientation errors inherently cause a corresponding position error of the MB center.
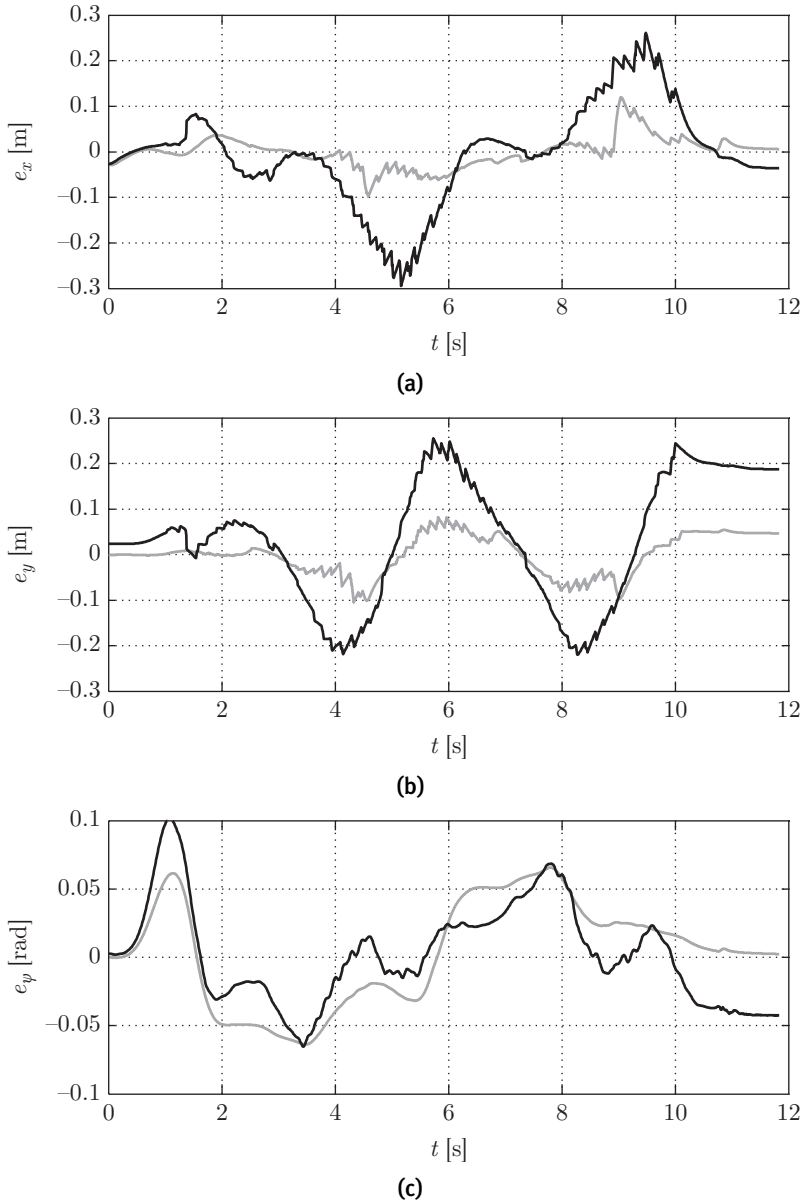
Figure 6.10: Controller results: Simulated signals (gray) and experiment measurements (black) of the MB error in (a) x-position, (b) y-position, and (c) yaw angle.

6.8 Conclusion

A multicycle controller for a four-wheel steered and driven WMR was designed, consisting of identical controllers for each wheel, thus regarding the WMR as a set of four unicycles. The unicycle controllers are based on input–output linearization by time-invariant state feedback, incorporating a linearized tire slip characteristic. In the multicycle approach, the overactuated nature of the robot is employed to determine the drive torque distribution across the wheels such that all tires have approximately the same amount of slip. The resulting controller can easily be adapted to other platform configurations. It is however necessary to have the longitudinal and lateral slip available, which requires a slip observer. To this end, two nonlinear slip observers were developed, one for the longitudinal and one for the lateral tire slip, which were proven to be asymptotically stable and appeared to perform adequately both in simulation and in practice. It must, however, be noted that the separation principle, stating that the stability of the controlled system with observers is determined by the individual stability of the observers and the controlled system without observers, may not hold in this nonlinear context and should be further investigated.

A possible improvement of the multicycle approach lies in the fact that the tire slip is still neglected on the multicycle level, i.e., at the kinematic determination of the reference steering angles. Furthermore, the nonlinear tire characteristic may be incorporated to achieve a more accurate behavior at high longitudinal and lateral accelerations.

The WMR serves as emulated traffic to provide sensory input for the onboard sensors of test vehicles that employ an advanced driver assistance system such as Cooperative Adaptive Cruise Control. Firstly, this test setup allows to characterize the onboard sensors with respect to accuracy and dynamical properties and, secondly, it allows for highly reproducible testing to evaluate and validate driver assistance control systems. As such, an intermediate development step is created between simulation-level controller design and practical testing under real-life circumstances, contributing to a thorough development procedure.

Chapter **7**

Conclusions and recommendations

This chapter summarizes the main conclusions from this thesis in Section 7.1 and identifies topics for future research as a result thereof in Section 7.2.

7.1 Conclusions

Limited highway capacity regularly causes traffic jams, which tend to increase over the years with respect to both the number of traffic jams and their length. An effective means to increase road capacity is to decrease the intervehicle distance while maintaining the same velocity level, decreasing fuel consumption due to reduced aerodynamic drag at the same time. To significantly decrease the intervehicle distance while not compromising safety, an automatic distance control system is required, taking over (part of) the driving task. Such a control system is subject to two main requirements: First, the preceding vehicle must be accurately followed, satisfying the adopted spacing policy, and second, the resulting string of controlled vehicles must be string stable, thereby preventing disturbance amplification along the string. To satisfy these requirements, wireless intervehicle communication is required, thus obtaining information for the vehicle's control system that cannot be obtained by onboard sensors such as radar. The design of such a control system, however, requires a rigorous and unambiguous definition of the notion of string stability, whereas the adopted controller design method should facilitate the explicit inclusion of the string stability requirement in the design specifications. Moreover, since wireless communication is subject to packet loss, a mechanism for graceful degradation must be designed to make the control system less vulnerable to the quality of the wireless link.

String stability is a property of a cascaded system, characterizing the evolution of the effects of disturbances over the interconnected systems constituting the cascaded system. In particular, string-stable behavior is an essential requirement for the design of automatic vehicle-following control systems, as it allows for short intervehicle distances in a vehicle platoon and scalability of the platoon with re-

spect to its length. Nevertheless, string stability is not unambiguously defined in literature. From a review of the main publications on this topic, it appeared that not only stability-like definitions were adopted, but also performance-based interpretations were proposed. The latter type of interpretation is typically applicable for strings of any length, whereas stability interpretations usually focus on infinite length strings, as is the case in the field of spatially invariant linear systems. Moreover, some definitions are tailored to a specific interconnection topology of the cascaded system under study, whereas others are of a more general nature. In addition, sometimes only perturbations in initial conditions are taken into account, as opposed to definitions that also include external disturbances. Finally, the performance-based interpretations commonly apply to linear systems only, whereas stability-like definitions also allow to include nonlinear system behavior.

Based on the aforementioned observations, a novel generic string stability definition was proposed in Chapter 2, employing the concept of $\mathcal{L}_p$ stability, which applies to both linear and nonlinear systems, while accommodating initial condition perturbations as well as external disturbances, independent of the interconnection topology. This approach basically allows for the application of existing methods for the analysis of $\mathcal{L}_p$ stability to assess the string stability properties. Specifically, the definition appeared to provide a rigorous basis for well-known string stability conditions, employing $\mathcal{L}_2$ and/or $\mathcal{L}_\infty$ gains, for linear unidirectionally interconnected systems. Employing these string stability conditions, it was shown, theoretically and practically, that Cooperative Adaptive Cruise Control (CACC) exhibits both $\mathcal{L}_2$ and $\mathcal{L}_\infty$ string-stable behavior for time gaps significantly smaller than 1 s, the latter being the minimum adopted value for nowadays Adaptive Cruise Control (ACC) systems. As a consequence, it can be concluded that CACC accommodates vehicular platooning at small distance while guaranteeing string stability. In turn, this allows to harvest potential benefits of close range platooning such as improved traffic throughput and increased fuel efficiency.

Furthermore, application of the $\mathcal{H}_\infty$ synthesis framework, as described in Chapter 3, appeared to allow for the explicit inclusion in the controller design specification of the $\mathcal{L}_2$ string stability requirement for linear unidirectionally interconnected systems, among which vehicle platoons. As a result, strict (preceding vehicle to follower vehicle) $\mathcal{L}_2$ string-stable behavior was obtained for a one-vehicle look-ahead communication topology whereas semi-strict (lead vehicle to follower vehicles) $\mathcal{L}_2$ string-stable behavior was realized for a two-vehicle look-ahead topology. In addition, it was found that the two-vehicle look-ahead topology provides a benefit with respect to minimum string-stable time gap when the communication delay exceeds a certain threshold. Moreover, the two-vehicle look-ahead controller appeared to be more robust against the presence of vehicles not equipped with wireless communication or, similarly, against failure of the wireless link for an extended period of time.

Focusing on the impact of wireless communication, it was shown that CACC performance in general, and string stability in particular, strongly depends on the availability of communicated information of the preceding vehicle(s). Since, however, wireless communication is subject to impairments such as packet loss, practical implementation of CACC requires a graceful degradation strategy in the

event of failure of the wireless link, such that minimum loss of CACC functionality is obtained. In addition, the preceding vehicle may not be equipped with wireless communication means, which essentially poses the same problem. To this end, a graceful degradation technique for CACC was proposed in Chapter 4, using an estimation of the preceding vehicle's current acceleration as a replacement to the desired acceleration which would normally (i.e., for CACC) be communicated over the wireless link. It was shown that, using this strategy, the degradation of string stability properties is limited, while maintaining the same time gap. Vice versa, a much smaller increase in time gap to regain string-stable behavior is required than with ACC, to which the controller effectively degrades in the absence of the graceful degradation mechanism. It is expected that this strategy can be combined with a multiple-vehicle look-ahead topology to further increase robustness against failures of the wireless link.

All theoretically obtained results regarding analysis of and controller synthesis for string stability, as well as the developed graceful degradation mechanism, were experimentally evaluated using a platoon of CACC-equipped passenger cars. As a result, it can be concluded that the practical experiments are consistent with the theoretical results, while illustrating the practical feasibility of CACC at the same time. From the experiment vehicle design, as described in Chapter 5, it appeared that practical implementation of CACC not only concerns the real-time implementation of the vehicle-following controller, but also requires position and velocity estimation of both the host vehicle and the target vehicle(s) to allow for association of the onboard sensor measurements with the corresponding wireless messages. Moreover, the driver must be allowed to interact with the system, and mechanisms for fault tolerance and graceful degradation need to be implemented. To manage the resulting complexity of the control software, a well-defined architecture appeared to be desired, at least distinguishing a perception layer, a control layer, and a supervisory layer. As opposed to the complexity of the control software, the actual hardware implementation basically only requires a GPS receiver and a wireless modem, provided that the vehicle is already equipped with ACC. Nevertheless, for research and development purposes, the necessary instrumentation is more extensive, among others including a rapid control prototyping system and a low-level computer system to enable a safe interaction with the native vehicle control systems.

Testing safety-critical cooperative driving applications, such as CACC, may require hardware-in-the-loop tests of the entire instrumented vehicle, while emulating other road users by means of motion-controlled wheeled mobile robots (WMRs). These robots must be four-wheel steered and driven to be able to drive the required trajectories. Within the scope of motion control of these WMRs, it was found that the so-called multicycle concept, in which the WMR is regarded as a set of four identical motion-controlled unicycles, is capable of achieving a high position accuracy. This result, as described in Chapter 6, is mainly due to the fact that the (linearized) tire slip characteristic is taken into account in the controller design. Consequently, a hardware-in-the-loop test setup was obtained that, firstly, allows to characterize the onboard sensors of the test vehicle with respect to accuracy and dynamical properties and, secondly, allows for highly re-

producible testing to evaluate and validate driver assistance control systems. As such, an intermediate development step is created between simulation-level controller design and practical testing under real-life circumstances, contributing to a thorough development process of ITS technologies such as CACC.

7.2   Recommendations

Vehicle platooning, as considered in this thesis, is a spatially one-dimensional cooperative driving application. As a consequence, the string stability analysis was confined to systems with scalar inputs and outputs. There is, however, no fundamental barrier to perform $\mathcal{L}_p$ string stability analysis on multivariable systems, which, for instance, arise in case of automated vehicle following, i.e., automation of both the longitudinal and the lateral motion of the vehicles in a platoon. Due to the relevancy of this more generic platooning scenario, being potentially increased safety of road transport, it is advised to further investigate multivariable $\mathcal{L}_p$ string stability, which is sometimes also referred to as mesh stability.

Another fundamental aspect of string stability concerns the development of methods for the assessment of this property. In this respect, it is noted that the $\mathcal{L}_p$ string stability definition, as proposed in this thesis, is an extension of the well-known notion of $\mathcal{L}_p$ stability. Hence, existing methods to analyze $\mathcal{L}_p$ stability, based on the formalism of Lyapunov stability, may be applied to analyze $\mathcal{L}_p$ string stability as well. This is particularly relevant for string stability analysis of nonlinear cascaded systems. In vehicle platooning, nonlinear behavior generally originates from the vehicle driveline or from the tire–road contact. Especially under extreme decelerations, which may occur during collision avoidance, tire behavior becomes severely nonlinear. It is, therefore, recommended to extend the string stability analysis for linear systems, as described in this thesis, to nonlinear systems, thus combining the fundamental aspect of $\mathcal{L}_p$ string stability of nonlinear systems with a relevant application in the mobility domain.

Notably, most results of this thesis apply to homogeneous systems only, thus inherently assuming that all vehicles in the string show identical dynamic behavior, in case of vehicle platooning. Obviously, this will not be the case in practice. Specifically for trucks, the dynamic properties may differ considerably, among others depending on the weight of the cargo. Consequently, the vehicle-following control system is required to be robust against these variations, not only guaranteeing string stability, but also guaranteeing a minimum vehicle-following performance level, for instance in terms of allowable distance error. Solutions to this challenge may be provided by adapting the low-level acceleration controller of each vehicle so as to enforce near-identical dynamic behavior, probably complemented by a robust vehicle-following controller that guarantees a minimum performance as well as string stability in the presence of uncertainties caused by variation in the behavior of the platooning vehicles. Due to its fundamental nature and its practical relevance at the same time, it is highly recommended to further investigate the topic of heterogeneous vehicle strings.

Next to these fundamental issues, vehicle platooning in everyday traffic also

involves several practical aspects to be solved. In this respect, the application of a communication-based "platoon-level" control system is recommended. Although this thesis advocates ad hoc platooning, it is likely that in the early phase of market introduction, such a high-level automation strategy is required to actively form a platoon of similar vehicles, i.e., vehicles with compatible instrumentation and corresponding vehicle-following control system. This strategy would avoid robustness issues due to varying vehicle dynamics (i.e., heterogeneity of the platoon) and non-communicating vehicles. In addition, this platoon-level control strategy could also support a controlled cut-in of equipped vehicles in an existing platoon by automatically increasing the intervehicle distance to allow the new vehicle to merge.

Arguably the most important issue in view of practical application of vehicle platooning strategies in everyday traffic, is the robustness of the control system against wireless communication impairments such as packet loss, with the extreme case being the presence of non-equipped vehicles in the platoon. It is, therefore, required to develop an overall strategy for fault tolerance and graceful degradation in the presence of unreliable wireless communication or non-equipped vehicles, taking into account the possible robustness measures as described in this thesis, i.e., multiple-vehicle look-ahead and acceleration estimation. Next to these measures, which apply to a failure of the wireless link over an extended period of time (or the absence of one), it is also required to take intermittent failures into account, for example leading to a varying latency of the wireless communication. To this end, the field of networked control systems provides a comprehensive set of tools for analysis of platooning performance in general and string stability in particular.

Yet another possibility to create robustness against wireless communication impairments may be sought in a fundamental change of the wireless communication protocol. Until now, time-driven communication is considered, in the sense that information is sent over the wireless link at equidistant time intervals. Here, the update time interval is determined by worst-case assumptions, i.e., rapid changes in the state of the communicating vehicles. Consequently, in the presence of a large number of transmitting nodes, the communication system may become overloaded, causing collisions of transmitted packets. Such a situation is very likely to occur at some point in the future, assuming an increasing degree of penetration of communicating vehicles. To cope with this situation, recent developments in the field of event-driven control systems may be applied. Such a system only executes a control action when the change in system state or output, expressed in terms of a norm on the state or output, exceeds a certain threshold. In other words, a message is only transmitted when its content has significantly changed since the last message. Consequently, event-driven communication for closed-loop cooperative driving applications is worthwhile investigating, as it may be the key to a successful large-scale introduction of these systems in everyday traffic.

Bibliography

Alam, A. Al, Gattami, A., and Johansson, K. H. (2010). An experimental study on the fuel reduction potential of heavy duty vehicle platooning. In *Proceedings of the 13th International IEEE Conference on Intelligent Transportation Systems*, Madeira Island, Portugal, September 19–22, 2010. p. 306–311.

Andréa-Novel, B. d', Campion, G., and Bastin, G. (1995). Control of wheeled mobile robots not satisfying ideal velocity constraints: A singular perturbation approach. *International Journal of Robust and Nonlinear Control*, 5(4), p. 243–267.

Arem, B. van, Driel, C. J. G. van, and Visser, R. (2006). The impact of cooperative adaptive cruise control on traffic-flow characteristics. *IEEE Transactions on Intelligent Transportation Systems*, 7(4), p. 429–436.

Åstrom, K. J. and Wittenmark, B. (1997). *Computer-controlled systems*. Prentice Hall, Upper Sadle River, NJ, USA, 3 edition.

Bamieh, B., Paganini, F., and Dahleh, M. A. (2002). Distributed control of spatially invariant systems. *IEEE Transactions on Automatic Control*, 47(7), p. 1091–1107.

Barbieri, E. (1993). Stability analysis of a class of interconnected systems. *ASME Journal of Dynamic Systems, Measurement, and Control*, 115(3), p. 546–551.

Barooah, P. and Hespanha, J. P. (2005). Error amplification and disturbance propagation in vehicle strings with decentralized linear control. In *Proceedings of the 44th IEEE Conference on Decision and Control*, Seville, Spain, December 12–15, 2005. p. 4964–4969.

Bendtsen, J. D., Anderson, P., and Pedersen, T. S. (2002). Robust feedback linearization-based control design for a wheeled mobile robot. In *Proceedings of the 6th International Symposium on Advanced Vehicle Control*, Hiroshima, Japan, September 9–13, 2002.

Besselink, I. J. M. (2000). *Shimmy of aircraft main landing gears*. Ph.D. thesis, Delft University of Technology, Delft, The Netherlands.

Borenstein, J. (1995). Control and kinematic design of multi-degree-of-freedom mobile robots with compliant linkage. *IEEE Transactions on Robotics and Automation*, 11(1), p. 21–35.

Bose, A. and Ioannou, P. A. (2003a). Analysis of traffic flow with mixed manual and semiautomated vehicles. *IEEE Transactions on Intelligent Transportation Systems*, 4(4), p. 173–188.

Bose, A. and Ioannou, P. A. (2003b). Mixed manual/semi-automated traffic: A macroscopic analysis. *Transportation Research Part C: Emerging Technologies*, 11(6), p. 439–462.

Brignolo, R., Zott, C., Spence, A., Brakemeier, A., Vivo, G., Bonnefoi, F., Mokaddem, A. K., Andreone, L., Cosenza, S., Zangherati, S., Zennaro, G., Visintainer, F., Schubert, R., and Bartels, C. (2008). Description of the integrated vehicle and infrastructure platform. http://www.safespot-eu.org/documents/D8.4.2_Integrated_vehicle_Infrastructure_Platforms.pdf [online], SAFESPOT Deliverable D8.4.2, April, 2008.

Bu, F., Tan, H.-S., and Huang, J. (2010). Design and field testing of a cooperative adaptive cruise control system. In *Proceedings of the American Control Conference*, Baltimore, MD, USA, June 30–July 2, 2010. p. 4616–4621.

Campion, G., Bastin, G., and Andréa-Novel, B. d' (1996). Structural properties and classification of kinematic and dynamic models of wheeled mobile robots. *IEEE Transactions on Robotics and Automation*, 12(1), p. 47–62.

Canudas de Wit, C., Siciliano, B., and Bastin, G. (1996). *Theory of robot control*. Springer-Verlag, London, U.K.

Chakravarthy, A., Song, K., and Feron, E. (2009). Preventing automotive pileup crashes in mixed-communication environments. *IEEE Transactions on Intelligent Transportation Systems*, 10(2), p. 211–225.

Chiang, R. Y. and Safonov, M. G. (1992). H^∞ synthesis using a bilinear pole shifting transform. *Journal of Guidance, Control, and Dynamics*, 15(5), p. 1111–1117.

Chiang, R. Y. and Safonov, M. G. (1998). *Robust control toolbox user's guide*. The MathWorks, Inc., 24 Prime Park Way, Natick, MA, USA.

Chien, C. C. and Ioannou, P. (1992). Automatic vehicle-following. In *Proceedings of the American Control Conference*, Chicago, IL, USA, June, 1992. p. 1748–1752.

Chu, K.-C. (1974). Optimal decentralized regulation for a string of coupled systems. *IEEE Transactions on Automatic Control*, 19(3), p. 243–246.

Corona, D. and Schutter, B. de (2008). Adaptive cruise control for a SMART car: A comparison benchmark for MPC-PWA control methods. *IEEE Transactions on Control Systems Technology*, 16(2), p. 365–372.

Curtain, R. F., Iftime, O. V., and Zwart, H. J. (2009). System theoretic properties of a class of spatially invariant systems. *Automatica*, 45(7), p. 1619–1627.

Desoer, C. A. and Vidyasagar, M. (2009). *Feedback systems: Input–output properties*. *Classics in Applied Mathematics*. Society for Industrial and Applied Mathematics (SIAM), Philadelphia, PA, USA.

Ding, S. X. (2008). *Model-based fault diagnosis techniques: Design schemes, algorithms and tools*. Springer-Verlag, Berlin Heidelberg.

Doyle, J. C., Glover, K., Khargonekar, P. P., and Francis, B. A. (1989). State-space solutions to standard $\mathcal{H}_2$ and $\mathcal{H}_\infty$ control problems. *IEEE Transactions on Automatic Control*, 34(8), p. 831–847.

Dunbar, W. B. and Caveney, D. S. (2012). Distributed receding horizon control of vehicle platoons: Stability and string stability. *IEEE Transactions on Automatic Control*, 57(3), p. 620–633.

Eckhoff, D., Sofray, N., and German, R. (2013). A performance study of cooperative awareness in ETSI ITS G5 and IEEE WAVE. In *Proceedings of the 10th Annual Conference on Wireless On-Demand Network Systems and Services*, Banff, Alberta, Canada, March 18–20, 2013. p. 196–200.

El-Sayed, M. L. and Krishnaprasad, P. S. (1981). Homogeneous interconnected systems: An example. *IEEE Transactions on Automatic Control*, 26(4), p. 894–901.

Eyre, J., Yanakiev, D., and Kanellakopoulos, I. (1998). A simplified framework for string stability analysis of automated vehicles. *Vehicle System Dynamics*, 30(5), p. 375–405.

Firooznia, A. (2012). *Controller design for string stability of infinite vehicle strings*. Master's thesis DC.2012.052, Eindhoven University of Technology, Department of Mechanical Engineering, Dynamics and Control Group.

Gehring, O. and Fritz, H. (1997). Practical results of a longitudinal control concept for truck platooning with vehicle to vehicle communication. In *Proceedings of the IEEE Conference on Intelligent Transportation Systems*, November 9–12, 1997. p. 117–122.

Geiger, A., Lauer, M., Moosmann, F., Ranft, B., Rapp, H., Stiller, C., and Ziegler, J. (2012). Team AnnieWAY's entry to the 2011 Grand Cooperative Driving Challenge. *IEEE Transactions on Intelligent Transportation Systems*, 13(3), p. 1008–1017.

Gietelink, O. J. (2007). *Design and validation of advanced driver assistance systems*. Ph.D. thesis, Delft University of Technology, Delft, The Netherlands.

Gietelink, O. J., Ploeg, J., Schutter, B. de, and Verhaegen, M. (2006). Development of advanced driver assistance systems with vehicle hardware-in-the-loop simulations. *Vehicle System Dynamics*, 44(7), p. 569–590.

González-Villaseñor, A., Renfrew, A. C., and Brunn, P. J. (2007). A controller design methodology for close headway spacing strategies for automated vehicles. *International Journal of Control*, 80(2), p. 179–189.

Guo, G. and Yue, W. (2012). Autonomous platoon control allowing range-limited sensors. *IEEE Transactions on Vehicular Technology*, 61(7), p. 2901–2912.

Haimovic, H. (2006). *Quantisation issues in feedback control*. Ph.D. thesis, School of Electrical Engineering and Computer Science, The University of Newcastle, Callaghan, Australia.

Hedrick, J. K., McMahon, D., Narendran, V., and Swaroop, D. (1991). Longitudinal vehicle controller design for IVHS systems. In *Proceedings of the American Control Conference*, Boston, MA, USA, June, 1991. p. 3107–3112.

Heemels, W. P. M. H. and Wouw, N. van de (2010). Networked control systems. A. Bemporad, M. Heemels, and M. Johansson (eds.). *Lecture Notes in Control and Information Sciences*, **406**, p. 203–253. Springer-Verlag, London, UK.

Hekmat, R. (2006). *Ad-hoc networks: Fundamental properties and network topologies*. Springer-Verlag, Dordrecht, The Netherlands.

Hespanha, J. P. (2009). *Linear systems theory*. Princeton University Press, Princeton, NJ, USA.

Heyer, L. J., Kruglyak, S., and Yooseph, S. (1999). Exploring expression data: Identification and analysis of coexpressed genes. *Genome Research*, 9(11), p. 1106–1115.

Hofmann-Wellenhof, B., Lichtenegger, H., and Collins, J. (2001). *Global positioning system – Theory and practice*. Springer-Verlag, Vienna, 5 edition.

Huppé, X., Lafontaine, J. de, Beauregard, M., and Michaud, F. (2003). Guidance and control of a platoon of vehicles adapted to changing environment conditions. In *Proceedings of the IEEE International Conference on Systems, Man, and Cybernetics*, Washington D.C., USA, October 5–8, 2003, **4**, p. 3091–3096.

International Organization for Standardization (2010). Adaptive Cruise Control systems – Performance requirements and test procedures. ISO Standard 15622, April, 2010.

Ioannou, P. A. and Chien, C. C. (1993). Autonomous intelligent cruise control. *IEEE Transactions on Vehicular Technology*, 42(4), p. 657–672.

Jovanović, M. R. and Bamieh, B. (2005). On the ill-posedness of certain vehicular platoon control problems. *IEEE Transactions on Automatic Control*, 50(9), p. 1307–1321.

Kato, S., Tsugawa, S., Tokuda, K., Matsui, T., and Fujii, H. (2002). Vehicle control algorithms for cooperative driving with automated vehicles and intervehicle communications. *IEEE Transactions on Intelligent Transportation Systems*, 3(3), p. 155–161.

Khalil, H. K. (2000). *Nonlinear systems*. Prentice-Hall, Inc., Pearson Eductation International, Upper Saddle River, NJ, USA, 3rd edition.

Khatir, M. E. and Davison, E. J. (2004). Decentralized control of a large platoon of vehicles using non-identical controllers. In *Proceedings of the American Control Conference*, Boston, MA, USA, June 30–July 2, 2004, **3**, p. 2769–2776.

Kianfar, R., Augusto, B., Ebadighajari, A., Hakeem, U., Nilsson, J., Raza, A., Tabar, R. S., Irukulapati, N. V., Englund, C., Falcone, P., Papanastasiou, S., Svensson, L., and Wymeersch, H. (2012). Design and experimental validation of a cooperative driving system in the Grand Cooperative Driving Challenge. *IEEE Transactions on Intelligent Transportation Systems*, 13(3), p. 994–1007.

Kim, S., Tomizuka, M., and Cheng, K. (2012). Smooth motion control of the adaptive cruise control system by a virtual lead vehicle. *International Journal of Automotive Technology*, 13(1), p. 77–85. 10.1007/s12239-012-0007-6.

Klinge, S. and Middleton, R. H. (2009a). String stability analysis of homogeneous linear unidirectionally connected systems with nonzero initial conditions. In *Proceedings of the IET Irish Signals and Systems Conference*, June 11–12, 2009a. p. 1–17.

Klinge, S. and Middleton, R. H. (2009b). Time headway requirements for string stability of homogeneous linear unidirectionally connected systems. In *Proceedings of the 48th IEEE Conference on Decision and Control*, Shanghai, P. R. China, December 16–18, 2009b. p. 1992–1997.

Lei, C., Eenennaam, E. M. van, Klein Wolterink, W., Ploeg, J., Karagiannis, G., and Heijenk, G. (2012). Evaluation of CACC string stability using SUMO, Simulink, and OMNeT++. *EURASIP Journal on Wireless Communications and Networking*, 116, p. 1–12.

Levine, W. S. and Athans, M. (1966). On the optimal error regulation of a string of moving vehicles. *IEEE Transactions on Automatic Control*, 11(3), p. 355–361.

Li, X. R. and Jilkov, V. P. (2001). A survey of maneuvering target tracking – part III: Measurement models. In *Proceedings of the SPIE Conference on Signal and Data Processing of Small Targets*, San Diego, CA, USA, July–August, 2001. p. 423–446.

Li, X. R. and Jilkov, V. P. (2002). A survey of maneuvering target tracking – part IV: Decision-based methods. In *Proceedings of the SPIE Conference on Signal and Data Processing of Small Targets*, Orlando, FL, USA, April, 2002. p. 4728–4760.

Li, X. R. and Jilkov, V. P. (2003). Survey of maneuvering target tracking. Part I: Dynamic models. *IEEE Transactions on Aerospace and Electronic Systems*, 39(4), p. 1333–1364.

Liang, C. H. and Peng, H. (1999). Optimal adaptive cruise control with guaranteed string stability. *Vehicle System Dynamics*, 32(4 & 5), p. 313–330.

Liang, C. Y. and Peng, H. (2000). String stability analysis of adaptive cruise controlled vehicles. *JSME International Journal, Series C, Mechanical Systems, Machine Elements and Manufacturing*, 43(3), p. 671–677.

Lidström, K., Sjöberg, K., Holmberg, U., Andersson, J., Bergh, F., Bjäde, M., and Mak, S. (2012). A modular CACC system integration and design. *IEEE Transactions on Intelligent Transportation Systems*, 13(3), p. 1050–1061.

Lijster, G. (2012). *A radar-based enhanced control algorithm for adaptive cruise control*. Master's thesis DC.2012.016, Eindhoven University of Technology, Department of Mechanical Engineering, Dynamics and Control Group.

Liu, X., Goldsmith, A., Mahal, S. S., and Hedrick, J. K. (2001). Effects of communication delay on string stability in vehicle platoons. In *Proceedings of the IEEE Conference on Intelligent Transportation Systems*, Oakland, CA, USA, August 25–29, 2001. p. 625–630.

Lu, M., Wevers, K., and Heijden, R. van der (2005). Technical feasibility of advanced driver assistance systems (ADAS) for road traffic safety. *Transportation Planning and Technology*, 28(3), p. 167–187.

Lu, X.-Y. and Hedrick, J. K. (2004). Practical string stability for longitudinal control of automated vehicles. *Vehicle System Dynamics*, supplement 41, p. 577–586.

Lu, X. Y., Shladover, S., and Hedrick, J. K. (2004). Heavy-duty truck control: Short inter-vehicle distance following. In *Proceedings of the American Control Conference*, June 30–July 2, 2004, **5**, p. 4722–4727.

Mårtensson, J., Alam, A., Behere, S., Khan, M. A. A., Kjellberg, J., Liang, K-Y., Pettersson, H., and Sundman, D. (2012). The development of a cooperative heavy-duty vehicle for the GCDC 2011: Team Scoop. *IEEE Transactions on Intelligent Transportation Systems*, 13(3), p. 1033–1049.

Maschuw, J. P., Keßler, G. C., and Abel, D. (2008). LMI-based control of vehicle platoons for robust longitudinal guidance. In *Proceedings of the 17th IFAC World Congress*, Seoul, Korea, July 6–11, 2008. p. 12111–12116.

Maybeck, P. S. (1979). *Stochastic models, estimation, and control*, *Mathematics in Science and Engineering*. **141**. Academic Press, Inc.

Meinsma, G. and Zwart, H. (2000). On $\mathcal{H}_\infty$ control for dead-time systems. *IEEE Transactions on Automatic Control*, 45(2), p. 272–285.

Melzer, S. M. and Kuo, B. C. (1971). Optimal regulation of systems described by a countably infinite number of objects. *Automatica*, 7(3), p. 359–366.

Middleton, R. H. and Braslavsky, J. H. (2010). String instability in classes of linear time invariant formation control with limited communication range. *IEEE Transactions on Automatic Control*, 55(7), p. 1519–1530.

Mori, S., Barker, W. H., Chong, C.-Y., and Chang, K.-C. (2002). Track association and track fusion with nondeterministic target dynamics. *IEEE Transactions on Aerospace and Electronic Systems*, 38(2), p. 659–668.

Motte, I. and Campion, G. (2000). A slow manifold approach for the control of mobile robots not satisfying the kinematic constraints. *IEEE Transactions on Robotics and Automation*, 16(6), p. 875–880.

Naus, G. J. L. (2010). *Model-based control for automotive applications*. Ph.D. thesis, Eindhoven University of Technology, Eindhoven, The Netherlands.

Naus, G. J. L., Bleek, R. A. P. M. van den, Ploeg, J., Scheepers, B. T. M., Molengraft, M. J. G. van de, and Steinbuch, M. (2008). Explicit MPC design and performance evaluation of an ACC stop-&-go. In *Proceedings of the American Control Conference*, Seattle, WA, USA, June 11–13, 2008. p. 224–229.

Naus, G. J. L., Vugts, R. P. A., Ploeg, J., Molengraft, M. J. G. van de, and Steinbuch, M. (2010). String-stable CACC design and experimental validation: A frequency-domain approach. *IEEE Transactions on Vehicular Technology*, 59(9), p. 4268–4279.

Nieuwenhuijze, M. R. I., Keulen, T. van, Öncü, S., Bonsen, B., and Nijmeijer, H. (2012). Cooperative driving with a heavy-duty truck in mixed traffic: Experimental results. *IEEE Transactions on Intelligent Transportation Systems*, 13(3), p. 1026–1032.

Nijmeijer, H. and Schaft, A. J. van der (1990). *Nonlinear dynamical control systems*. Springer-Verlag, New York, USA.

Nunen, E. van, Kwakkernaat, M. R. J. A. E., Ploeg, J., and Netten, B. D. (2012). Cooperative competition for future mobility. *IEEE Transactions on Intelligent Transportation Systems*, 13(3), p. 1018–1025.

Nunen, E. van, Ploeg, J., Morales Medina, A., and Nijmeijer, H. (2013). Fault tolerancy in cooperative adaptive cruise control. In *Proceedings of the 16th International IEEE Annual Conference on Intelligent Transportation Systems*, The Hague, The Netherlands, October 6–9, 2013. p. 1184–1189.

Öncü, S. (2014). *String stability of interconnected vehicles: Network-aware modelling, analysis and experiments*. Ph.D. thesis, Eindhoven University of Technology, Eindhoven, The Netherlands.

Öncü, S., Wouw, N. van de, and Nijmeijer, H. (2011). Cooperative adaptive cruise control: Tradeoffs between control and network specifications. In *Proceedings of the 14th International IEEE Conference on Intelligent Transportation Systems*, Washington D.C., USA, October 5–7, 2011. p. 2051–2056.

Öncü, S., Wouw, N. van de, Heemels, W. P. M. H., and Nijmeijer, H. (2012). String stability of interconnected vehicles under communication constraints. In *Proceedings of the IEEE 51st Annual Conference on Decision and Control*, Maui, HI, USA, December 10–13, 2012. p. 2459–2464.

Pacejka, H. B. (2002). *Tire and vehicle dynamics*. Butterworth-Heinemann, Oxford, U.K.

Patel, R. V. and Munro, N. (1982). *Multivariable system theory and design*. Pergamon Press, Oxford (UK), NY, USA.

Peppard, L. (1974). String stability of relative-motion PID vehicle control systems. *IEEE Transactions on Automatic Control*, 19(5), p. 579–581.

Piao, J. and McDonald, M. (2008). Advanced driver assistance systems from autonomous to cooperative approach. *Transport Reviews*, 28(5), p. 659–684.

Pintelon, R. and Schoukens, J. (2012). *System identification: A frequency domain approach*. Wiley-IEEE Press, 2 edition.

Ploeg, J., Knaap, A. C. M. van der, and Verburg, D. J. (2002). ATS/AGV – Design, implementation and evaluation of a high performance AGV. In *Proceedings of the IEEE Intelligent Vehicles Symposium*, Versailles, France, June 18–20, 2002, **1**, p. 127–134.

Ploeg, J., Vissers, J. P. M., and Nijmeijer, H. (2006). Control design for an overactuated wheeled mobile robot. In *Proceedings of the 4th IFAC Symposium on Mechatronic Systems*, Heidelberg, Germany, September 12–14, 2006. p. 127–132.

Ploeg, J., Schouten, H. E., and Nijmeijer, H. (2009). Position control of a wheeled mobile robot including tire behavior. *IEEE Transactions on Intelligent Transportation Systems*, 10(3), p. 523–533.

Ploeg, J., Scheepers, B. T. M., Nunen, E. van, Wouw, N. van de, and Nijmeijer, H. (2011). Design and experimental evaluation of cooperative adaptive cruise control. In *Proceedings of the 14th International IEEE Conference on Intelligent Transportation Systems*, Washington D.C., USA, October 5–7, 2011. p. 260–265.

Ploeg, J., Shladover, S., Nijmeijer, H., and Wouw, N. van de (2012). Introduction to the special issue on the 2011 Grand Cooperative Driving Challenge. *IEEE Transactions on Intelligent Transportation Systems*, 13(3), p. 989–993.

Ploeg, J., Semsar-Kazerooni, E., Lijster, G., Wouw, N. van de, and Nijmeijer, H. (2013). Graceful degradation of CACC performance subject to unreliable wireless communication. In *Proceedings of the 16th International IEEE Annual Conference on Intelligent Transportation Systems*, The Hague, The Netherlands, October 6–9, 2013. p. 1210–1216.

Ploeg, J., Shukla, D. P., Wouw, N. van de, and Nijmeijer, H. (2014a). Controller synthesis for string stability of vehicle platoons. *IEEE Transactions on Intelligent Transportation Systems*. http://ieeexplore.ieee.org/stamp/stamp.jsp?arnumber=06683051 [online]. To be published.

Ploeg, J., Wouw, N. van de, and Nijmeijer, H. (2014b). $\mathcal{L}_p$ string stability of cascaded systems: Application to vehicle platooning. *IEEE Transactions on Control Systems Technology*, 22(2), p. 786–793.

Rajamani, R. (2006). *Vehicle dynamics and control. Mechanical Engineering Series*. Springer-Verlag, 2333 Spring Street, New York, NY, USA.

Rajamani, R. and Shladover, S. E. (2001). An experimental comparative study of autonomous and co-operative vehicle-follower control systems. *Transportation Research Part C: Emerging Technologies*, 9(1), p. 15–31.

Rajamani, R. and Zhu, C. (2002). Semi-autonomous adaptive cruise control systems. *IEEE Transactions on Vehicular Technology*, 51(5), p. 1186–1192.

Rajamani, R., Tan, H.-S., Law, B. K., and Zhang, W.-B. (2000a). Demonstration of integrated longitudinal and lateral control for the operation of automated vehicles in platoons. *IEEE Transactions on Control Systems Technology*, 8(4), p. 695–708.

Rajamani, R., Choi, S. B., Law, B. K., Hedrick, J. K., Prohaska, R., and Kretz, P. (2000b). Design and experimental implementation of longitudinal control for a platoon of automated vehicles. *ASME Journal of Dynamic Systems, Measurement, and Control*, 122(3), p. 470–476.

Ramakers, R., Henning, K., Gies, S., Abel, D., and Max, H. (2009). Electronically coupled truck platoons on German highways. In *Proceedings of the IEEE International Conference on Systems, Man, and Cybernetics*, San Antonio, TX, USA, October 11–14, 2009. p. 2409–2414.

Russo, F., Galgani, D., Segarra, G., Lübke, A., Paulus, I., Busch, A., Kulp, I., Strassberger, M., and Seeberger, D. (2008). Deliverable D18: Standardisation activities. http://www.comesafety.org/uploads/media/COMeSafety_DEL_D18_StandardisationActivities_v2.0_01.pdf [online], COMeSafety Deliverable D18, October, 2008.

Safonov, M. G. (1987). Imaginary-axis zeros in multivariable H$^\infty$-optimal control. In *Proceedings of the NATO Advanced Research Workshop on Modelling, Robustness, and Sensitivity Reduction in Control Systems*, New York, NY, USA, 1987. p. 71–81, Springer-Verlag New York, Inc.

Santhanakrishnan, K. and Rajamani, R. (2003). On spacing policies for highway vehicle automation. *IEEE Transactions on Intelligent Transportation Systems*, 4(4), p. 198–204.

Sastry, S. (1999). *Nonlinear systems: Analysis, stability and control*. Springer-Verlag, New York, USA.

Seiler, P. and Sengupta, R. (2005). An H_∞ approach to networked control. *IEEE Transactions on Automatic Control*, 50(3), p. 356–364.

Seiler, P., Pant, A., and Hedrick, K. (2004). Disturbance propagation in vehicle strings. *IEEE Transactions on Automatic Control*, 49(10), p. 1835–1842.

Shaw, E. and Hedrick, J. K. (2007a). Controller design for string stable heterogeneous vehicle strings. In *Proceedings of the 46th IEEE Conference on Decision and Control*, New Orleans, LA, USA, December 12–14, 2007a. p. 2868–2875.

Shaw, E. and Hedrick, J. K. (2007b). String stability analysis for heterogeneous vehicle strings. In *Proceedings of the American Control Conference*, New York City, NY, USA, July 11–13, 2007b. p. 3118–3125.

Sheikholeslam, S. and Desoer, C. A. (1990). Longitudinal control of a platoon of vehicles. In *Proceedings of the American Control Conference*, San Diego, CA, USA, May 23–25, 1990. p. 291–296.

Sheikholeslam, S. and Desoer, C. A. (1992a). Control of interconnected nonlinear dynamical systems: The platoon problem. *IEEE Transactions on Automatic Control*, 37, p. 806–810.

Sheikholeslam, S. and Desoer, C. A. (1992b). A system level study of the longitudinal control of a platoon of vehicles. *ASME Journal of Dynamic Systems, Measurement, and Control*, 114(2), p. 286–292.

Sheikholeslam, S. and Desoer, C. A. (1993). Longitudinal control of a platoon of vehicles with no communication of lead vehicle information: A system level study. *IEEE Transactions on Vehicular Technology*, 42(4), p. 546–554.

Shladover, S. E. (2005). Automated vehicles for highway operations (automated highway systems). *Proceedings of the Institution of Mechanical Engineers, Part I: Journal of Systems and Control Engineering*, 219(1), p. 53–75.

Shladover, S. E. (2012). Recent international activity in cooperative vehicleŪhighway automation systems. Technical Report, University of California PATH Program, Richmond, CA, USA.

Shladover, S. E., Nowakowski, C., Cody, D., and O'Connell, J. (2009). Cooperative adaptive cruise control: Field testing of driver use and acceptance. In *Proceedings of the 16th World Congress & Exhibition on Intelligent Transport Systems and Services*, Stockholm, Sweden, September 21–25, 2009.

Shladover, S. E., Su, D., and Lu, X.-Y. (2012). Impacts of cooperative adaptive cruise control on freeway traffic flow. In *Proceedings of the 91st TRB Annual Meeting*, Washington, D.C., January 22–26, 2012. p. 1–17.

Singer, R. A. (1970). Estimating optimal tracking filter performance for manned maneuvering targets. *IEEE Transactions on Aerospace and Electronic Systems*, AES-6(4), p. 473–483.

Skogestad, S. and Postlethwaite, I. (2005). *Multivariable feedback control*. John Wiley & Sons.

Stanković, S. S., Stanojević, M. J., and Šiljak, D. D. (2000). Decentralized overlapping control of a platoon of vehicles. *IEEE Transactions on Control Systems Technology*, 8(5), p. 816–832.

Stoica, P. and Moses, R. L. (1997). *Introduction to spectral analysis*. Prentice-Hall, Upper Sadle River, NJ, USA.

Ström, E. G. (2011). On medium access and physical layer standards for cooperative intelligent transport systems in Europe. *Proceedings of the IEEE*, 99(7), p. 1183–1188.

Sugiyama, Y., Fukui, M., Kikuchi, M., Hasebe, K., Nakayama, A., Nishinari, K., Tadaki, S., and Yukawa, S. (2008). Traffic jams without bottlenecks – Experimental evidence for the physical mechanism of the formation of a jam. *New Journal of Physics*, 10 (033001), p. 1–7.

Swaroop, D. (2002). A note about the stability of a string of LTI systems. *ASME Journal of Dynamic Systems, Measurement, and Control*, 124(3), p. 472–475.

Swaroop, D. and Hedrick, J. K. (1996). String stability of interconnected systems. *IEEE Transactions on Automatic Control*, 41(3), p. 349–357.

Swaroop, D. and Hedrick, J. K. (1999). Constant spacing strategies for platooning in automated highway systems. *ASME Journal of Dynamic Systems, Measurement, and Control*, 121(3), p. 462–470.

Swaroop, D., Hedrick, J. K., Chien, C. C., and Ioannou, P. (1994). A comparison of spacing and headway control laws for automatically controlled vehicles. *Vehicle System Dynamics*, 23(1), p. 597–625.

Swaroop, D., Hedrick, J. K., and Choi, S. B. (2001). Direct adaptive longitudinal control of vehicle platoons. *IEEE Transactions on Vehicular Technology*, 50(1), p. 150–161.

Teo, R., Stipanović, D. M., and Tomlin, C. J. (2010). Decentralized spacing control of a string of multiple vehicles over lossy datalinks. *IEEE Transactions on Control Systems Technology*, 18(2), p. 469–473.

Toledo-Moreo, R., Gruyer, D., and Lambert, A. (2011). A theoretical analysis of the extended kalman filter for data fusion in vehicular positioning. In *Proceedings of the 11th International Conference on ITS Telecommunications*, St. Petersburg, Russia, August 23–25, 2011. p. 305–310.

Tse, D. and Viswanath, P. (2005). *Fundamentals of wireless communication*. Cambridge University Press, Cambridge, UK.

Vahidi, A. and Eskandarian, A. (2003). Research advances in intelligent collision avoidance and adaptive cruise control. *IEEE Transactions on Intelligent Transportation Systems*, 4(3), p. 143–153.

Vahidi, A., Stefanopoulou, A., and Peng, H. (2005). Recursive least squares with forgetting for online estimation of vehicle mass and road grade: Theory and experiments. *Vehicle System Dynamics*, 43(1), p. 31–55.

Venhovens, P., Naab, K., and Adiprasito, B. (2000). Stop and go cruise control. *International Journal of Automotive Technology*, 1(2), p. 61–69.

Wang, J., Wu, X., and Xu, Z. (2006). Input-to-state stability analysis of a class of interconnected nonlinear systems. In D. Yeung, Z.-Q. Liu, X.-Z. Wang, and H. Yan (eds.), *Advances in Machine Learning and Cybernetics*, *Lecture Notes in Computer Science*, **3930**, p. 122–132. Springer-Verlag, Berlin, Heidelberg.

Wang, M., Hoogendoorn, S. P., Daamen, W., Hoogendoorn, R. G., and Arem, B. van (2012). Driver support and cooperative systems control design: Framework and preliminary results. In *Proceedings of the American Control Conference*, Fairmont Queen Elizabeth, Montréal, Canada, June 27–29, 2012. p. 5751–5756.

Yadlapalli, S. K., Darbha, S., and Rajagopal, K. R. (2006). Information flow and its relation to stability of the motion of vehicles in a rigid formation. *IEEE Transactions on Automatic Control*, 51(8), p. 1315–1319.

Yanakiev, D. and Kanellakopoulos, I. (1998). Nonlinear spacing policies for automated heavy-duty vehicles. *IEEE Transactions on Vehicular Technology*, 47(4), p. 1365–1377.

Zhou, K., Doyle, J. C., and Glover, K. (1996). *Robust and optimal control*. Prentice Hall, Englewood Cliffs, NJ, USA.

Zwart, H., Firooznia, A., Ploeg, J., and Wouw, N. van de (2013). Optimal control for non-exponentially stabilizable spatially invariant systems with an application to vehicle platooning. In *Proceedings of the 52nd Conference on Decision and Control*, Florence, Italy, December 10–13, 2013. p. 3038–3042.

Samenvatting

Analyse en ontwerp van regelaars voor coöperatief en automatisch rijden

De afgelopen decennia is de intensiteit van het transport over de weg van personen en goederen sterk toegenomen. Verdere ontwikkeling van het huidige wegtransport wordt echter belemmerd door een beperkte capaciteit van het wegennetwerk. Daarnaast bestaat er een toenemende maatschappelijke druk om brandstofverbruik te verminderen en het aantal verkeersongevallen verder te reduceren. Naast het aanleggen van meer wegen kan de capaciteit worden verhoogd door de verkeersefficiëntie, als algemene maat voor doorstroming en reistijd, te verhogen. Deze wordt vooral bepaald door de interactie tussen de wegvoertuigen en niet zozeer door de eigenschappen van de individuele voertuigen en hun bestuurders. Daarnaast kunnen brandstofverbruik en verkeersveiligheid verder worden verbeterd door de individuele voertuigen te optimaliseren, maar echt nieuwe mogelijkheden hiervoor zullen pas ontstaan als in verkeerskundige zin wordt onderkend dat de voertuigen onderdeel zijn van een verkeerssysteem. Vanuit deze systeembenadering is het gebied van de Intelligente Transportsystemen in het afgelopen decennium ontstaan.

Een veelbelovende toepassing van deze systeembenadering staat bekend onder de naam *Cooperative Adaptive Cruise Control* (CACC). Dit is een systeem dat voorliggende voertuigen volgt met een kleine onderlinge afstand door automatisch gas te geven en te remmen, daarbij gebruikmakend van op het voertuig gemonteerde sensoren en van draadloze communicatie tussen de voertuigen. Het CACC-systeem moet voldoen aan eisen ten aanzien van de prestatie van het systeem (zoals de reactiesnelheid en de nauwkeurigheid), en aan de veiligheid en het comfort van de inzittenden. Om deze doelstellingen te kunnen realiseren moet een peloton van CACC-voertuigen ketenstabiel (Eng.: string stable) zijn. Dit betekent dat het effect van verstoringen, zoals bijvoorbeeld snelheidsvariaties, in stroomopwaartse richting uitdempt. Hierdoor wordt congestie door zogeheten spookfiles voorkomen. Het begrip ketenstabiliteit is echter niet eenduidig gedefinieerd in de literatuur omdat het zowel in termen van prestatie als in termen van stabiliteit

wordt beschreven. Om deze reden wordt in dit proefschrift een nieuwe definitie van ketenstabiliteit geïntroduceerd, gebaseerd op ingangs–uitgangsstabiliteit van niet-lineaire gecascadeerde systemen. Als een specifieke toepassing van deze nieuwe definitie kunnen de uit de literatuur bekende condities voor ketenstabiliteit van lineaire systemen worden afgeleid. Aan de hand van deze condities wordt vervolgens de ketenstabiliteit geanalyseerd van een specifiek CACC-systeem dat gebruik maakt van informatie van de directe voorligger.

Op basis van de condities voor ketenstabiliteit van lineaire systemen wordt vervolgens een methode voor regelaarontwerp ontwikkeld waarbij ketenstabiliteit als expliciete ontwerpeis kan worden geformuleerd. Hierdoor is iteratieve aanpassing van de regelaarparameters om ketenstabiliteit te realiseren niet langer nodig. Deze ontwerpmethode wordt geïllustreerd door toepassing ervan op het ontwerp van een CACC-systeem waarbij de draadloze informatie van één en van twee directe voorliggers wordt gebruikt. In beide gevallen leidt dit tot ketenstabiliteit. Tevens blijkt dat het gebruik van informatie van twee voorliggers vooral effectief is bij een relatief grote tijdvertraging in de draadloze communicatie tussen de verzending van een bepaald bericht en de ontvangst ervan in een andere auto.

Om de theoretische analyse te valideren, is een prototype van een CACC-systeem ontwikkeld en vervolgens geïmplementeerd in zes passagiersvoertuigen. De meetresultaten van de experimenten, die met deze voertuigen zijn uitgevoerd, laten een duidelijke overeenkomst zien met de resultaten van de theoretische analyse, waarmee dus de praktische haalbaarheid van een CACC-systeem wordt aangetoond. De experimenten geven echter ook de noodzaak aan van een mechanisme voor geleidelijke degradatie (Eng.: graceful degradation) om het optreden van fouten, die inherent zijn aan het gebruik van draadloze communicatie, op te vangen. Een voorbeeld van een dergelijke fout is het niet aankomen van verzonden informatie (Eng.: packet loss). Om deze reden wordt een regelstrategie ontwikkeld die in staat is de ketenstabiliteit tot op zekere hoogte te behouden in geval van informatieverlies.

De ontwikkeling van bestuurderondersteunende systemen zoals CACC wordt gefaciliteerd door experimenten waarbij een testvoertuig op een rollenbank wordt geplaatst terwijl rijdende robots het overige verkeer nabootsen. Omdat elk van de vier wielen van de robots onafhankelijk kan worden aangedreven en gestuurd terwijl de regeldoelstelling slechts drie graden van vrijheid kent in het platte vlak (namelijk de positie in twee richtingen en de oriëntatie), wordt de robot "overgeactueerd" genoemd. In wezen zijn deze robots te beschouwen als geautomatiseerde voertuigen, zij het dat hun manoeuvreerbaarheid ruimschoots die van de huidige wegvoertuigen overtreft. Vanuit het oogpunt van reproduceerbaarheid van de experimenten wordt een nauwkeurige positieregeling voor de robots ontworpen, rekening houdend met de slip tussen de banden en het wegdek. Deze positieregeling is gebaseerd op linearisatie van het ingangs–uitgangsgedrag door middel van toestandsterugkoppeling, waarbij de robot wordt beschouwd als vier afzonderlijke, identieke eenheden, elk bestaande uit een wiel, een aandrijfmotor en een stuurmotor. Deze regelaar beoogt dus de beweging van de vier wielen te synchroniseren, zodanig dat hun gemeenschappelijke doelstelling, namelijk positionering van de robot als geheel, wordt bereikt. Dit regelprobleem komt in essentie overeen met

het bovengenoemde probleem van het volgen van wegvoertuigen in een peloton, hetgeen eveneens betrekking heeft op coördineren van de beweging van diverse systemen, in dit geval hele voertuigen. Praktijkexperimenten met de positiegeregelde robot laten zien dat deze een gewenst pad nauwkeurig volgt, waardoor het reproduceerbaar testen van intelligente voertuigen in een controleerbare omgeving mogelijk is.

Samenvattend kan worden gesteld dat dit proefschrift zich richt op zowel theoretische als praktische aspecten van het regelaarontwerp voor coöperatief en geautomatiseerd wegtransport. Een belangrijke conclusie is dat een systeem voor het automatisch volgen van een voorligger op kleine onderlinge afstand, zoals CACC, technisch haalbaar is. Dit is ten eerste het gevolg van de beschikbaarheid van draadloze communicatie met een kleine tijdvertraging en ten tweede van het verworven fundamentele inzicht in het mechanisme van propagatie van verstoringen in elkaar volgende voertuigen. Daarbij is de implementatie van een strategie voor geleidelijke degradatie in geval van communicatiefouten een belangrijke voorwaarde. Veiligheidskritische toepassingen van coöperatief rijden, zoals CACC, vereisen dus een zorgvuldig ontwikkelproces. De beschikbaarheid van testmethoden waarmee het gehele systeem in een virtuele omgeving kan worden getest, draagt hier in belangrijke mate aan bij.

Dankwoord

Promoveren doe je niet alleen. Zeker in mijn geval, waarbij de promotie wordt gecombineerd met een baan, zijn er veel mensen op één of andere manier bij betrokken. Hen wil ik middels onderstaande woorden graag bedanken.

In de eerste plaats wil ik graag Henk Nijmeijer en Nathan van de Wouw bedanken voor de wetenschappelijke ondersteuning die ze mij hebben gegeven en voor de stimulerende atmosfeer die ze hebben gecreëerd, waardoor ik met heel veel plezier aan deze promotie heb gewerkt. Henk, bedankt dat je mij deze gelegenheid hebt geboden. Ik heb een grenzeloos respect voor het feit dat je, ondanks je drukke agenda, toch telkens weer de ruimte maakte om een technisch-inhoudelijke discussie te voeren. Nathan, je hebt me *rigorous thinking* geleerd: compromisloos tot de kern van het probleem doordringen; de essentie van een promotie. Daarnaast ben ik je heel veel dank verschuldigd voor het zeer zorgvuldig becommentariëren van een niet aflatende stroom aan voortgangsrapporten, publicaties en proefschrift-hoofdstukken. Hoewel niet direct betrokken bij mijn promotie, gaat mijn dank ook uit naar Maarten Steinbuch. Maarten, jij hebt ooit de kiem gelegd voor mijn fascinatie voor regeltechniek.

Mijn dank gaat ook uit naar Bart van Arem, Paul van den Bosch, Steven Shladover en Hans Zwart voor het feit dat zij in mijn commissie wilden plaatsnemen en voor het opbouwende commentaar dat zij hebben gegeven op mijn concept-proefschrift. Steven, I am grateful that you are willing to fly across the ocean for me. You are one of the founders of the field of cooperative and automated driving, and I consider it a great honor to have you as a member of my doctorate committee.

Natuurlijk mag TNO hier niet ontbreken. Zeer veel collega's hebben mij op verschillende manieren bijgestaan. Bedankt daarvoor! Het zijn er teveel om hier allemaal te noemen, maar enkelen van hen wil ik toch graag vermelden. Als eerste Egbert-Jan Sol. Met de woorden "Jij gaat promoveren. Als je afdelingshoofd moeilijk doet, laat het dan maar weten." heb je mij het duwtje gegeven dat ik nodig had om hieraan te beginnen. Ik heb ook zeer veel te danken aan Leo Kusters, Riné Pelders en San Hendrickx. Leo, ooit hebben jij en Ineke voor Liesbeth en mij bij ons thuis gekookt, na ons verkeersongeluk in India. Jaren later heb je mij de kans geboden te gaan promoveren. Dankjewel voor je steun in

zulke uiteenlopende situaties. Riné, jij hebt telkens weer een deel van je budget gereserveerd ter financiering; San, na afloop van het Connect & Drive-project droogde mijn voornaamste financieringsbron op, maar jij hebt ervoor gezorgd dat ik door kon gaan. Beiden dank daarvoor. Verder wil ik hier Hanno Schouten en John Vissers noemen, ooit mijn afstudeerders en nu al geruime tijd collega's. Hanno, John, bedankt voor jullie grote bijdrage aan het regelingontwerp van de Moving Base. Mijn dank gaat verder uit naar Elham Semsar. Elham, you started writing the conference paper that appeared to become the basis for Chapter 4 of this thesis. Thanks! Last but not least wil ik Ellen van Nunen en Bart Scheepers noemen. Bart, zonder jou waren er geen testvoertuigen geweest en was dit boekje half zo dik geweest. Ellen, jouw analytische bijdrage aan de ontwikkeling van CACC, je bereidheid om telkens weer een testrit te maken, je positieve instelling en vrolijke aanwezigheid hebben ontzettend veel voor mij betekend.

In dit rijtje mogen ook de Connect & Drive-partners en met name de initiatiefnemer, Alex Serrarens, niet ontbreken. Alex, jij bood mij hiermee de mogelijkheid dit promotiewerk te starten en bent mede bepalend geweest voor de richting waarin ik ben gegaan.

Voor wat betreft mijn collega-promovendi van de TU/e, wil ik vooral Sinan Öncü bedanken. Sinan, your willingness to discuss technical and mathematical problems was invaluable to me. As in any Ph.D. project, there were times of joy and times of frustration. I greatly appreciated it that I could share these with you and I'm very happy to have you as a colleague now. Verder wil ik ook graag Geertje Janssen en Petra Aspers bedanken. Het doorgronden van de procedures en regelingen van één organisatie is lastig, maar in het geval van twee organisaties wordt het een schier onmenselijke opgave. Geertje, Petra, jullie stonden altijd klaar om me hierbij te helpen en stelden mij daardoor in staat me te concentreren op mijn werk. Tot slot gaat mijn dank ook uit naar Gerrit Naus. Gerrit, jouw promotiewerk, deels op het gebied van CACC, is een uitstekend uitgangspunt geweest voor het mijne.

Ik mag mijzelf gelukkig prijzen met Guido Lijster en Dipan Shukla, de afstudeerders die ik heb begeleid in het kader van mijn promotietraject. Guido, dankjewel voor je afstudeerwerk; het heeft uiteindelijk tot een publicatie en een hoofdstuk geleid! Dipan, you did a marvelous job regarding controller design for CACC and I consider myself very lucky that you were willing to do your graduation project at TNO.

Tenslotte wil ik graag degene bedanken zonder wie ik dit traject nooit had kunnen volbrengen. Liesbeth, je hebt het soms zwaar te verduren gehad, maar je bent nooit opgehouden me te steunen. Dankjewel voor jouw liefde en voor alles wat je hebt gedaan. Ik hoop dat er nog vele jaren zullen volgen waarin ik hetzelfde voor jou kan betekenen.

Jeroen Ploeg
Helmond, 9 februari 2014

Curriculum vitae

Jeroen Ploeg was born on July 11, 1964 in Velsen, The Netherlands. After finishing his pre-university education in 1982 at the Coornhert Lyceum in Haarlem, The Netherlands, he studied mechanical engineering at Delft University of Technology in Delft, The Netherlands. In 1988, he received his M.Sc. degree on the control of wind turbines under partial load.

From 1989 to 1999, he worked as a researcher at Koninklijke Hoogovens (currently Tata Steel) in IJmuiden, The Netherlands, where his main focus was on the dynamic process control of large-scale industrial plants. Since 1999, he is a Senior Research Scientist at TNO in The Netherlands; he is currently working within the Integrated Vehicle Safety department in Helmond, The Netherlands. His current research interests are focusing on the control system design for cooperative and automated vehicles. He works in close cooperation with the Dynamics and Control group of the Mechanical Engineering department of Eindhoven University of Technology in Eindhoven, The Netherlands. In 2009, he started a Ph.D. project at Eindhoven University of Technology, of which the results are presented in this dissertation.